Mineralogical study and melt-fluid evolution of the Noumas I pegmatite, Northern Cape, South Africa.

Thesis submitted in fulfillment of the requirements

for the degree of

MAGISTER SCIENTIAE

by

Nequita MacDonald

At the Department of Geology

In the Faculty of Science
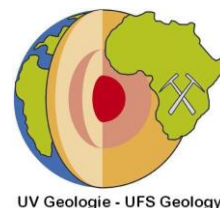
Of the University of the Free State

Bloemfontein

South Africa

Supervisor: Prof. Christoph D.K. Gauert

Co-supervisor: Dr. F. Roelofse

June 2013

UFS UV

UV Geologie - UFS Geology

DECLARATION

I, Nequita MacDonald, hereby declare that the content of this thesis submitted for the degree of Magister Scientiae at the University of the Free State, apart from the help recognized, is my own, unaided work and has never formally been submitted to another University for a previous degree.

N. MacDonald

Bloemfontein, June 2013

ABSTRACT

The motivation for this petrological study of the Kibaran aged, Noumas I pegmatite is based on the economic importance of lithium-bearing spodumene [$LiAl(Si_2O_6)$] as an electronic metal and its role in the crystallization process associated with the formation of complex lithium-rich LCT pegmatites.

Spodumene is found within the mineral assemblage of the Namaqualand pegmatites in the Northern Cape. It is one of the principle sources of lithium occurring in granodiorites. The host rocks are pegmatites in granites typically associated with dykes and veins consisting of quartz, microcline-perthite, albite, plagioclase, muscovite, columbite-tantalite, garnet, accessory beryl, spodumene, schorl and other Li-bearing phases.

An extensive literature study shows that economic lithium pegmatites have well defined intermediate and replacement zones with various Li-bearing mineral phases. Macroscopic mapping of narrow and dyke-like Noumas I pegmatite reveals mineralogical zones, namely border, wall, intermediate and core zones with distinct mineral assemblages. XRD and SEM-EDS analyses determined alkali feldspars, plagioclases and the lithium minerals spodumene, lepidolite and lithiophilite, petalite and amblygonite.

The geochemistry suggests that the Noumas I pegmatite compares well to a typical lithium enriched granite. Mass balance calculations show that its lithium content of 40.5 ppm requires a 6878.20% enrichment in lithium. Petrography, mineralogy and geochemistry suggest that the Noumas I pegmatite crystallized from a slow cooling, fluid rich melt. Jahns-Burnham's model of extreme fluid enrichment during secondary boiling better explains the crystal morphology and trace element enrichment. The major element compositions show a depletion of TiO_2, Fe_2O_3 and CaO compared to upper continental crust, indicative of a S-type source rock.

A concentration of water and fluxing elements (F, B, Li and P), in the Noumas I pegmatite, lowered the crystallization temperature, and made the magma less viscous. Based on the various analyses (XRF, XRD, SEM-EDS, ICP-MS) the classification for the Noumas I pegmatite is a lithium, columbite-tantalite pegmatite derived from s-type, peraluminous granites that concentrate Li, Rb, Cs, Be, Sn and Ta > Nb in the presence of B, P, F.

Microthermometry studies, established hydrothermal fluid properties in the wall, intermediate and core zones as fluids dominated by NaCl, K/NaCl <Mg+$CaCl_2$ and K/NaCl. The primary inclusion trapping temperatures were determined between 390-560°C at 5.5-6 kbar pressure for a deep emplacement of 17-20km. Secondary inclusion trapping temperatures for a shallow (6-7km) emplacement range between 100-170°C at pressures of 2-2.5 kbar. Although a liquid and a gas phase are identified within the fluid inclusions, the majority of them are liquid dominated with CO_2, CH_4 and H_2O identified by RAMAN and FTIR spectrometry.

Keywords: spodumene, lithium, Kibaran, Noumas, fluid inclusions, peraluminous granite

ACKNOWLEDGEMENTS

CONTENTS

CHAPTER 1: INTRODUCTION

CHAPTER 2: GEOLOGICAL SETTING

CHAPTER 3: DETAILED FIELD OBSERVATIONS

CHAPTER 4: PETROGRAPHY, MINERALOGY and GEOCHEMISTRY

CHAPTER 5: FLUID INCLUSION STUDY

CHAPTER 6: DISCUSSION

CHAPTER 7: CONCLUSIONS   107

CHAPTER 8: REFERENCES   108

LIST OF FIGURES

LIST OF TABLES

ABBREVIATIONS

BSE	back-scattered electron image
C	Core zone
FI	Fluid inclusion
FIA	Fluid inclusion assemblage
Ga	billion years
GPS	global positioning system
LLD	lower limit of detection
LOI	loss on ignition
Lpd	lepidolite
I	intermediate zone
M	middle zone
Ma	million years
Mcc	microcline
Musc	muscovite
NMB	Namaqua mobile belt
NMP	Namaqualand Metamorphic province
Plg	plagioclase
Pyx	pyroxene
Qtz	quartz
SEM-EDX/WDX	scanning electron microscope-Energy dispersive/wavelength dispersive spectrometer
Spd	spodumene
Te	eutectic temperature
Tf	formation/ trapping temperature
Th	homogenization temperature
Tm	total melting temperature of ice
Tm_{cl}	melting temperature of clathrate
Tm_{CO_2}	melting temperature of CO_2
XPL	cross-polarized light
XRD	x-ray diffraction
XRF	x-ray fluorescence
Eq. wt% NaCl	Quantity of NaCl that yields the same Tm_{ice} value. NaCl concentration of solution at room temperature
wt%	weight percentage

Chapter 1: INTRODUCTION

Pegmatite intrusions associated with REEs (rare earth elements) show enrichment in lithium, beryllium and tantalum. The lithium pyroxene, spodumene *(LiAl(SiO$_3$)$_2$)*, is the only exploitable Li-mineral in South Africa (Bullen,1998). South Africa imports Li as spodumene or as a compound (lithium oxide, hydroxide, and carbonate). It is therefore of economic interest to identify viable lithium deposits or a classification system to identify large extractable deposits, that would be of benefit to the economy of South Africa.

1.1 Literature review

Landes (1933) and 60 years later, Anderson and Bodnar (1993) defined pegmatites, as large coarse-grained rocks or graphically textured material of intrusive origin. Whereas today, pegmatites are defined as mineral associations crystallized in-situ, decidedly more coarse-grained than similar mineral associations in the form of ordinary rocks, and differing from these in having a more irregular fabric of the mineral aggregates. Pegmatites are multifaceted in shape, size and continuity. The recovery of economic minerals from pegmatites is considered small when looking at the tonnage of rock that needs to be moved for it to become viable (Minnaar and Theart, 2006). In general, pegmatites are frequently associated with dykes and veins of aplite, consisting of quartz, microcline, albite, orthoclase, muscovite and tourmaline (Cairncross, 2004).

Lithium is an economically viable metal used in a multitude of metallurgical, electronic, petrochemical, plastic and chemical processes. Lithium is used in three basic forms, as ore and concentrate, metal and manufactured chemical compounds. Glass, ceramic and porcelain industries use Li ore and concentrates. Petalite, lepidolite and amblygonite can be used without prior beneficiation, whereas spodumene must be beneficiated by grinding, flotation, leaching and magnetic separation (Kennedy, 1990). Lithium provides high mechanical strength and thermal shock resistance as well as chemical resistance within internal nucleation conditions during crystallization (Garret, 2004). The United States Geological Society estimated that Chile holds approximately 73% of the world's lithium resources, China 13%, Canada 4.5% and Australia just over 4% (Kennedy, 1990). Lithium resources occur in two types, as lithium minerals and lithium-rich brines. Lithium minerals can be derived from pegmatites and brines as

principle sources (Boelema and Hira, 1994). Canada and Australia have the most significant hard-rock lithium resources, with Chile having the dominant lithium brine resources.

Lithium pegmatites of southern Africa are associated with the ±1 Ga Namaqualand Metamorphic Province (NMP) located in the northwestern Cape (Figure 1-1 and Figure 1-2). The lithium minerals found in the berrylliferous western portion of the pegmatite belt include spodumene, amblygonite *(Li, Na)AIPO$_4$(F, OH),* lepidolite *KLi$_2$Al(Al, Si)$_3$O$_{10}$(F, OH)$_2$,* petalite and lithiophillite *Li(Mn, Fe)PO$_4$* (Nesse, 2004). Lithium pegmatites are generally found in granitiod terranes, of Precambrian age (540 Ma), in high-grade metamorphic environments. Economic lithium pegmatites are well defined and appear to have complex zones where the lithium minerals occur in various mineral phases (Thomas et al., 1994).
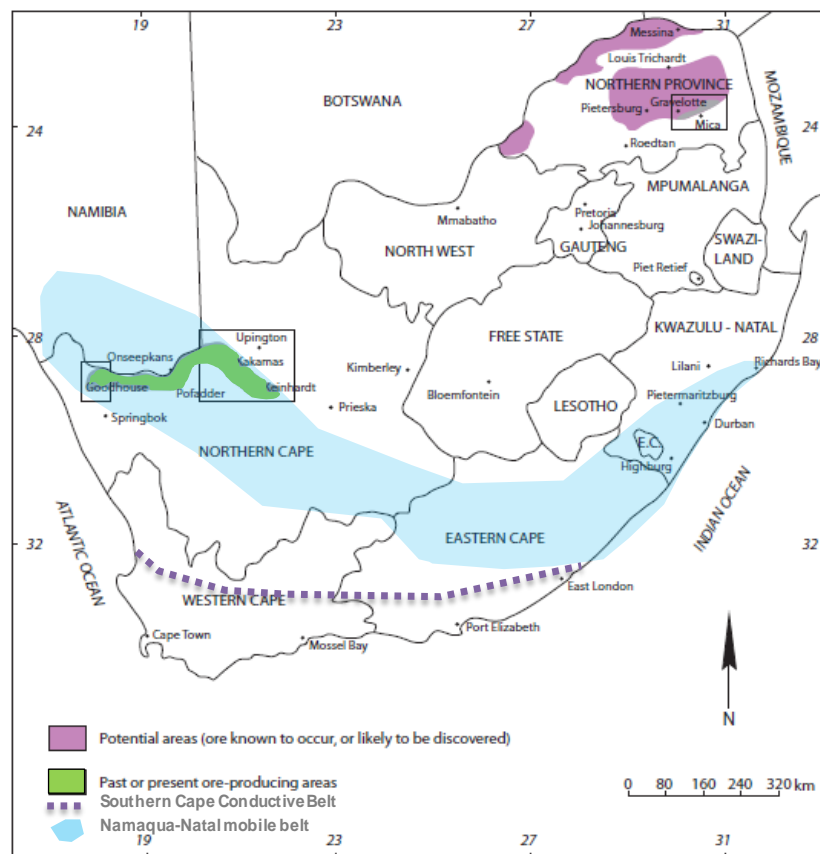
Figure 1-1: Distribution of pegmatites in the Republic of South Africa after (Boelema, 1998).

Hugo (1970) identified homogeneous and two types of heterogeneous pegmatites in the Northern Cape area. However, only heterogeneous pegmatites, simple and complex types, are found in the study area, NW Namaqualand around the Noumas I pegmatite. The major

difference between simple and complex pegmatites is the zonation and shape found in each type.
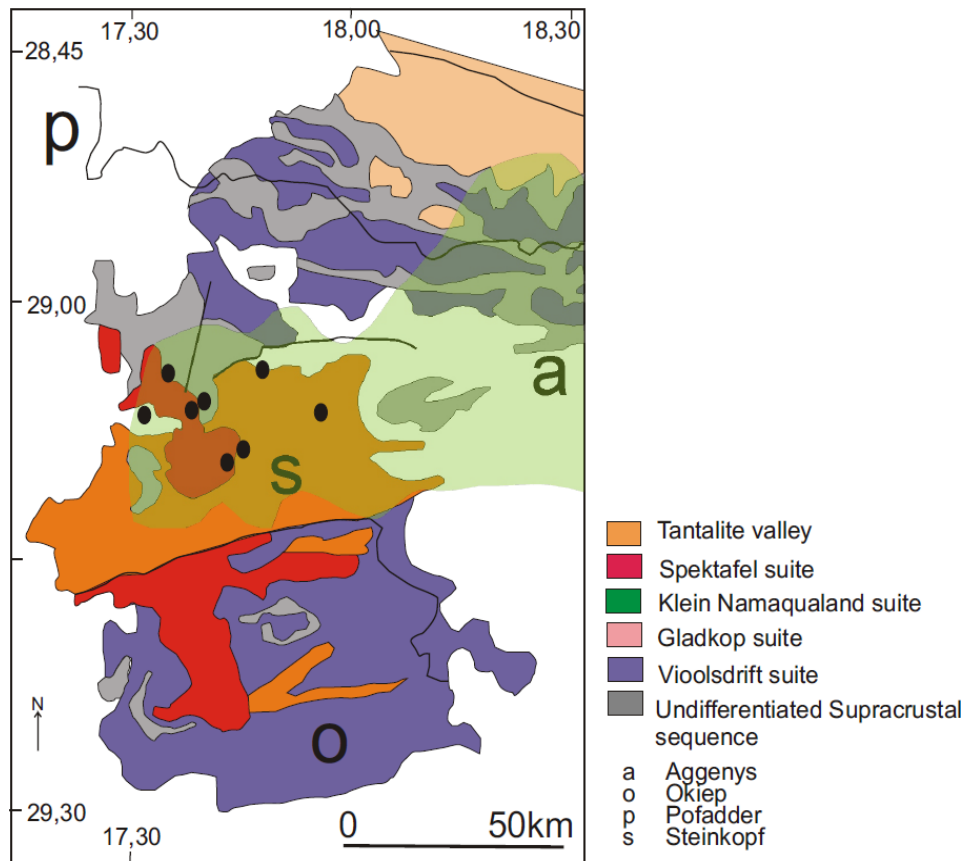
Figure 1-2: Enlarged study area of the pegmatite belts. There is a distribution of lithium mineralized pegmatites (black circles) hosted in the Namaqualand Metamorphic Province (after Thomas et al., 1994 & Minnaar and Theart, 2006).

Simple pegmatites have a well-developed zonation with four zones. i) The wall zone consisting of microcline perthite, quartz and plagioclase, ii) the intermediate zone of perthite with plagioclase, accessory andalusite and rare-earth minerals, iii) the core entirely of quartz and iv) a replacement zone can occur in some cases. The outer margin of the intermediate zone and the core is where the main concentration in REEs is found.

Complex pegmatites have large and irregular crystal shapes, with the wall zone consisting of quartz, perthite, plagioclase, muscovite and lesser amounts of schorl, biotite, magnetite and garnet. The intermediate zone consists of albite, quartz and muscovite with accessory beryl, spodumene, perthite, apatite, tantalite-columbite and rarely topaz, schorl, triplite, zircon and REEs.

There are various classifications for pegmatites such as those of Hugo (1970), Von Backstrom (1973) and Blignault (1977). Most, however, turn to Cerny's (1991) pegmatite classification. The classification combines the depth of emplacement, metamorphic grade and minor element content. The four main classes are 1) the Abyssal (high grade, high to low pressure), 2) Muscovite (high pressure, lower temperature), 3) Rare-element (low temperature and pressure) and 4) Miarolitic (shallow level). More in depth classification of rare-element classes are based on the compositions. They are divided into the lithium, cesium and tantalum (LCT) enriched and niobium, yttrium and fluorine (NYF) enriched families.

1.2 Hypothesis - The economic viability of the Noumas pegmatite, South Africa

Li-pegmatites have certain features that make them mineralogical and geochemically unique from other pegmatites. They are usually dyke-like, complexly zoned, with an intricate mineralogy of multiple Li- and hydrous- mineral phases, large crystals and are characteristically associated with rare-metal phases (Thomas et al., 1994). Spodumene and petalite are two most important hard rock sources of lithium ore. According to Glover et al. (2012), Li-rich evaporates and their brines are the current global source of lithium. Spodumene and petalite are only found in highly fractionated rare-element pegmatites, associated with the Li-Cs-Ta or LCT family of deposits originating from aluminous (S-type) granites (Cerny et al., 2012). The LCT pegmatite emplacement is controlled at least in part by shear zones (London, 2008).

Several models have been proposed for the formation and genesis of these Li-pegmatites. The main argument is how the large well-formed crystals formed. Was it as a result of supercooling or the presence of volatile concentrations (Thomas et al., 2009). Studies from Fuertes-Fuente, 2000; Raeside, 2003; Ackerman et al., 2007; and Thomas et al., 2009 and the references there in, have attempted to explain the origin of the fluids present within the melts that form the pegmatites and to classify them according to different pressure-temperature variations or tie them to specific conditions of formation using fluid inclusion studies.

The aim of the study was thus to 1) assess the various factors that were involved during the formation of the Noumas I pegmatite 2) the time, influence and origin of fluids and 3) to classify the pegmatite and compare results accordingly.

Several important questions remain:

- What quantity of lithium enrichment within the source rocks was needed to produce the lithium-rich melts that formed the Noumas I pegmatite?

- Is Noumas a simple or complex pegmatite formation?

- Do mineralogical and chemical variations occur within the various zones of the Noumas pegmatite?

- What is the timing of pegmatite formation in relation to the deformation of the surrounding area?

- Do the fluid inclusion properties of the Noumas pegmatite reflect a magmatic or meteoric origin for the fluid?

- What major and trace element distributions are present within the fluid inclusion phases?

- Do any oxidation changes occur within the Noumas I pegmatite?

1.3 Historical perspective and previous studies

The first exploitation of pegmatites in South Africa was in 1900, between Kakamas and Kenhardt on the farm N'Rougas Noord 108. During this time mica was extracted from Straussheim No.1. In the late 1920s the beryllium price and demand increased causing further exploitation of the pegmatites. The government-sponsored exploration programme created a renewed interest in the 1940s while focusing on strategic minerals (Boelema, 1998). Beryl production was steady during the 1950s, until 1959 when the price dive forced diggers to exploit other minerals such as muscovite, spodumene, feldspar and cassiterite.

The first pegmatites to be exploited and mined in 1925, was the Noumas I pegmatite, due to the mineral enrichment of native bismuth (Schutte, 1972). In the 1920s, shortly after mining activities had started, the demand and price of beryl increased drastically. The Namaqualand was investigated by geological surveys that focused on the areas of Steinkopf, Vioolsdrift and Goodhouse during 1935 and 1936.

After the Second World War, the focus of surveys shifted to strategic minerals (tungsten, scheelite) along the western parts of the Orange River. In the mid-1940s the interest in nuclear reactor minerals and material (beryllium, uranium) led to further surveys but this time focused specifically on pegmatites (Von Backstrom, 1969). This was due to their element enrichment of beryllium, lithium and REEs.

Gevers et al., (1937) were the first to give a detailed description of the Namaqualand pegmatites, followed by Von Backstrom (1964) and Hugo (1970). During the 1960s a variety of elements of interest were surveyed; beryllium (Nel, 1965), lithium (Nel, 1965), niobium-tantalum (Von Backstrom and Nel, 1968), and REEs (Von Backstrom, 1969). The mapping of Von Backstrom in 1964 led to the discovery of an extensive pegmatite belt located along the Orange River.

The work done by Hugo (1970) on the two different types of heterogeneous pegmatites, gives a better understanding of their distribution along the Orange River in the Upington area of the Northern Cape. Simple heterogeneous pegmatites normally don't show a huge difference in appearance, composition and internal structure. They are limited in both shape and size. Complex heterogeneous pegmatites are large irregular bodies. They are believed to have formed during an advanced stage of magmatic processes. This caused the enrichment of incompatible elements with lower temperature and pressures. Beukes (1967 & 1973) thoroughly investigated minerals and the distribution of REEs in the Gordonia-Kenhardt area. His research places a constraint on the distribution of REEs within a pegmatite host, to the intermediate perthite zones of complex heterogeneous pegmatites.

1.4 Granite related deposits

The Strong (1988) model is used for mineral deposits genetically associated with granitoid rocks. Two types of granite-related deposits exist namely, 1) typically associated with peraluminous mica granites and 2) less abundantly with metaluminous to peralkaline suites. Peraluminous granites are high Na, K and low Ca granites. Ore minerals are zoned and chalcophile elements occur furthest from the intrusive contact. The distribution of granite-related deposits are found in virtually every tectonic setting and age, this includes stable Precambrian cratons of the Bushveld, Mesozoic extensional environments in Nigeria and Cenozoic subduction zones in South America (Robb, 2005).

The minerals within these deposits tend to concentrate towards the pluton contact zones, as cupolas, stocks, disseminations, pegmatites and veins. Four main granite-related mineral deposit types reflect the stages of progressive decrease in temperature and pressure. These consist of magmatic disseminations, pegmatites, porphyries and veins (Strong, 1988) with magmatic, pegmatitic, pneumatolitic and hydrothermal stages. Stages are explained as the function of crystallization where fracturing and escape of fluid occurs. Early fracturing results in

pegmatite deposits, late fracturing produces hydrothermal deposits and no fracturing would result in disseminations (Strong, 1988).

The formation of granitic rocks can occur by crystallization and differentiation of less silicic magmas or partial melting of different source rocks, with temperature and water pressure as the two most important controlling variables. When aqueous fluids coexist with silicate melts, the behavior of the elements is governed by fluid-melt partitioning. Compounds such as HCl, CO_2 and NH_3 may cause the melting temperatures of granitic liquids to rise, while H_2O, P_2O_5, HF, B_2O_3 and LiO_2 will have the opposite effect, namely the lowering the melting temperature. The effects that the different compounds have on the melting temperature for granitic compositions are shown in Figure 1-3.

Strong (1980) subdivides the granophile elements into three groups, namely the large highly charged cations Sn^{4+}, W^{6+}, U^{4+}, Mo^{6+}, the small variably charged cations Be^{2+}, B^{3+}, Li^+ and P^{5+} and lastly the anions or anionic complexes CO_3^{2-}, Cl^-, F^-. These are respectively recalled SWUM, BEBLIP and CCF. The BEBLIP groups are also associated with Na, Rb, Cs and REE's. The BEBLIP groups play a critical role in controlling the genesis of magmas and subsequent solidification behavior.
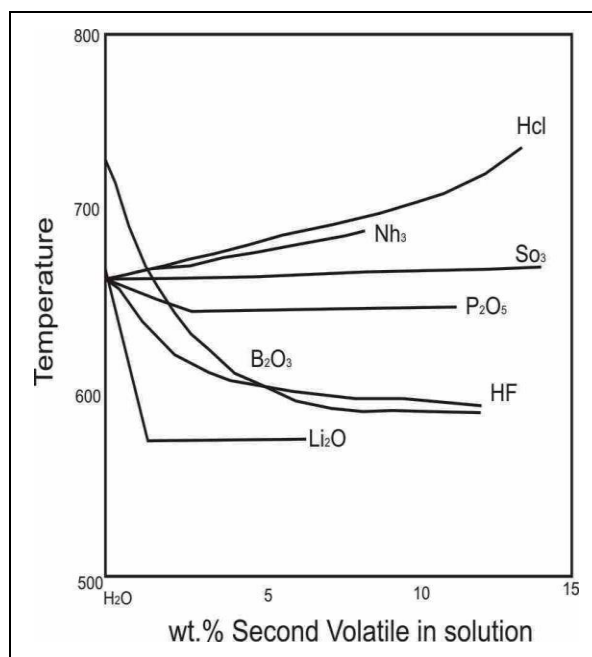
Figure 1-3: The effects different components have on the melting temperature of a granitic composition (Strong, 1988).

The effects of these components on the temperature are reflected by the fluid-melt partitioning of the elements, increasing from Li_2O to HCl. Experimental studies by Stewart (1978) showed the effect that Li has on lowering the melting temperatures in granites and at the same time, promotes extreme differentiation of Li-bearing melts. According to Figure 1-3 Li or B concentrate in late stage residual melts. An element such as B increases the solubility of water in melts. Fluorine has the opposite effect by lowering the solubility of water in melts. This would explain the exsolution that occurs earlier in fluorine-rich melts. The zonation patterns present within pegmatite deposits are mainly controlled by differing temperatures during deposition.

Transport and deposition of litho- and chalcophile elements, within a deposit, is a complex process and depends on several factors such as the concentration of metals, the Cl and S content in the aqueous fluid, and temperature and pressure. This produces differing conditions of deposition and complex mineral assemblages. The different patterns of paragenesis and zonation can be related to differing metal solubility's, which reflect the temperature variations related to temporal and spatial characteristics of the cooling pluton.

For pegmatite deposits to form the lithophile elements (Li, Be, F, Nb, Ta, B) that are readily partitioned into aqueous fluids must first be retained by silicate melts, through extreme differentiation to concentrate these elements in the brine. The typical minerals that these elements partition into include spodumene, lepidolite, beryl, fluorite, columbite-tantalite, ilmenite and tourmaline.

The metal tenor of granite-related mineral deposits depends on whether the elements of interest were dispersed or concentrated during crystallization or partial melting producing pegmatites that form from a magmatic concentration process, during cooling of the water-saturated melt, when the elements are preferentially partitioned into the aqueous phase. In the case of a water-undersaturated magma, the elements are preferentially partitioned into the silicate melt requiring extreme degrees of fractionation to produce economic concentrations.

1.5 Pegmatite formation model

The general consensus opinion for pegmatite genesis is that these form by means of primary crystallization from a volatile-rich, siliceous melt (Jahns and Burnham, 1969; Cerny 1991; London, 1990). The melts of rare element pegmatites are related to highly differentiated granitic magmas and represent strongly fractionated residual melts in terms of silica, alumina, alkali

elements, water, lithophile elements and rare metals. Cerny (1991) suggested that the lithology of the source rocks for melts is a major control on the ultimate composition of the formed rare element pegmatite. Undepleted upper crustal lithologies thus result in peraluminous granites that give rise to pegmatites enriched in Li, Cs and Ta.

During the cooling of magma the partially solidified rock becomes unstable and can fracture. A pegmatite is formed when the remaining molten material is forced into the fracture. Pegmatites are thus formed as part of the cooling and crystallization process of intrusive rocks. The progressive cooling of the parental magma results in a sequential crystallization process that concentrates volatile constituents such as B, F, H_2O and P in the residual magma (Sinclair, 1996). The presence of residual water within a magma produces favourable conditions for the magma to cool slowly enough to allow coarse crystal growth for a simple pegmatite. More complex pegmatite results from numerous striking volatiles that are eventually incorporated into rare minerals (Sinclair, 1996).

As the melt forming pegmatite raises towards the surface, the pressure imposed on the magma by the surrounding rocks decreased (Figure 1-47). The decrease in pressure causes the amount of H_2O and CO_2 that can dissolve in the melt, to also decrease (Philpotts and Ague, 2009). This process is known as first boiling and will exsolve the dissolved gases from the melt as the decrease in pressure continues (Robb, 2005), at A in Figure 1-4. Second boiling will occur as soon as the mineral-forming constituents are removed from the melt (Robb, 2005), at B in Figure 1-4.

Concentric mineral zones are produced during inward pegmatite crystallization. The zones are enriched in rare elements. During this crystallization the progressive evolution of a coexisting supercritical aqueous phase assists the growth of large crystals and helps to concentrate elements not easily incorporated in silicate minerals (Sinclair, 1996). At various stages of pegmatite formation the aqueous phase can react with earlier formed minerals to produce metasomatic zones. These metasomatic zones are enriched in lithophile elements and rare metals.
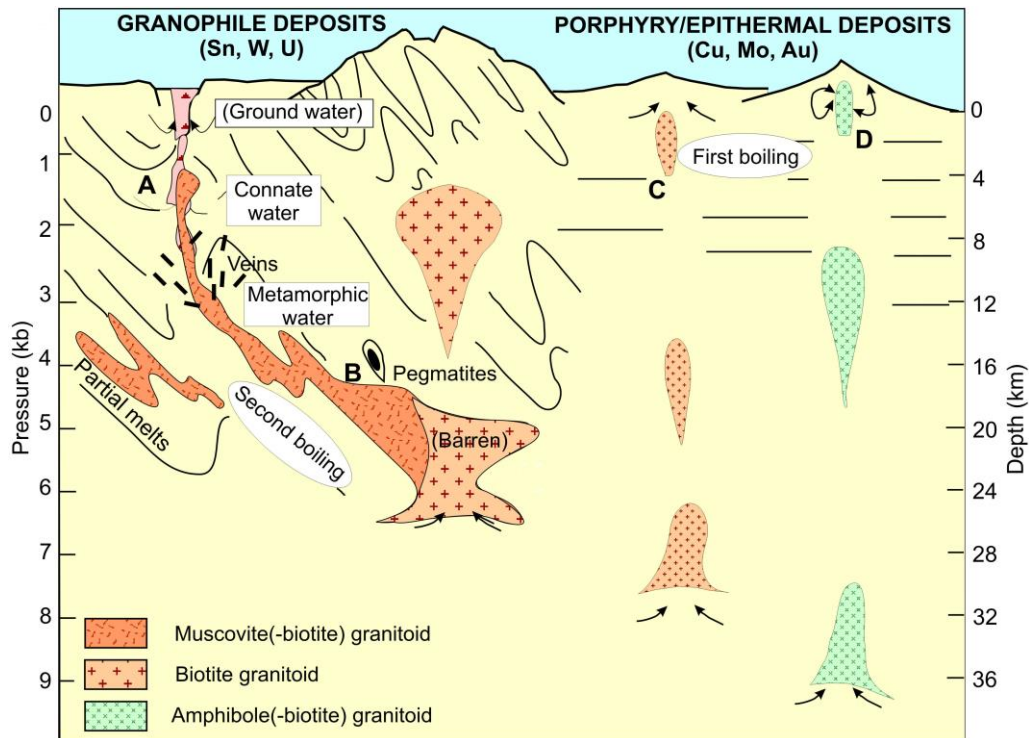
Figure 1-4: Schematic illustration of the emplacement style and metallogenic character of granites (Strong 1999)

1.6 Objectives of investigation

The paper focuses primarily on the following:

1. Qualitative and quantitative characterization of the pegmatite mineral assemblage at the Noumas I pegmatite;

2. Investigate the physico-chemical properties of the fluids involved in ore formation (fluid inclusions);

3. Interpretation of the mineralization history or paragenetic scheme of events during pegmatite or fluid evolution.

Chapter 2: GEOLOGICAL SETTING

The study area consisted of 1) partly mineralized pegmatites intruded into granodiorites of the Vioolsdrift Suite and 2) leucocratic alkali-granites of the same suite, which were intruding barren pegmatites. The Noumas I pegmatite is situated ± 15km south of Vioolsdrift. This is the largest known mineralized pegmatite belt in Namaqualand. It was mined for feldspar and bismuth but also contains beryl and tantalite/columbite (Minaar and Theart, 2006). The minerals commonly occur with quartz.

The Noumas I pegmatite varies from fine to coarse grained leucogranite in composition and is found in a granodioritic host rock. The granodiorite is hosted within the Steinkopf terrain. The pegmatites in the surrounding area are found within the Gaarseep gneiss (medium-grained, mesocratic hornblende gneiss). The study area falls within the Namaqua-Natal metamorphic province (NNMP) as part of the Namaqua mobile belt (NMB).

2.1 Regional Geology

The NMB forms part of the Mesoproterozoic system of mobile belts, see Figure 2-1. The NMB is the result of the overlapping of crustal fragments with the southwestern margin of the Kaapvaal craton. The belt is contained on its southern margin by the Southern Cape Conductive Belt (SCCB) and further south the Cape Fold Belt (CFB). The main periods of igneous activity in the area is dated at ±1700-2000 Ma and 1000-1200 Ma (Blignault et al., 1983). The NMB underwent folding and metamorphism ±1000-1200 Ma ago (Figure 2-1) and left an interrelation between magmatic and deformation processes in the central part of the belt (Blignault et al., 1983). The Namaqua tectogenesis is prominently seen in the south-west of the Namaqua front as high-grade metamorphism, a thermal event and magmatism (Blignault et al., 1983). The Namaqua front is interpreted by Blignault et al., (1983) as a major zone of movement. It is a shear system of continental proportions with the later part of the movement postdating the main Namaqua tectogenesis.
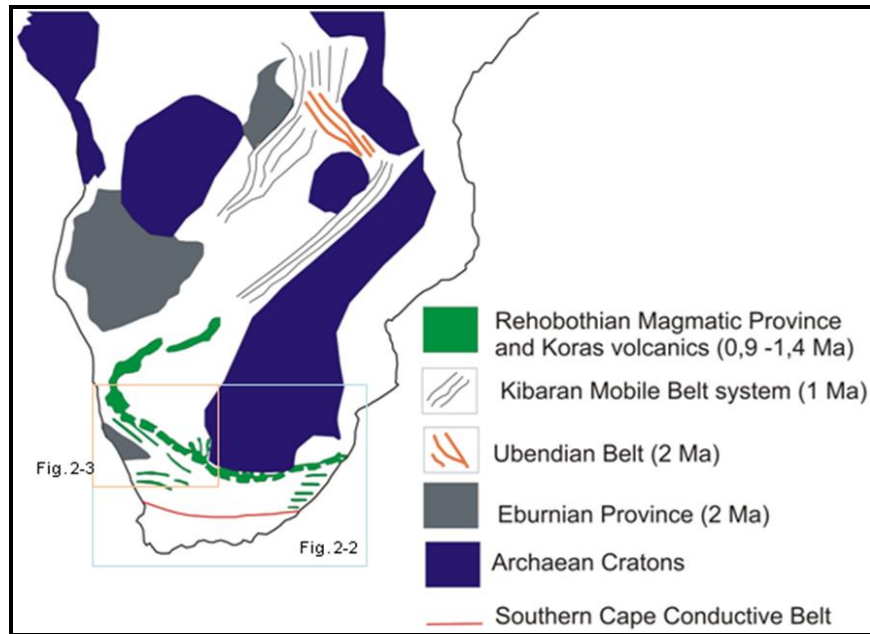
Figure 2-5: The distribution of Archean and Proterozoic tectonic provinces on a map of Southern and central Africa (after Blignault et al., 1983).

The Namaqua-Natal metamorphic province (NNMP) formed in the Mokolian era, Proterozoic Eon, ±1000-1800 Ma ago, during the collision of the Congo- and Kaapvaal-Zimbabwe cratons (Figure 2-2). This resulted in high grade metamorphic NMB, wrapping around the western and southern parts of the Kaapvaal craton (McCarthy and Rubidge, 2005).
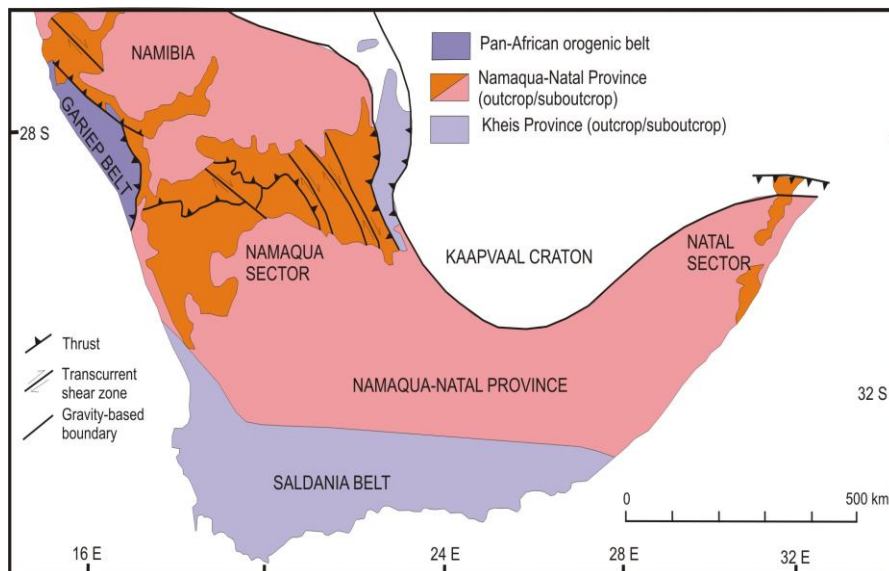
Figure 2-6: Geological setting of the Namaqua-Natal Province (after Cornell et al., 2006).

The NNMP can be subdivided into tectonostratigraphic subprovinces and terranes based on changes in lithostratigraphy. These domains (Figure 2-3) are 1) the Richtersveld Subprovince (~2000 Ma low- to medium-grade supracrustal rocks), 2) the Bushmanland Terrane (~2000 Ma granitic gneisses, 1600 to 1200Ma amphibolites to granulite grade supracrustal rocks, 1200 Ma to 1000 Ma granitoids), 3) the Kakamas Terrane (possibly ~2000 Ma supracrustal metapelite, Namaquan granitoids), 4) the Areachap Terrane (juvenile ~1300Ma arc-related supracrustal rocks, 1000 Ma granitoids) and 5) the Kaaien Terrane (Kheisian metaquartzites) (Cornell et al., 2006). The study area falls within the Bushmanland terrane.

The Bushmanland group consists of a mixture of Paleoproterozoic island arcs and ocean floor sediments, which were deformed and metamorphosed during the craton collision (McCarthy and Rubidge, 2005). The main deformation event and the peak prograde metamorphism to amphibolite grade are closely associated, with temperatures of 650-700ºC and pressures of 3.5-4.5 kbar. The timing of this event is 1171±31 Ma (Dewey et al., 2006). During a Kibaran crustal shortening and thickening (1199 - 1175 Ma) major recumbent folds developed (Dewey et al., 2006). Sheets of mesocratic and leucocratic granite gneiss were injected along the folds and weak zones.

The Bushmanland can stratigraphically and geochronologically be divided into three distinct age groups namely the basement granitic rocks of 1700-2050 Ma, mixed supracrustal sequences of sediments and volcanics around 1200, 1600 and 1900 Ma and lastly intrusive bodies emplaced during late and post-formational stages at about 1200 Ma (Cornell et al., 2006). The terrane is divided by shear zones, into smaller terranes with different lithological units. The sub terranes include Aggenys, Gariep, Granau, Okiep, Poffadder and Steinkopf. The Noumas I pegmatite is situated in the Steinkopf terranne of the Bushmanland Group, see Figure 2-4.

The Steinkopf terrain is bound on its eastern margin by the Groothoek thrust of the Gezelschap Bank area, the Richtersveld domain (Figure 2-3) to the north and by the Skelmfontein thrust/shear of the Okiep region to the south. The overprinting of the Dabbiknik structures, due to the open folding of the Ratelpoort shearing, led to the complex outcrop pattern of the regional foliation in the Steinkopf area (Van der Merwe, 1986).

The Bushmanland Group of sedimentary rocks was deposited during the Kibaran event 1100 Ma. The rocks were intensely folded and metamorphosed by the intrusion of granites (McCarthy and Rubidge, 2005). Alluvium, tertiary and quaternary sediments cover the majority of the area.
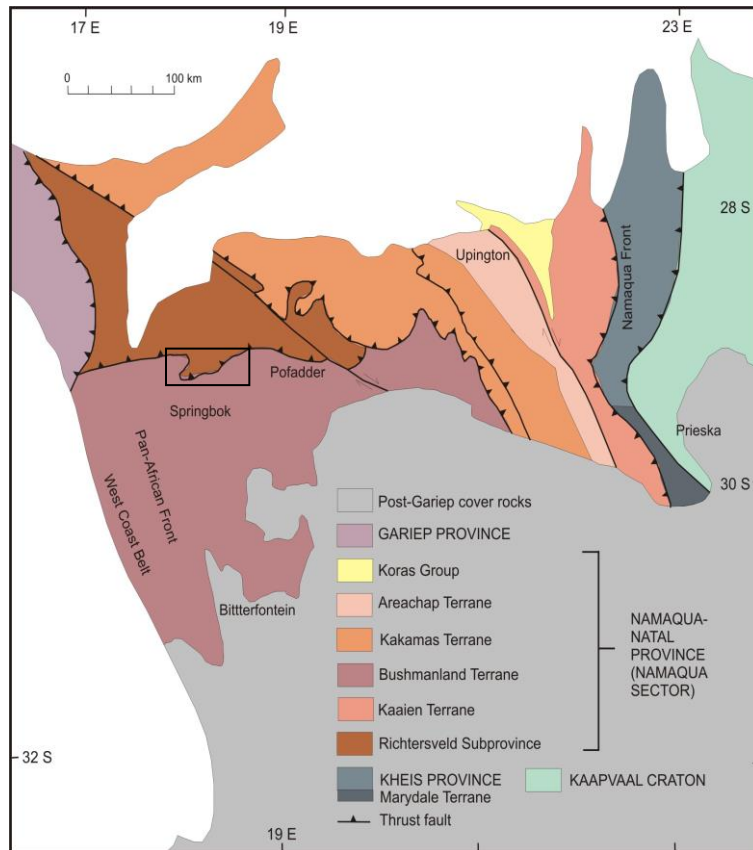
Figure 2-7: Tectonic subdivision of the Namaqua sector (Cornell et al., 2006).
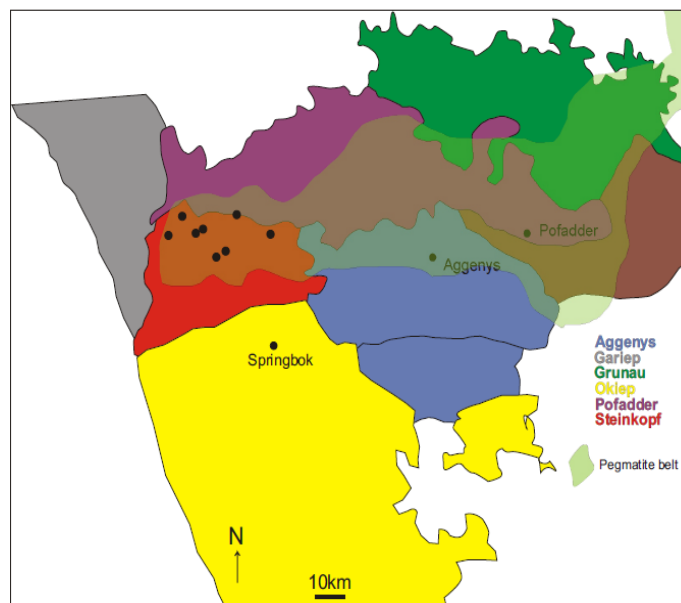
Figure 2-8: Tectono-stratigraphic terranes of the western part of the Namaqua mobile belt (Collinston and Schoch, 2002; Thomas et al., 1994 and Minnaar and Theart, 2006). The black dots represent the lithium-bearing pegmatite distribution along the pegmatite belt and in the various terrains.

2.2 Steinkopf Terrain

The Steinkopf terrain (Figure 2-4) comprises mainly Kheisian age metamorphic rocks of the Gladkop and Bushmanland groups (2050–1700 Ma). The terrane is divided almost vertically by the occurrence of a north, north-east trending grabens; formed by the down-thrusting of a central region bound by two major sets of faults. This terrain contains the majority of the north-east trending dykes in the region as well as many of the faults. Among those, the Steinkopf fault is the dominant fault in the area (Van der Merwe, 1986). The graben has been filled with younger Nama sedimentary rocks. The fault occurrence is the youngest deformation phase in the region as all structures, shear zones, folds and all bedding have all been displaced by the faulting. The intruding Noumas I pegmatite appears to have been unaffected by the fault and is suspected to have used the faults and fractures as pathways for the crystallizing material.

Van der Merwe (1986) divided the structural development of this area into two main structural groups. 1) An older group of sub-horizontal structures formed by the Gladkop and earlier Namaqua deformation and 2) a later sub-vertical set of structures formed due to thrusting in the area. The Noumas I pegmatite intruded after the deformation events and can be regarded, based on the rheology in the surrounding country rocks, as the more recent event to have occurred in this area.

2.3 Local Geology and Mineralogy

The pegmatites located in the region of the study area, consists mainly of plagioclase, K-feldspar, quartz, biotite and varying amounts of chlorite and epidote. Hornblende alteration products are seen in the weathered granodiorite (Vioolsdrift Suite) country rock (Minnaar and Theart, 2006).

The Noumas I pegmatite is found within the Vioolsdrift suite granodiorite (Figure 2-5). The distribution of the pegmatites varies in shape and size. Irregular pegmatite bodies are typically large with dykes and smaller veins. The continuity of the pegmatite body in depth is connected to the dimensions, the strike and the outline of the pegmatite bodies. The intruding body is thus limited not only by the space available but also by the size of the joints and fractures it intruded along.
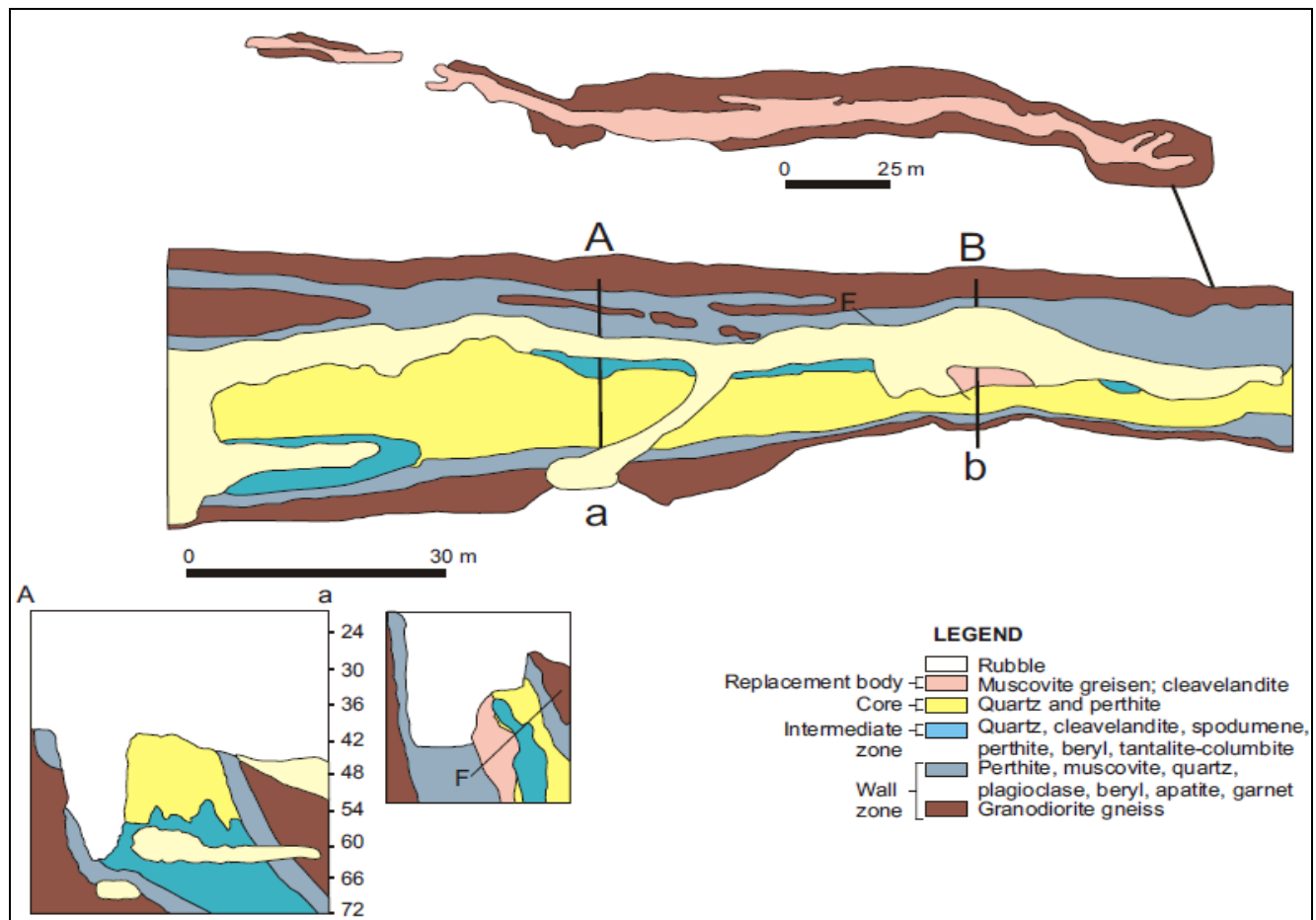
Figure 2-9: The geology of the Noumas I pegmatite as seen from the top view (Schutte, 1972). Cross-sections A-a and B-b are included at the bottom left.

The Noumas I pegmatites are more resistant to weathering than the wall rocks they are situated in and form ridges. Low angle dipping pegmatite bodies and most northwest striking bodies that are discordantly emplaced have large surface exposures (Minnaar and Theart, 2006). They also strike parallel to the country rock foliation. The rheology of the country rocks controlled the behavior of the pegmatite during intrusion. The different pegmatite zones identified in the Noumas I pegmatite include border, wall, intermediate and core (Table 2-1).

Although not evenly distributed, homogeneous and heterogeneous pegmatites are recognized in the pegmatite belt. Homogeneous simple pegmatites consist of aggregates of quartz, feldspar and accessory minerals, and are typically found in groups or swarms with no economically important minerals. Heterogeneous pegmatites usually have a systematic arrangement of constituents and zones that varies in mineralogy and texture (Hugo, 1970).

The mode of emplacement for the Noumas pegmatite dykes are ascribed to fluid emplacement (Minnaar and Theart, 2006). The lenticular dyke- and vein-like shapes of the pegmatites seem to have been injected into pre-existing tensional openings. Lenticular bodies appear to have been both passively and forcefully injected (Minnaar and Theart, 2006).

Table 2-1 Mineral zonation found within the Noumas I and II pegmatites. These patterns correlate with the rare-element classification of Ginsburg (1960) (Minnaar and Theart 2006).

Pegmatite	Zonation	Dimensions (outcrop) Wall rock (m)	Comments
Noumas I	**Border zone**: microcline, plagioclase, qtz, muscovite, [garnet] **Wall zone**: muscovite, qtz, plagioclase, microcline-perthite, [beryl, bismuth minerals, apatite, triplite, garnet] sugary albite assemblage: resembles chilled border zone. albite, qtz, garnet, apatite, microcline **First intermediate (capping) zone**: graphic pegmatite, [beryl, tantalite-columbite] **Second intermediate (spodumene) zone**: spodumene, albite (cleavelandite), qtz, [micro-perthite, beryl, tantalite-columbite] **Core**: milky qtz, microcline-perthite **Undifferentiated pegmatite**: cleavelandite, qtz, [microcline, muscovite, spodumene, beryl, tantalite-columbite] **Replacement bodies**: muscovite, cleavelandite, [micro-perthite, tantalite-columbite, microcline, thorite, orangite, gummite]	1000x25 Granodiorite	Mined for beryl, bismuth, tantalite-columbite, spodumene, feldspar and mica
Noumas II	**Wall zone**: qtz, albite (cleavelandite), microcline-perthite, muscovite, [beryl, bismuth minerals, tantalite-columbite] **Core**: qtz, microcline-perthite **Replacement bodies**: muscovite greisens	250x15 Granodiorite	

2.4 Mining-Economic significance

The Noumas I pegmatite measures roughly 1000x140x25m (Minaar and Theart, 2006) making it the largest zoned pegmatite to the west of the pegmatite belt. Compared to other giant zoned Greenbushes pegmatite in Australia (3300x500x400m) and Tanco in Manitoba (1650x800x125m) the Noumas' reserves are small and it would not be viable to apply mechanized mining operations.

Until the 1960s, beryl, bismuth and tantalite-columbite were the main products extracted from Noumas I. Due to high transport costs of the lower-priced minerals such as spodumene, feldspar and muscovite those could not be profitably marketed. Difficulties such as remoteness, decreasing market and decline in demand caused the production from the Noumas I pegmatite to end mining production in the late 1970s. Extensive mining has left the mineral enriched Noumas I pegmatite as open quarries that reveal the regular and somewhat asymmetrical zonal structure of the body (Table 2-2).

Table 2-2 Definition of the different zones located and noted at the Noumas I pegmatite (Schutte, 1972). qtz = quartz, musc=muscovite

a)	**Border zone**	Fine-grained border zone. 1 and 15cm wide on both foot and hanging-wall contacts. Microcline, plagioclase, qtz, musc and accessory garnet
b)	**Wall zone**	Present on both foot and hanging-wall and varies in thickness 1 to >6m. Musc, qtz, plagioclase, microcline-perthite accessory beryl, bismuth minerals, apatite, triplite and garnet. Musc books ±75 cm in site concentrated along contact with the border zone. Mica production averages 100 tonnes per month from the hanging-wall
c)	**Sugary albite assemblage**	Fine-grained material near the contacts resembling a chilled border zone. But it's not confined to contacts. Also occurs as irregular bodies and lenses towards the centre of the pegmatite. Albite is the dominant mineral with qtz, garnet, apatite and accessory microcline in places. Garnet and apatite concentrated in layers parallel to contacts and appear banded. Material is closely associated with wall zone and may represent an earlier variety of it.
d)	**First intermediate (capping) zone**	The capping zone is confined to higher SE part of the pegmatite where it caps the other zones. Graphically intergrown qtz and feldspar. Capping zone grades downwards into underlying zones. Beryl and tantalite-columbite occur sparingly in capped zoned.
e)	**Second intermediate (spodumene) zone**	Intermediate zone between 6 and 8cm wide consists of spodumene, albite, qtz and accessory micro-perthite, beryl and tantalite-columbite. Between wall and the core zone. Developed on the footwall side of the pegmatite and dips at an angle 30° underneath core. Mined for spodumene, beryl and tantalite-columbite by a wide stope approximately 70m long.
f)	**Core**	Consists of anhedral milky white qtz and large subhedral crystals of microcline-perthite.
g)	**Undifferentiated pegmatite**	Wall zones gradually merge with spodumene zone to form relatively homogeneous pegmatite with no clearly defined structural and lithological units. Abundant albite and qtz with additional microcline, musc, altered spodumene, beryl and tantalite-columbite also present. Little mining has been carried out in this part due to scarce development.
h)	**Replacement bodies**	Replacement bodies consist of fine muscovite, albite accessory microcline-perthite, tantalite-columbite, microcline, thorite, orangite and gummite scattered along contact of footwall between wall and spodumene zone.

2.5 Source of Pegmatites

The origin of the magma, forming and enriching the pegmatite in incompatible elements, has been widely debated over the last 100 years. From this the various processes have been assigned to the formation. Geochronological studies on both the Namaqualand and Bushmanland Terranes indicated an episodic history in the Mesoproterozoic crustal development (Dewey et al., 2006). A major pulse of magmatism accompanied the Namaqua event sequence around 1060 and 1030Ma, with granite sheets intruding during this time interval. Hugo (1970) described the granites in this complex to be of magmatic origin, as well as reconstituted sedimentary and granitoid rocks. Until thus far there is no satisfactory explanation for the genetic relationship of the pegmatites occurring in the pegmatite belt of the area. The pegmatites cannot be related to any intrusive body in the area as discussed by Gevers et al., (1937) and Sohnge and De Villiers (1946).

The pegmatites are mainly developed in the granodiorite of the Vioolsdrift Suite, dated at around 1900Ma for mafic members and 1730Ma for felsic members (Minnaar and Theart, 2006). Two phases of pegmatite intrusion in the pegmatite belt are determined, an older phase at 1000Ma associated with the closing stages of the Namaqua orogeny and a younger phase at 950 Ma related to the intrusion of granitoid bodies (Beukes, 1967; Hugo, 1970). Such a close association between the pegmatites with the granitoids of the Vioolsdrif Suite suggests that the granitoids acted as the parent magmas.

The Namaqua orogeny is dated at 1200Ma and the termination of it around 1100Ma, during which easterly trending shear zones formed (Colliston and Schoch, 2002). This suggests the pegmatite formed after the termination of the Namaqua orogeny. If the formation is associated with the closing stages of the Namaqua orogeny around 1000 Ma, then the development occurred simultaneous with the shear zones. The easterly trending shear zones correlate with the northwest striking pegmatites, indicating that the pegmatite formed prior to 1000 Ma.

Chapter 3: DETAILED FIELD OBSERVATIONS

In the vicinity of the Noumas I pegmatite the pegmatite bodies cut across the fabric in the somewhat folded country rock which also is draped around the shape of the intrusion. The shape of the pegmatite bodies are reflected in the outlines of the hills. A vertical zonation was observed at the Noumas I pegmatite along with an almost vertical dip of 85°. The Noumas I pegmatite was systematically sampled along the strike of the pegmatite and in the width.

3.1 Mapping and Sampling

The sampling in the area between Steinkopf and Vioolsdrift delivered 40 samples that were hand specimens obtained from heap dumps. The samples were pre-sorted and located not far from the original pegmatite (Appendix 1). Due to the particular zoning of the pegmatite the non-in-situ material could be linked to mineralogical zones. Minerals such as spodumene had been removed from the pegmatite and were only enriched in the intermediate zone within the Noumas I pegmatite. A number of pegmatites were found, traced and sampled around the area, see Figure 2-4.

The only intensely mineralized pegmatite, Noumas I is described in this study. The narrow, dike-like, NW striking intrusion showed a vertical zonation. The pegmatite intrusion occurred post-deformation, as evidenced by the cross-cutting foliated host rock (Figure 3-1). This suggested a formation age younger than approximately 1Ga, after the metamorphic event in the area.
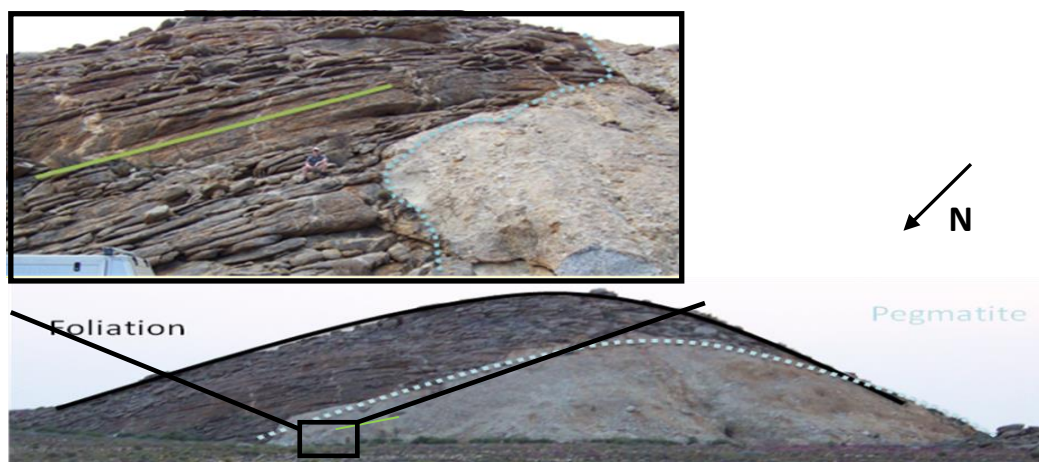
Figure 3-10: Intruding pegmatitic dike through country rock. Inserted photo shows the foliation visible from the folded host. The sharp contact between the host and intruding pegmatite.

The Noumas I pegmatite, documented during the sampling campaign, stretches ±350m long and ±25m wide. It has a NW strike. Pegmatites in the immediate area cross-cut the foliation of their host rocks (Figure 3-1), and follow the layering within the host rock, producing the same shape as the folded host rock. This suggests that the pegmatite body formed after the granodiorite, and is thus younger than the host.

The zonation within the pegmatite is in the vertical (Figure 3-2). There is also a border zone (grey) around the wall zone consisting of quartz, feldspar, garnet and mica. The zone is a few centimeters thick and has fine grained minerals of quartz, plagioclase, muscovite and feldspar distributed within it. Large spodumene crystals (±50cm) are distributed along with lepidolite in the middle of the Noumas I pegmatite.

Systematic sampling took place along the strike of the pegmatite (Figure 3-3) in intervals of 20 meters in length and 3 meters across. The sampling showed the chemical differences of the material within the zones. The majority of the pegmatite material had been removed towards the north-eastern part of the pegmatite. The samples from the small sections that were left on the sides of the host rock consisted mainly of coarse grained quartz and feldspar with large mica crystals. The Noumas I pegmatite thinned out towards the NE and thickened towards the SW.
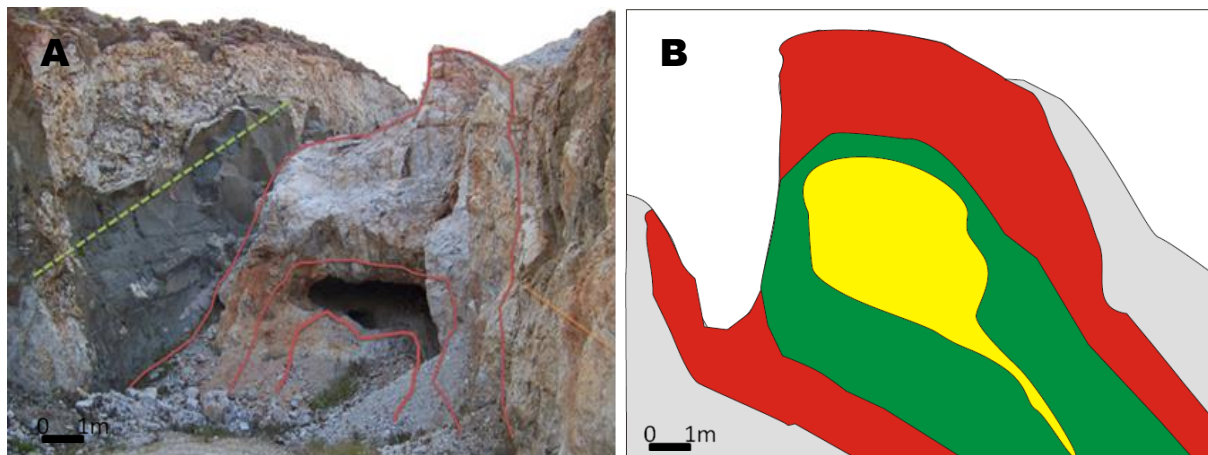
Figure 3-11: A) The mined Noumas I pegmatite, within the granodioritic host (green line). B) Illustration of the observed zones from the Noumas I pegmatite showing the border (grey), wall (red), intermediate (green) and core (yellow) zones.

Figure 3-12: A satellite image of the Noumas I pegmatite with inserted photos (a-d) that show sample sites along the strike of the pegmatite. a) Remnant mineralization clear, b) quarter of the Noumas I pegmatite, c) middle of the pegmatite, d) gradually thinning towards the NE (Google image, 2011).

Xenoliths of a coarser, almost hornblendite-like appearance are present in the granodioritic host rock, see Figure 3-4. The vertical zonation (wall, intermediate and core) was visible on a macroscopic scale, with clearly distinguishable mineralogy. The core zone has been removed (Figure 3-2) but remnants of beryl crystals are found in the intermediate zone with mica, spodumene and intergrown quartz and feldspar crystals (Figure 3-5). The study of the different zones present at the Noumas I pegmatite revealed an intrusive body that pinched towards the top. This places the Noumas I pegmatite at a post-metamorphic and deformation where the intrusions' shape followed that of the folds within the host rock.
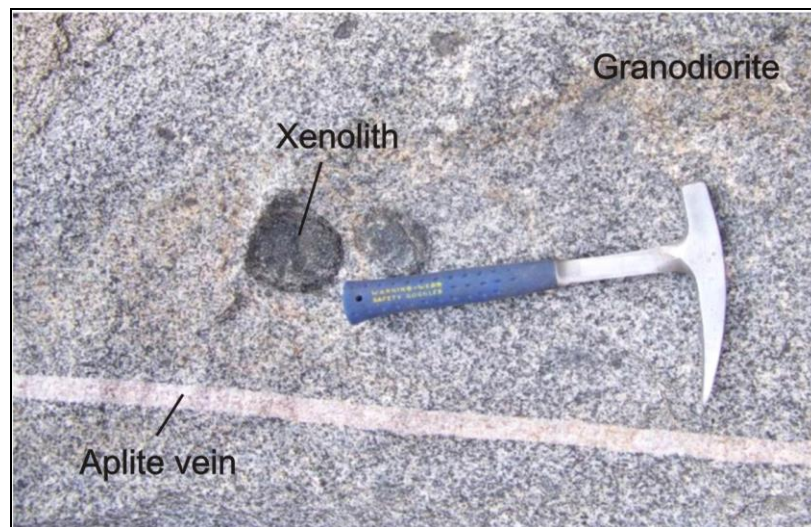
Figure 3-13: Granodiorite host rock with aplite vein and xenolith located on the south western limb.
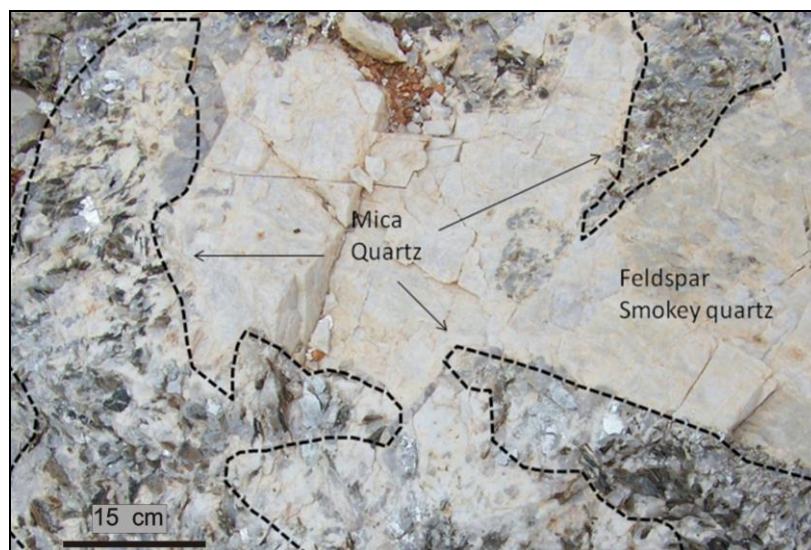
Figure 3-14: The mineral distribution and intergrowths found from the wall zone of the Noumas I pegmatite.

3.2 Overall Physical Appearance of Noumas I pegmatite

The pegmatite consists of quartz, feldspar, muscovite, spodumene, lepidolite, beryl, garnet and plagioclase. Mining has completely removed the economic mineralization. There are remnants of the different minerals present in some of the zones, such as large spodumene crystals surrounded by mica. The Noumas I pegmatite consists of a border that is a few cm wide, wall, intermediate and core zone. There are minerals such as quartz and mica that are found over the entire pegmatite and minerals that seem to concentrate in specific areas such as spodumene in the intermediate and tourmaline in the wall zone. The observations of the various zones are described in Table 3-1, with their macroscopic differences.

Table 3-3: Characterization of the various zones based on the macroscopic properties of the pegmatite. Qtz-quartz, Fspr-feldspar, spd-spodumene, lep-lepidolite, musc-muscovite.

	Wall zone	Intermediate zone	Core zone
Mineralization	Qtz, beryl, garnet, mica	Qtz, fspr, spd, lep, mica	Qtz, fspr, beryl, garnet, mica
Size	± 1-12m	± 1-10m	± 1-4m
Comments	Qtz of zone appears to be entirely qtz with musc On the border with the granodioritic host the garnets and musc is large relative to the other minerals.	Remnants of beryl still left on the border walls of the mined core. Intergrown qtz and spd Symplectically intergrown textures between qtz and spd.	Not visible Not visible, only material directly underneath the upward pinched intrusion.

The Li-pyroxene, spodumene, was found as massive crystals within the intermediate zone. In some areas within the intermediate zone these spodumene crystals have started to alter to the respective clay mineral weathering products. The alteration is due to surface weathering under humid climate conditions. The green (hiddenite), pink and purple (kunzite) varieties of spodumene are found at the Noumas I pegmatite.

Macroscopically the size of crystals for garnet and muscovite change within the pegmatite from the core to the wall zones (smaller crystals found closest to the granodioritic host). The areas in direct contact with the granodioritic host have mica and garnets distributed throughout them. The opposite applies for intergrown quartz and feldspar with massive sizes (Figure 3-6A). Small pockets of tourmaline (Figure 3-6B) occur, in between pure quartz and muscovite layers, within

the wall zone of the Noumas I pegmatite. Beryl embedded within quartz was found in the wall and core zones (Figure 3-6B). Li-mica (lepidolite) from the intermediate zone is present in banded sections (Figure 3-6C). The large spodumene crystals are surrounded and outlined by mica crystals (Figure 3-6D).
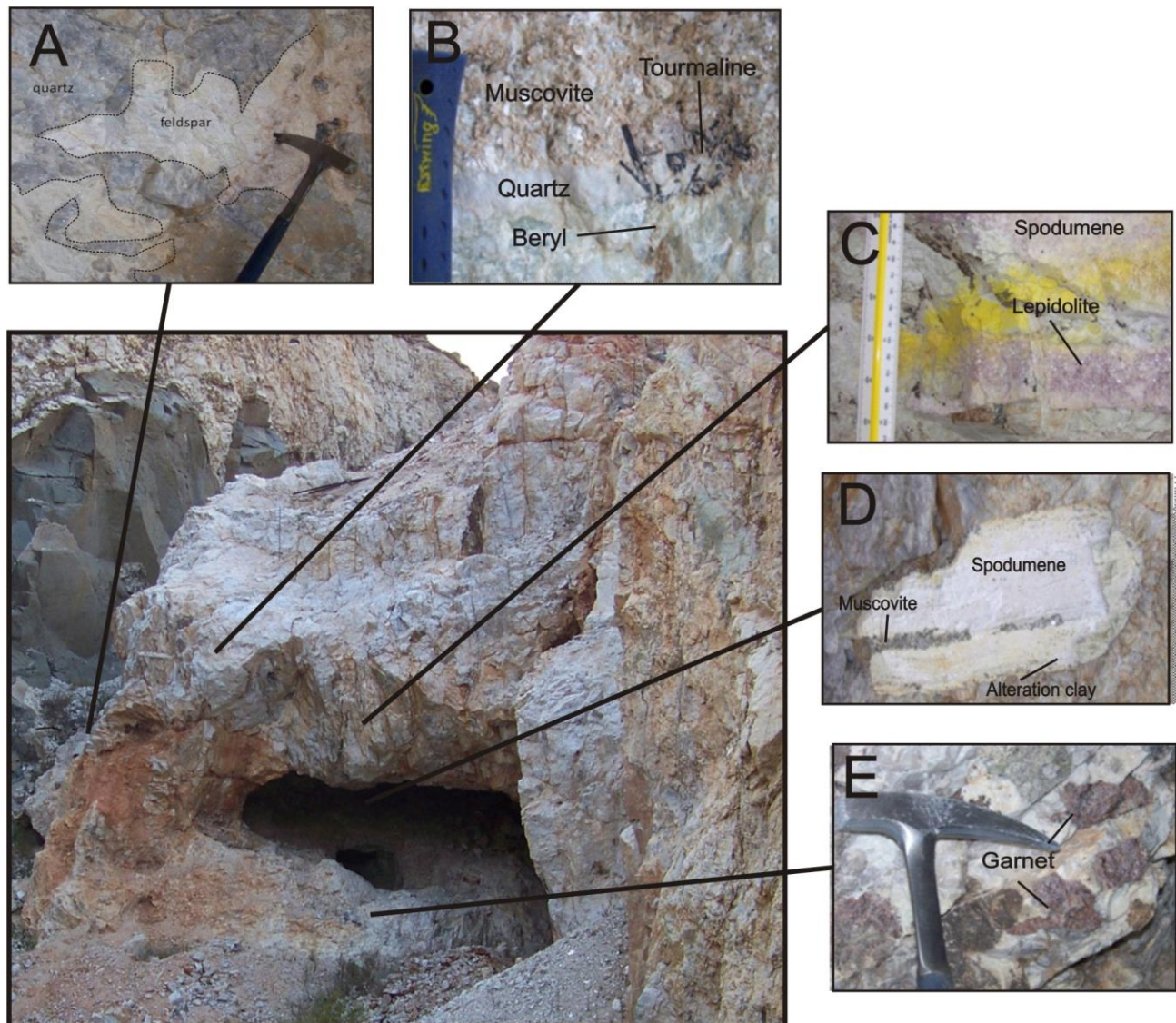
Figure 3-15: The Noumas I pegmatite: a) wall zone with intergrown quartz and feldspar, b) wall zone with tourmaline pockets, intergrown quartz and muscovite and beryl crystals, c) lepidolite bands in the intermediate zone along with quartz and spodumene crystals, d) large spodumene within the intermediate zone surrounded by small muscovite crystals, alteration to clay at the bottom, e) large red variety garnet at the core zone.

The veins (Figure 3-7) found in the host (granodiorite) rocks consist of quartz. The veins are perpendicularly orientated to the intruded pegmatite and parallel to the contact. The veins cut

through fractures and joints in the granodiorite. This suggests that the Noumas I pegmatite formed after the metamorphism as it assumes the shape of the intruding host that has been folded after the metamorphic event.

The fine-to medium crystalline granodiorite host rock consists of the minerals quartz, plagioclase, feldspar, hornblende and amphibole/biotite. The small crystal size may indicate a fast cooling rate and a shallow intrusion depth. The pegmatite mineralogy in direct contact with the granodiorite host consists of muscovite and garnets (Figure 3-7).
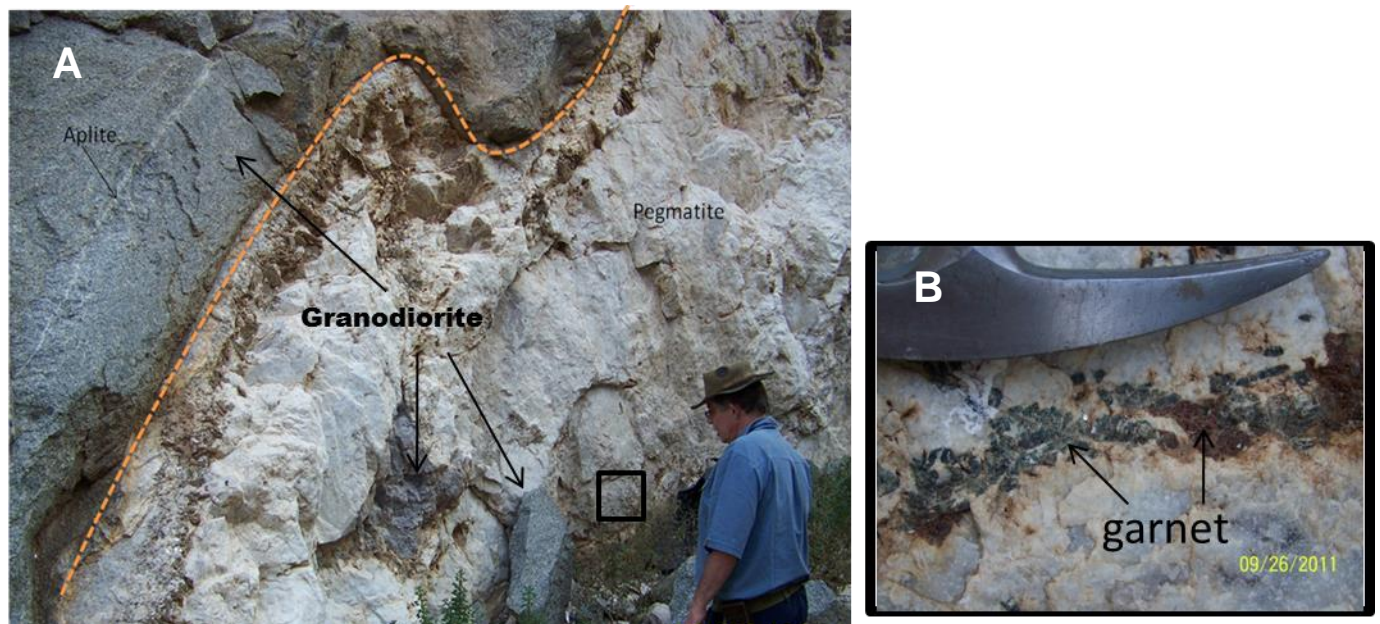
Figure 3-16: At the contact zone with the host rock, massive mica crystals between 2-20cm. in the pegmatite green and red garnets (to right) that vary in size along with quartz and feldspar intergrowths are found.

3.3 Emplacement

Deformation in the area led to faults and fractures that acted as pathways and weak zones for the pegmatite magma to intrude along. Figure 3-8. The intruding pegmatite caused displacement along forced apart sections. After foliation, fracturing and folding, the Noumas I pegmatite intruded. There appears to be a relationship between the occurrence of certain minerals and the distance from the intrusive body.

Figure 3-17: The granodioritic host material intruded by the pegmatite along weak joints (j) and fracture (f) zones.

The minerals distribution within the pegmatite, are arranged in a specific way. Beryl occurs closer to the host rock contact than spodumene, while tourmaline extends further than spodumene minerals within the wall zone. Mica minerals are present throughout the entire pegmatite. Larger crystals are found in direct contact with the granodiorite (Figure 3-9). The mica crystals decrease in size from the wall towards the core zone. The intermediate zone (Figure 3-2) consists of larger crystals, due to the influence of the host rock on the intruding pegmatite allowing the pegmatite to cool down slower.
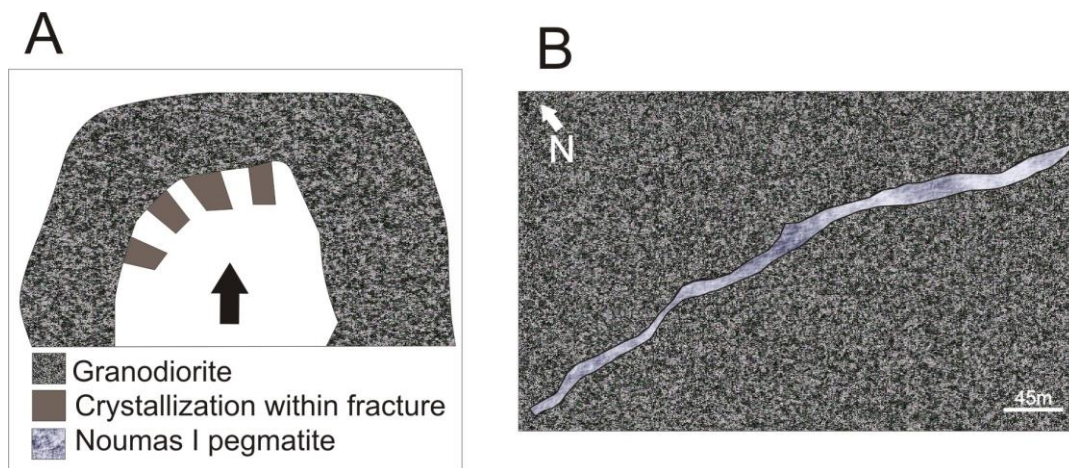
Figure 3-18: A) The crystallization from the intruding magma, B) The plan view of the Noumas I pegmatite within the granodiorite host.

Chapter 4: MINERALOGY, PETROGRAPHY AND GEOCHEMISTRY

Petrographic, mineralogical and whole rock geochemical analyses were conducted on representative samples that were taken from the different zones of the Noumas I pegmatite (Sample locations, Appendix 1). Studies were done with, a conventional optical microscope with a secondary electron microscope (SEM-EDS). X-ray diffraction (XRD) and X-ray fluorescence (XRF) analyses were done. The various methodologies used, their specifications and the appropriate standards (where relevant) are summarised in Appendix 2. The different techniques together, provide insight into the major and minor mineral phases and their chemical compositions and the relationships between various minerals from each zone. The combination of macroscopic descriptions and field observations show clear differences in the mineralization attributed to the various wall, intermediate and core zones. The integration of microscopical techniques established and confirmed the various constituents found within the zoned pegmatite and the textural characteristics between the minerals. It it important to note that the sample representativeness places a major limitation on the study. The amount of samples taken for such a coarse grained pegmatite can not be as representative as needed.

4.1 Mineralogy

The overall mineralogy consists of quartz, K-feldspar, spodumene, plagioclase and mica that make up the bulk of the samples within the different zones. Optical microscopy also revealed the presence of lepidolite, beryl and apatite in smaller quantities (Table 4.1). Ore microscopy positively identified the presence of bismuthinite in small quantities.

Table 4-4: The macroscopic identification of the minerals in the W-wall, I-intermediate and C-core zones (>45%=1, 45-20%=2, 20-5%=3, 5-1 %=4).

Sample	Zone	Minerals	Texture
SW1	W	Quartz (1), K-feldspar (2), beryl (4), mica (3), tourmaline (4), garnet (4)	Large areas dominantly coarse grained quartz, coarse grained single beryl, tourmaline pockets, fine grained garnet.
SW2	I	Quartz (2), K-feldspar (2), spodumene (3), lepidolite (3), mica (3)	Intergrown coarse grained crystals.
SW3	I	Quartz (2), K-feldspar (2), spodumene (3), lepidolite (3), mica (3)	Intergrown crystals, spodumene has started to alter to clay mineral
SW4	C	Quartz (1), K-feldspar (2), beryl (4), mica (3), garnet (4)	Intergrown coarse grained crystals.
SSO8	C	Quartz (1), K-feldspar (1), mica (2), garnet (4)	Intergrown crystals, irregular shape of very coarse grained minerals

4.1.1 Macroscopic descriptions of zones

Samples from the Noumas I pegmatite are summarised in Table 4-1. The zones consist of various silicates, with mica and pyroxene and K-feldspar from the major mineral phases, followed by lesser beryl, tourmaline, garnet and lepidolite. Quartz is the dominant mineral in the zones with grain sizes, ranging from fine (<1cm) to coarse (>10cm) crystalline.

Outer/Wall zone

Minerals are intergrown and have a preferred orientation, visible on a macroscopic scale (Figure 4-1). An intergrowth of feldspar and quartz from the wall to the core zone is found in the pegmatite. The euhedral sheet micas range from long (30cm) to short (1cm). Green beryl is found within quartz and around coarse-grained mica sheets. Single beryl crystals are widely distributed within the wall zone. Small grossular and almandine garnets, range in size from 1cm to 5mm.

Middle/Intermediate zone

Quartz is present as both clear and smoky varieties, intergrown with K-feldspar and plagioclase. Coarse-grained mica sheets are found along the borders of minerals such as spodumene and smaller in appearance (<3cm). The minerals lepidolite, quartz and feldspar are irregularly intergrown. Spodumene laths are included in intergrown quartz and feldspar and surrounded by small mica sheets along the mineral contacts (Figure 4-1).

Core

Milky quartz is the only variety found within the core zone. The mica mineralization is distributed consistently in the core (Figure 4-1). The granodioritic host rock is found as xenoliths. Large garnet crystals, are present within this zone.

The important Li-rich minerals, found within the intermediate zone displays intense alteration features, spodumene is altered among others to kaolinite clay. This section has varying amounts of coarse lepidolite and intergrown K-feldspar and plagioclase. Finely crystallized quartz grains are found concentrated with muscovite around larger subhedral- to anhedral quartz grains (Figures 4-2 and 4-3).
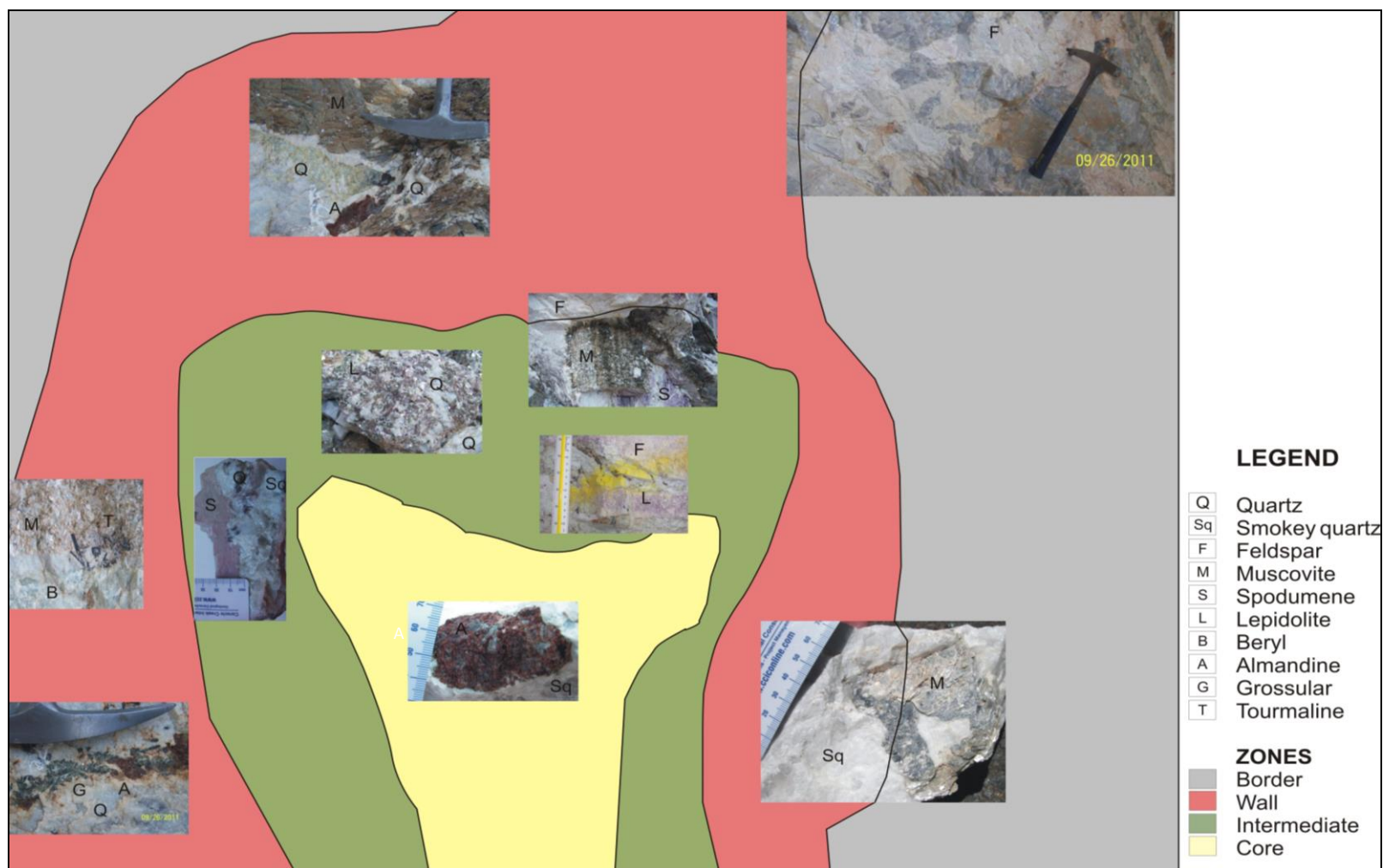
Figure 4-19: Illustration of the different zones: Wall, intermediate and core found at the Noumas I pegmatite; inserted photographs are from the specific zones. Note the texture and grain size differences from the outer wall towards the core zone.
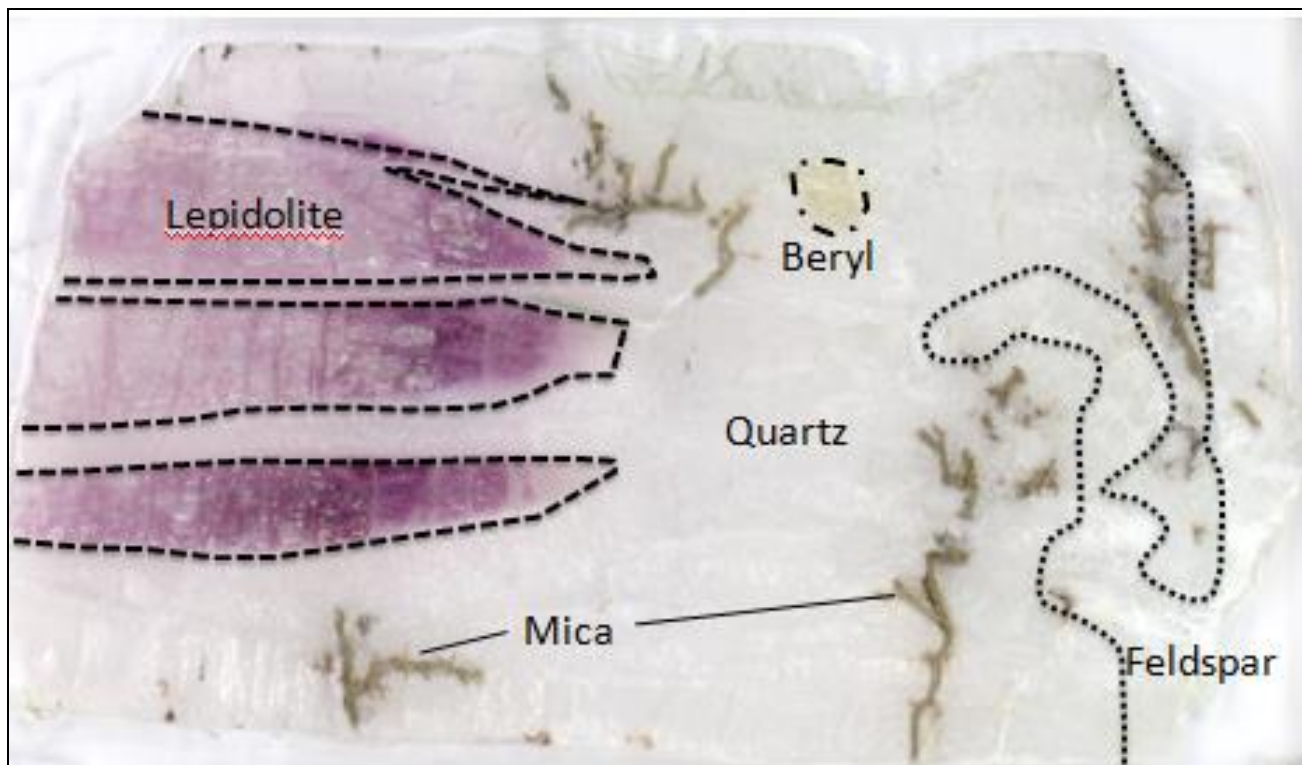
Figure 4-20: Annotated polished section (5cm) of sample SW3 (intermediate zone).
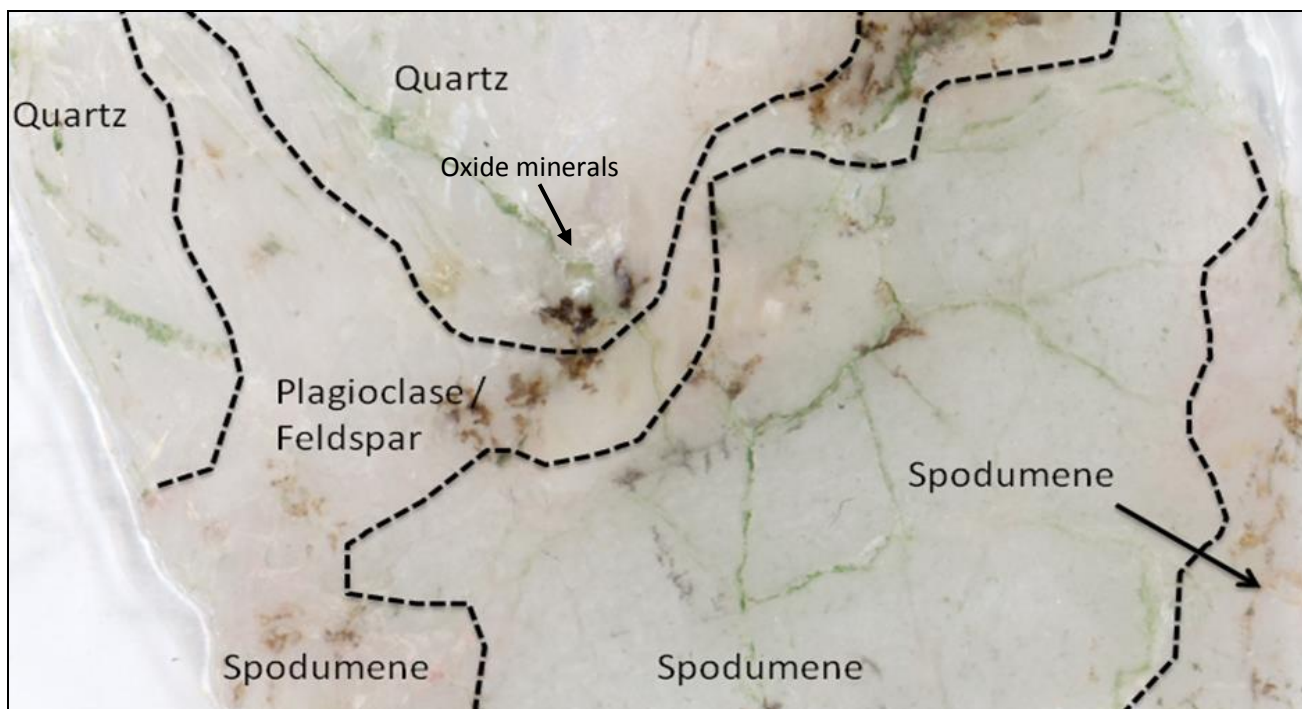
Figure 4-21: Annotated polished section (5cm) of sample SW2 (intermediate and wall zone).

Table 4-5: Estimated modal mineral proportions (in vol. %) of the main mineral content in 33 investigated polished thin sections (qtz=quartz, spd=spodumene, fsp=feldspar, plag=plagioclase, alm=almandine, gross=grossular, lpd=lepidolite). W=wall/outer zone, I=middle/intermediate, C=core zone, B=border.

Sample	Zone	qtz	spd	mica	K-fsp	plag	alm	gross	lpd	Total
SSO1	B	55	-	30	-	-	-	15	-	100
SSO2	B	65	-	35	-	-	-	-	-	100
SSO3	B	50	-	25	-	-	-	25	-	100
SSO4	B	55	-	35	-	-	-	10	-	100
SSO5	B	60	-	10	-	-	15	15	-	100
SSO6	W	65	-	20	-	-	-	15	-	100
SSO7	W	60	-	10	-	-	12	18	-	100
Bkq4.2	W	45	-	-	25	-	18	12	-	100
Bkq4-1	W	40	-	-	60	-	-	-	-	100
Bkq4-1b	W	40	-	12	48	-	-	-	-	100
Bkq4-2	W	45	-	8	47	-	-	-	-	100
Bkq4-3b	W	40	-	-	35	-	15	10	-	100
Bkq5.2a	W	35	-	-	30	-	20	15	-	100
Bkq5.5b	W	40	-	-	50	-	10	-	-	100
Bkq5-1a	W	40	-	10	20	-	10	20	-	100
SW1	W	63	-	-	37	-	-	-	-	100
14.17.5a	I	40	22	-	10	10	-	-	18	100
14.17.5c	I	45	25	-	5	5	-	-	20	100
Bb3	I	20	65	-	-	-	-	-	15	100
Bb3-1	I	15	67	-	-	-	-	-	18	100
Bb4	I	28	20	15	8	13	-	-	16	100
Bb5	I	17	34	29	10	10	-	-	-	100
Bb5-5b	I	24	40	26	5	5	-	-	-	100
SW2	I	52	23	5	10	10	-	-	-	100
SW3	I	55	20	15	5	5	-	-	-	100
Bb1a	C	52	-	40	-	-	5	3	-	100
Bb1b	C	45	-	20	-	-	25	10	-	100
Bb2-1	C	40	-	25	-	-	20	15	-	100
Bb2-9	C	45	-	33	-	-	12	10	-	100
Bb2a	C	45	-	35	-	-	15	5	-	100
Bb2b	C	42	-	20	-	-	24	14	-	100
Bb2c	C	42	-	30	-	-	16	12	-	100
SSO8	C	3	-	22	10	65	-	-	-	100
SW4	C	42	-	25	-	-	23	10	-	100

4.1.2 Mineral description:

Host rock

The coarse-grained masses of granodiorite, associated with granitic batholiths, adjacent to the Noumas I pegmatite body consist of quartz, orthoclase, biotite, plagioclase, amphibole and aplitic veins filled with albite and quartz. The medium- to coarse-grained granodioritic rock hosts the intruded pegmatite bodies. The colour index of the host rock ranges between 10-25%.

4.1.2.1 Major mineral phases of the Noumas I pegmatite:

Quartz

Quartz is present in the majority of the thin sections as constituents of the matrix. The crystals are closely associated with K-feldspar and plagioclase. Myrmekitic textures are found with quartz and plagioclase forming small wormlike bodies. Late-stage quartz not only makes up the major unit within the zones but forms a fine crystalline filling in cracks (Figures 4-4 A and E, 4-7 A and C, 4-8 E and F). Quartz crystals are widely distributed and found in the entire pegmatite body. There is a gradual change from clear to smoky and milky varieties quartz, from the wall to the intermediate zone. According to Von Backstrom (1973), the radio-active mineral thorite is found within the middle zone. Using a handheld scintillometer thorite [(Th, U) SiO_4], the radio-active mineral as described in literature, was identified. This could be the cause for the colour variations within the quartz. Smoky quartz is a direct result of the radiation. Milky quartz is caused by tiny cavities and CO_2 gas bubbles or water trapped during crystal growth and ultimately results in the change from transparent to translucent.

Beryl

Hexagonally shaped beryl is found within the quartz host in the wall zone of the pegmatite (Figure 4-2). Beryl ranges in volume percent between 1-5% of the overall crystals present in the wall zone. This characteristically shaped green mineral is present in the core zone. The average crystal size ranges between 10-15 cm, except in the intermediate zone (<2cm). Coarse-grained isolated crystals of beryl are widespread throughout the wall and core zones of the Noumas I pegmatite. They occur as tabular hexagonal prisms, as well as anhedral interstitial grains within the quartz host of the wall and core zone.

K-feldspar

Euhedral and anhedral feldspars are abundant within the intermediate and core zones of the Noumas I pegmatite (Figures 4-7 A, 4-8 E and F). K-feldspar constitutes about 45-20% of the minerals present within the wall, intermediate and core zones. The average crystal sizes range from 2 mm, to as large as 15 cm. In these shallow intrusive rocks, perthite textures are typical; exsolutions consist of either albite or oligioclase in a K-feldspar matrix and can only be observed at a microscopic scale (Figure 4-4 E). Both polysynthetic and Carlsbad twins are present in the samples (Figure 4-4 D).

Plagioclase

Euhedral, tabular crystals of plagioclase are distributed through the intermediate and core zones (Figures 4-4 F, 4-5 A, D and F). The average crystal sizes of plagioclase ranges from 500μm to larger crystals sizes of 5cm. The plagioclase mineral present in the intermediate and core zone make up about 10-15%. Myrmekitic textures of plagioclase and quartz are present in the intermediate zone. This intrusion contains plagioclase with intermediate degrees of order, where the An compositions based on the extinction angles of plagioclase are between An_5 and An_{36}.

Spodumene

Spodumene is a characteristic mineral of Li-bearing granite pegmatites (Deer et al., 1997). At Noumas I, spodumene is present as euhedral and anhedral crystals in the intermediate zone (Figures 4-4 B to E, 4-5 B, D and F). Spodumene makes up about 67-16% of the minerals present within the intermediate zone. It occurs as euhedral laths and as isolated crystals rimmed by mica flakes. The crystal sizes range between 10 μm, to crystals as large as 70cm. Fragments of spodumene are found as tiny inclusions within veins (Figure 4-4 A). In some places with the correct conditions or change in composition, spodumene is transformed to muscovite. An ideal reaction for such a change in solution would be (Deer et al, 1997):

$3LiAlSi_2O_6 + 2H_2O + K^+ \rightarrow KAl_2(Si_3Al)O_{10}(OH)_2 + 3Li^+ + 3SiO_2 + 2(OH)^-$

Spodumene   Muscovite

The symplectically intergrown texture of spodumene with quartz (Figure 4-4 B) is characteristic of spodumene that has replaced petalite from the series. Spodumene generally shows little compositional variations with minor amounts of Na to replace Li and Fe^{3+} that might replace Al within the chemical structure of the mineral (Nesse, 2004).
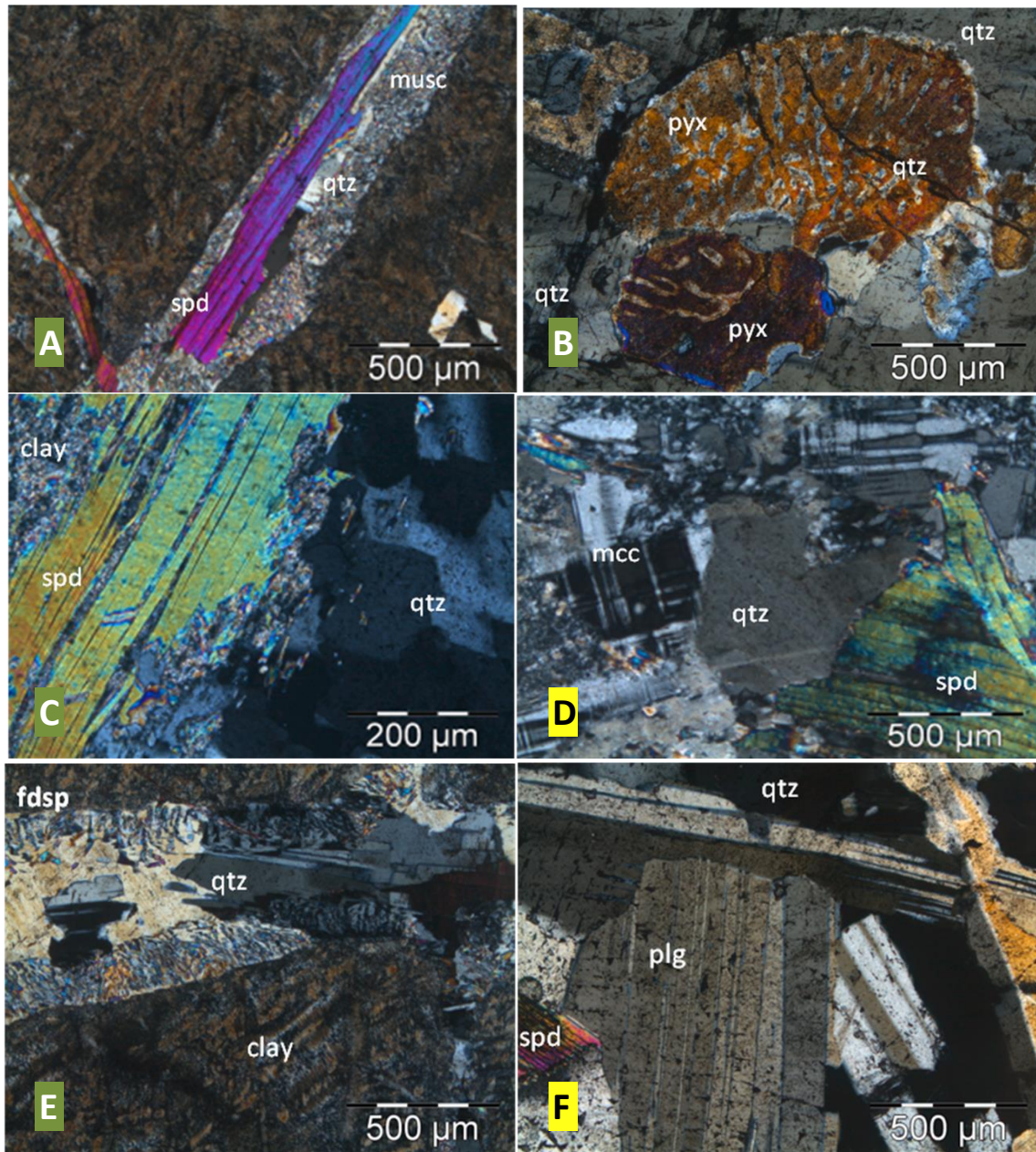
Figure 4-22: Under transmitted light, crossed polars, SW3A: Vein filled by fine crystalline quartz (qtz) and muscovite (musc) within a quartz host and inclusions of spodumene (spd) laths found within the veins, SW3B: A symplectitic intergrowth of quartz (qtz) and pyroxene (pyx), embedded in quartz (qtz) grains. SW2C: Quartz, spodumene (spd) lath with alteration (clay) along the rim of the crystal grain, SW3D: Coarse-grained spodumene crystal, microcline (mcc) intergrown with quartz, SW2E: Coarse-grained spodumene altered to clay enclosing quartz crystals, typical myrmekite textures between plagioclase and quartz are observed, SSO8F: Euhedral plagioclase laths in quartz matrix. Red=wall zone, green=intermediate zone and yellow=core zone.
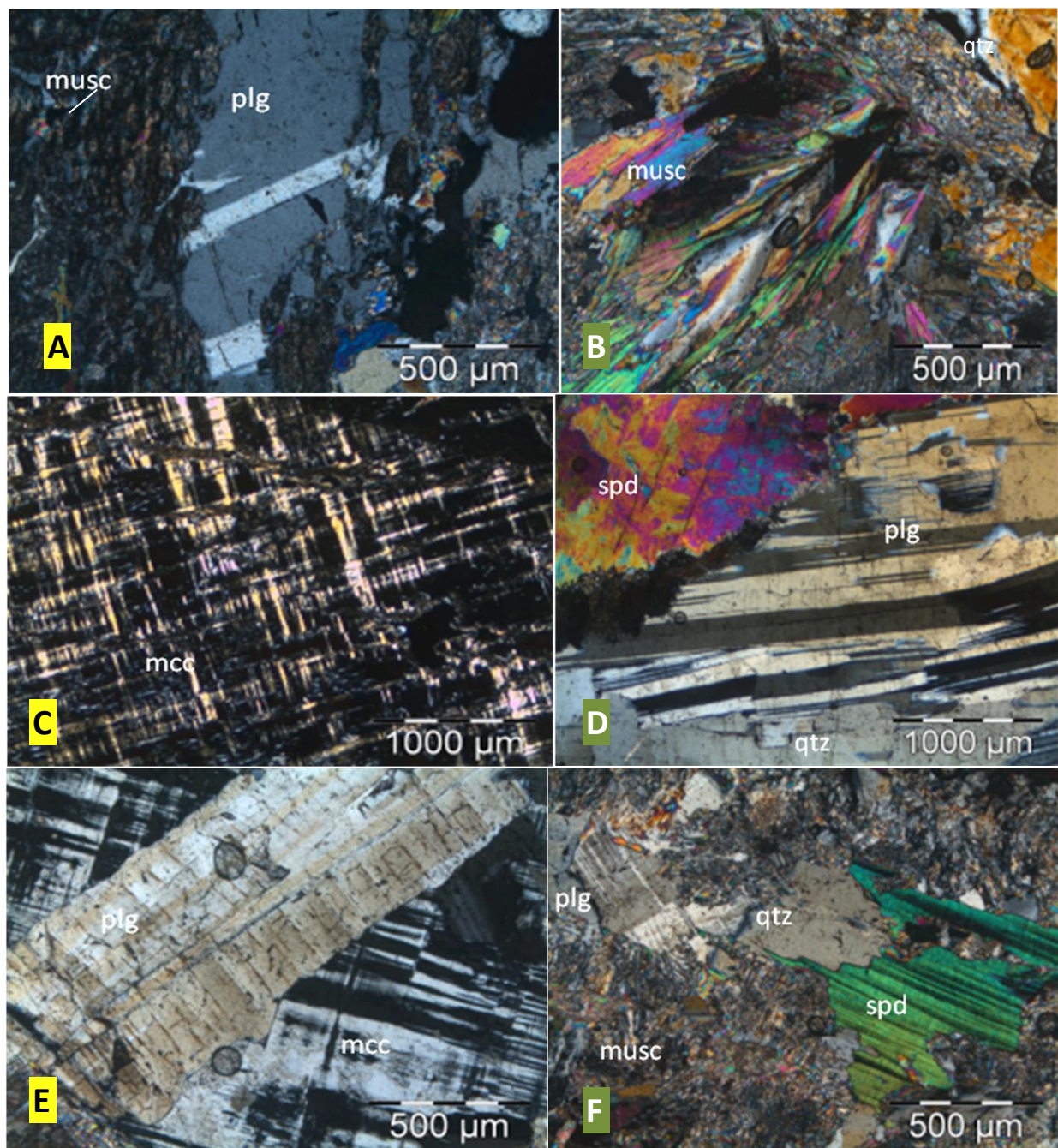
Figure 4-23: Under transmitted light, crossed polars, SS08A: Plagioclase (plg) in quartz and muscovite (musc), SW2B: Muscovite (musc) in quartz, SSO8C: Microcline (mcc) perthite texture with exsolution lamella of albite, SW3D: Spodumene crystal with alteration along rim where crystals are in direct contact with plagioclase, quartz is found distributed along the sides of euhedral plagioclase, SSO8E: Plagioclase in microcline matrix, SW2F: Coarse-grained anhedral spodumene crystal within an intergrowth fine crystalline matrix of muscovite, quartz and plagioclase crystals. Red=wall zone, green=intermediate zone and yellow=core zone.

Mica

The mica minerals biotite (K_2(Mg, Fe)$_6$Al$_2$Si$_6$O$_{20}$(OH, F)$_4$), muscovite (KAl$_2$(AlSi$_3$O$_{10}$)(OH)$_2$) and lepidolite (K(Li, Al)$_3$(Si, Al)$_4$O$_{10}$(F,OH)$_2$) are all found within the Li- bearing Noumas I pegmatite. Muscovite flakes are distributed in patchy and isolated crystals. The grains vary in size from 20µm to 30cm (Figures 4-4 F, 4-8 C). These minerals make up 40-8% of the minerals present in the zones. The muscovite mineralization decreases in size towards the core. Muscovite is the alteration product of lepidolite. Lepidolite is classified under micas because of its similarities to muscovite, but contains lithium within its crystal chemistry. Lepidolite is found in patches or bands within the Noumas I pegmatite with a pink to purple colour and vitreous luster. The average grain size ranges between 100µm to large crystals of 7 cm (Figure 4-5 F). The thin flexible sheets have perfect cleavage. A distinguishing feature of lepidolite is the K interlayer that is substituted by Rb, Na or Cs, resulting in substantial amounts of these elements associated with lepidolite (Nesse, 2004). Euhedral lepidolite crystals of Noumas are surrounded by intergrown quartz and feldspar crystals. Biotite is found in the granodiorite host rock along with quartz, plagioclase and mafic constituents (amphibole). Biotite crystals have an average grain size of about 1 cm.

Garnet

Two types of garnets could be distinguished, a green grossular (Ca$_3$Al$_2$ [Si$_3$O$_{12}$]) and red or rose coloured almandine (Fe$_3^{2+}$ Mg$_2$Al [Si$_3$O$_{12}$]) garnet (Appendix 5). The average crystal size ranges from 0.5 cm to larger crystals of 4cm. The garnet minerals make up about 5-35% of the minerals present within the wall and core zones. Almandine acts as a scavenger for manganese. The appearance of almandine in rocks of appropriate bulk chemistry is favoured by high-pressure environments so it is stable in most of the higher grades of metamorphism (Deer et al., 1997). In the Noumas I pegmatite it does not appear to be a xenocryst but a primary entrained magmatic constituent. Grossular is typically found in regionally metamorphosed impure calcareous rocks that have undergone calcium metasomatism (Deer et al., 1997). Grossular is found as coarse-grained crystals of 0.5 - 2cm in diameter. The grain sizes decrease to 1mm, towards the intermediate zone. In the core zone only almandine is found.

Tourmaline

Tourmaline is found in granitic pegmatites and as accessory mineral in granite and granodiorite. At Noumas I tourmalines have euhedral, stubby columnar crystals. The black tourmaline found in the wall zone occurs as "pockets" or irregular masses with varying orientation of the crystals.

They are distributed in minute amounts and make up about 1-2% of the minerals present within the wall zone. Tourmaline crystals are found associated with hexagonal beryl crystals.

4.1.2.2 Minor mineral phases of Noumas I pegmatite:

Thorite

In the intermediate zone of the pegmatite, the radio-active mineral thorite [(Th, U) SiO_4] is found in small quantities of <1%. Thorite was not visible with the naked eye but Von Backstrom (1973) identified the presence of the radio-active mineral. The scintillometer positively identified the presence of a radio-active mineral. The smoky quartz variety is a direct result of radiation from the radio-active thorite mineral.

Bismuthinite

The bulk of the mineralization has been mined out between 1925 to 1961 (Bullen, 1998); nevertheless bismuthinite was found in a sample, thought to be purely quartz, from the wall zone. The samples collected from the wall/outer zone were viewed under a reflected light (ore) microscope. A sporadic and very small amount of bismuthinite was detected microscopically in only one sample (Figure 4-6). This single crystal is <2mm in diameter.
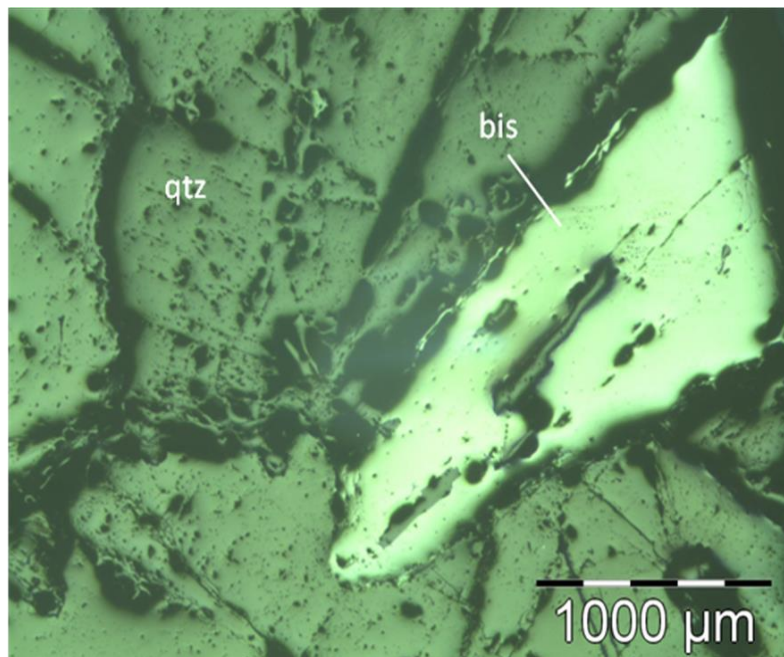
Figure 4-24: Microscopic photograph under reflected light shows the gangue mineral (qtz) and the anhedral bismuthinite (bis) crystal formed within the host mineral.

4.1.3. Mineral phases and chemistry

The backscattered electron images obtained using the SEM-EDS show the intergrowth relationship of the various mineral phases from the wall to the core zone (Figures 4-7, 4-8 and 4-9).

The wall zone shows intergrown quartz and K-feldspar minerals with tourmaline, beryl, muscovite, garnet and apatite. The irregular crystal grains are better defined with the backscattered electron images than under the microscope. Small cavities (dark black lines) are present within the samples and clearly visible. Bismuthinite, the only sulphide mineral identified, is found in this zone.

In the middle zone; the minerals present within the middle or intermediate zone (lepidolite, spodumene) also have a unique association. The Li-rich minerals are only present within this zone and not in any other. On a macroscopic scale lepidolite is found as "strings or thick bands" within quartz and small irregular crystals surrounded by intergrown K-feldspar and quartz.

In the core zone graphic intergrowth is observed. The dominant minerals present here are quartz and K-feldspar with minor muscovite, beryl and illite.

X-ray diffraction spectra (Appendix 3) positively identified triplite *[Li(Fe, Mn)PO$_4$]* in the intermediate zone. Petalite is also present in the intermediate zone. Most fractures have been filled in by albite and quartz. The mineral identified and their abundances within the wall, intermediate and core zones have been summarized in Table 4-3.
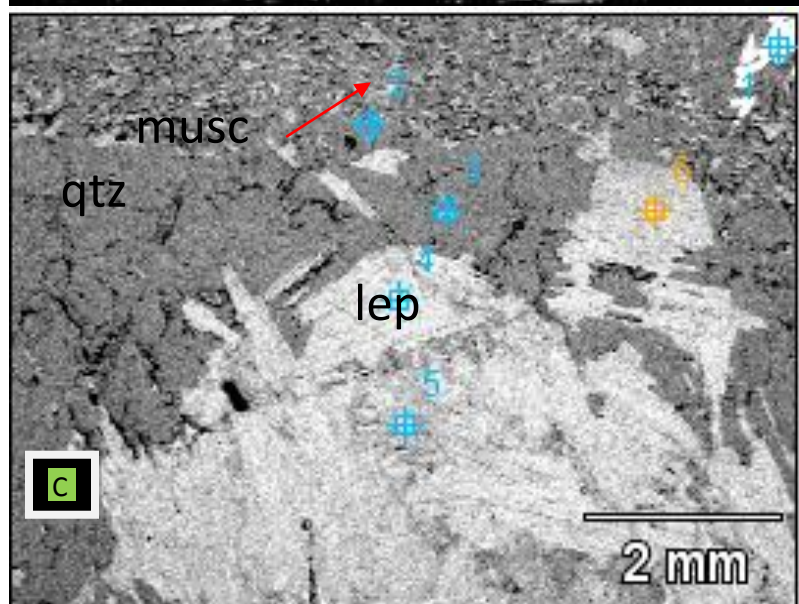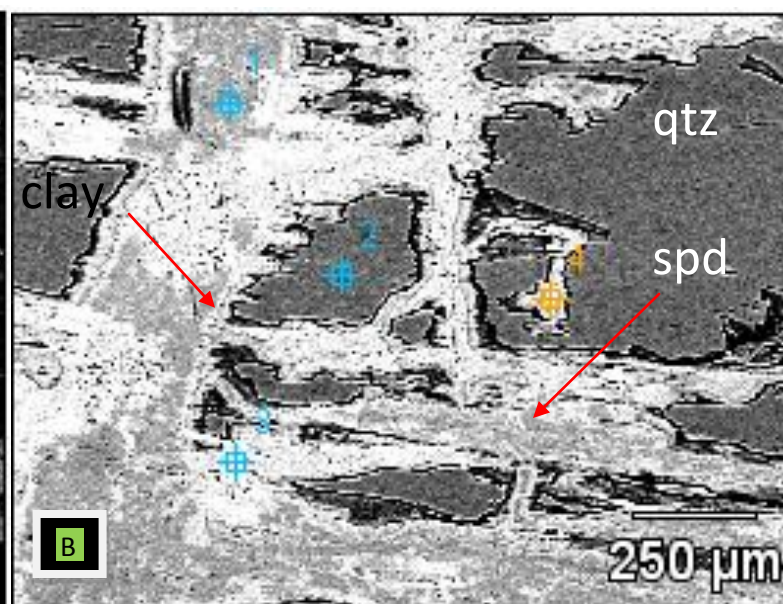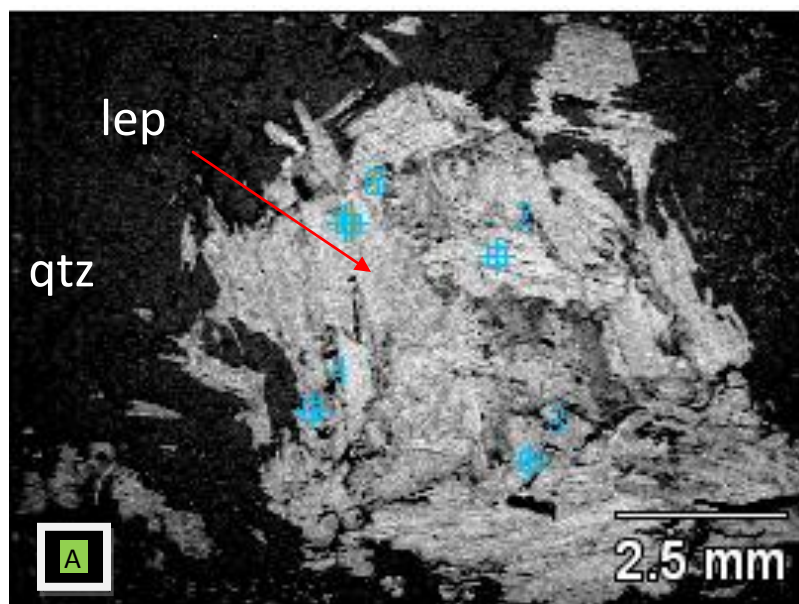
Figure 4-25: Annotated SEM backscattered electron images showing the relationships of the mineral components within the zoned pegmatite. A) *Intermediate zone* has intergrown quartz and lepidolite textures, the needle-like structures of lepidolite is clearly visible B) *Intermediate zone* shows the alteration of the spodumene to clay (kaolinite equivalent), embedded in quartz C) *Intermediate zone*, quartz is surrounded and in certain areas intergrown with muscovite, it appears to have a micro-layering that grades into smaller crystals, large lepidolite is also present.
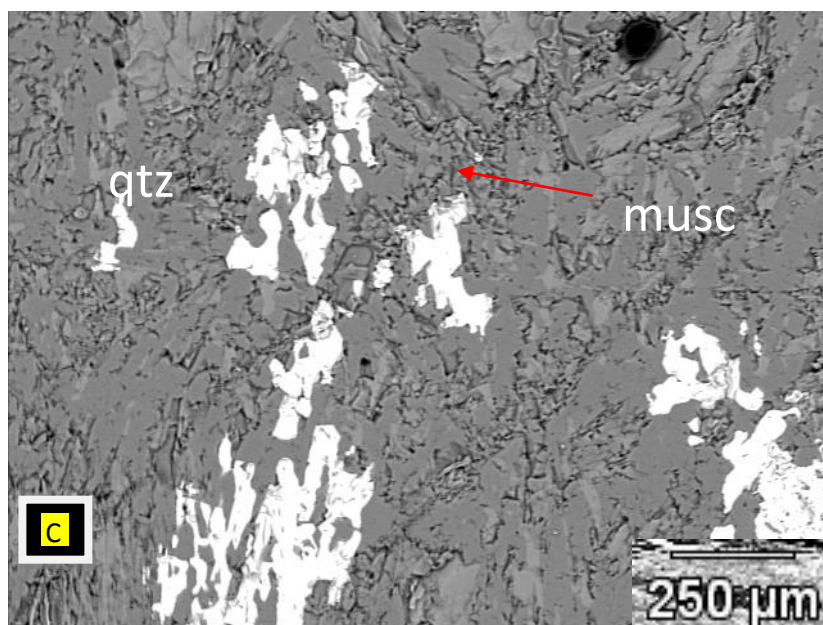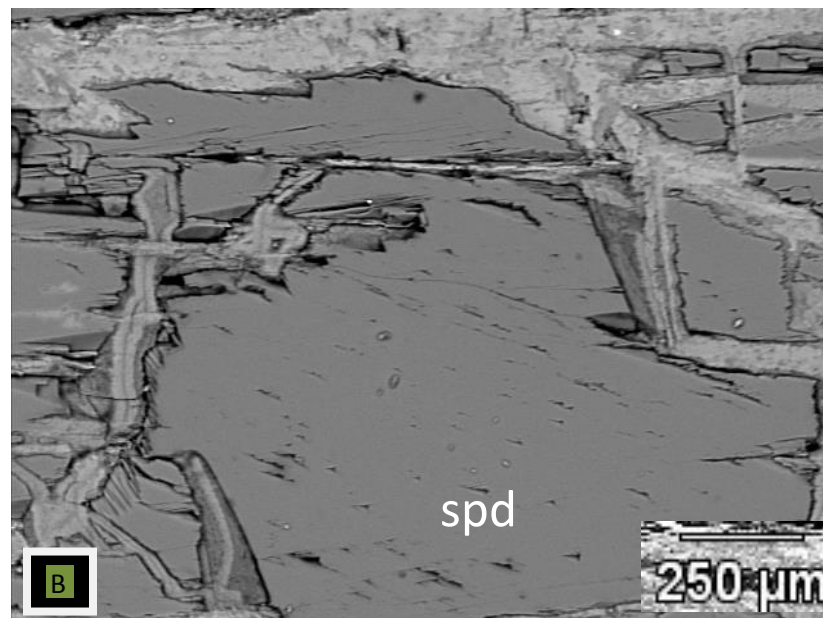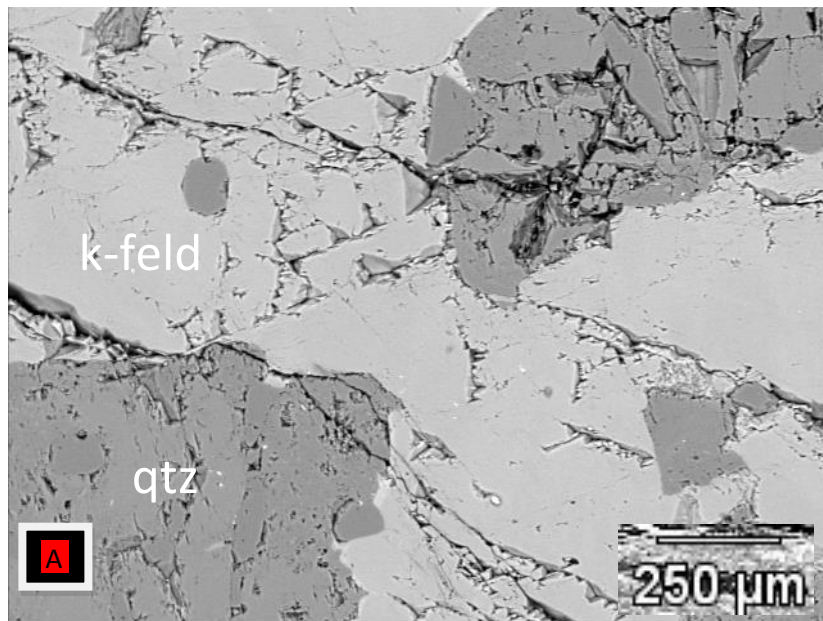
Figure 4-26: Annotated SEM backscattered electron images showing the relationships of the mineral components within the zoned pegmatite. A) *Wall zone* **has intergrown quartz and K-feldspar textures on a micro-scale, B) I***ntermediate zone* **shows the clear alteration of the spodumene to its kaolinite clay equivalent, C) C***ore zone,* **and quartz is surrounded by muscovite that formed in the micro-fractures with a skeletal mineral intergrown in the quartz host.**
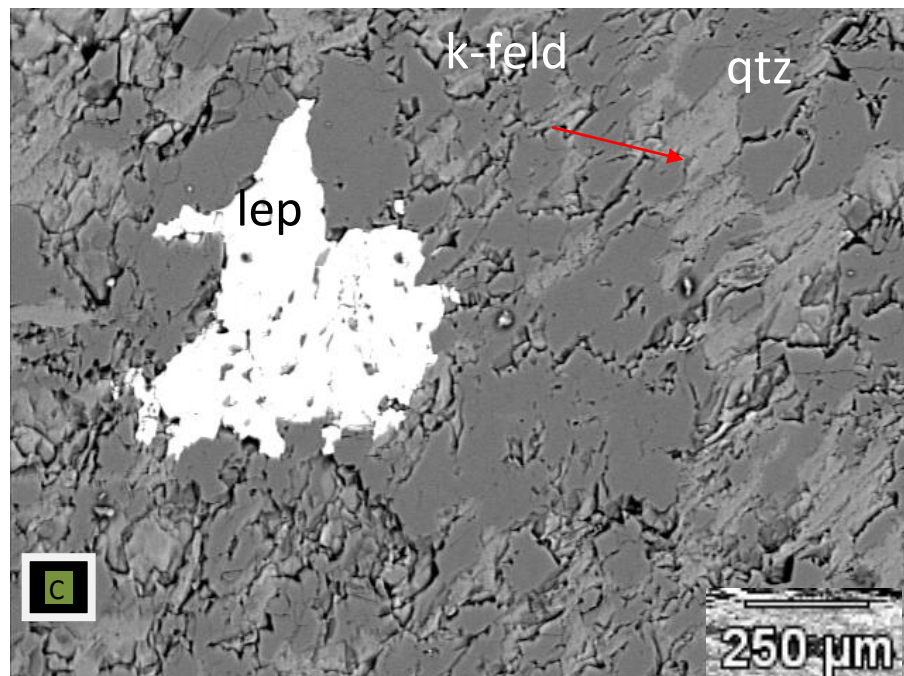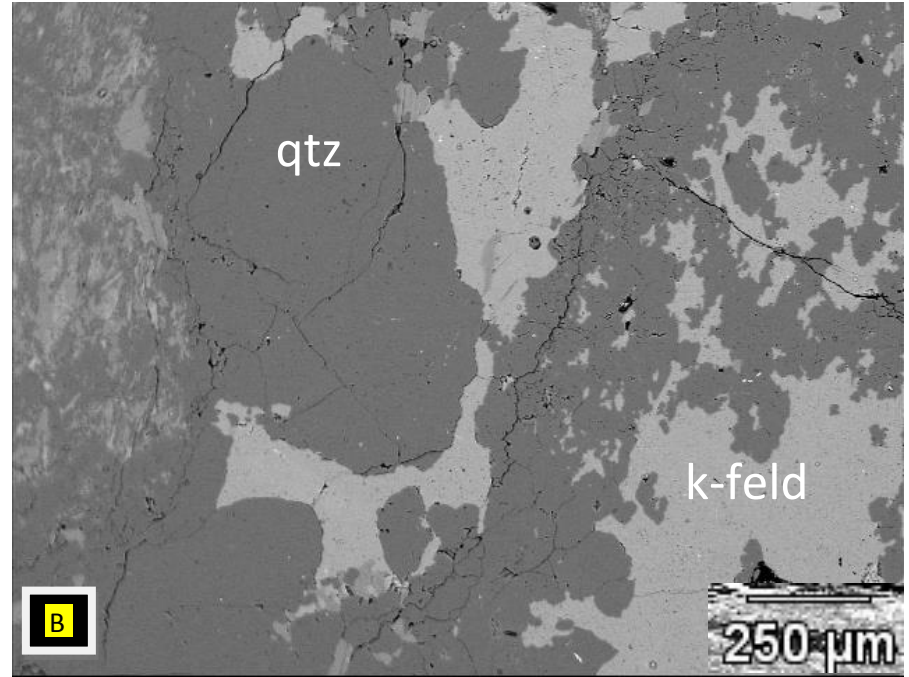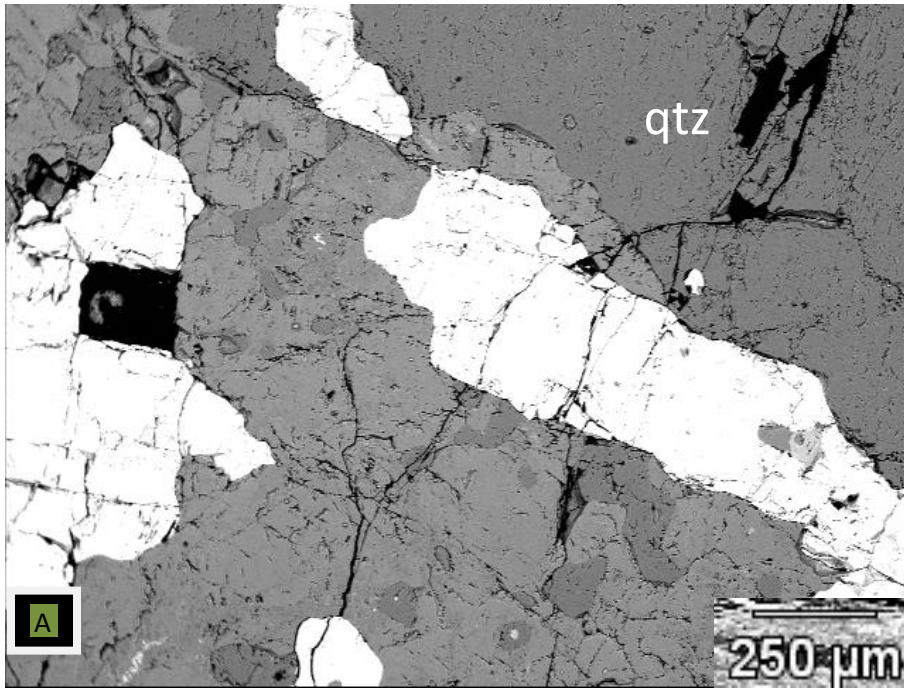
Figure 4-27: Annotated SEM backscatter electron images showing the relationships of the mineral components within the zoned pegmatite. A) *Intermediate zone* small cavities in between mica sheets, B) *Core zone*, granular intergrowth or simultaneous crystallization of quartz and K-feldspar, C) *Intermediate zone*, quartz is intergrown with K-feldspar, lepidolite found as isolated grains.

Table 4-6: Summary of minerals identified and mineral abundances within the Noumas I pegmatite (minerals identified with XRD and SEM-EDS).

Mineral	W	I	C	Occurrence
K-feldspar	Common	Common	Common	Intergown
Quartz	Very common	Very common	Very common	Intergown, dominant mineral
Muscovite	Common	Common	Rare	Coarse-grained and small phenocrysts, euhedral to anhedral
Plagioclase	Common	Common	Common	Intergown
Garnet	Rare		Common	Blebs in core, pockets at contact with wall zone
Lepidolite		Common		Limited to intermediate zone
Spodumene		Very common		Common in the Li-rich intermediate zone
Beryl	Rare		Rare	Sporadic, coarse-grained hexagonal crystals
Triplite		Very rare		Together with spodumene in intermediate zone
Apatite	Very rare			Small quantities in wall zone
Illite		Rare	Rare	Alteration product
Bismuthinite	Very rare			Ore mineral; small quantities in wall zone
Petalite		Very rare		Found in the intermediate zone
Tantalite-columbite		Very rare		Mined out; occurred in the intermediate zone

Legend:
- Very common >40%
- Common 10-30%
- Rare 1-5%
- Very rare <1%

4.2 Petrography

4.2.1 Petrographic descriptions of individual zones:

Descriptions are based on the thin sections taken from the wall, intermediate and core zones.

Sample: SW1

Position: Wall zone (Figure 4-1, Table 4-2)

Constituents: quartz 63%, K-feldspar 37%

Description: This section (Figures 4-2 and 4-7 A) is dominated by quartz crystals showing undulatory extinction with intergrown K-feldspar. No other minerals were found within the section except for bismuthinite. The dull greyish-white opaque mineral forms an anhedral crystal within its quartz host with strong anisotropic colours. The mineral was observed under reflected light and the grain is more than 2mm in size.

Sample: SW2

Position: Intermediate zone (Figure 4-1, Table 4-2)

Constituents: quartz 52%, spodumene 23%, plagioclase10%, muscovite 5%, clay minerals 5% K-feldspar 5%

Description: The sections (Figures 4-5 C, E; 4-6 B, F) are dominated by quartz crystals showing undulatory extinction. Myrmekite is visible in all the sections from the intermediate zone. Large euhedral to anhedral shaped crystals of spodumene are found in major amounts within the intermediate zone (Figures 4-5 C, 4-6 F). The spodumene laths are in some areas altered to the clay mineral, koalinite (Figure 4-7 B). Muscovite appears to fill or form around spodumene crystals. Euhedral plagioclase laths with typical polysynthetic twinning are found in smaller quatities spread interstitially throughout the zone. The minerals occur showing interstitial textures and there appears to be an association within the mineralization of the zone, of pyroxene (spodumene) with quartz and mica (muscovite). Even where microfractures are filled with quartz small amounts of euhedral spodumene crystals are found within the filled fractures.

Zone: SW3

Position: Intermediate zone (Figure 4-1, Table 4-2)

Constituents: quartz 55%, spodumene 20%, muscovite 15%, clay 6%, plagioclase 2% and k-feldspar 2%.

Description: The section (Figures 4-5 A, B; 4-6 D) is dominated by anhedral quartz found as intergranular matrix, along with skeletal pyroxene (spodumene) forming symplectitic intergrowth textures with quartz (Figure 4-5 B). Anhedral spodumene laths are present in a finer crystalline texture surrounded by muscovite and quartz crystals. Kaolinite clay is found as an alteration product next to the filled fractures. Muscovite crystals surround the spodumene laths forming smaller rim structures. Large anhedral plagioclase laths are found along with spodumene and granular quartz (Figure 4-8 F). Typical lammellar twinning of plagioclase crystals is present. Anhedral spodumene crystals are found as interstitial occurences within the quartz matrix.

Zone: SSO8

Position: Core zone (Figure 4-1, Table 4-2)

Constituents: plagioclase 65%, muscovite 22%, K-feldspar 10%, quartz 3%.

Description: The sample from this zone (Figures 4-5 D, F; 4-6 A, C, E) is dominated by euhedral plagioclase phenocrysts. The plagioclase laths have typical lammelar twinning with An contents as low as that of albite as determined by optical estimation. The minerals from the feldspar series also included orthoclase. The orthoclase also showed perthite exsolution along with characteristic Carlsbad twinning. Cross-hatched twinning of microcline was observed. Exsolution lamellar of microcline was also noted (Figure 4-6 C). Fine-crystalline muscovite flakes surround the euhedral laths of plagioclase and quartz matrix in between cavities (Figure 4-7 C).

4.3 Geochemistry

4.3.1 X-ray Fluorescence Analyses

The Noumas I pegmatite consists of a wide variety of minerals. Using X-ray Fluorescence spectometry (Appendix 3), the major and trace element distributions throughout the various zones of the pegmatite are investigated. This establishes a better understanding of the crystallization or solidification evolution that occurred within the Noumas I pegmatite. There is a clear variation, of the trace element concentration and distribution from the wall, through the intermediate to the core zone.

The various zones of the Noumas I pegmatite were compared to the average distribution of trace elements for granite to establish trends. The sampled data were compared with the continental crust composition as stated by Taylor and McLennen (1985) and Thompson (1982). The magma composition is compared to the compositional melt evolution as the pegmatite formed. Major and trace elemental plots help to establish the compositional trends that are found in the various zones of the pegmatite.

The major element distribution relatively homogeneous within the single zones; however there are compositional trends present between the various zones of the Noumas I pegmatite. The samples from the border zone (grey), with minor differences, are relatively consistent with increased Fe_2O_3, MnO, MgO and P_2O_5 content relative to the wall, intermediate and core zones. The samples taken from the border zone, along the pegmatite body, show an increase in the content of these element oxides due to the differentiation of the pegmatite itself (Figure 4-10 to Figure 4-15).

The granitic pegmatite from Noumas I showed typical high SiO_2 values and depleted K_2O values when compared to a standard quartz granodiorite analysis (Geringer et al., 1988). During the melting or removal of quartz and feldspar Si, Al, Na, K and Ca are removed and elements such as Fe and Mg remain in the residual melt.

The border zone (grey) contains relatively constant SiO_2 and Al_2O_3 values. MgO and Fe_2O_3 values appear to increase towards the wall zone of the pegmatite. This increase is attributed to the presence of tourmaline, garnets and biotite within the wall zone. The wall zone (red) the furthest from the mineralized pegmatite has higher TiO_2, CaO and MgO values with high SiO_2

and Al_2O_3 values than the intermediate zone. These higher values are attributed to the feldspar-plagioclase-quartz mineralization found in the exterior wall zones.

The intermediate zone (green) has relatively higher Al_2O_3 than the rest of the zoned areas. The high Na_2O and K_2O values are a reflection of the abundant feldspar-plagioclase from this zone. A high Al_2O_3 with lower Na_2O can also be indicative of a sedimentary protolith source rock.

The core zone (yellow) consists of similar values for major elements compared to the border, wall and intermediate zones. Higher Na_2O and K_2O values are found and it is due to the feldspar-plagioclase abundance. SiO_2 distribution within the various zones differ significantly. The higest silica content is found within the core, wall and border zones. The opposite is known for the Al_2O_3 content of the zones (Figure 4-11). The Na_2O content varies over most zones of the Noumas I pegmatite (Figure 4-12). The high Na_2O content can be attributed to the plagioclase and albite minerals. The highest K_2O values are found within the wall zones (Figure 4-13). Over the core and intermediate zones the K_2O content varies. The MgO content throughout the Noumas pegmatite varies significantly (Figure 4-14). The Fe_2O_3 values within the border, zones gradually increase towards the wall zone of the pegmatite (Figure 4-15).
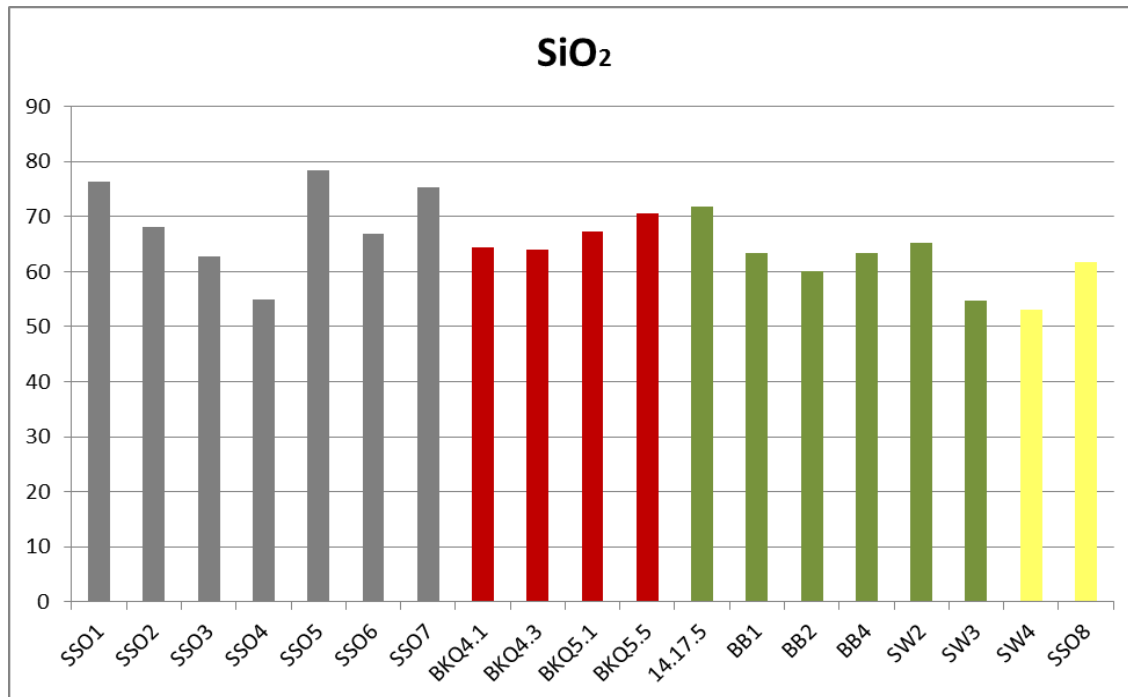
Figure 4-28: Major element distribution within the Noumas pegmatite, samples appear from the border (SSO1) furthest from the center to the core (SSO8). Grey= border, red= wall, green= intermediate, yellow= core.
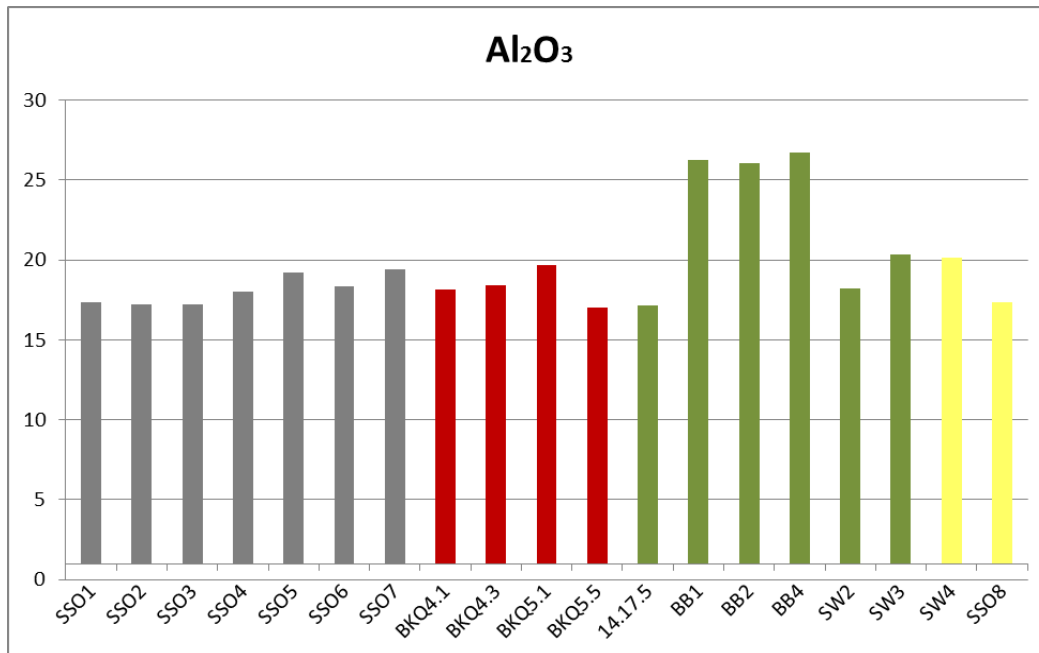
Figure 4-29: Major element distribution within the Noumas pegmatite, samples appear from the border (SSO1) furthest from the center to the core (SSO8), grey= border, red= wall, green= intermediate, yellow= core.
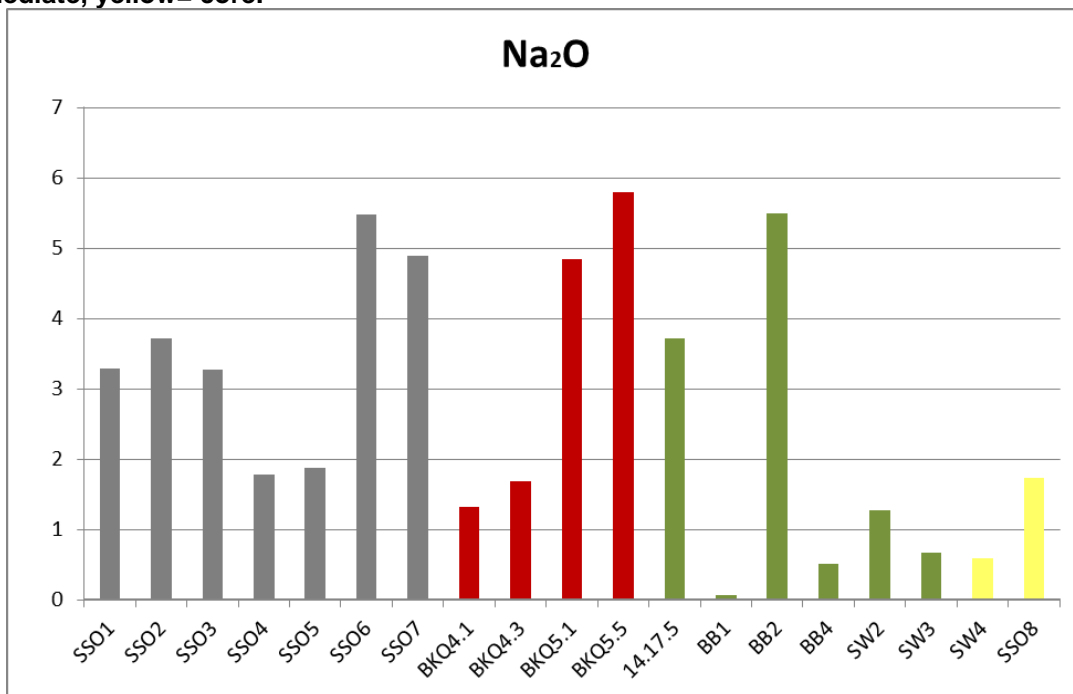
Figure 4-30: Major element distribution within the Noumas pegmatite, samples appear from the border (SSO1) furthest from the center to the core (SSO8) grey= border, red= wall, green= intermediate, yellow= core.
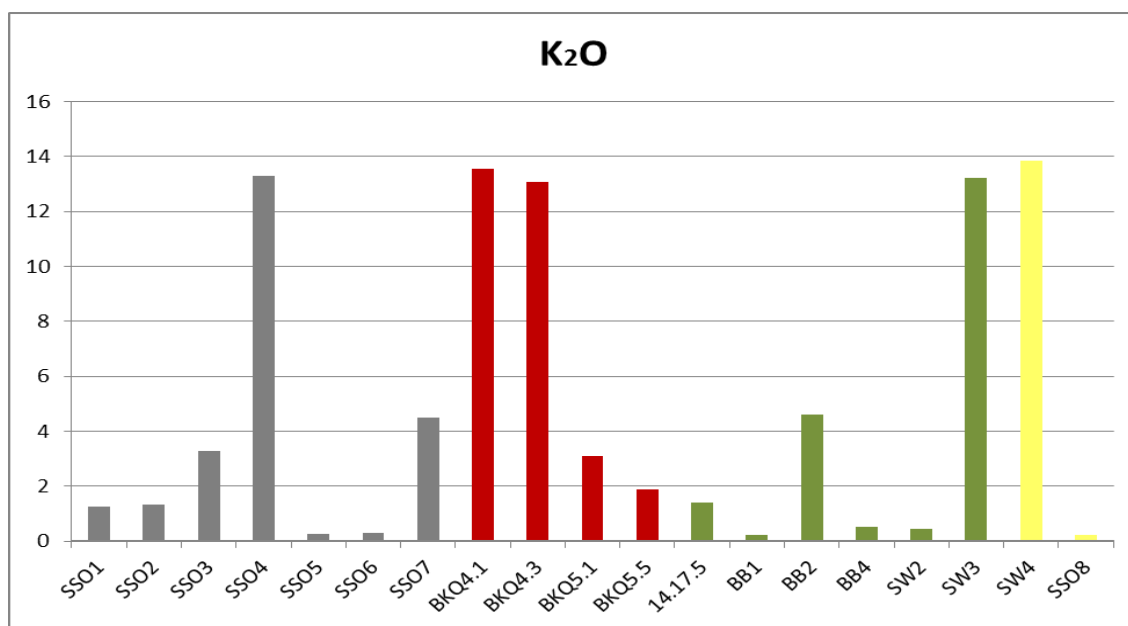
Figure 4-31: Major element distribution within the Noumas pegmatite, samples appear from the border (SSO1) furthest from the center to the core (SSO8) grey= border, red= wall, green= intermediate, yellow= core.

The MgO content for the Noumas I pegmatite reflect the accessory compositions from Fe-Mg bearing mineral such as garnet and tourmaline (Figure 4-14).
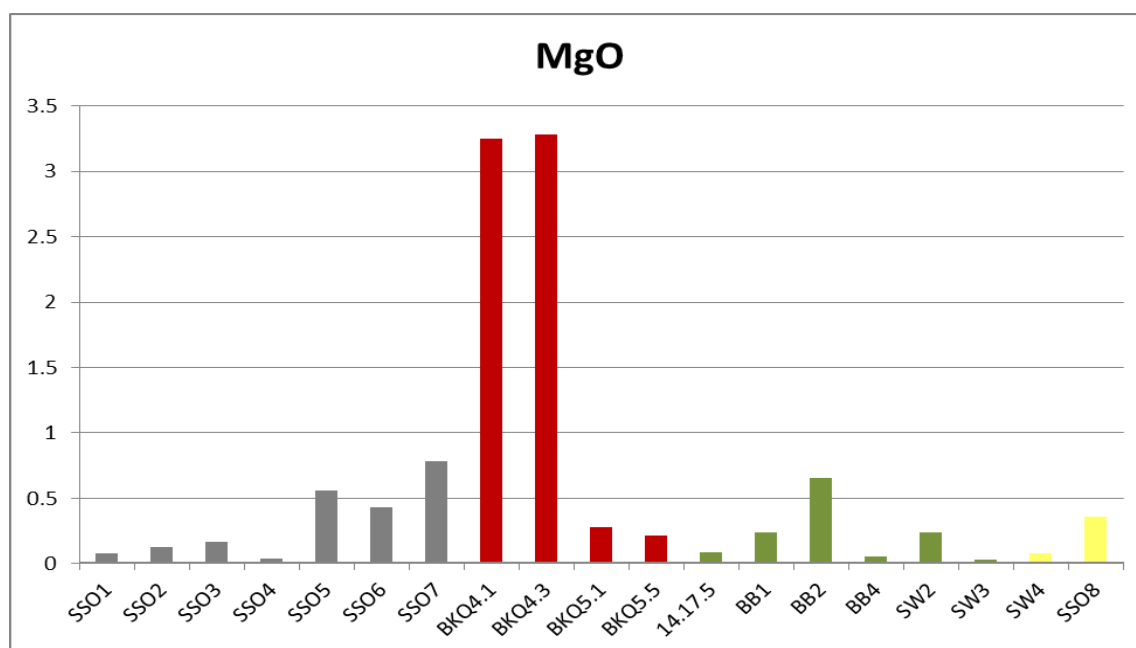
Figure 4-32: Major element distribution within the Noumas pegmatite, samples appear from the border (SSO1) furthest from the center to the core (SSO8) grey= border, red= wall, green= intermediate, yellow= core.
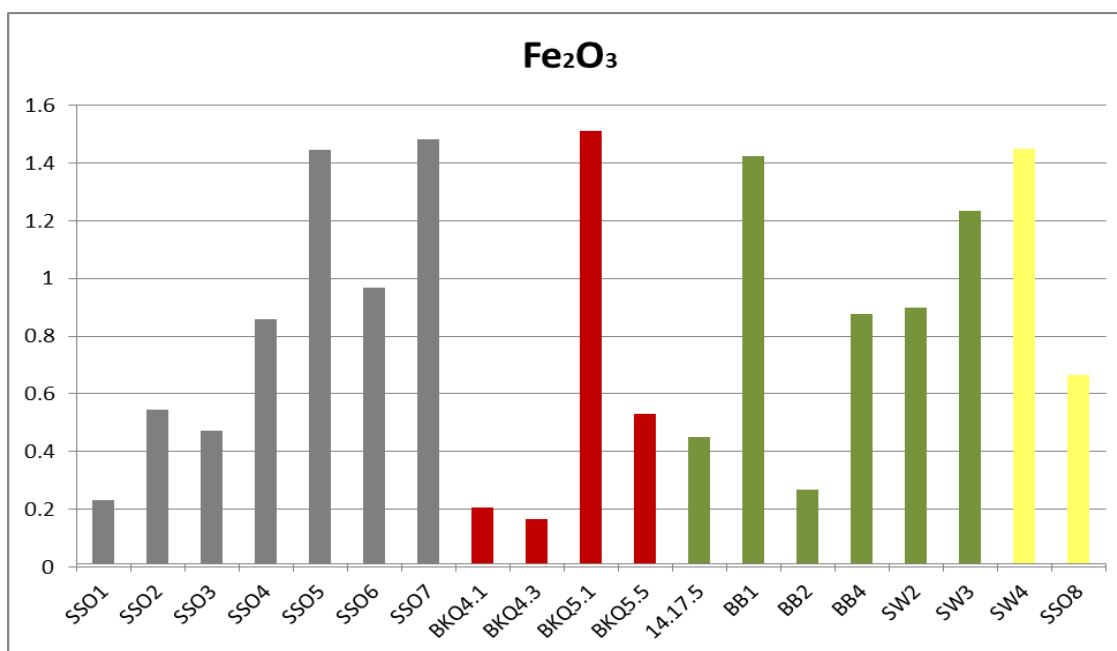
Figure 4-33: Major element distribution within the Noumas pegmatite, samples appear from the border (SSO1) furthest from the center to the core (SSO8) grey= border, red= wall, green= intermediate, yellow= core.

Webster et al., (1997) used the (Al_2O_3/CaO + Na_2O +K_2O) (aluminum saturation index) and established a range between 1.3 and 2 that was able to classify the pegmatite source as peraluminous. The same was calculated for the different zones of the Noumas I pegmatite see Table 4-5. The samples that correspond to the 1.3 to 2 ratio are highlighted within Table 4-5.

Table 4-7: The calculated values for pegmatite source distinction, based on Webster et al., 1997

Sample	Zone	Al_2O_3/CaO+Na_2O+K_2O	Sample	Zone	Al_2O_3/CaO+Na_2O+K_2O
SSO1	B	1.11	BKQ5.5	W	1.45
SSO2	B	1.61	14.17.5	I	1.48
SSO3	B	0.94	BB1	I	1.43
SSO4	B	1.62	BB2	I	1.57
SSO5	B	1.47	BB4	I	1.12
SSO6	B	0.45	SW2	I	1.37
SSO7	B	1.49	SW3	I	2.14
BKQ4.1	W	3.40	SW4	C	0.46
BKQ4.3	W	1.94	SSO8	C	0.77
BKQ5.1	W	1.38			

The Noumas I pegmatite were normalized with the compositions for the upper crust from Taylor and McLennan (1985). The major, transition, rare and high field strength elements were plotted against the normalized upper continental crust in order to establish the enrichment or depletion for the group elements (Figure 4-16 to Figure 4-18).

Trace elements normalized to the upper continental crust have large discrepancies due to the higher variability in trace element concentrations. Rudnick and Gao (2003) stated that less evolved melts would have a lower SiO_2, higher Fe_2O_3, MgO and CaO but similar P_2O_5 and Na_2O values. The solubility of the transition elements would indicate if minerals crystallized directly from the silicate liquids (Webster et al., 1997).

The major elements from the border, wall, intermediate and core zones of the Noumas I pegmatite were normalized against the upper continental crust, see Figure 4-16. The diagram shows the bulk of the melt has either enriched elements (> 1) or depleted elements (< 1) from the various zones. SiO_2 and Al_2O_3 are highly enriched in all the zones, at above two orders magnitude. The elements MgO, CaO and Na_2O show large discrepancies over the various zones.

There is depletion in FeO, for samples from the wall zone. All the samples show depletion in CaO, with a higher magnitude of depletion from the wall zone. In the border, wall, intermediate and core zones, K_2O has a wide spread of both enrichment and depletion. Such a large depletion could be due to the removal of the element from the melt during crystallization within another zone.

Minerals found within the Noumas I pegmatite of Ca-bearing nature include apatite and grossular. The Fe-bearing minerals form the Noumas I pegmatite are tantalite, triplite and almandine. The wide discrepancies for K can possibly be due to the minerals such as microcline, muscovite and lepidolite all found at various modal proportions in the Noumas I pegmatite.

It should also be noted while sampling from a pegmatite, it is difficult to get a representative sample for the entire area, as the grain sizes of minerals present are large. The amount that is sampled should be rather large in order to truly represent the various zones under investigation.

The whole rock data for the Noumas pegmatite (Figure 4-34) when compared to upper continental crust shows enrichment of SiO_2 samples in the continental crust. The crust is also

enriched in Al_2O_3 four times higher than crustal abundances. The different zones appear to be depleted in Fe_2O_3 and TiO_2, and highly depleted in CaO. This could be indicative of a S-type rather than and I-type source rock. The main reasons for these large discrepancies would be a direct result of non-representative sampling that occurred.
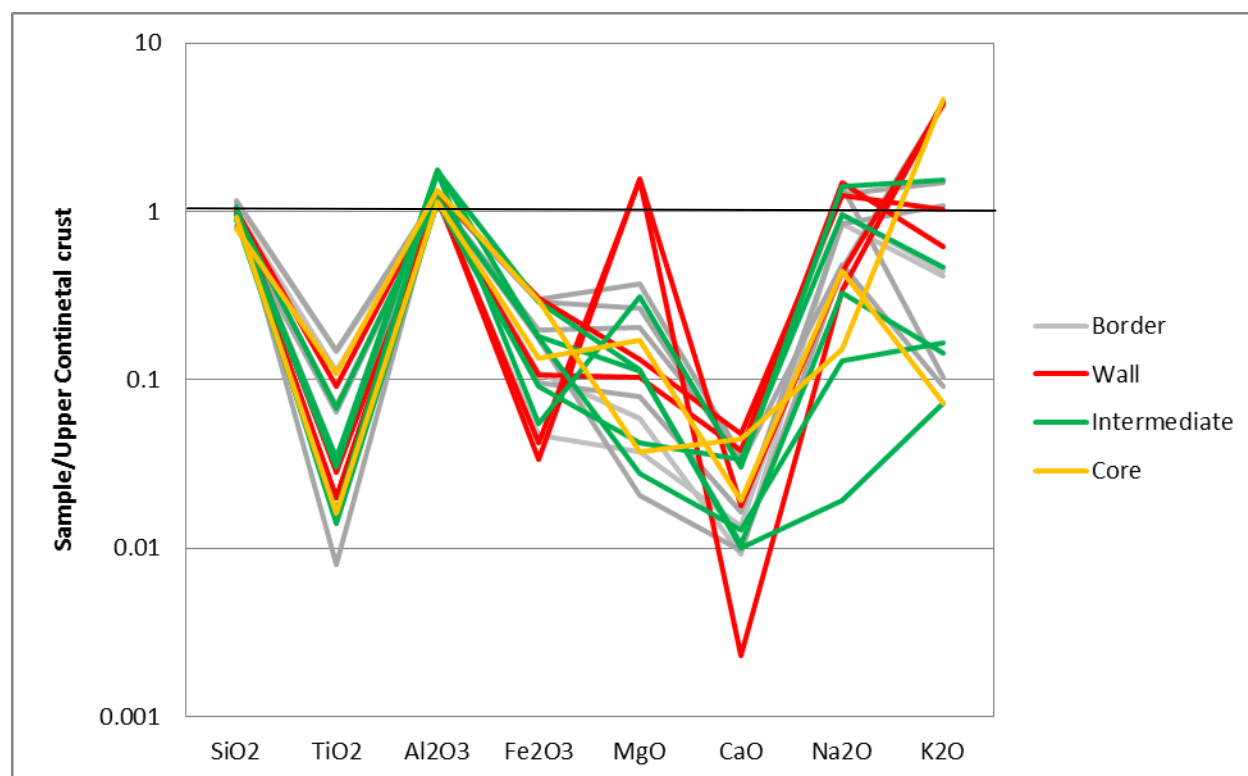
Figure 4-34: Major elements of the Noumas I pegmatite, samples normalized against upper continental crust (Taylor and McLennan, 1985) from the border, wall, intermediate and core zones.

The REE plot shows bulk enrichment in all the elements for the core, suggesting more evolved and therefore enriched in incompatible REE's. The wall and intermediate zones are depleted in Ce, Nd and Pr. The Ce anomaly in a sample indicates a state of oxidation within the Noumas I pegmatite (Figure 4-17). In the sample area that has been highly oxidized, most Ce occurs as Ce^{4+}. In the event of oxidation fractionation occurs within the zones.

The core zone is more oxidized based on the positive Ce anomaly. The high oxidized state causes the elements such as Ce, to be leached from the melt at the outer zones (wall and intermediate) leading to negative Ce anomalies compared to the upper continental crust.
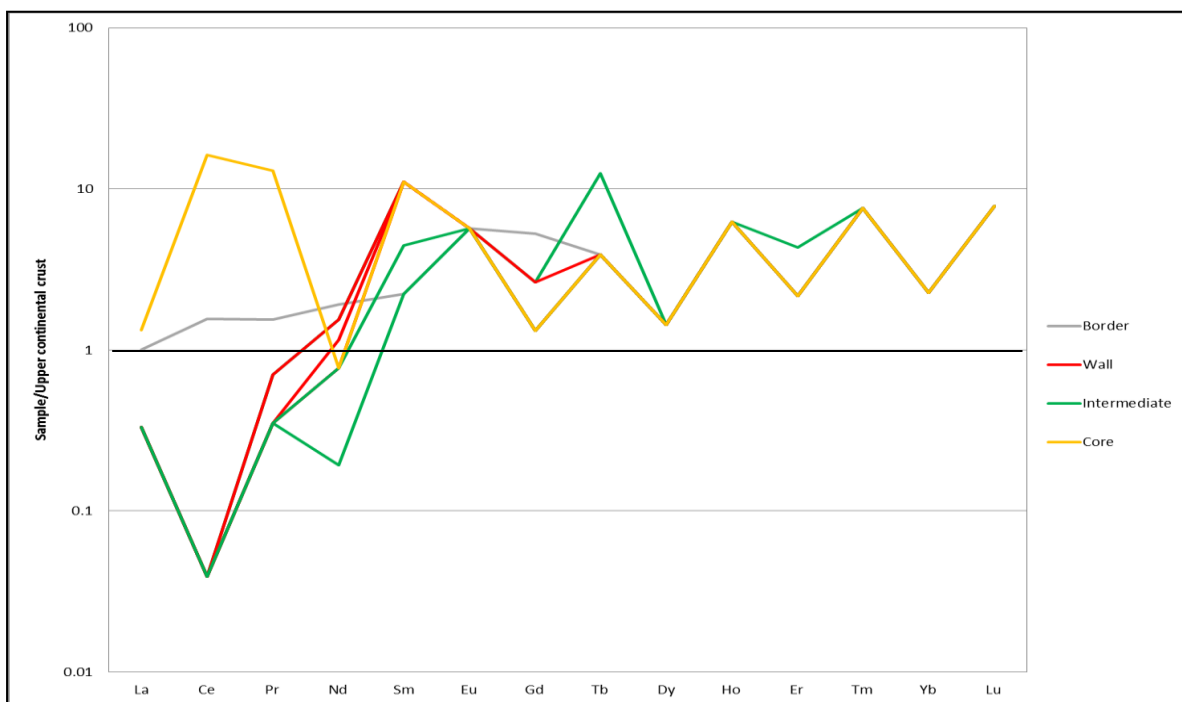
Figure 4-35: REE of the Noumas I pegmatite, samples normalized against upper continental crust (Taylor and McLennan, 1985) from the border, wall, intermediate and core zones.
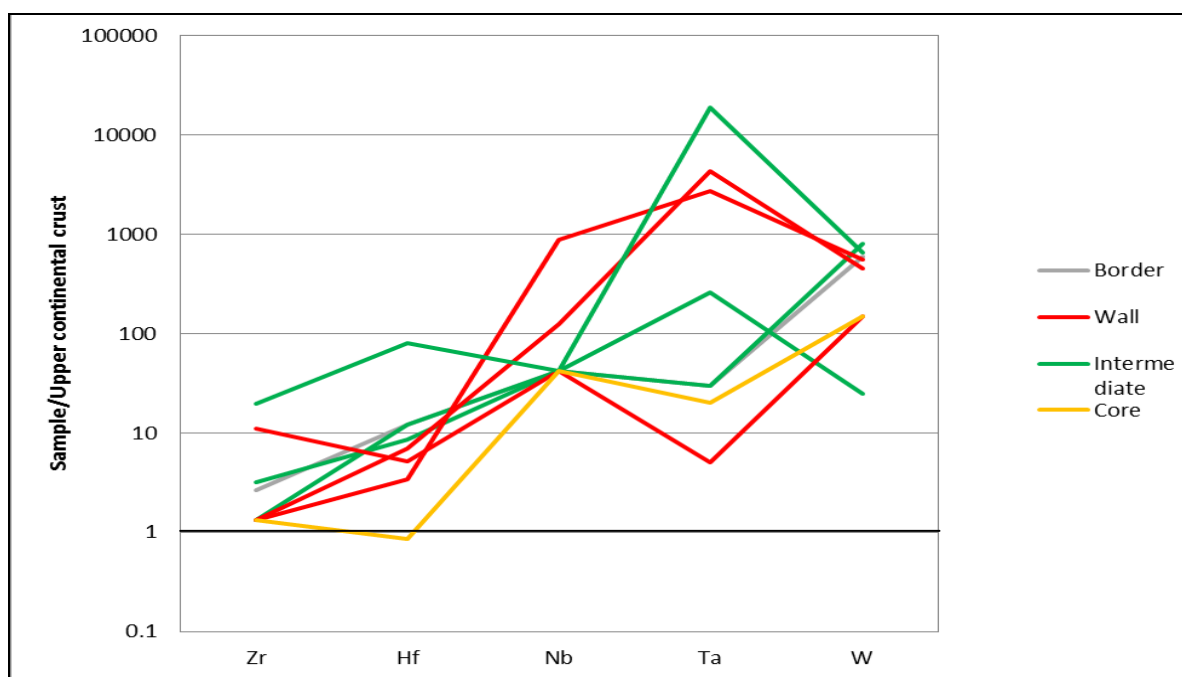
Figure 4-36: High field strength elements of the Noumas I pegmatite, samples normalized against upper continental crust (Taylor and McLennan, 1985) from the border, wall, intermediate and core zones.

The high field strength elements (Figure 4-18) show a strong enrichment in Zr, Hf, Nb, Ta and W for all four zones of the Noumas I pegmatite. The Ta distribution ranges over 4 orders of magnitude enrichment, indicating its variable occurance in the pegmatite.

Major element variation diagrams show the relationship between the cooling magma and the crystallized rocks. The samples submitted for XRF analyses were taken from the border, wall, intermediate and core zones. The large sections sampled from the pegmatite, were crushed and powder pellets and fusion discs made. The data was placed on Harker diagrams against SiO_2 (Figures 4-19 to 4-26).

The chemical compositions for the minerals quartz, alkali-feldspar and albite taken from Deer et al. (1997), were plotted on the Harker diagrams to indicate possible composition similarities for the samples from the border, wall, intermediate and core zones. During the melting or removal of quartz, plagioclase and feldspar the elements Si, Al, Na, K and Ca are depleted and Fe and Mg were concentrated in the melt. The major elements and the mineral compositions (quartz, albite and alkali-feldspar) are discussed according to the major elements.

The Al_2O_3 vs. SiO_2 diagram (Figure 4-19) suggests a combination of alkali-feldspar, albite and quartz compositions. The Fe_2O_3 values of the wall and core samples have a higher range than albite and alkali-feldspar compositions (Figure 4-20). The majority of the MgO values in the wall, intermediate and core samples tend towards the alkali-feldspar compositions (Figure 4-21).

The dominant resemblances within the Na_2O samples (Figure 4-22) are towards quartz mineral compositions. The K_2O values of the intermediate and core zone samples tend towards an alkali-feldspar composition but the majority of the samples are compositionally close to an composition between albite and quartz (Figure 4-23). The border, wall, intermediate and core samples are low in CaO compared to the expected amount for an alkali-feldspar composition (Figure 4-24). The low CaO values of all the zones, wall, intermediate and core samples are near to that of an albite composition. The TiO_2 values for the border and intermediate samples group around an albite towards quartz composition than alkali-feldspar (Figure 4-25). The P_2O_5 content from the intermediate and border zones tend towards albite compositions, with border and intermediate zone samples lying close to an alkali-feldspar composition (Figure 4-26).
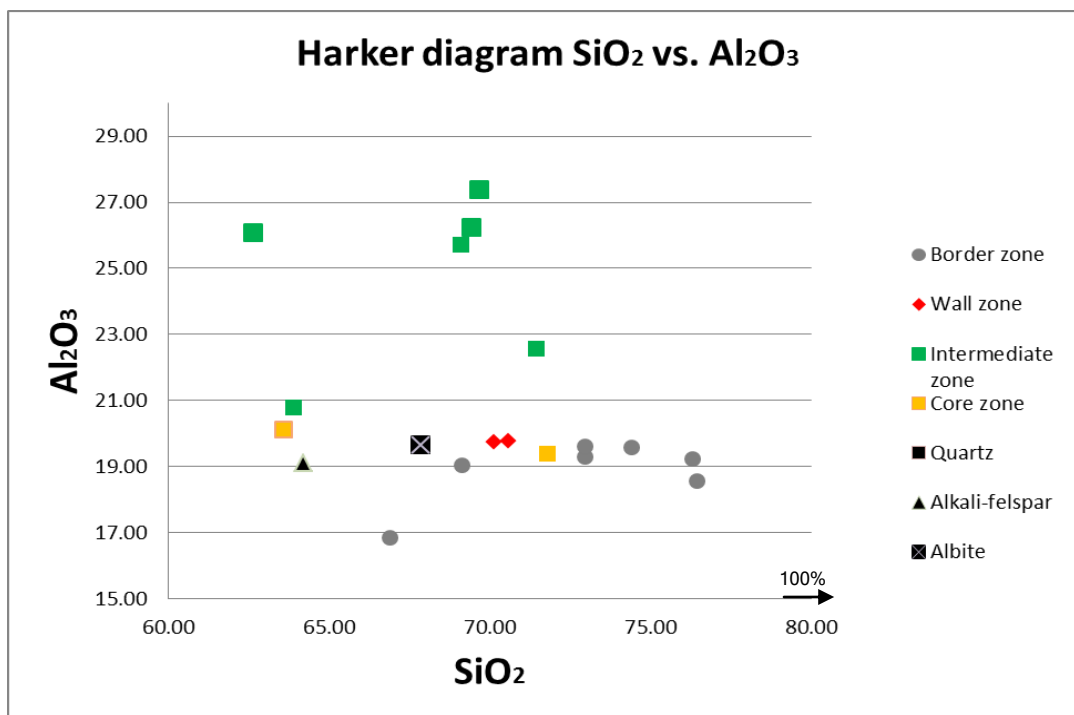
Figure 4-37: Harker diagram for Al$_2$O$_3$ versus SiO$_2$.
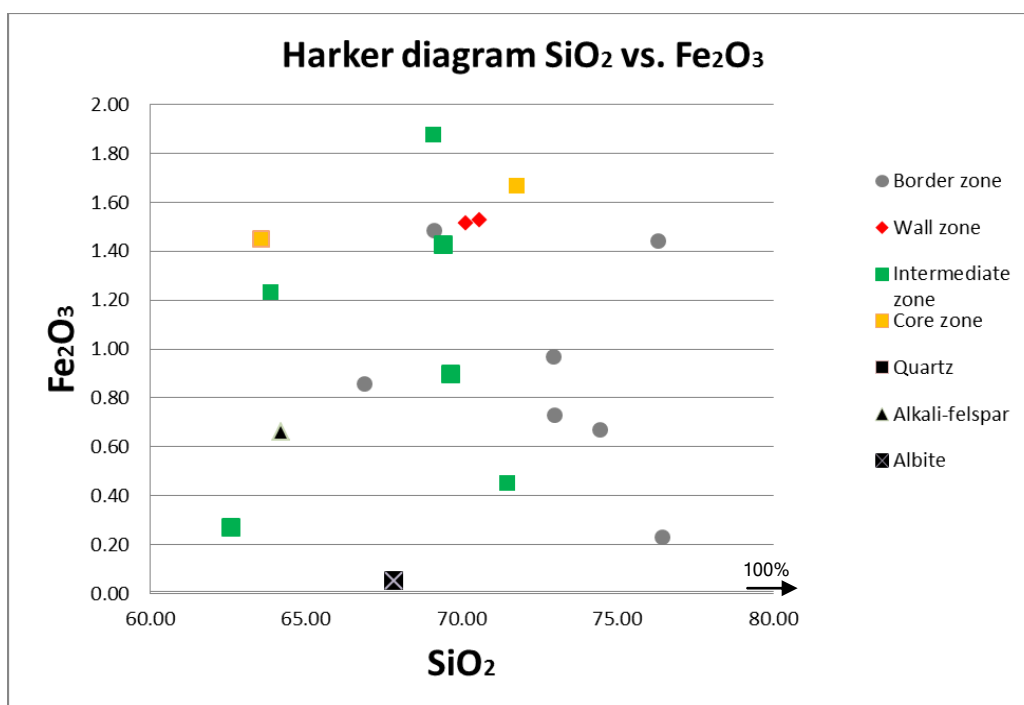
Figure 4-38: Harker diagram for Fe$_2$O$_3$ versus SiO$_2$.
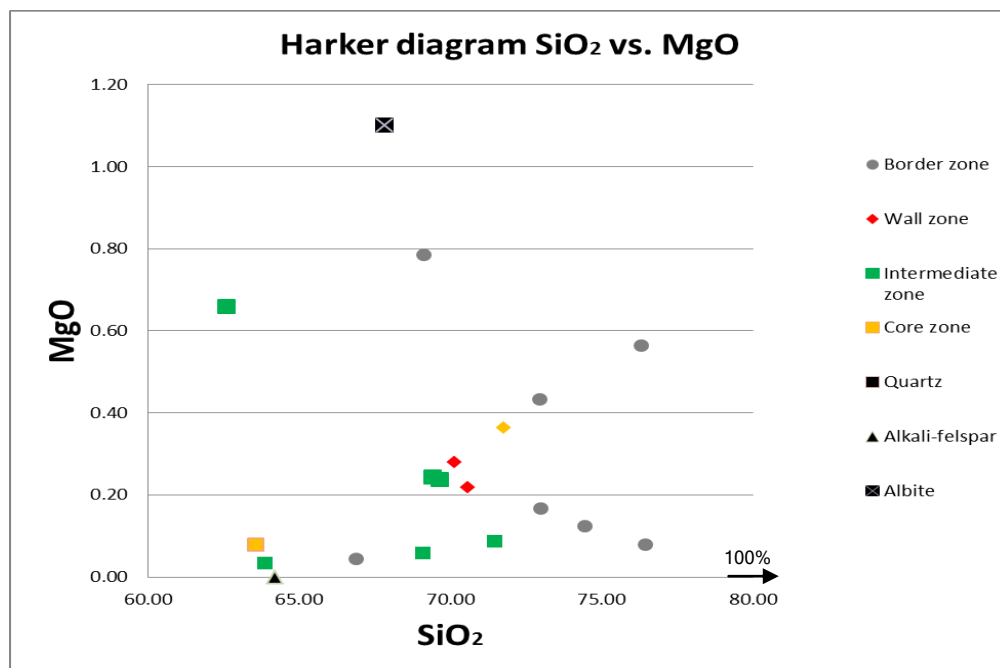
Figure 4-39: Harker diagram for MgO versus SiO$_2$.
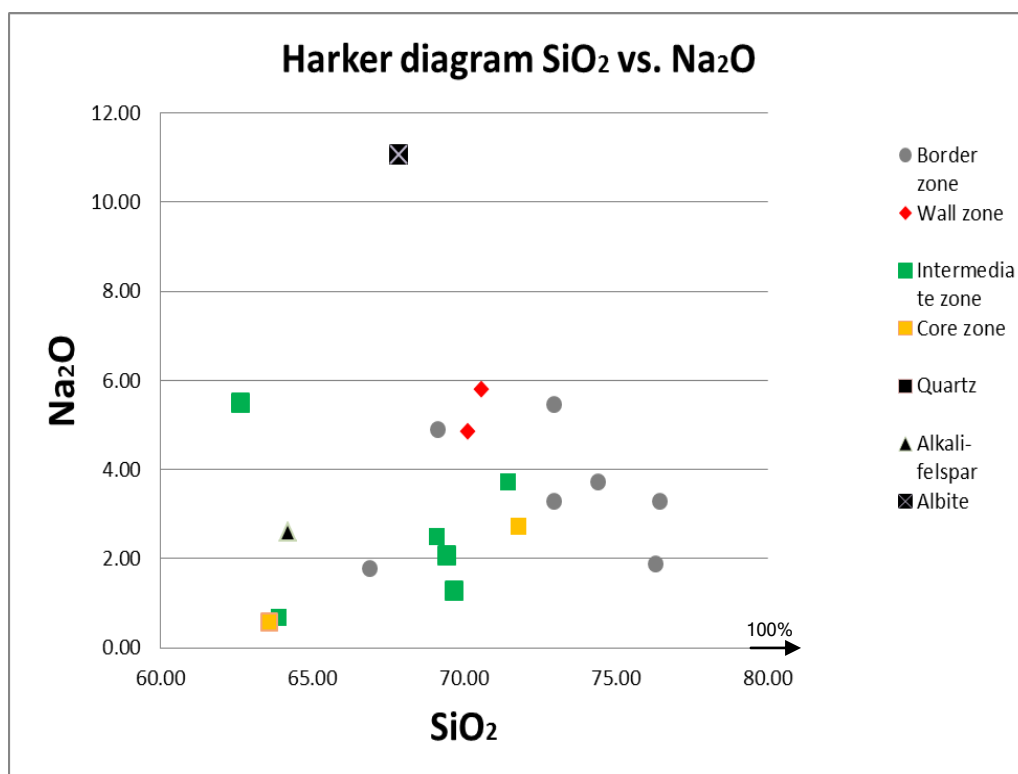
Figure 4-40: Harker diagram for Na$_2$O versus SiO$_2$.
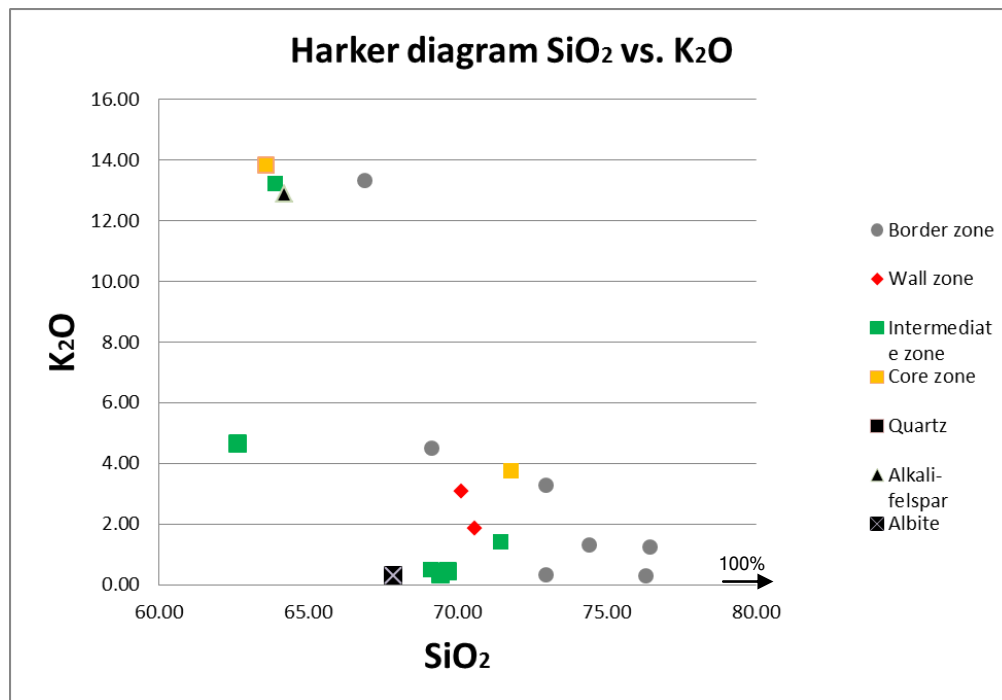
Figure 4-41: Harker diagram for K_2O versus SiO_2.
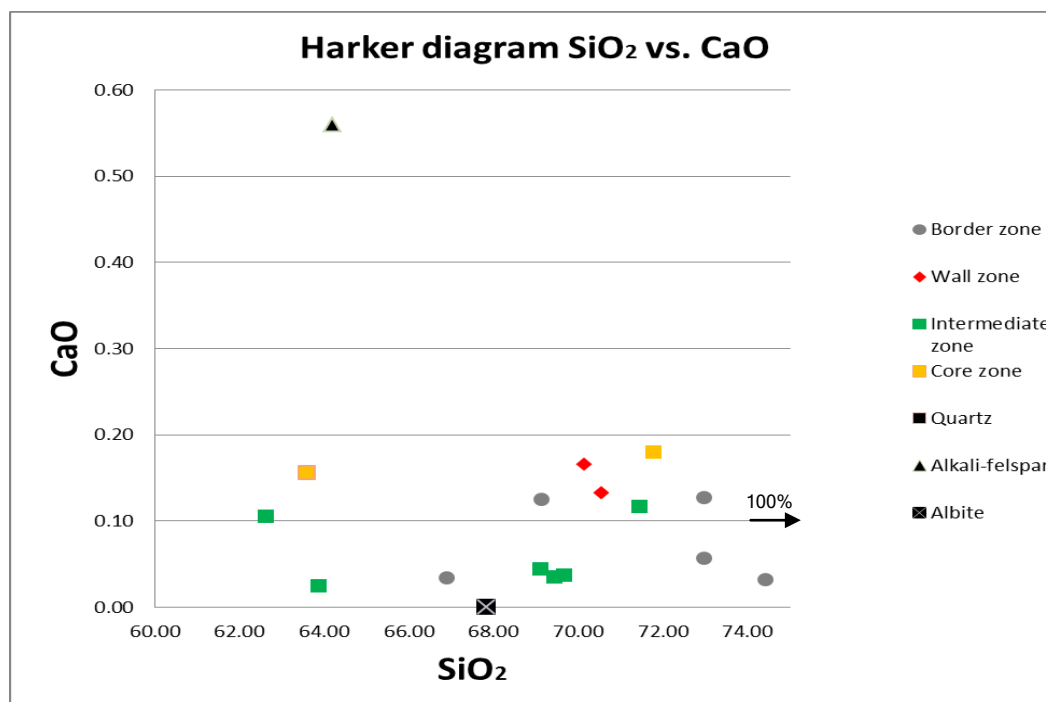
Figure 4-42: Harker diagram for CaO versus SiO_2.
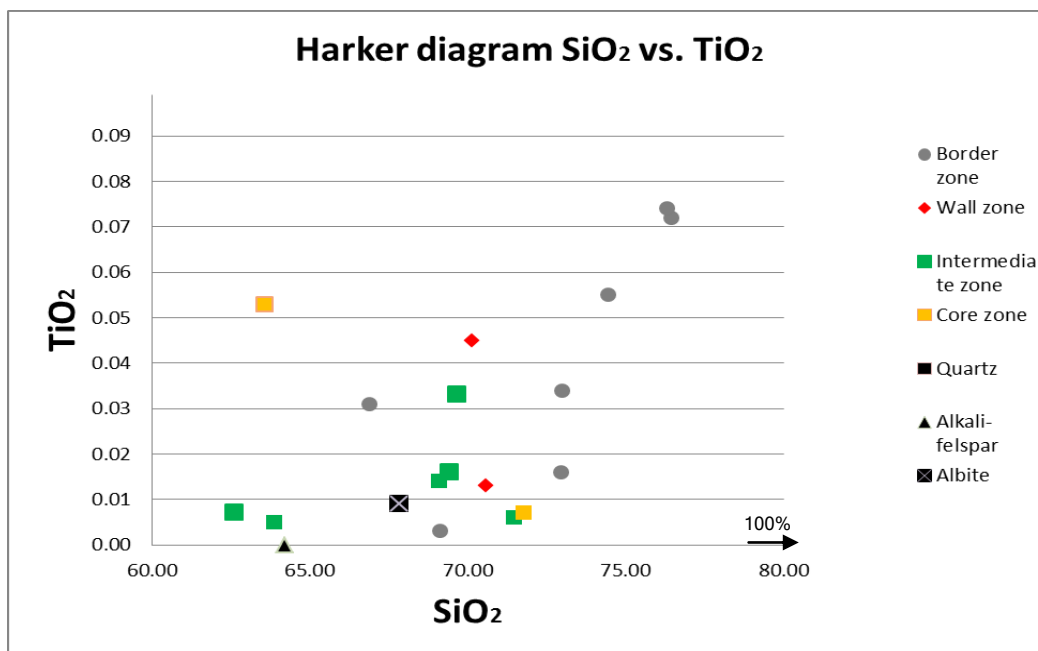
Figure 4-43: Harker diagram for TiO$_2$ versus SiO$_2$.
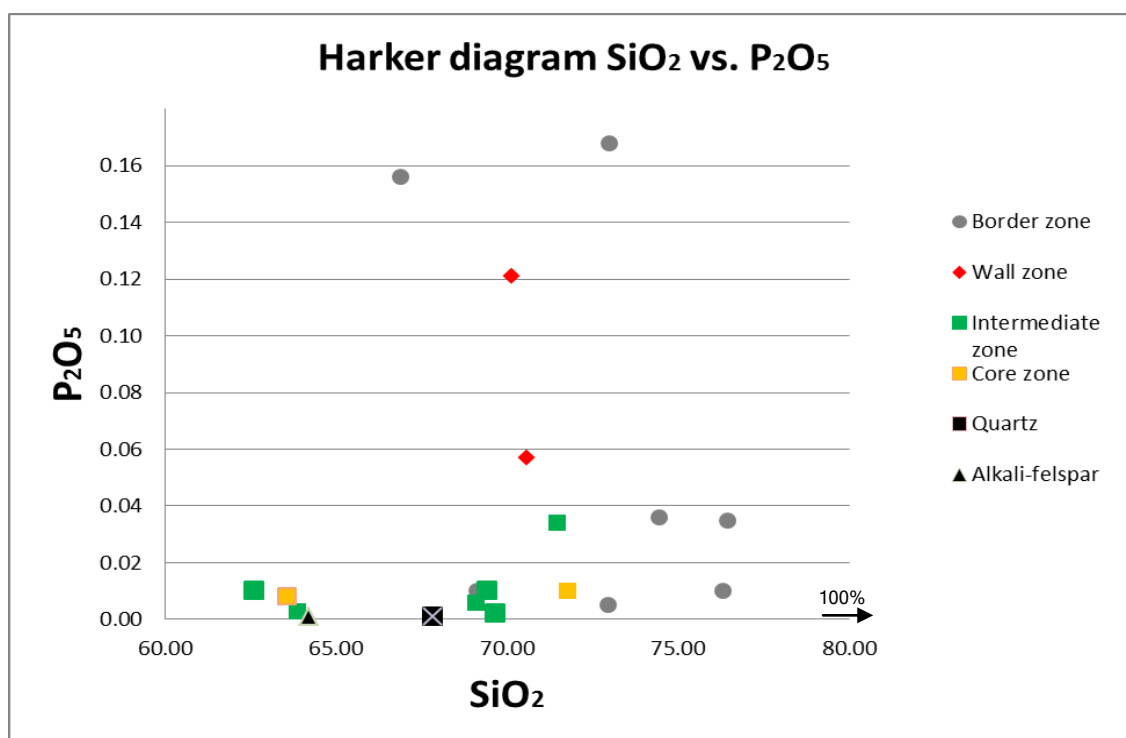
Figure 4-44: Harker diagram for P$_2$O$_5$ versus SiO$_2$.

The sample distributions for the various plots against SiO_2, do not show any correlated differentiation trends, the samples are scattered over the compositions of albite, alkali-feldspar and quartz. This is not the typical chemical distribution for igneous rocks and again the non-representative sampling can be the main reason for the lack of the differentiation trends.

The trace element distribution data graphically shows the concentrations within the Noumas I pegmatite (Figure 4-28). The pie charts illustrate the trace element contributions within the different zones (%) as well as along the pegmatite. The trace elements erratic distribution of minerals is due to the minerals that they are found in. The trace element Rb has relatively high values in the zoned area of the pegmatite and tends to decrease for samples taken along the strike of the pegmatite.

Rb is a highly incompatible element and during fractional crystallization it will stay in the magmatic melt than become part of mantle minerals (Jacobsen et al., 2000). The element Sr during fractional crystallization is concentrated in plagioclase. Sr is low in the zoned areas of the pegmatite and higher concentrations are found along the pegmatite and within the border zone (Figure 4-27). The Rb/Sr ratio would increase, during fractional crystallization, in the mineralogical order of plagioclase, hornblende, K-feldspar, biotite and muscovite (Faure, 2001).

Rb and Sr concentration data was used in order to determine if the magma had been highly fractionated. The Rb/Sr ratio in Figure 4-28 decreases from the wall zones to the core zone. The highest Rb values are expected within the core zone and the highest Sr within the border zones. The Noumas I pegmatite has a higher Rb and Sr concentration in the wall zones. The high Rb/Sr ratios, according to Halliday et al., (1991) can be explained by sub-solidus fluid-rock interaction.
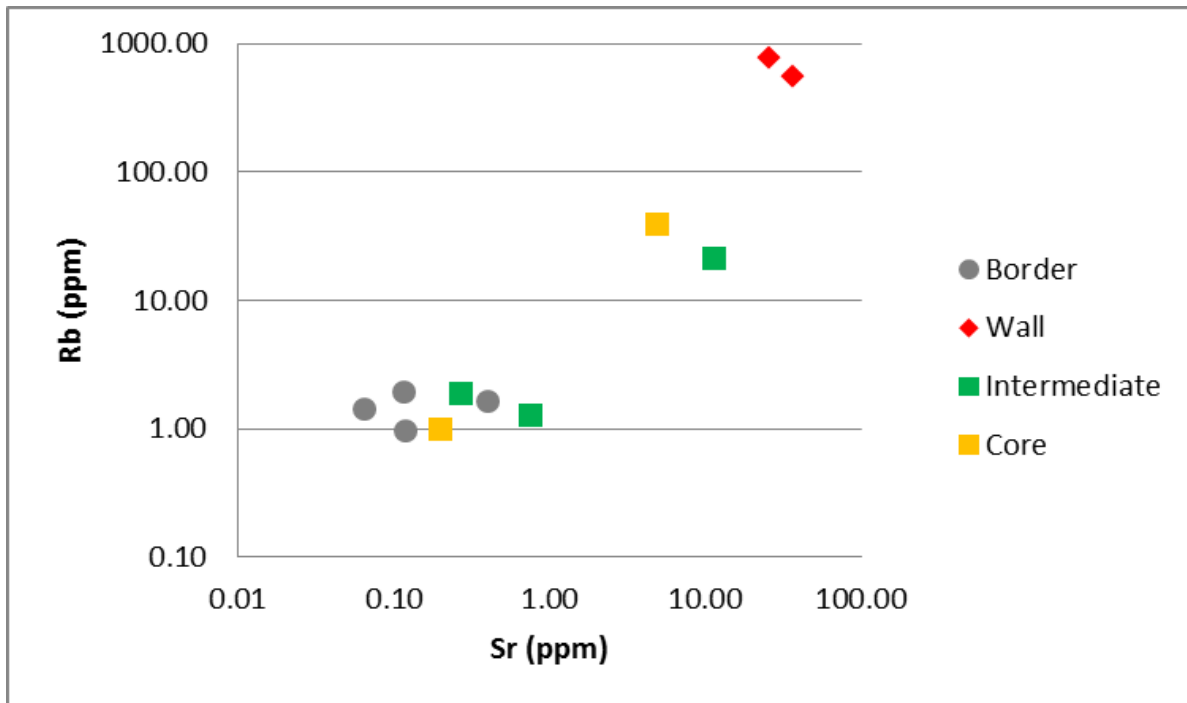
Figure 4-45 The Rb vs. Sr concentrations within the border, wall, intermediate and core zone of the Noumas I pegmatite.

The Nb concentration is generally low or the same along the pegmatite for the wall, intermediate and core zones. The only increase in Nb is found in the border zone at the direct contact with the wall zone (Figure 4-28). A possible reason for the increase of Nb would be the occurrence of the mineral columbite-tantalite. Zr gradually decreases along the pegmatite (Figure 4-28), during zircon crystallization the Zr is removed from the magma, depleting the pegmatite forming magma of Zr. The Th concentration is higher within the intermediate zone of the pegmatite but again decreases along the length of the pegmatite. The presence of the mineral thorite will show enrichment in the trace element Th.

Cu, Ni, Cr, Zn and Pb concentrations are higher in the core and intermediate zones (Figure 4-28). Sb concentrations from the intermediate zones of the pegmatite are high in comparison to the border, wall and core zones (Figure 4-28).

Trace element concentrations of the various zones of the pegmatite were normalized to chondritic compositions of Thompson (1982) and were plotted in an order of increasing compatibility. Deposits associated with felsic igneous rocks often have higher concentrations of lithophile elements such as Li, Be, F, Sn, W, U and Th. The enrichment of these lithophile

elements within the differentiated melts is caused by their geochemically incompatible nature (Wood et al., 1979).

The trace elements for the Noumas I pegmatite have relativley high concentrations of large ion lithophile elements (LIL) such as Rb, Ba, Cs, Sr and moderate field strength elements (HFS) such as Zr, Hf, Nb, Ta, U, Th, Y (Figure 4-29). High-transition metal contents such as Ti are also present. The moderate values of HFS probably reflect the presence of accessory minerals such as zircon. The mobility of LIL elements are largely controlled by the behavior of fluid phases. HFS element concentrations are controlled by the chemistry of the magma source compositions and crystal/melt processes that take place during the evolution of the melts.

Individual minerals such as zircon, apatite and plagioclase strongly control the concentrations of Zr, P and Sr. The ionic charges of incompatible elements cause them to be excluded from the crystallization sequence. Instead they are concentrated into differentiated residual magmas. More mobile LIL element concentrations are controlled by aqueous fluids that are concentrated in the continental crust and used as an indicator for crustal contamination of magmas. Figure 4-28 shows a spider diagram of pegmatite trace element compositions normalized against chondrite after Thompson (1982). An overall strong enrichment for most elements is expected for highly differentiated and thus more evolved pegmatites.

The spider diagram normalizing values for Rb, Th and K with a slightly lower Nb correlates with that of chondrite. There is also a dip/decrease in more compatible element ratios towards the right. At the Noumas I pegmatite, these elevated sample/chondrite values indicate a shallower depth of intrusion based on the elemental values dominantly from the upper continental crust.
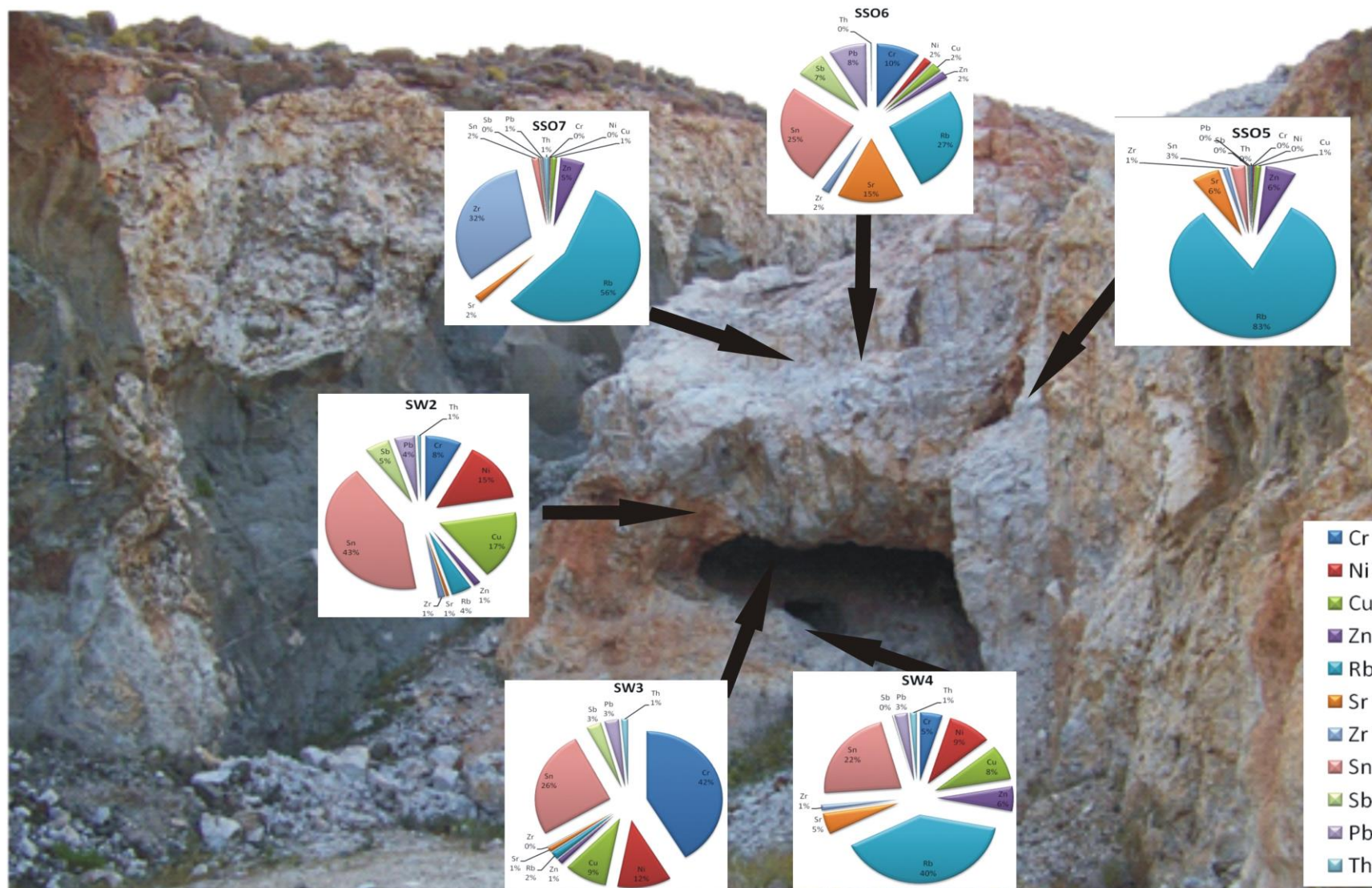
Figure 4-46: Trace element distribution based on XRF data (wt. %) through the various zones sampled as well as along the pegmatite.

The values of Rb, La, P and Ti are high and indicate that the melt is derived from the crust. The precipitation of secondary phases as well as sorption and co-precipitation processes influence the retention or release of trace elements (Lottermoser and Ashley, 2006). It is possible to have an enriched Li, Cs, Ta pegmatite with other elements such as Sr, P and Zr below the detection limit.

The same geochemical characteristics apply to the Ehrenfriedersdorf pegmatite in Germany. This pegmatite contains Li in thousand parts per million and weight percentage levels of Rb and Cs but Ta is below the detection limit (Linnen et al., 2012). For more evolved pegmatites, the concentration of incompatible Rb and Li increases with a decrease of Ba during differentiation, placing the more evolved pegmatites at later stages of differentiation and highly enriched in incompatible elements. Noumas I is highly enriched in incompatible elements and is regarded as an evolved pegmatite as a result of this, as well as the complex mineralogy found within the zoned pegmatite.
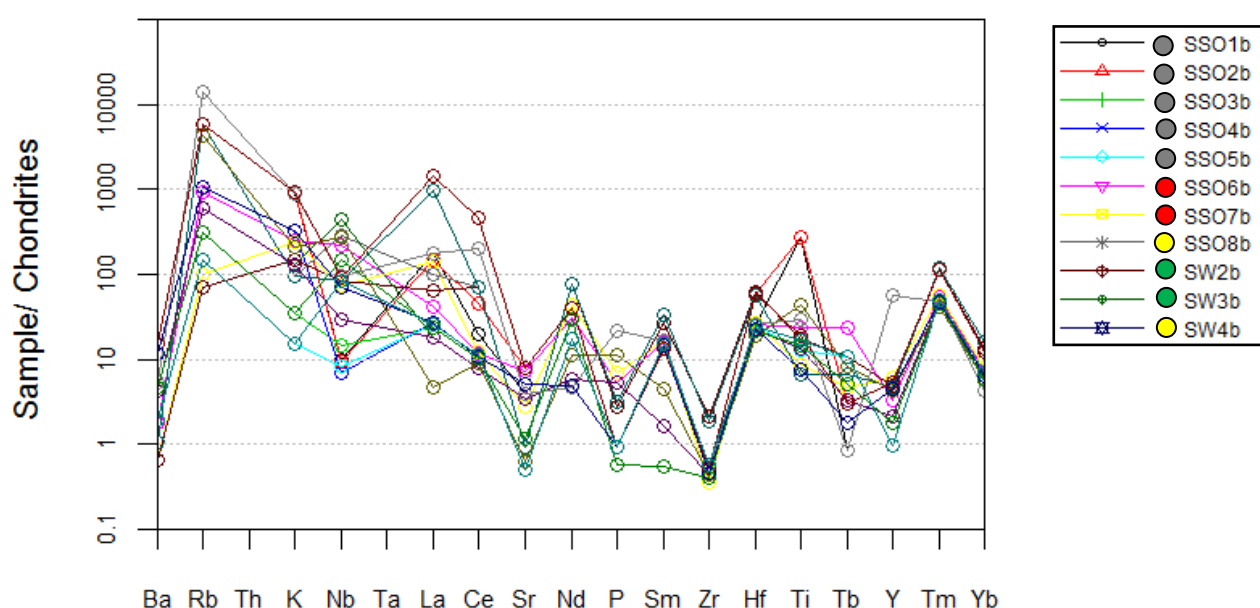
Figure 4-47: Noumas I pegmatite samples normalized against chondritic values (Thompson, 1982) the border (grey), wall (red), intermediate (green) and core (yellow) represent the different zones of the Noumas I pegmatite.

The overall trend in Figure 4-29 shows a negative dip towards more compatible elements. The Noumas I pegmatite for the samples taken from the border show lower values for Sr, P and Zr. Ti tends to be higher and the Zr lower, suggesting that zircon melted out of the parent magma. A possibility for the depletion of these elements would be the early crystallization of plagioclase, zircon and apatite that removes the elements before the

pegmatite crystallized. Thus the pegmatitic melt was depleted in the Zr, Sr and P (Figure 4-30).
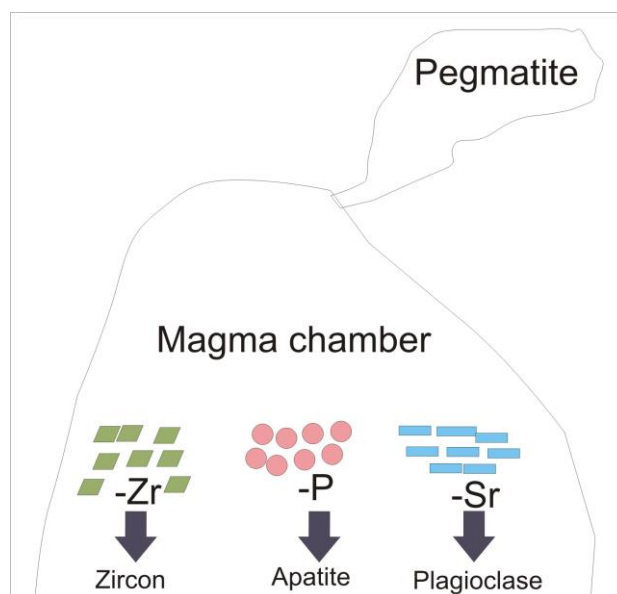
Figure 4-48: An illustration of the parental magma for the Noumas I pegmatite melt.

4.4 Estimation enrichment for the source granite melt

In order to have an approximate estimation of the amount of enrichment the granitic melt underwent to produce the Li-rich intermediate zone within the Noumas I pegmatite, a mass balance calculation based on the stoichiometric values for each Li-bearing mineral within the intermediate zone was carried out. The concentration of Li within the intermediate zone for the minerals spodumene, lepidolite, amblygonite and triplite was taken from Deer *et al.*, (1997) and Garret (2004). The concentrations of the specific minerals are then multiplied by the estimated amount and the volume that the intermediate zone occupied. The value is divided by the total volume of the pegmatite.

First the area was estimated for the 350 m long and 25 m wide Noumas I pegmatite, using the formula for a circle (Figure 4-31), it was assumed that the pegmatite zones are concentric in shape ($A = \pi \cdot r^2$). The total area for each zone is shown in Table 4-6.
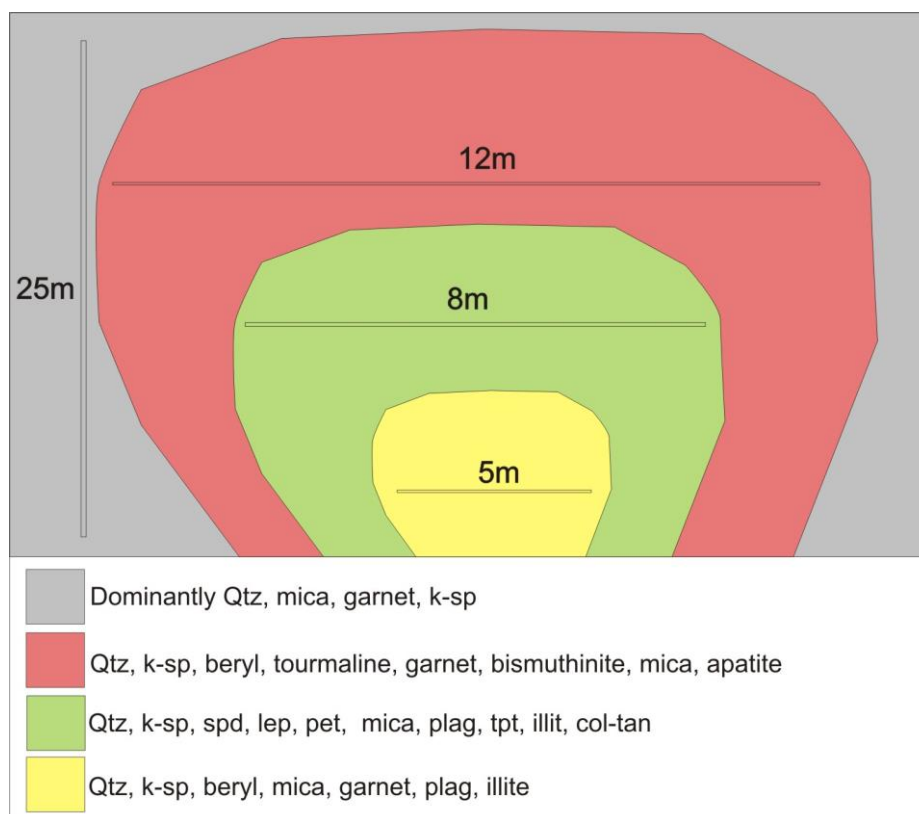
Figure 4-49: The mineral distribution and well as the dimensions of the Noumas I pegmatite, on which the enrichment equitation was based.

In order to obtain the volumes of the various zones the other areas should be subtracted from the entire volume. For example, the wall zone has a total area of 113.10m^2, but the area occupied by the intermediate zone should be removed before the volume for just the wall zone can be calculated (Table 4-6). For Li$_2$O= $(6.941)^2$ + (15.994) =29.88 g/mol. The Li (wt %) was worked out and is given in Table 4-7 along with the ppm values for the specific lithium minerals.

Table 4-8: The area and volume determined for the wall, intermediate and core zones of the Noumas I pegmatite (z=zone, L=length, A=area,r =radius)

Zone	Area ($A = \pi \cdot r^2$)	Volume ((A-z)*L)
Wall	6^2 22/7 =113.10m^2	21990.5m^3
Intermediate	4^2 22/7 =50.27m^2	10720.5m^3
Core	$2.5^2$22/7 =19.64m^2	6874m^3

Table 4-9: Li$_2$O content (wt%) used to determine the lithium enrichment of the granite source rock.

Mineral	Avg.Lithium (wt%Li_2O)	Lithium (wt% Li)	Lithium content (ppm)	Resource
Spodumene	4.2	1.928	19280.56	Deer *et al.*, 1994
Lepidolite	4.4	2.021	20209.74	Deer *et al.*, 1994
Ampblygonite	7.0	3.252	32521.42	Garret 2004
Petalite	4.4	2.021	20209.74	Deer *et al.*, 1994
Triphylite	9.7	4.504	45042.17	Garret 2004
Lithiophillite	10.7	4.966	49664.85	Garret 2004

After the area and the volume (m^3) were estimated (Figure 4-32 and Table 4-6) the bulk mass (kg) for the Noumas I pegmatite was determined (Table 4-8). The area is assumed as a concentric circle and the areas that overlap are subtracted before the volume can be determined for the wall, intermediate and core zones. The average density of the granite is assumed for this exercise at 2650 kg/m^3. In order to estimate the lithium reserve the mass for each zone needs to be established. This is done by multiplying the density (kg/m^3) with the volume (m^3).

Table 4-10: The mass (kg) for the wall, intermediate and core zones.

Zone	Volume x Density	Mass (kg)
Wall	21990.5*2650	58274825
Intermediate	10720.5*2650	28409325
Core	6874*2650	18216100
Total mass		**104900250**

The average lithium minerals observed in Table 4-7 for all the samples from the intermediate zone was determined by taking the average Li-minerals determined by the modal proportions multiplied by the Li (wt %). In the samples from the intermediate zone the only lithium minerals present was spodumene and lepidolite ($\sum$Avg.$_{Spod}$ x 1.928 wt % Li + $\sum$Avg.$_{lpd}$ x 2.021 wt % Li = 1.028596 %). The concentration of lithium within the intermediate zone was calculated by taking the mass of the intermediate zone multiplied by the concentration of Li within the intermediate zone. 28409325 x 1.028596/100. Mass of Li within the intermediate zone will then be 292217.2. To get the Li concentration for the entire pegmatite

(Equation 1), the lithium within the intermediate zone is divided by the total mass for the intermediate zone x 100.

$[Li]_{intermediate\ zone}$ /mass $Li_{(pegmatite)}$ x 100 **Equation 1**

292217.2/104900250 x 100= 0.2786%

In order to convert 0.2786% to ppm it is multiplied with 10000.

According to Levinson (1974) the trace element distribution patterns in parent pegmatite rocks with Li, Be and Ta range between 25-300 ppm and a probability estimation for Li at 40.5 ppm. After the Li content within the intermediate zone is calculated, an estimate for the enrichment that has occurred in the parental granite is done. The 40.5 ppm was converted to wt% (0.00405). In order to determine the enrichment in the granite, the concentration of lithium in the whole pegmatite (Equation 2) is divided by the concentration lithium in the source granite.

Enrichment= [2785.67 ppm]/ [40.5 ppm]* 100 =6878.20% **Equation 2**

The total enrichment of lithium in the Noumas I pegmatite compared to a typical lithium enriched granite of 40.5 ppm is 6878.20%.

4.5 Summary of results

The various zones documented in the field for the Noumas I pegmatite are illustrated in Figure 4-32. The zones are estimated and divided into the wall, intermediate and core zones based on the mineralogical differences seen within the zones. These minerals provide clear boundaries to divide the pegmatite into the different zones.

The different analytical techniques (XRD, Microscopy, XRF, ICP-MS, SEM-EDX) employed at the Noumas I pegmatite showed the correlations and the differences over the wall, intermediate and core zones. The major differences for the mineralogy, petrology and geochemistry have been summarised in Table 4-9. This includes the structural and textural differences for the wall, intermediate and core zones of the Noumas I pegmatite.
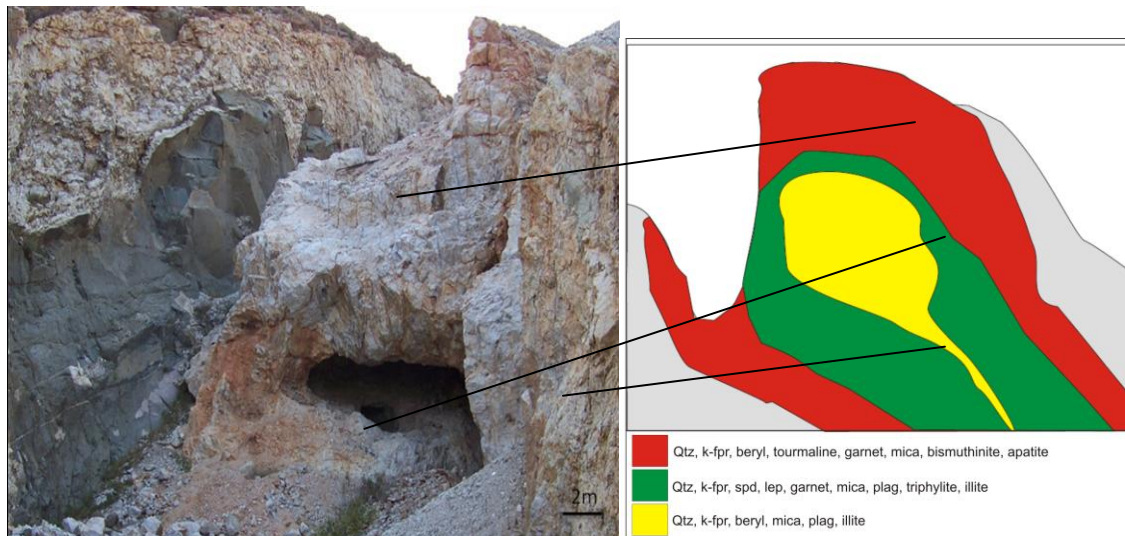
Figure 4-50: Noumas I pegmatite with the border (grey), wall (red), intermediate (green) and core (yellow) zones. The differentiations of the zones are based on mineralization within the pegmatite.

Table 4-11: Summary for the different analyses done on the Noumas I pegmatite of the wall, intermediate and core zones. Coarse(>5cm), medium(1-5cm) and fine (<1cm). high = >1.5 ppm , low = <1.5 ppm .

Zone	Zone 1	Zone 2	Zone 3
Area	Wall/outer	Intermediate/middle	Core
MINERALOGY **XRD**	Qtz , K-fsp, beryl, tourmaline, garnet, mica bismuthinite , apatite	Qtz, K-fsp, spd, lep, garnet, mica plag, triphyllite, illite	Qtz, K-fsp, beryl, mica plag, illite
PETROGRAPHY Crystallinity Crystal size Crystal shape	Large intergrowntexture between qtz and k-fsp Holocrystalline Coarse Idiomorphic	Intergrown texture between qtz and K-fsp Holocrystalline Coarse and medium Hypidiomorphic	Exsolution texture (Perthite) Holocrystalline Coarse and fine Hypidiomorphic
GEOCHEMISTRY Major elements Trace elements	Distribution constant (SiO_2, Al_2O_3). Na_2O increases as K_2O decreases towards middle zone Distribution increases towards the middle zone (MgO, Fe_2O_3) Low: Cr, Rb, Sr, V (compared to zone 2 & 3) High: Zr, Nb, Sb	Distribution relatively constant (SiO_2, Al_2O_3). Na_2O increases as K_2O decreases towards core zone Distribution fluctuates towards the core zone (MgO, Fe_2O_3) Low: Zr, Nb, Rb, Sr (compared to zone 1 & 3) High: Cr, Sb, V	Distribution relatively constant (SiO_2, Al_2O_3). Na_2O increases as K_2O decreases away from the middle zone Distribution fluctuates (MgO, Fe_2O_3) Low: Zr, Nb, Sb (compared to zone 1 & 2) High: Cr, Rb, Sr, V

Chapter 5: MICROTHERMOMETRY & RAMAN-FTIR STUDIES

Petrographic studies using the Olympus BX51 microscope was used to identify the presence of fluid inclusion assemblages, of both heterogeneously and homogeneously entrapped fluids, within the doubly polished thick sections. Initially primary inclusions were identified as well as a distinctive mix of secondary inclusions with lower homogenization temperatures and salinities.

Microthermometric analyses were conducted on samples from the border, wall, intermediate and core zones of the Noumas I pegmatite (Appendix 4). A limited number of Fourier Transform Infrared (FTIR) and Raman spectroscopic analyses were done to constrain the chemistry within the fluid inclusions of selected minerals. The combination of microthermometry, FTIR and RAMAN studies performed on fluid inclusions, determined the physiochemical properties of exsolved magmatic fluid, the formation temperature, salinity and chemistry of solutes.

Fluid inclusions are more than just temperature indicators during formation of the deposit. The main goal of fluid inclusion measurements have changed from determining the temperature of various geological processes to estimating the pressure and depth at the time of inclusion trapping and is used to determine the density of ore fluids (Roedder and Bodnar, 1980; Roedder, 1984; Raeside, 2003).

5.1 Petrography of fluid inclusions hosted in quartz

Fluid inclusions discussed in this chapter may be subdivided into two general types, namely those with low to moderate salinities and those with higher salinities. These two types are further distinguishable based on size, cooling rate and volatile content influence. The low to moderate salinity type of fluid inclusions appear to have similar shapes and sizes for vapour to liquid ratios. The higher salinity type inclusions appear more isolated and somewhat larger in size than surrounding inclusions. The various inclusion types and their distributions are illustrated to show the prominent differences amongst them (Figures 5-1 to 5-4).

The different sizes and shapes as well as the compositional variations provide evidence for multiple fluid generations during the crystallization event of the Noumas I pegmatite. The sizes and shapes of the inclusions measured within the zones of the Noumas I pegmatite vary significantly (Figure 5-1 to Figure 5-8). The inclusions are dominantly aqueous phases with a gas phase sealed within it. In some cases, both gas (CO_2) and solid phases are found

in the aqueous phase. Large, dark inclusions, gaseous in nature, also exist within the observed inclusions.
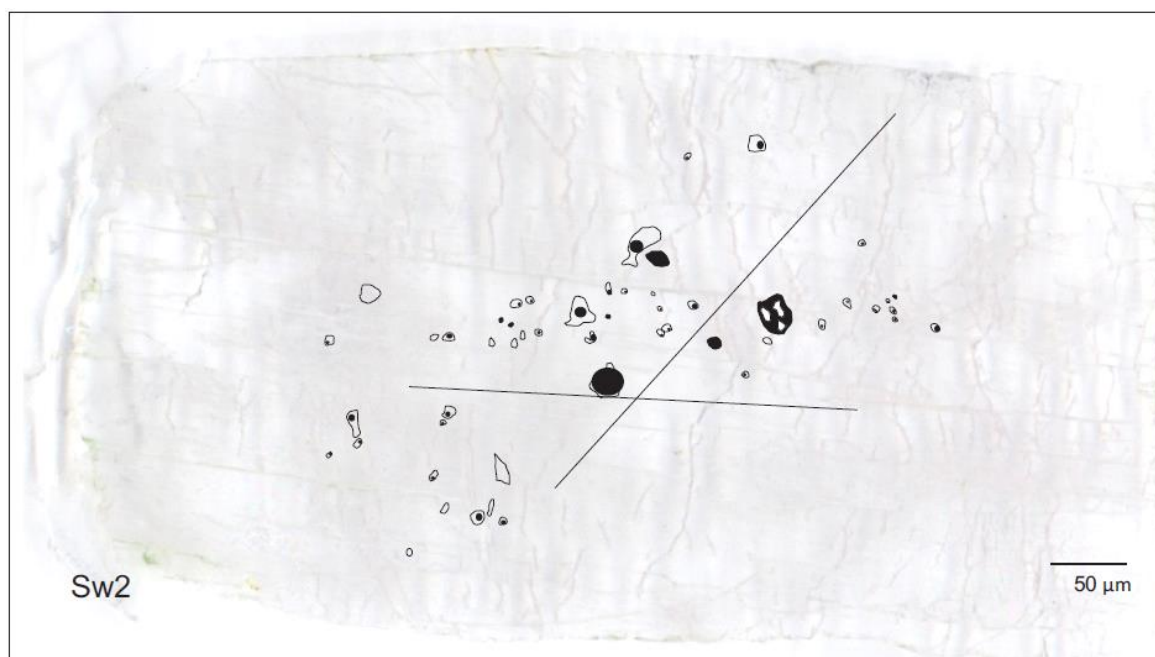
Figure 5-51: Overlay of fluid inclusions onto a thick section scan as observed in sample SW2 (intermediate zone). Inclusions appear to be a mixture of primary and secondary.
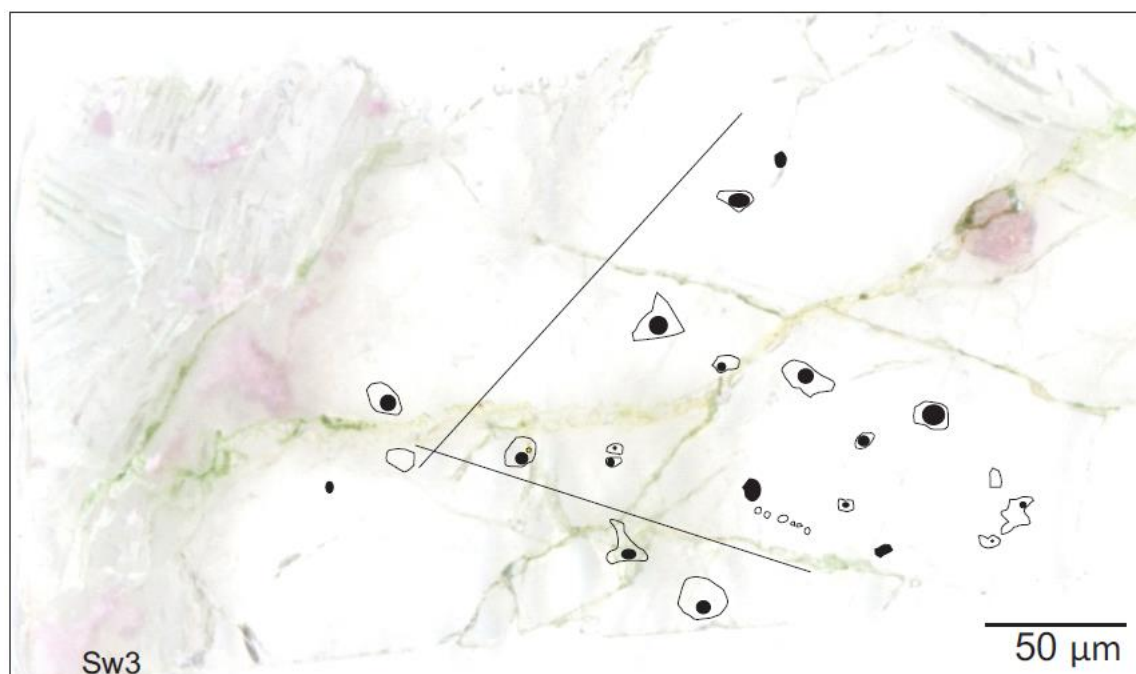
Figure 5-52: Overlay of fluid inclusions onto a thick section scan as observed in sample SW3 (intermediate zone). Inclusions appear to be mainly primary.
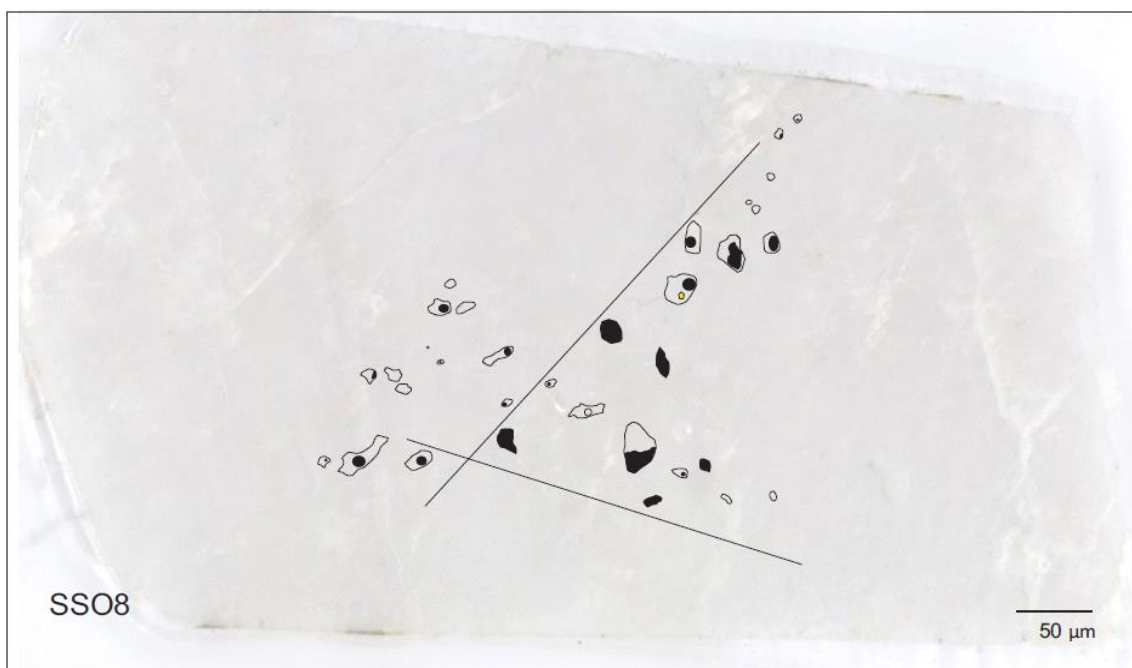
Figure 5-53: Overlay of fluid inclusions onto a thick section scan as observed in sample SSO8 (core zone). Inclusions appear to be mainly primary.

Figure 5-54: Overlay of fluid inclusions onto a thick section scan as observed in sample SW4 (core zone). Inclusions appear to be mainly primary.

The various inclusion types, shapes and sizes are all present in a quartz host and the distributions of some of the inclusions are limited to core and intermediate zones of the pegmatite. Large isolated inclusions are found in all the zones from border inwards to the core zone. Secondary inclusions found in all the zones except for the core zone. Although the majority of inclusions are aqueous, gas dominated inclusions are found in the middle/intermediate and the core zones (Figure 5-7 to Figure 5-12).

The shapes within the same quartz host can be very different (Figure 5-5 and Figure 5-6A). Inclusions vary considerably in size and are orientated in a direction (Figure 5-5B and Figure 5-6A). Both mono- and di-phases are present as one trail of inclusions. The large size distributions are liquid dominated, where gas-rich inclusions are normally smaller (30µm). The size of vapour and liquid was recorded in 217 fluid inclusion samples from the wall, intermediate and core zones of the Noumas I pegmatite during microthermometry and shown in Figure 5-7 and Figure 5-8.
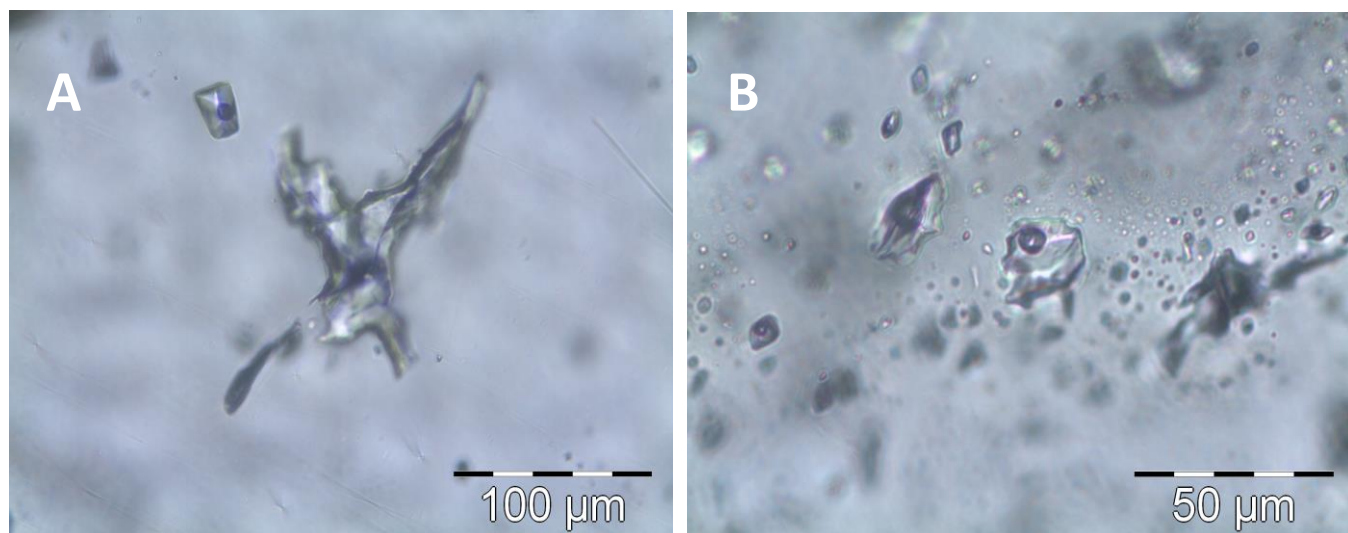
Figure 5-55: Microphotographs of fluid inclusions in doubly polished thick sections from quartz crystal host at room temperature. A) Large inclusion di-phase with an almost symmetrical shaped inclusion also di-phase. Both have dominant liquid phases SW2, B) Small trails with larger isolated inclusions with clear orientation of the inclusions SW3.
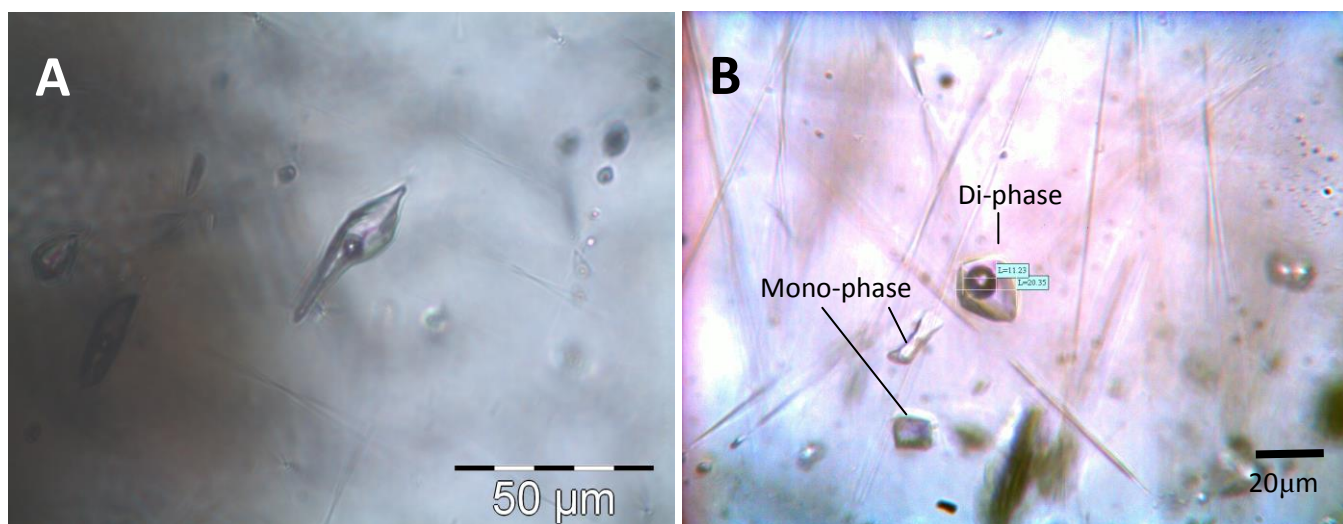
Figure 5-56: Microphotographs of fluid inclusions in doubly polished thick sections from quartz crystal host at room temperature A) large isolated inclusion di-phase with a necking effect suggesting extension in one direction and compression in the other in the zones of the pegmatite SSO8, B) mono and di-phase inclusions, gas phase relatively large compared to the liquid phase of the other liquid dominated inclusions in the zones of the pegmatite SW4.
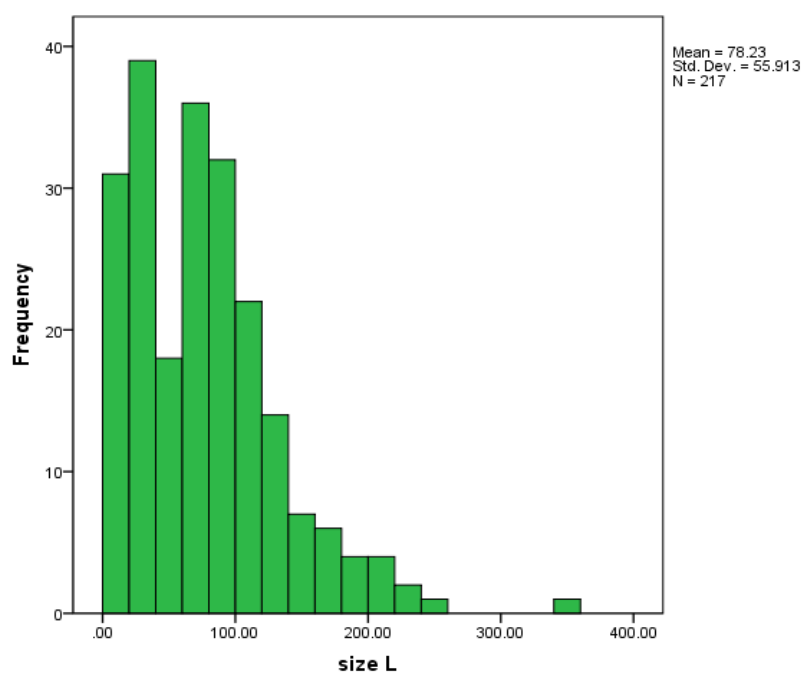
Figure 5-57: Frequency distribution in the observed fluid inclusions based on size (µm) of the trapped liquid phase.
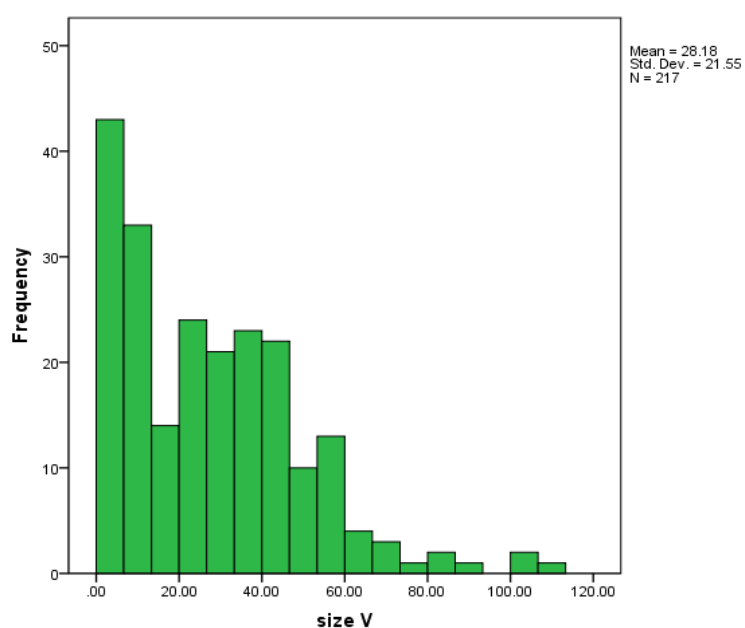
Figure 5-58: Frequency distribution in the observed fluid inclusions based on size (µm) of the trapped vapor phase.

From these observations the dominant type of inclusions within the wall, intermediate and core zones of the Noumas I pegmatite have been illustrated (Figure 5-9). The samples are found above the 1:1 ratio line indicating the fluids are more liquid or aqueous than gas dominated.
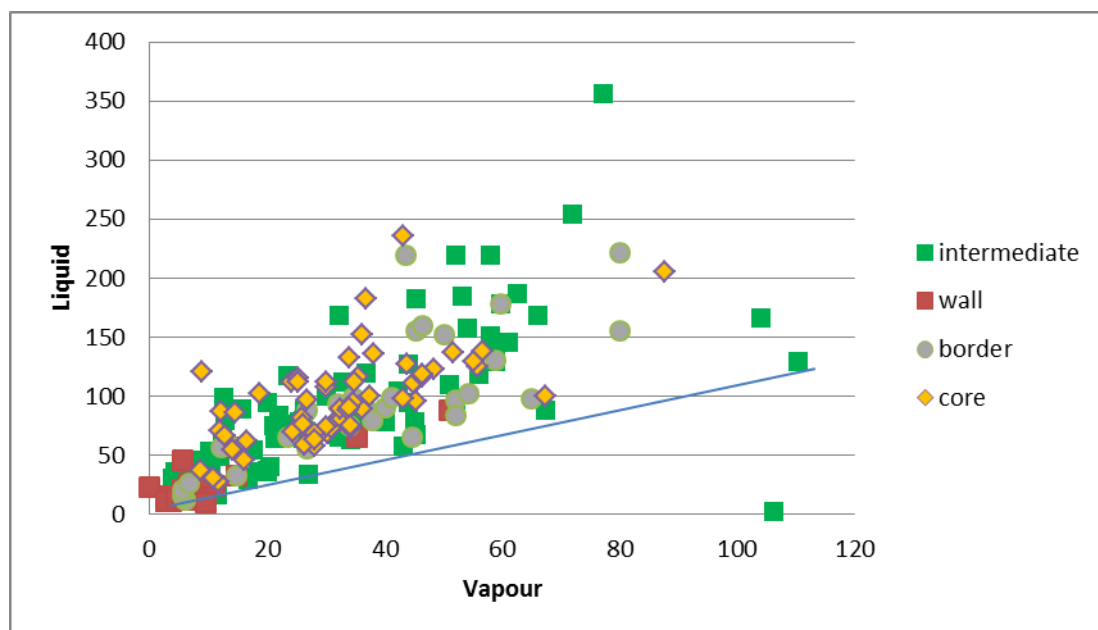
Figure 5-59: The dominant fluid inclusion type within the wall zone, v=vapour and l= liquid based on the 1:1 ratio.

5.2 Microthermometry

Initially fluid inclusion assemblages (FIA) for the wall, intermediate and core zone samples were selected. This is a fluid inclusion trapping event that can be identified based on the petrography and it is assumed these assemblages formed at the same time with the same temperature and pressure.

The microthermometry determined the melting (T_m) and homogenization (T_h) temperatures over the various zones of the Noumas I pegmatite. The temperature of homogenization is the total homogenization and the temperature of fluid formation is known as the trapping temperature (T_f). When these two temperatures were compared the different classifications of the inclusions observed could be noted. The correlations suggest the presence of more than one type of inclusion present based on the salinity ranges, with type 1 of low to moderate and type 2 of high salinity.

For both types (1 and 2) the difference between these two is the high and low T_h temperatures. So the compositions in the different types will also be different, as some metals are more soluble in higher salinities. A comparison of type 1 and type 2 inclusions are made to show the similarities as well as differences between them (Table 5-1 and Figure 5-10).

A correlation found between fluid inclusions and the mineralization event (especially when applying the fluid inclusion studies to hydrothermal ore deposits) was made by Huizenga

(2010). In order to understand the fluid entrapment the host mineral formation was petrographically studied to identify primary or secondary assemblages.

Table 5-12: Comparison between type 1: low to moderate salinity inclusions and type 2: high salinity inclusions of observed fluid inclusion investigations.

Type 1: Low-salinity (high and low temp)	Type 2: High-salinity (high and low temp)
• Very abundant through the various zones (wall, intermediate, core) • Large shaped inclusions • Occur as isolated inclusions and in trails • Initial melting ranges between -25.4 and -21.3°C • T_h between +100 and +300°C • Salinities vary between 0.63 to 6.8 wt% NaCl	• More abundant in specific zones (core) • Regular, irregular shaped inclusions • Occur as isolated inclusions and in trails • Initial melting ranges between -66.2 and -42.9°C • T_h between +150 and +330°C • Salinities vary between 11.7 and 22.1 wt% NaCl
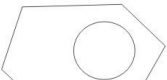
Inclusion type	Description	W	I	C
I	Monophase aqueous			
II A	CO_2 + Laq			
II B	Laq +Vapor >80% liquid			
II C	Laq +Vapor >50% liquid			

Present   Common   Abundant

Figure 5-60: Types, abundance and mode of occurrence of fluid inclusions in the W-wall, I-intermediate and C-core zones.

The distribution of the T_h temperatures ranges between 39 and 340°C. The dominant T_h within the inclusions are found at 100 - 215°C (Figure 5-11). The salinities of the fluid inclusions were determined by using Bodnar and Vityk's (1994) equation. The equation requires the melting temperature (T_m) in order to determine the salinity of the inclusion

(Figure 5-12). The salinities are also distributed over wide ranges, of 0.35 to 23 (wt. % NaCl equivalents). The effects of fluid inclusion sizes have an effect on the T_h as well as the density (Fall et al., 2009). The T_h seems to be higher in aqueous inclusions.
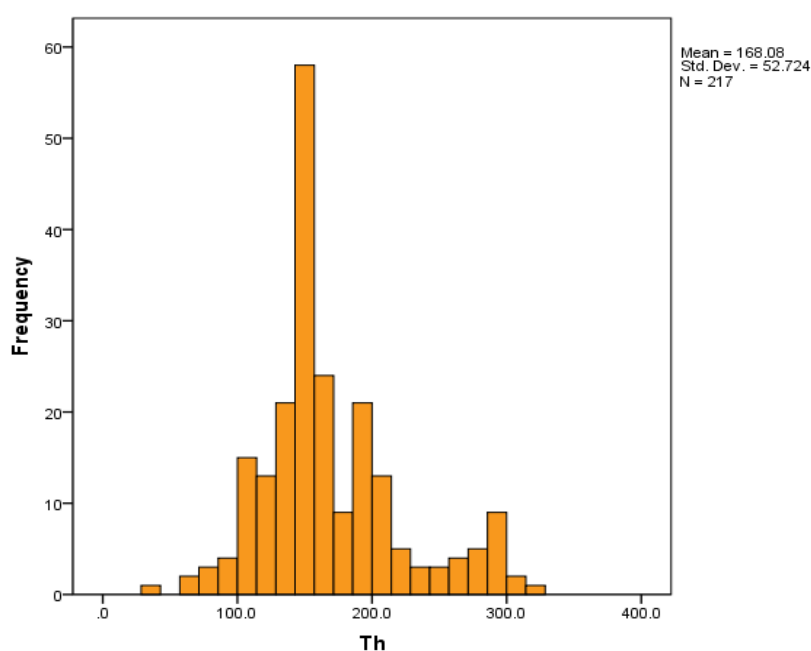
Figure 5-61: Frequency distribution of homogenization temperatures (Th) of fluid inclusions in the investigated zones within the pegmatite for both (°C).
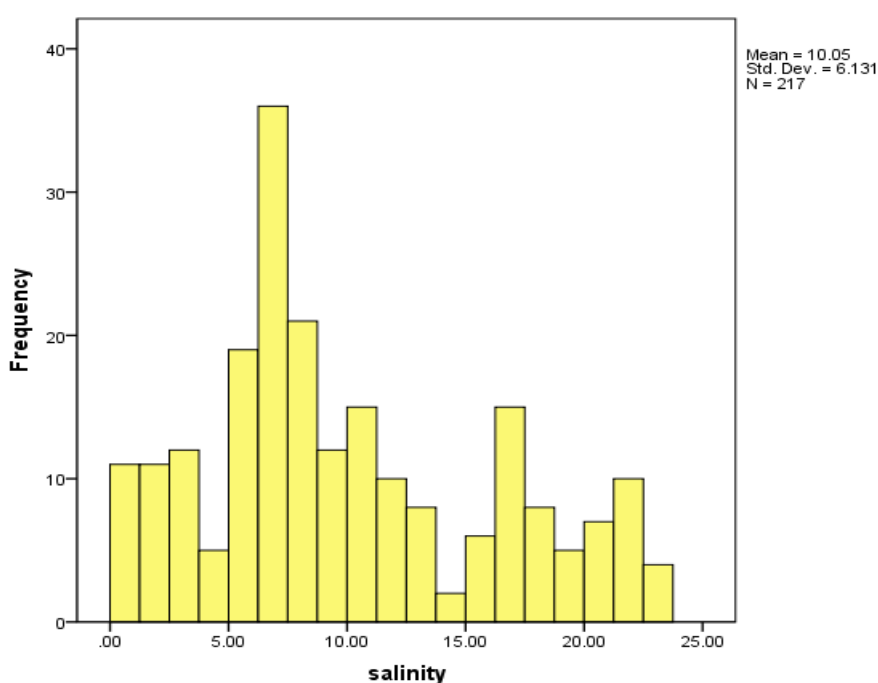
Figure 5-62: Frequency distribution of salinity (wt% NaCl) estimated based on Bodnar's (1994) equation.

The Tf were determined from the homogenization temperatures. The Tf for primary and secondary fluid inclusions are shown in Figures 5-13 to 5-19.

Wall zone: The fluid inclusion analyses done for sample SSO1 are grouped in the low salinities (between 0-15 wt.% NaCl) and medium Th (100 - 200°C). The Tf estimated at a pressure of 2.5 (kbar), ranges between 320-360°C, for a shallow scenario. At a higher pressure of 5.5-6 (kbar) the Tf range between 350-540°C.

Intermediate zone: Samples SW2 and SW3 have two different salinity and Th, but were sampled from the same zone. SW2, the sample closer to the wall zone, have high Th (220 - 310°C) and cover a wider salinity range (0 - 22 wt % NaCl). Interestingly SW3, the sample located closer to the core, has a consistent Th range (110 - 170°C) but again a wide spread in salinity (5 - 21 wt % NaCl). The Tf estimated at a pressure of 2.5 (kb), ranged between 300-360°C, for secondary inclusions. The deeper pressure at 5.5-6 (kbar), gave Tf values that range between 360-570°C.

Core zone: Same as with the two samples from the intermediate zone, SW4 and SSO8 have different Th and salinities. When compared to the wide range of the intermediate zone the distribution for the samples from the core is not as wide. Sample SW4 have salinity values ranging between 5 - 12 wt % NaCl, with Th of 179 -190°C. For sample SSO8, the salinity distribution stretches from 3 - 10wt %NaCl and Th between 129 - 175°C. The Tf estimated at a pressure of 5.5-6 (kbar), ranges between 370-510°C. Only primary fluid inclusions were identified in the core samples.

In order to determine a constrain regarding the evolution of temperature and fluid salinity during crystal growth within the different zones of the Noumas I pegmatite, the T_f and salinity data from the border, wall, intermediate and core zones (Figure 5-13 to Figure 5-16) are separated. Using scatter plots of T_f and salinity, the evolution of the fluid inclusion can be determined. This shows which of the inclusions came first, but due to the paragenetic occurrence of quartz over the entire span of the Noumas I pegmatite formation; it is difficult to infer the appropriate sequence of formation for each of the fluid inclusion assemblages. The T_f is plotted against salinity to show the possibility of multiple injections during the formation and crystallization for the mineral quartz. The secondary inclusions temperature corrections are shown in Figures 5-17 to 5-19.
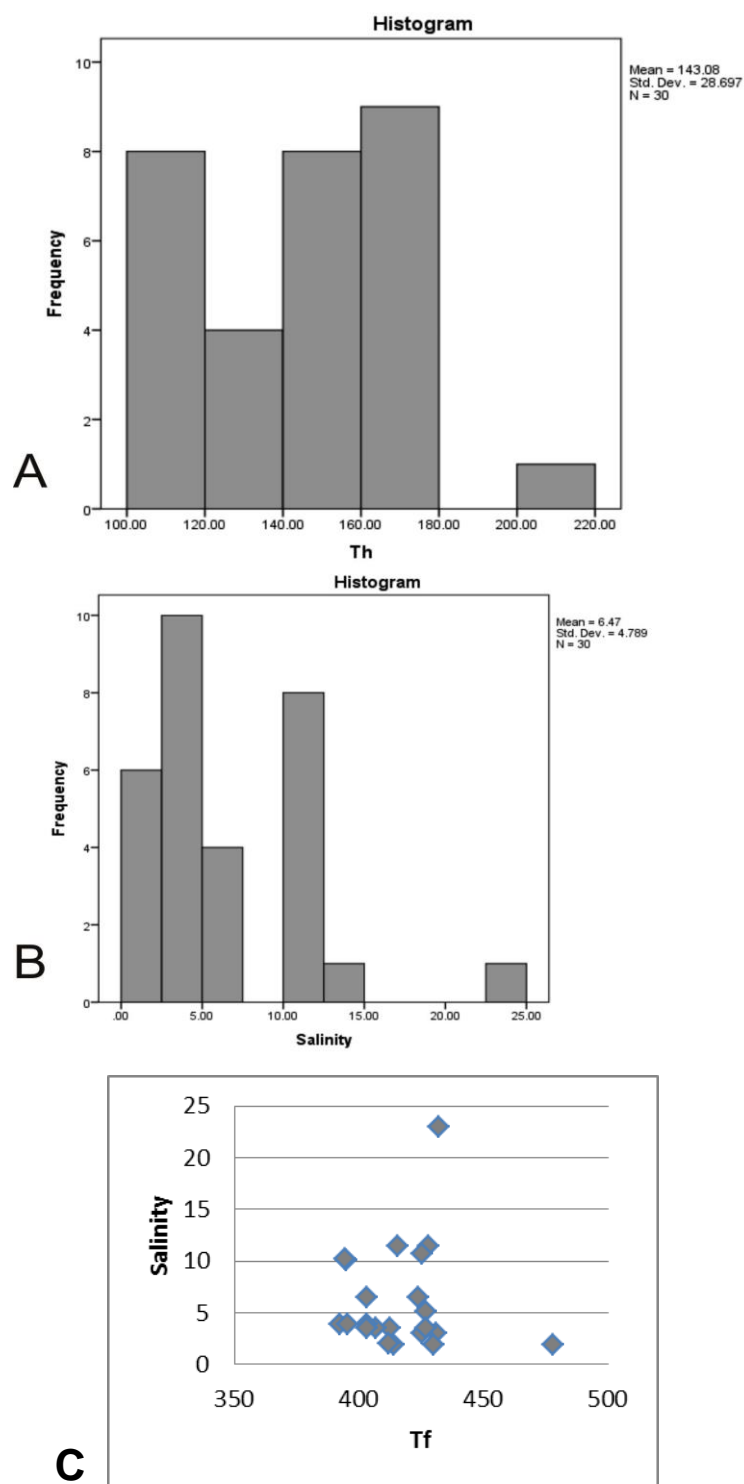
Figure 5-63: A) Th distribution of fluid inclusions from the border zone. B) Salinity distribution of fluid inclusions from the quartz crystal. C) Primary Tf inclusions versus salinity.
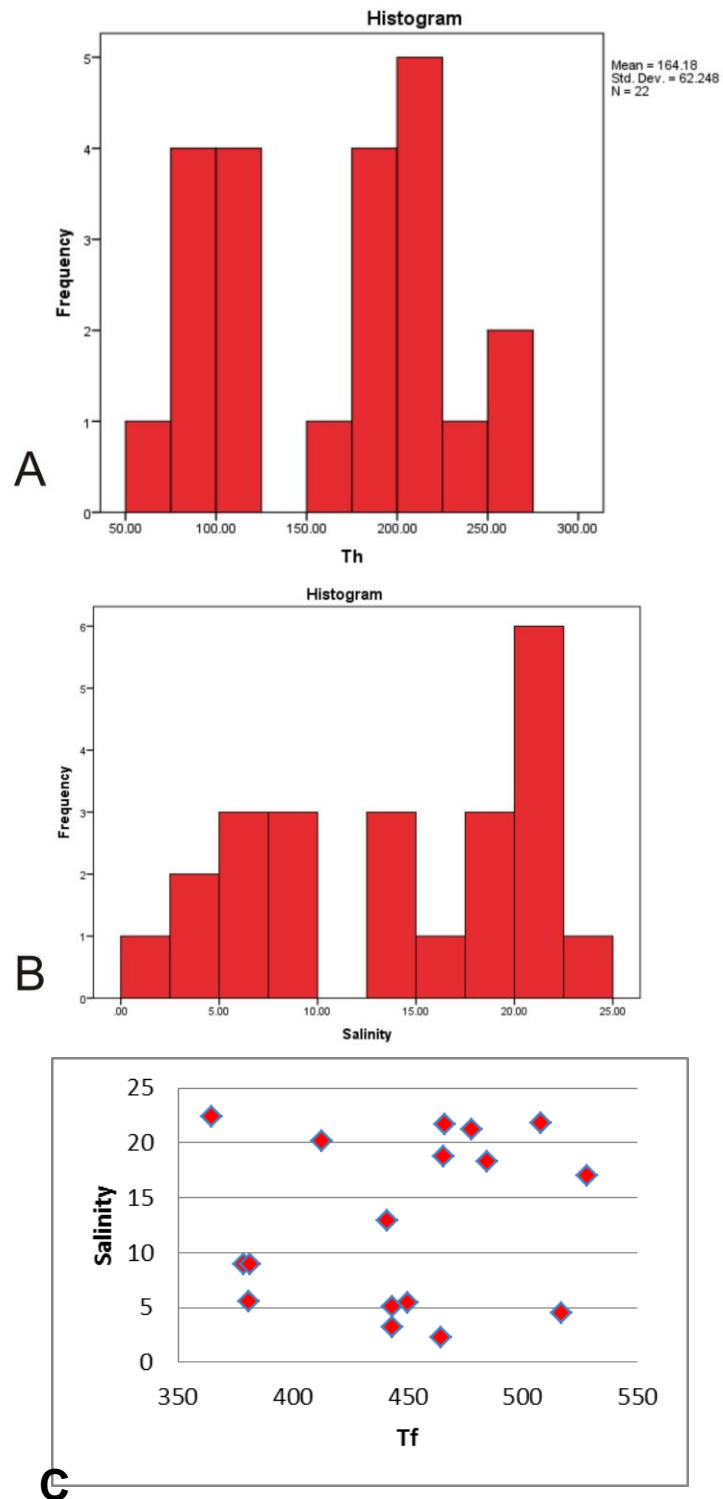
Figure 5-64: A) Th distribution of fluid inclusions from the wall zone. B) Salinity distribution of fluid inclusions from the quartz crystal. C) Primary Tf inclusions versus salinity.
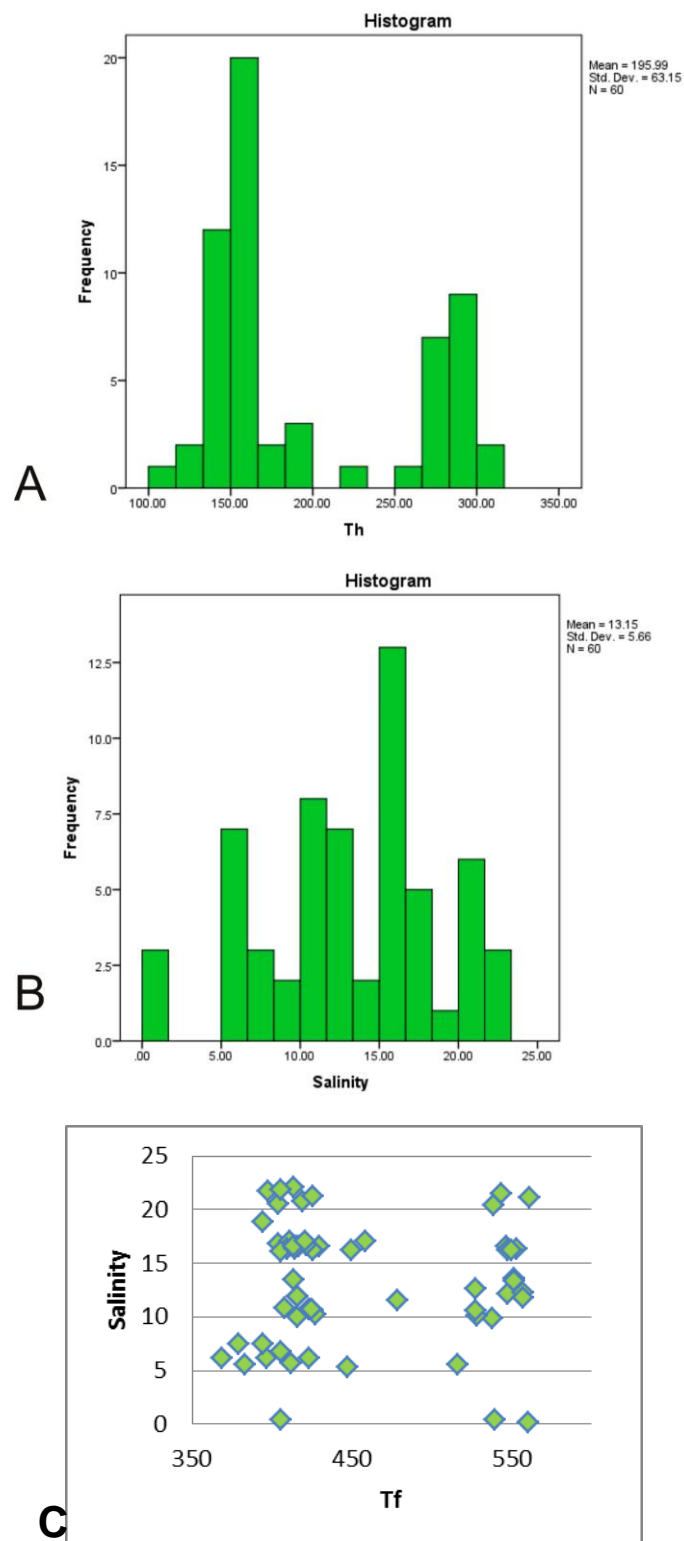
Figure 5-65: A) Th distribution of fluid inclusions from the intermediate zone. B) Salinity distribution of fluid inclusions from the quartz crystal. C) Primary Tf inclusions versus salinity.
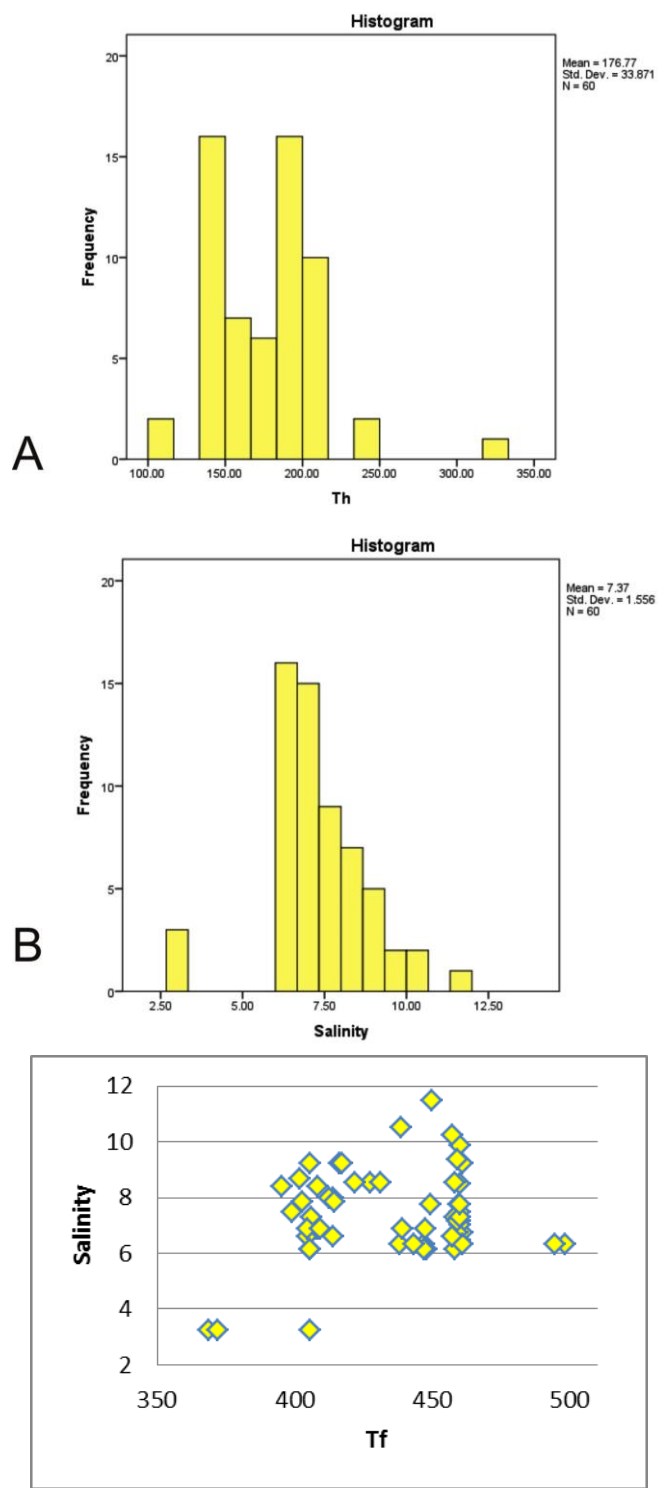
Figure 5-66: A) Th distribution of fluid inclusions from the core zone. B) Salinity distribution of fluid inclusions from the quartz crystal. C) Primary Tf inclusions versus salinity.
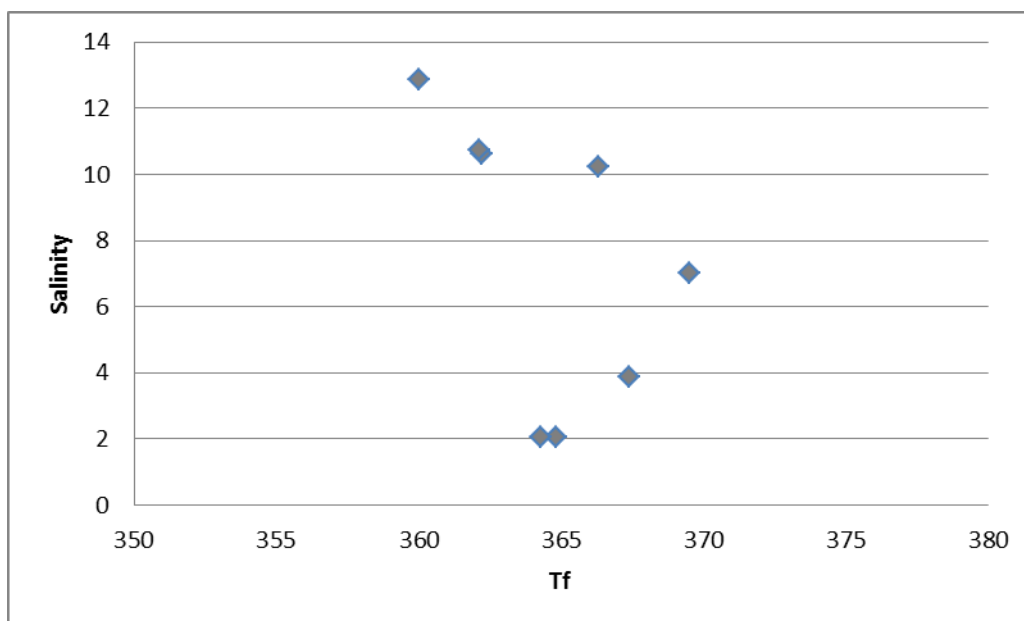
Figure 5-67: Trapping temperatures for secondary inclusions form the border zone.

Figure 5-68: Trapping temperatures for secondary inclusions form the wall zone.

Figure 5-69: Trapping temperatures for secondary inclusions form the intermediate zone.

5.3 FTIR and RAMAN results

The two complementary analytical techniques, FTIR and Raman, identify the chemical compositions for the fluid inclusion content more accurately when used together (Figures 5-20 to 5-23). The compositions measured in the zones are saturated with CH bonds and contain H_2O and CO_2. Methane (CH_4) was also identified in samples SW2 and SW3 (middle/intermediate zone). A Raman spectrum was obtained and used as a database for the rest of the samples. H_2O, CO_2, C-F and C-Br bonds were identified from the middle/intermediate zone (Figure 5-23).

The aqueous solution plays an important role during ore deposition. The solution helps to transport and precipitate ore, in high concentrations and far from the original source. This is seen where the pegmatite intrudes over 25km and the mineralization changes towards the "top" or furthest point form the source.

The multi-component phases found in entrapped inclusions are typical for situations where H_2O was a solvent for minerals and gases under deeper crustal conditions. Based on inclusion records the gas-bearing aqueous fluids found in the crust can be binary or ternary systems (Roedder, 1984). Results of the inclusions, Raman and FTIR suggest that Noumas inclusions can be characterized in a ternary system of either CO_2-H_2O-NaCl or CH_4-H_2O-NaCl or possibly in a mixture of CO_2-H_2O-CH_4-NaCl.
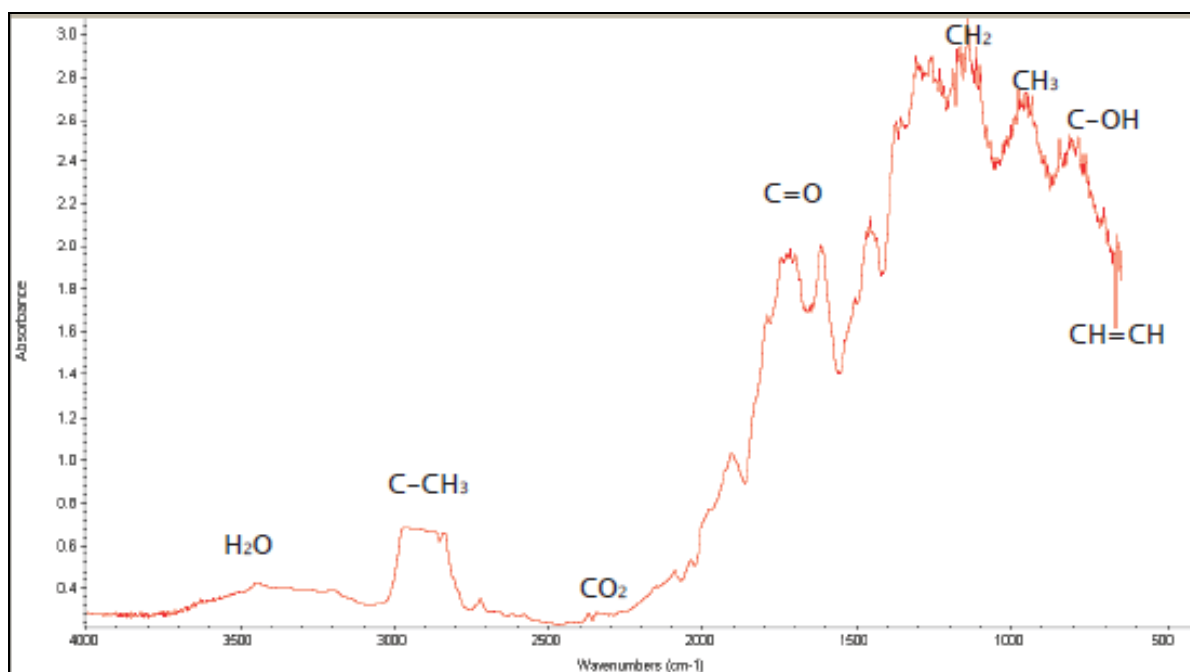
Figure 5-70: FTIR spectra of a CH4-bearing H_2O-CO_2 fluid inclusion (quartz host). The spectrum is saturated with CH bonds. CH_4, H_2O and CO_2 positively identified in sample SW2.
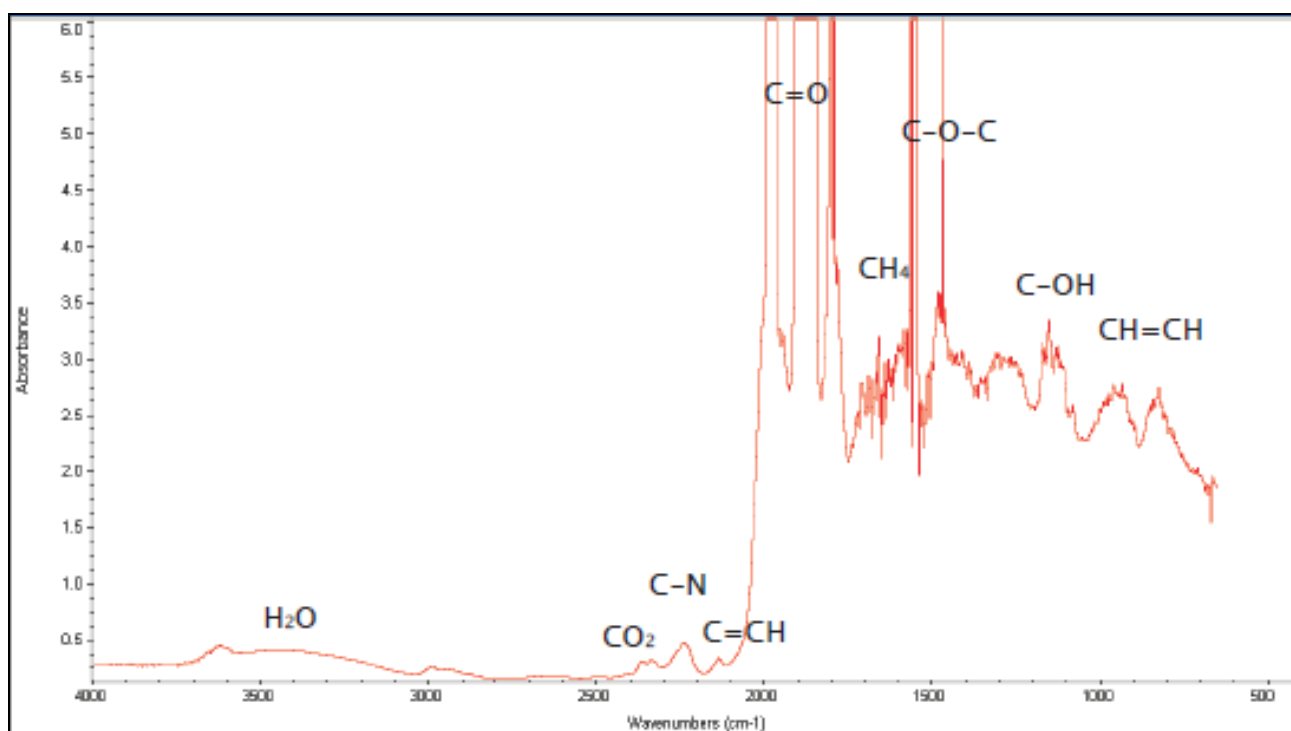
Figure 5-71: FTIR spectra of a CH_4-bearing H_2O-CO_2 fluid inclusion (quartz host). The spectrum is saturated with CH bonds. CH_4, H_2O and CO_2 positively identified in sample SW3.
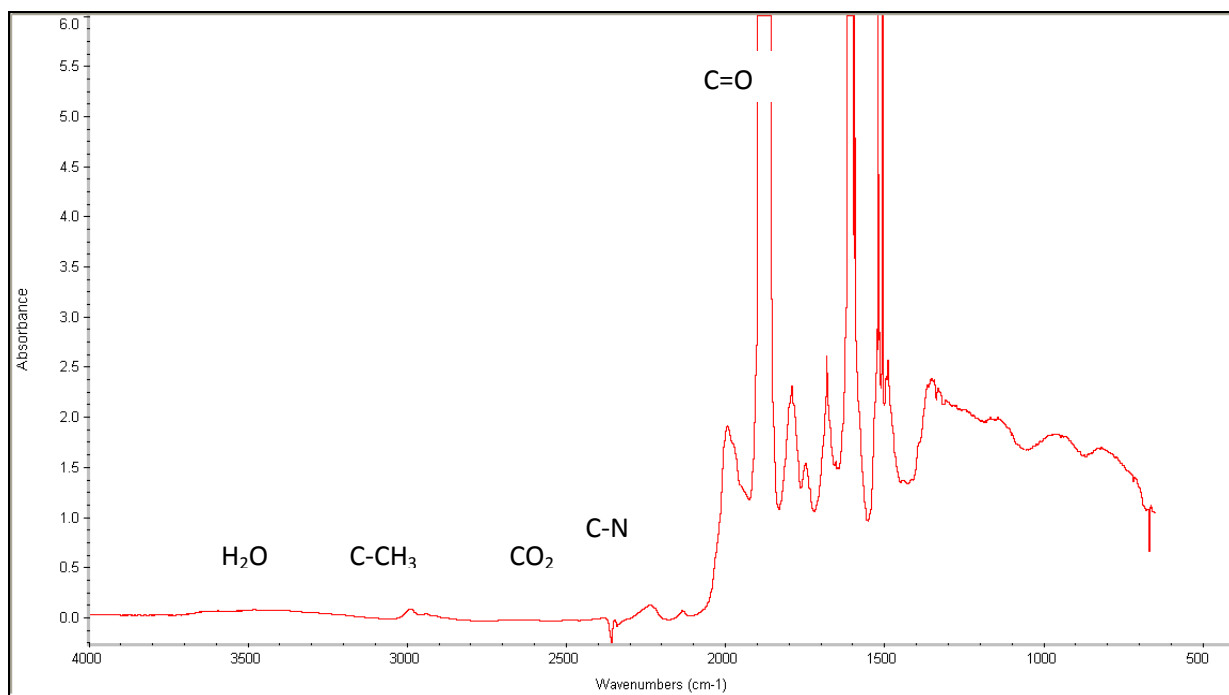
Figure 5-72: FTIR spectra of H_2O-CO_2 fluid inclusion (quartz host). The spectrum is saturated with CH bonds. H_2O and CO_2 positively identified form sample SW4.
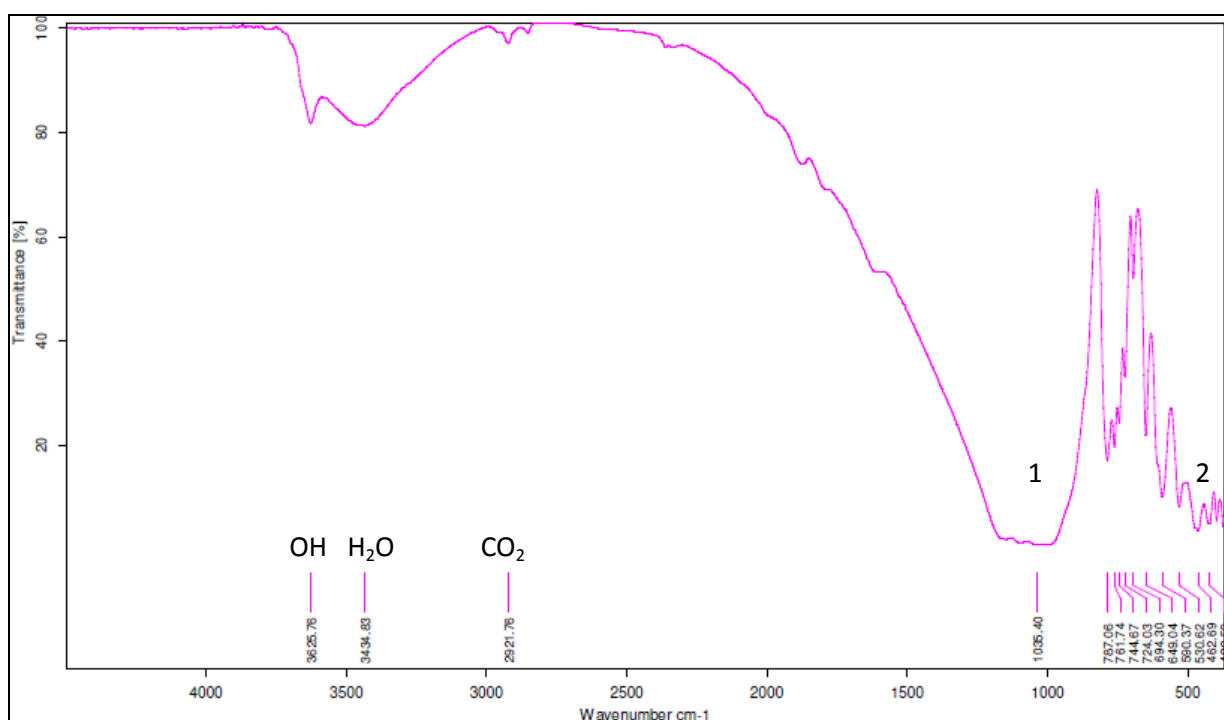
Figure 5-73: Raman spectrum form the middle/intermediate zone. During analysis it was used as a reference spectrum (database) for the sample measurements. Sample consists of OH, H_2O,CO_2, (1) C-F or amblygonite overlaps and (2) C-Br bonds.

The average eutectic (T_e) temperature over the whole pegmatite varies significantly making it hard to accurately determine the nature of the cations (Table 5-2). Based on the work of Huizenga (2010) the low T_e of -91.8°C are indicative of co-existing Ca^{2+}, Fe^{2+}, Mg^{2+} cations

and in some cases Li and/or Br. The T_e values between -20°C and -13°C indicates NaCl-(KCl) compositions dominate in the inclusions.

Table 5-13: The average eutectic temperature (T_e) and estimated compositions of the Noumas I pegmatite (values after Huizenga, 2010), W-wall, I-intermediate, C-core zone.

Sample	Zone	T_e (°C)	Dominant compositions
SSO1	W	-17.58	NaCl dominated
SW2	I	-23.74	NaCl dominated
SW3	I	-32.42	K/NaCl dominated, $<Mg+CaCl_2$
SSO8	C	-20.95	K/NaCl dominated
SW4	C	-27.91	K/NaCl dominated, $<Mg+CaCl_2$

5.4 Pressure and temperature estimations during time of formation

Th and Tf temperatures for aqueous inclusions in quartz occupy a wide temperature range (Figure 5-14B, 5-15B and 5-16B) over the wall, intermediate and core zones. The program BULK was used to calculate bulk fluid density and composition. After which the hypothetical bulk composition and densities are entered into the program ISOC to calculate corresponding isochores. This program automatically selects the relevant equations based on the fluid composition.

An oversimplified temperature and pressure diagram (Figure 5-24), based on the quartz-saturated phase relationships for lithium minerals along with the temperatures from fluid inclusion analyses provided estimation for the depth of emplacement at two different pressures of 2-2.5kbar and 5.5-6kbar. The pressure was then used in Strong's (1988) model for the relative emplacement depth at around 6-8 km for a shallow and a deeper scenario at 17-20 km.

A system, in this case H_2O-CO_2-CH_4, was predefined and the relative composition of the homogenous non-aqueous phases of CO_2 and CH_4 was chosen between 0 and 1. The amount of substance fraction for CO_2 was determined from the averaged Raman analysis (Figure 5-20 to 5-23). The fractions for CO_2 and CH_4, are estimated at 0.61 and 0.39 as the Raman intensities are directly proportional to the concentration of the species.
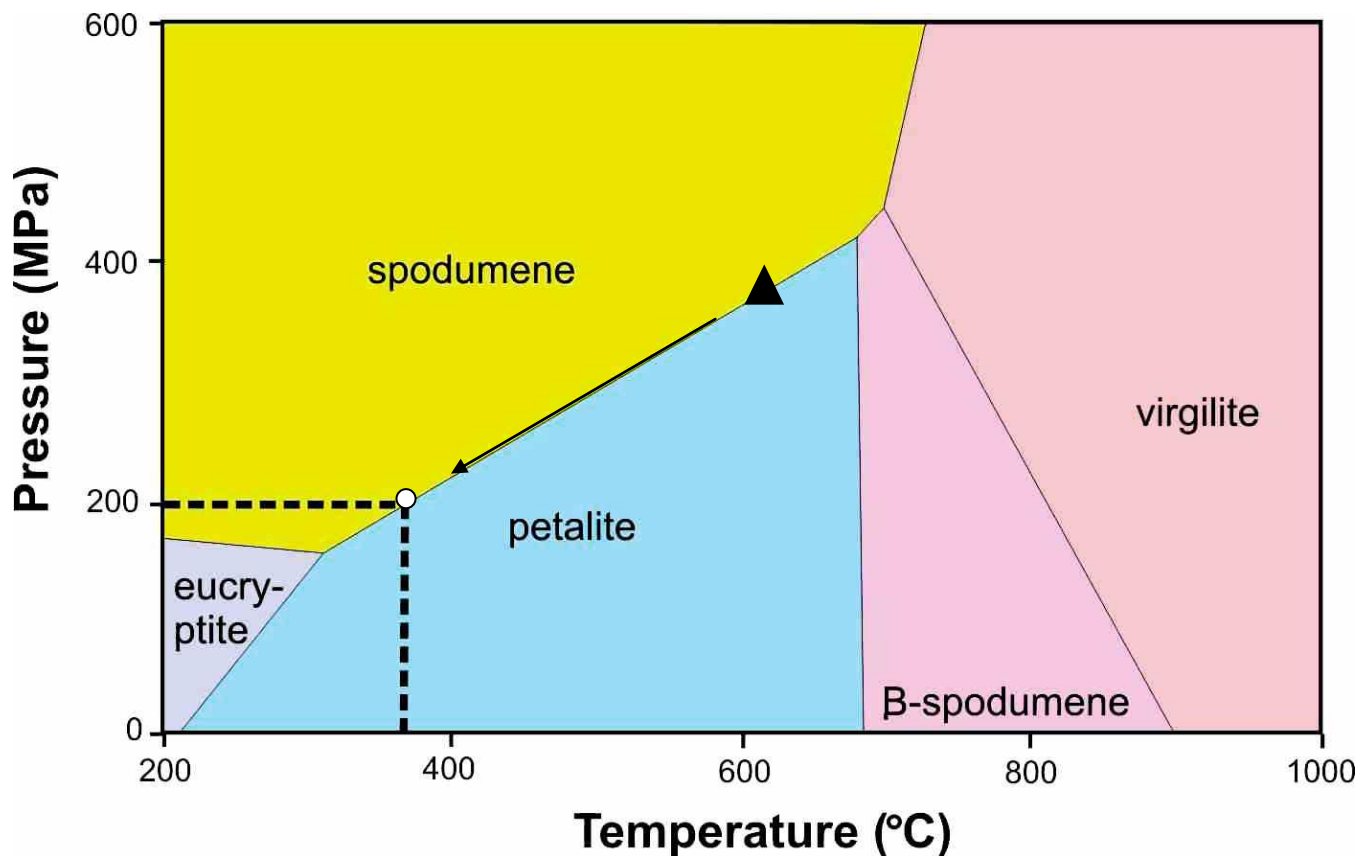
Figure 5-74: An oversimplified diagram of quartz-saturated phase relationships for Li minerals (after Linnen et al., 2012; London, 2005). White dot-Noumas I pegmatite, triangle-granitic melt.

The corresponding isochores were estimated by using the homogenization temperatures to determine the formation temperature for the fluid inclusions. In P-T diagram the intersection of isochores for trapped end member fluids is located at a unique point, which is the same as the intersection of their solvus curves (Diamond, 1994). Figure 5-25 is an example of how the T_f values were estimated for secondary fluid inclusions at a shallow depth of emplacement. A second emplacement depth was estimated at a deeper depth of 17-20 km. The two scenarios are shown in Table 5-3.

Table 5-14: The estimation for shallow and deeper emplacement of the Noumas I pegmatite.

Scenario	Shallow	Deep
Depth (km)	6-8	17-20
Pressure (kb)	2-2.5	5.5-6
Average Tf (°C)	226.90	427.63

The T_h values were used at the constant pressure for the shallow and deep scenario (Table 5-3) to determine the T_f. The estimated T_f values were higher when compared to the T_h (Appendix 4). Table 5-4 shows the difference between fluid inclusions of a secondary and

primary nature. The average formation temperature for each zone of the Noumas I pegmatite is given in Table 5-5.
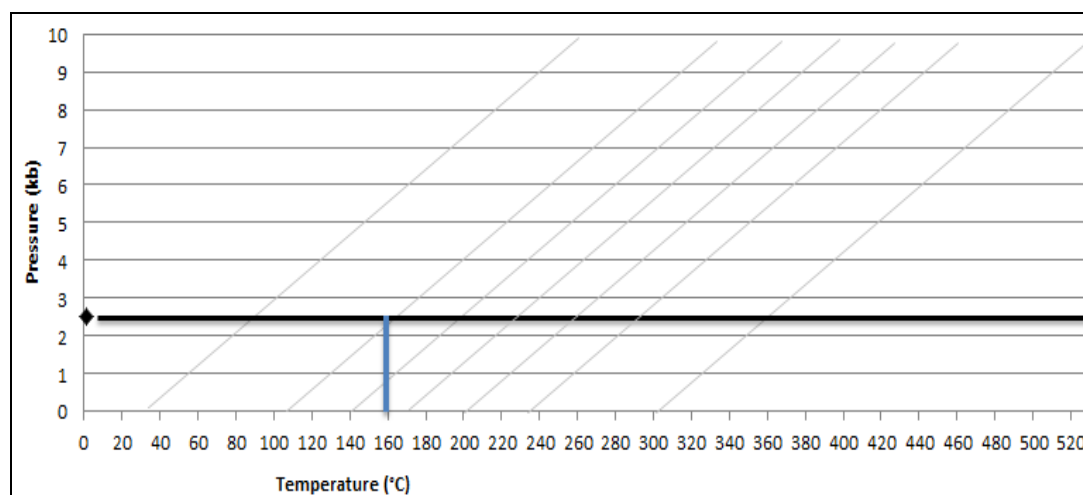
Figure 5-75: P-T diagram in a H_2O-CO_2-CH_4 system. The isochores (grey) used to generate the T_f from the T_h at a pressure of 2.5 (kb) (black line). The estimated T_f along specific isochores (blue line), in this case corrected from a T_h of 110°C.

5.5 Summary of results

The microthermometric analyses of fluid inclusions in quartz crystals, within the Li-, Ta- and Be-rich Noumas I pegmatite confined the temperature, salinity and general composition of the several fluid inclusion generations. These components help to establish the compositional evolution of the fluid from the crystallizing magma. The inclusions have formation temperatures ranges between 300-370°C for secondary inclusions and higher temperatures for primary inclusions between 390-570 °C within the wall, intermediate and core zone of the Noumas I pegmatite (Figure 5-26 and Tables 5-4 to 5-5).

The lower trapping temperatures show the shallow emplacement depth scenario is suited for the secondary inclusions that have been altered during a possible uplift of the pegmatite, while the higher trapping temperatures for a deeper scenario can be related to the primary fluid inclusions. The classification where deposits are related to the general features of alteration and associated mineral assemblages to the depth of formation form Strong (1988), suggest the trapping temperatures for primary inclusions is greater than the 6-8km emplacement depth.

The majority of inclusions contain two phases (liquid and vapour, liquid dominated), mono- and multiple- phases (liquid, vapour and solid) are also present in clusters in the wall, intermediate and core zones of the Noumas I pegmatite samples. The phases within the inclusions consist of dark rimmed vapour phases (assumed to be CO2) and possibly

complex solutions with various types of salts (daughter crystal of NaCl). The most important gas compositions found in fluid inclusions of the Noumas I pegmatite are H_2O, CO_2 and CH_4, and a solid phase halite (NaCl).

The early fluid inclusion populations could have been altered and or destroyed by late stage exsolved magmatic fluids, and therefore not represent the initial crystallization conditions.

Avg. Sal (wt% NaCl)	Avg. Te (°C)	Fluid composition
6.47	-17.58	NaCl dominated
12.03	-28.08	K/NaCl dominated
7.37	-24.43	K/NaCl dominated
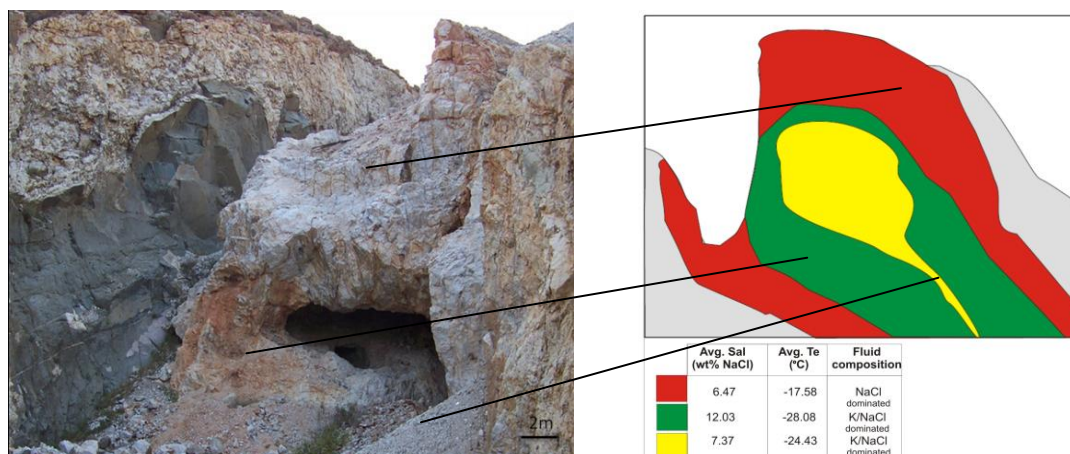
Figure 5-76: Illustrates the various zones, wall (red), intermediate (green) and core (yellow) for Noumas I pegmatites where Table 5-1 (zone 1-3 are taken from).

Table 5-15: Summary of the primary and secondary inclusions identified in the Noumas I pegmatite from the border, wall, intermediate and core zones.

	Primary inclusions	Secondary inclusions
Avg. Th (°C)	176.01	87.96
Avg. Salinity (wt % NaCl	9.93	10.80
Avg. Tf $_{shallow}$ (°C)	235.71	148.49
Avg. Tf $_{depth}$ (°C)	436.01	267.33
Estimated depth (km)	17-20	6-8
Estimated pressure (kbar)	5.5-6	2-2.5

Table 5-16: Summary of the mineralogy and microthermometry for the wall (W), intermediate (I) and core (C) zones in quartz samples from the Noumas I pegmatite.

Zone	Zone 1	Zone 2	Zone 3
Area	Wall/outer	Intermediate/middle	Core
MINERALOGY	Qtz , K-fsp, beryl, tourmaline, garnet	Qtz, K-fsp, spd, lep, garnet, mica	Qtz, K-fsp, beryl, mica
XRD	Bismuthinite , apatite	Plag, triphyllite, illite	Plag, illite
MICROTHERMOMETRY			
Dominant phase in FI	Liquid	Liquid	Liquid
Avg. Salinity (wt % NaCl)	6.47	12.03	7.37
Std. dev. avg. Sal.	3.62	2.74	0.34
Avg. Te (°C)	-17.58°C	-28.08°C	-24.43°C
St. dev. Avg. Te	8.18	18.93	5.17
Avg. Th (°C)	164.18	169.86	176.77
St. dev. Avg. Th	42.25	25.85	25.37
Avg. Tf $_{shallow}$ (°C)	221.7	229.86	236.4
Avg. Tf $_{depth}$ (°C)	427.02	455.98	436.77
Salt composition in fluids	NaCl dominated	K/NaCl dominated $<Mg+CaCl_2$	K/NaCl dominated
Compositional phases identified	H_2O, CO_2	H_2O, CO_2 and CH_4	H_2O, CO_2

Chapter 6: DISCUSSION

6.1 Genesis, emplacement and source rocks

The Noumas pegmatites are developed in the granodiorite of the Vioolsdrift Suite, dated at around 1900Ma (mafic members) and 1730Ma (felsic members) (Minnaar and Theart, 2006). Two phases of pegmatite intrusion is evident in the pegmatite belt. The older phase (1000 Ma) is associated with the closing stages of the Namaqua orogeny and a younger phase (950 Ma) is related to the intrusion of granitoid bodies (Beukes, 1967; Hugo, 1970). The pegmatites cannot be related to any of the intrusive bodies found in the Orange River along the Namaqualand (Gevers, 1937; Sohnge and De Villiers, 1946). During a Mesoproterozoic crustal shortening and thickening (1199 - 1175 Ma) major recumbent folds developed (Dewey et al., 2006). Sheets of mesocratic and leucocratic granite gneiss were injected along the folds and weak zones. If the source melt is associated with the closing stages of the Namaqua orogeny (1100 Ma), then the development occurred simultaneous with the easterly striking shear zones (Hugo, 1970; Martens, 1979; Colliston and Schoch, 2002; Cornell et al., 2006). This might explain the northwest strike of the pegmatites. The alignment of the Noumas I pegmatite conforms to the foliation in the granodiorite host rock. This puts an age estimate of younger than 1000 Ma on the intrusive Noumas I pegmatite after the host rock.

The general consensus for pegmatite formation is that they form by primary crystallization from a volatile-rich siliceous melt (Jahns and Burnham, 1969; Cerny 1991; London, 1990). The melts of rare element pegmatites are related to highly differentiated granitic magmas and represent strongly fractionated residual melts in silica, alumina, alkali elements, water, lithophile elements and rare metals. Cerny (1991) suggested that the lithology of the source rocks of the melt is a major controlling factor on the ultimate composition of the rare elements in the pegmatite. Peraluminous granites, from undepleted upper crustal lithologies, give rise to pegmatites enriched in Li, Cs and Ta. The aluminum saturation index of Webster et al., (1997), estimated for the Noumas I pegmatite, correlated with a peraluminous granitic melt. The volatile distribution and the major element estimations (Chapter 2, Figure 2-7; Chapter 4, Table 4-5) also agree with a peraluminous source rock. As the melt forming pegmatite raised towards the surface, the pressure imposed on the magma by the surrounding rocks decreased. The decreased pressure caused a decrease in the amount of H_2O and CO_2 available during primary boiling (Strong, 1988). The dissolved gases exsolve from the melt, as the pressure continues to decrease (Strong, 1988).

The Noumas I pegmatite was averaged against both chondritic and upper continental crust (Chapter 4, Figure 4-16 to Figure 4-18), no differentiation trend was established due to non-representative sampling. The element Ce, can have a valence state of +3 as well as +4 (Akagi and Masuda, 1998). The different valences cause anomalous behavior of those elements in the REE patterns (Akagi and Masuda, 1998). These anomalies reflect the redox conditions within the sample. The negative Ce anomaly is related to a relatively oxidizing condition (Akagi and Masuda, 1998). The negative Ce anomaly (Figure 4-17) indicates an oxidation period within the formation of the Noumas I pegmatite for the core zone, with relatively reducing conditions in the wall and intermediate zone. The mineral bismuthinite (Bi_2S_3) hosted within the wall zone was formed in a reducing environment. The oxidation state within the magma at the time of formation, allow for the transport of elements and affect the solubility of metals being transported (Rudnick and Gao, 2003).

6.2 Mineralogy, petrography, chemical variations and fluid characteristics within the zones of the Noumas I pegmatite

During pegmatite crystallization, volatile and soluble components within the magma directly influence the physical character and chemical properties of the magma. A water and flux compounds, such as F, cause the magma to become less viscous with the depression of the eutectic crystallization temperature of the magma. Minerals form from such solutions by one or more changes, resulting in the saturation of the solution before precipitation can occur. The following steps or changes occur prior the precipitation of minerals near the source of the magma (Table 6-1).

Table 6-17: Changes within magma prior the precipitation of minerals (Quirke and Kremers, 1943)

1) lowering of temperature
2) release/escape of some or all of the volatile elements or precipitation of mineral involving the element
3) Saturation of the magma with a particular component due to solution of country rock, /previously formed pegmatite material.

The low temperatures of crystallization have been attributed to rare components (volatiles) playing the role of fluxes in lowering the melting and crystallization temperatures (Fuertes-Fuente et al., 2000; Veksler et al., 1986; London and Burt, 1982). The fluxing components most often cited are B, F and P (Chapter 5, Figure 5-17 to 5-20). These occurred in the Noumas I pegmatite. The fluxing elements such as Li and B lower the solidification temperatures within the magma (Keppler, 1993).

6.2.1. Mineralogy and petrology

The three main processes namely cooling rate, nucleation and diffusion involved in the mineral development have a great influence on the ultimate texture of the final rock. The crystallization rate that is the slowest will have the biggest control on the crystallization of the minerals (Philpotts and Ague, 2009). The paragenetic sequence of spodumene, columbite-tantalite, lepidolite, beryl, garnet and tourmaline have been reconstructed for the Noumas I pegmatite (Figure 6-1).
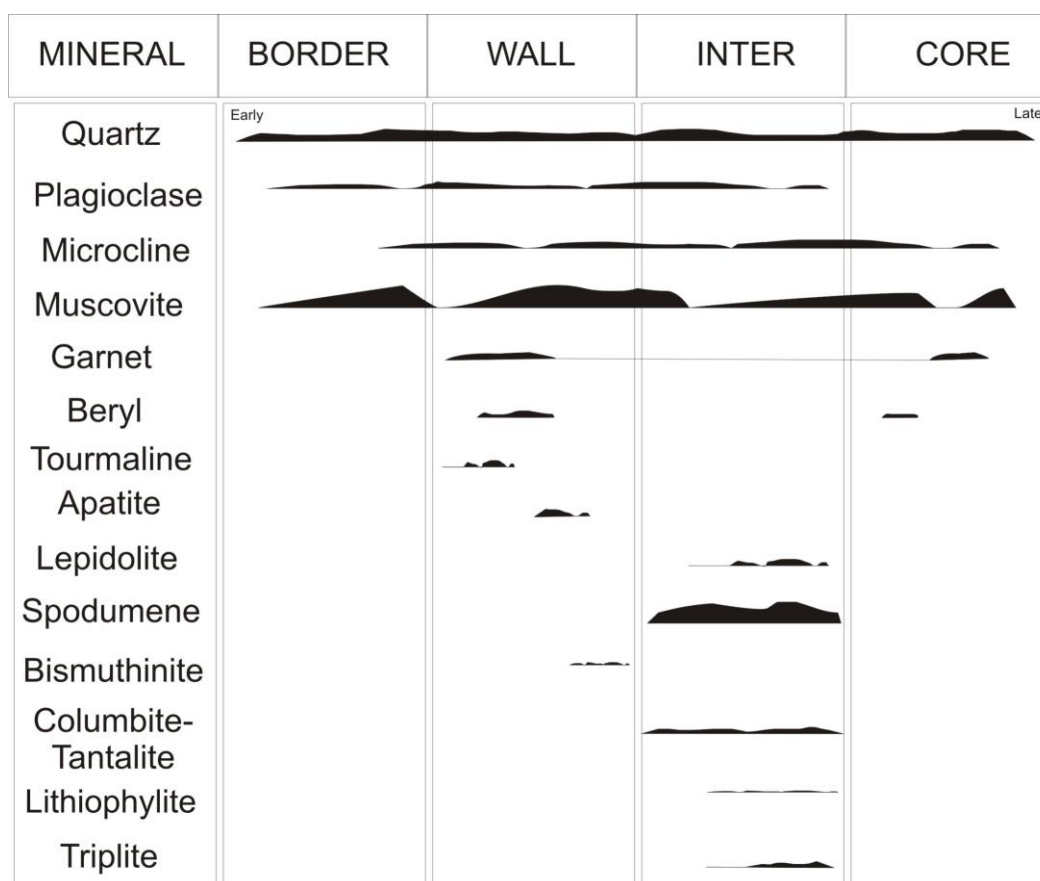
Figure 6-77: Paragenetic scheme of the Noumas I pegmatite mineralization within the border, wall, intermediate and core zones.

The border contains minerals microcline, plagioclase, quartz, muscovite and garnet. The wall zone consists of quartz, plagioclase, microcline perthite, muscovite, albite, beryl and triplite with accessory bismuthinite, apatite and columbite-tantalite. The intermediate zone showed quartz and feldspar graphically intergrown with spodumene, lepidolite, amblygonite and triplite. The core consists of milky quartz, large microcline perthite, muscovite, garnet and beryl crystals

The Li (Mn, Fe) P and columbite-tantalite minerals appear later in the paragenetic sequence as ($LiMnPO_4$) lithiophylite and ($MnNb_2O_6$) columbite. These are the only mafic phases

identified during the study in the intermediate zones. Shigley et al. (1986) states that among the accessory minerals, found in some granitic pegmatites, the phosphate species, lithiophylite-triplite is important. Looking at the mode of occurrence for the phosphates it is probable that their crystallization occurred during the earlier stages of pegmatite formation. The variations in the mineral assemblages and zonation suggest the Noumas I pegmatite is a complex, heterogeneous pegmatite.

The Noumas I pegmatite is a more evolved member of the rare-element pegmatites. The more alkaline components promote localized alteration that occurred after coarser-grained minerals. Within the lithium alumino-silicates, Li is exchanged for Na or K to produce pseudomorphism by fine-grained albite or albite and muscovite (London and Burt, 1982). During the replacement of lithiophylite-triplite (Li (Mn, Fe) PO_4) Mn or Fe are substituted by Ca with the related loss of Li (London and Burt, 1982). XRD analysis positively identified the presence of both minerals within the intermediate zone of the Noumas I pegmatite (Appendix 3).

The euhedral, subhedral and anhedral shapes for albite, microcline and muscovite minerals of the same mineral suggested multiple fluid generations. The low-salinity inclusions observed in the quartz are most likely pseudo-secondary inclusions, which formed during the growth of the crystal and are thus the oldest. A possibility regarding the origin of the high-salinity inclusions is that they might have been derived from pre-existing low-salinity fluids which during hydration of surrounding rock the low-salinity content increased causing high-salinity fluid to be trapped (Chapter 5, Table 5-1 and Table 5-6).

Kerr (1950) suggested that the presence of both illite and kaolinite in a formation indicates a source area, with two types of weathering. At the Noumas I pegmatite, the illite and kaolinite are most likely due to weathering of the minerals spodumene and mica. Garnets are not common in igneous rocks but are found as accessory minerals in peraluminous granites, aplites, syenites and granitic pegmatites (Whitworth, 1991). The grossular and almandine varieties are also found in the wall zone of the Noumas I pegmatite.

Tourmalines are resistant to post-ore metamorphism, hydrothermal alteration, weathering and abrasion (Jiang et al., 2004). London (1990) proposes that the tourmaline-rich borders of pegmatites arise by mixing of pegmatite-derived components (Na, B, Al, and Si) and wallrock-derived components (Mg, Fe). The granodioritic host (Mg, Fe) at Noumas provides the components necessary for mixing to produce the small quantities of tourmaline. The large masses of tourmaline associated with granites and pegmatites mark the sites of fluid mixing. As the border zone of the Noumas I pegmatite crystallized and sealed the cavity, the

tourmaline incorporated the Fe from the country rock in the magma. After the external source of Fe was exhausted tourmaline crystallization ceased. This explained the scarcely crystallized pockets of tourmaline found within the wall zones of the Noumas I pegmatite as described in Chapter 3. This is also observed where the magma injected within the wall zone of the Noumas I pegmatite.

The Noumas I pegmatite is enriched in Na_2O and depleted in CaO and Sr (Chapter 4, Figure 4-28) with the exception of volatile phases Li, B and Be compared to chondritic values. The enriched Na_2O and depletion of CaO and Sr are indicative for magmatic evolution of pegmatites (Schwartz, 1990; Tredoux, 2009).

6.2.2. Fluid evolution and crystallization

Crystallization pressure-temperature conditions for pegmatites, rich in Li, to crystallize have been constrained by Ackerman et al., (2007) between 500 - 570°C and 310 - 430 MPa. The trapping temperature range of the samples from Noumas I pegmatite, varies between 116 - 350°C, a very low temperature range and representative of a secondary fluid that entered the pegmatite system after the initial formation of the pegmatitic fluids (Appendix 4) The higher temperatures between 400-650 ^{o}C are the trapping temperatures of the primary inclusions

The pressure and temperature for primary and secondary inclusions differ (Chapter 5, Table 5-5). This showed that the secondary fluids have a lower pressure and temperature than the calculated temperature and pressure of primary fluid inclusions. The shallow 6-8km at 2-2.5kbar scenario is applicable to the secondary inclusions, while the deep17-20km at 5.5-6kbar scenario is ascribed to the primary fluid inclusions.

Initially the parental melt contains OH^- and CO_3^{2-} at the start of crystallization; it begins to exsolve as H_2O and CO_2. CO_2-rich inclusions were detected within the quartz crystals (Chapter 5, Figure 5-5 to 5-6); and believed to have exsolved at lower temperatures of 95-110°C. The water-undersaturated pegmatite forming melt starts crystallizing from the wall of the pegmatite body. At the start of crystallization the melt undergoes boiling. The presence of distinct inclusion types, both high and low salinities, provided the evidence for fluid exsolution from the magma (Chapter 5, Figure 5-10, Table5-1 and Table 5-3) and indicated a slower cooling had occurred at the time of crystallization.

The concentration of CO_2 determined by Raman spectroscopy within the inclusions appears to be low. According to Thomas et al., (2009), this is due to the low solubility of CO_2 in felsic melts. During the cooling of the melt the evolution of the gas phases will result in volume

changes and create an increase in pressure. During the crystallization of the graphic granite the pegmatite forming melt reacts with the wall rock in order to achieve chemical equilibrium.

The microthermometric analyses of quartz crystals from the wall zones, within the Li-, Ta- and Be- Noumas pegmatite were carried out to confine the equilibrium temperature, salinity and general composition of the fluid inclusion generations (Chapter 5, Table 5-2 and Figure 6-4). The analysis and interpretation of the inclusions led to the discovery of two possible fluid generations from the Noumas I pegmatite (Chapter 5, Figure 5-10).

Before the minerals can precipitate from the saturated solution certain changes need to occur. These changes include lowering of the temperature leading to the formation of minerals, the escape of volatile elements or the precipitation of a mineral that will remove the volatiles from the melt. The geological setting of the Noumas I pegmatite within the granodiorite and the metamorphic environment suggests a crustal depth at which it would have been too warm to have cooled down fast. The levels of formation for slower cooling as evidenced by the crystal morphologies are at shallow levels. During deeper, slower cooling secondary boiling processes are active (Robb, 2005). Based on the crystal shapes and sizes, a slow cooling process was active during the formation of the Noumas I pegmatite. The presence of primary inclusions throughout the zones of the Noumas I pegmatite indicate the continuous exsolution and trapping during pegmatite crystallization (Figure 6-1).

The quartz crystal textures within the wall zone of the Noumas I pegmatite consist of graphic intergrowth. The tabular shapes and intergrown structures of crystals from the wall, intermediate and core zones indicate what appears to be slow cooling during the development of the Noumas I pegmatite. The Noumas I pegmatite consists of a quartz-rich zone with a cluster of perthitic-microcline crystals that occupy the centre of the dyke. As mentioned the wall zone contains quartz and tourmaline needles, that project in a downward direction. The wall zone crystallized from the outside inward, into an intergrowth of quartz, K-feldspar with muscovite. The graphic albite and quartz intergrowths appear to have nucleated around the small garnet and pockets of tourmaline.

The zonation found within all complex pegmatite dykes, shows that the compositional changes that occur at the boundary layers, stimulate crystallization to occur (London, 2005). In the final stages of crystallization within the residual melt, the boundary layer will consist of a different composition and as it grows it will become more evolved. This change in the mineral chemistry produces evolved minerals with rare compositions. This could have produced the gem-quality beryl, spodumene and lepidolite found in the wall and intermediate zones of the Noumas I pegmatite.

6.2.3. Chemistry of fluid inclusions

The mineralogy varies considerably over the zoned pegmatite (Figure 6-1). Taking the distinct fluid inclusion populations into consideration, the possibility of a replenished melt-fluid system with multiple fluid generations seems likely. The processes developed, from deep in the crust within the parental rocks, and include partial melts from source rock anatexis and crystal fractionation during magma ascent. Cerny et al. (2012) considered the chemical and tectonic links between the pegmatites and their source rocks. Secondary boiling is the main mechanism of fluid enrichment in pegmatites; it is not expected to find a preserved fluid inclusion record at the source (Roedder, 1984).

Within the Noumas I pegmatite B, F, Li, CH_4 was identified within fluid inclusions (Chapter 5, Figure 5-18 to Figure 5-21). Fluid inclusions suggested that there was more than one fluid generation (Chapter 5, Figures 5-13 to 5-16). The presence of volatiles was confirmed by FTIR, Raman and fluid inclusion salinities.

FTIR identified two possible fluid compositions of either CO_2-H_2O-NaCl or CH_4-H_2O-NaCl system. The Noumas I pegmatite consisted of both aplite veins and pegmatites found within the same granodioritic host. This represents simultaneous crystallization of both the melt and water-rich phases (Stern et al., 1986).

In order to understand the evolution of the mineralizing fluid found in inclusions at the Noumas I pegmatite, a bivariate diagram for the T_f and the salinities of the fluid inclusions was plotted (Figure 6-2). It is clear that for the middle/intermediate zone there is a wide spread in salinity. This can be explained by the occurrence of a wider variety of minerals in this zone. The salinity variations allow larger amounts of cations to be transported within the middle/intermediate zone. The fairly constant values are found in the border and core zones. The differences for the primary and secondary inclusions are noticeable in Figure 6-2. Primary inclusions (Figure 6-2, square) are at higher trapping temperatures with the salinity over a wider range between 0.1-23 (wt. % NaCl equivalents). The secondary fluid inclusions also spread over the same salinities but at lower trapping temperatures. The highly variable salinity of both primary and secondary inclusions (Figure 6-2) can be indicative of the heterogeneous nature of pegmatitic melt and fluids.
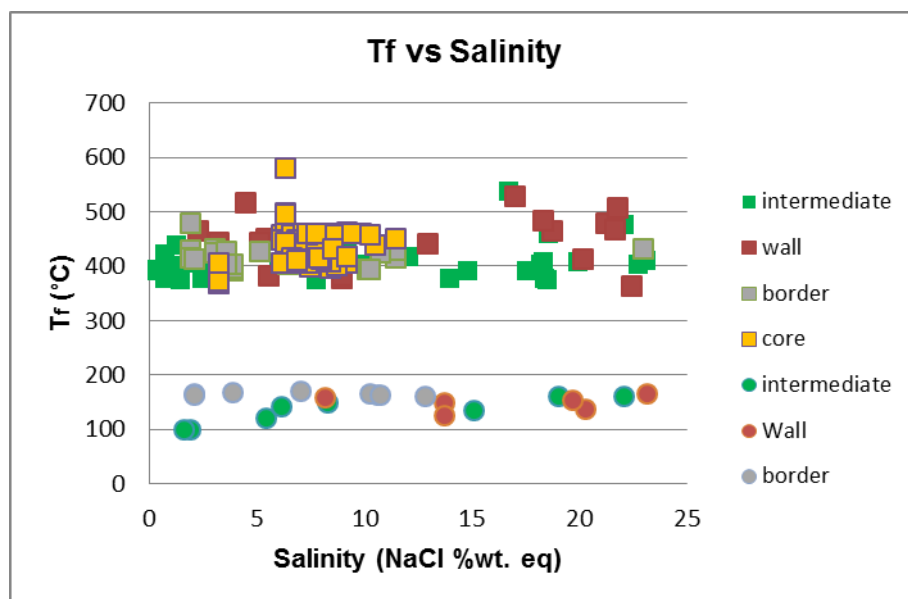
Figure 6-78: Bivariate diagram of salinity (wt. % NaCl) vs. homogenitization temperature (°C) for two-phased inclusions of the various zones of the Noumas I pegmatite. Squares= primary fluid inclusions and circles= secondary fluid inclusions.

There is a definite and distinctive variation in both the salinities and the homogenitization temperatures for the wall, intermediate and core zones of the Noumas I pegmatite (Figure 6-3). Both (T_h and salinity) are higher in the intermediate zone. Within this zone more complex minerals such as spodumene, lepidolite, triplite that are enriched in Li, P, F elements occur. The higher salinities provide a way to transport the elements, making this zone more evolved in mineralization. The salinities are characteristic of the various zones they occupy. The highest salinities are found closest to the pegmatite intrusion (wall zone) and decreases towards the core/inner zones of the pegmatite. A possible explanation for the lower homogenitization temperatures present in the outside wall zones would be the mixing with meteoric waters.
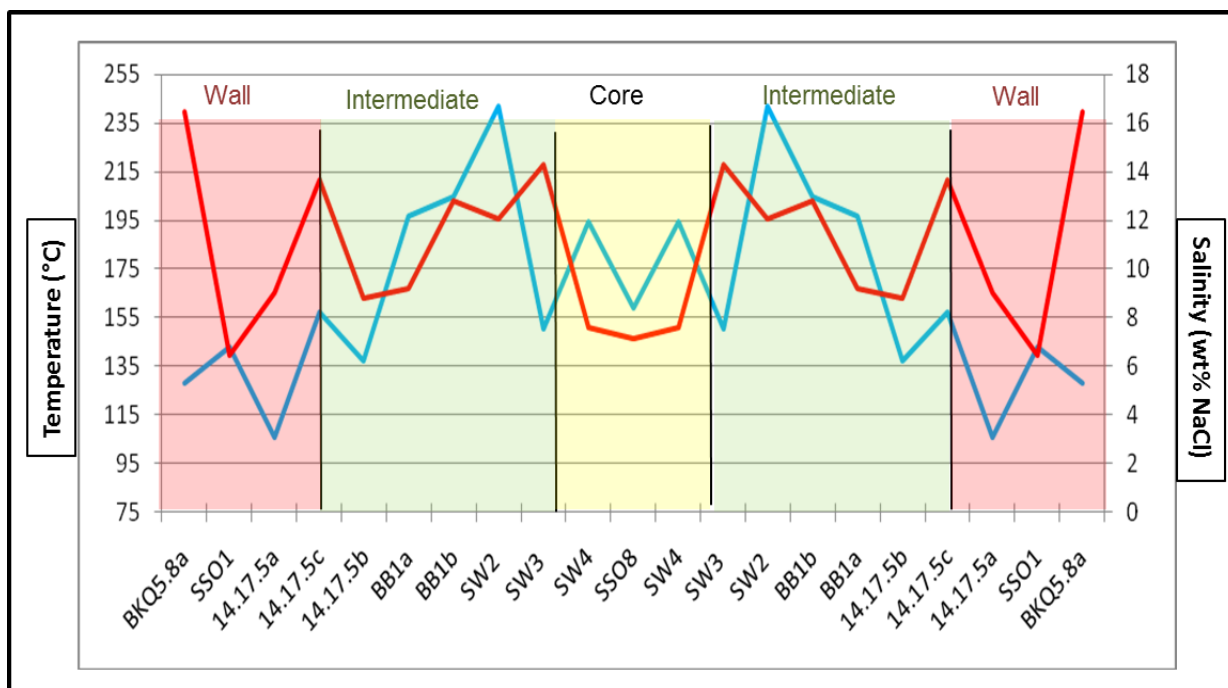
Figure 6-79: The T_h (blue) and salinity (red) distribution within the Noumas pegmatite over the wall, intermediate and core zones.

Quartz crystals were sampled from the intersections within the zoned areas of the Noumas I pegmatite. The observations regarding the evolution of the fluids are made in the different sampled sections from the pegmatite in quartz minerals. These zones represent the evolving magma from the outside to the inside. The occurrences of the various phases in the inclusions are dependent on the geological conditions under which the minerals were formed such as fluid composition, primary and secondary boiling, and interaction of magmatic and metamorphic fluids.

Rapid cooling inhibits the fluid exsolution process (Thomas and Davidson, 2007). The fluids indicate that slower cooling had to have occurred for the Noumas I pegmatite. This supports the data found (Chapter 4) suggesting slower cooling. The chemical evolution of the minerals within the Noumas I pegmatite is controlled by the evolving melt composition and by the occurrence of specific volatiles (prohibiting the crystallization or influencing the formation temperature), and will change once the volatiles have been withdrawn from the system (Figure 6-1).

During the precipitation of albite, quartz, tourmaline and Li-Be ore minerals the removal of B, Mg, Fe, Na, K, Al, Si, Li and Be elements from the melt leads to the precipitation of other minerals. An example of this is the crystallization of tourmaline from fluids between 470 -

420°C that removes borate from the melt. After the crystallization of these minerals the remaining fluid is composed of a low-density NaCl-CO_2 aqueous fluid.

An oversimplified diagram of temperature and pressure based on the quartz-saturated phase relationships for lithium minerals showed in Chapter 5, Figure 5-21, provided estimations on the depth of emplacement (6-8 km) and the pressure (2-2.5 kb). A granitic melt would plot around 650°C (Triangle in Figure 5-21), as the magma forming the pegmatite was exposed to secondary boiling or mixing with meteoric fluids the temperature was reduce to the 350°C found at the Noumas I pegmatite where both spodumene and petalite minerals co-crystallize.

The presence of fluxing elements such as F, B, Li and P can affect the solidification temperature of magma by substantially lowering it. These fluxing elements control the depth of emplacement allowing the magma to rise and intrude at shallower levels (Cerny et al., 2012). The more enriched the pegmatite is in the fluxing elements the shallower the crystallization depth. The Noumas I pegmatite is enriched in F, Li and B.

Table 6-18: Summary of the results for mineralogy, petrography, geochemistry and microthermometry. Grain sizes are as follows: coarse (>5cm), medium (1-5cm) and fine (<1cm).

Area	Wall/outer	Intermediate/middle	Core
MINERALOGY XRD	Qtz , K-fsp, beryl, mica, plag tourmaline, garnet bismuthinite , apatite	Qtz, K-fsp, spd, lep, mica plag, triplite, illite, petalite	Qtz, K-fsp, beryl, mica, garnet plag, illite
PETROGRAPHY Crystallinity Crystal size Crystal shape	Large intergrown texture between qtz and K-fsp Holocrystalline Coarse Idiomorphic	Intergrown texture between qtz and K-fsp Holocrystalline Coarse and medium Hypidiomorphic	Exsolution texture (Perthite) Holocrystalline Coarse and fine Hypidiomorphic
GEOCHEMISTRY **Major elements**	Distribution constant (SiO_2, Al_2O_3). Na_2O increases as K_2O decreases towards middle zone. Distribution of MgO and Fe_2O_3 increases towards the middle zone	Distribution relatively constant (SiO_2, Al_2O_3). Na_2O increases as K_2O decreases towards core zone Distribution of MgO and Fe_2O_3 fluctuates towards the core zone	Distribution relatively constant (SiO_2, Al_2O_3). Na_2O increases as K_2O decreases away from the middle zone. Distribution of MgO and Fe_2O_3 fluctuates
FLUID INCLUSIONS Dominant FI Avg. Salinity (wt% NaCl) Te (°C) Composition of fluids	Liquid 6.47 -17.58°C NaCl dominated	Liquid 12.03 -28.08°C K/NaCl dominated, <Mg+$CaCl_2$	Liquid 7.37 -24.43°C K/NaCl dominated

6.3 Origin and classification of the Noumas I pegmatite

Over the last 100 years the origin and enrichment of the pegmatitic magma has been widely debated and is still a controversial topic among authors (Cameron et al., 1949; Beukes, 1973; Blignault et al., 1983, Cornell et al., 2006). London and Kontak (2012) regarded pegmatites to have bulk compositions of minimum-temperature melts in a hydrous granitic system ($NaAlSi_3O_8$-$KAlSi_3O_8$-SiO_2-H_2O) where the most chemically evolved pegmatites

would have only a few viscosity-reducing components such as H_2O, B, P and F. The two most widely used models to classify pegmatites are the Cameron et al. (1949) model and Jahns and Burnham (1969) model. The two models are summarized with in Table 6-3 along with the Noumas I pegmatite.

Table 6-19: The two models compared with the Noumas I pegmatite.

	Cameron et al. (1949)	Jahns and Burnham (1969)	London (2005)	Noumas I pegmatite
Source magma	Silicate melt that scavenges elements from the host rock, to produce zones of distinctive deposition.	The source of constituents from silicate melts, textures and mineralogical zonation of the pegmatites.	Pegmatites originate by extended crystal fractionation of large magma bodies	Mixing of magmatic fluids with meteoric fluids after magma was depleted of Sr, P and Zr.
Crystallization of pegmatite	The chemical evolution of pegmatites can be attributed to fractional crystallization of melts. During this process, rare elements such as Li, Be and Ta, fluxes such as B, P and F and other volatile components such as H_2O and Cl are concentrated by the initial crystallization of quartz and feldspars to concentrate inward into a diminishing fraction of residual melt. This melt eventually becomes saturated in rare components and then forms minerals containing them.	Crystallization from an aqueous fluid that scavenged and redistributed particular elements from the melt to growing crystals (London and Kontak, 2012).	Crystallization occurs under conditions of strong undercooling relative to the liquidus. In granitic pegmatites, the boundary between granitic compositions rich in rare minerals marks the transition from crystallization of the bulk melt through the flux-rich boundary layer to crystallization of the flux-rich medium.	The evolving magma will crystallize minerals during the cooling process in the following sequence (Table 6-2).The Noumas I pegmatite contains flux elements (B, F, Li and P) of which enrichment occurred during the crystallization of quartz. Fractional crystallization reduced Fe, Mg, Ti, Ca and Na and at the same time enriched the melt in K and Si. The enrichment led to crystallization of alkali-feldspar and quartz.
Internal zonation	The internal zonation is very distinct with the difference in mineralogy identifying the zones enriched in more rare elements. The zonation is controlled by the presence of mobile elements; they have a specific sequence in which they crystallize from the melt.	The internal zonation and crystallization order of the main minerals in the pegmatites as the result of equilibrium crystallization, from a granitic water-saturated magma. The exsolved water-dominated fluid of evenly distributed phase in the residual pegmatitic magma should be responsible for the giant crystal size and concentration	Mineralogical zonation due to igneous fractional crystallization. Fractional crystallization of vapour-undersaturated but volatile-rich melt approximates characteristic zonation found in pegmatites.	The internal zonation was established as the wall, intermediate and core zones. The zones are determined based on the mineralogy present within them. The parental magma crystallized zircon, apatite and plagioclase (Figure 4-30) leaving a depleted magma that mixed with meteoric fluid as it started to crystallize.

	Cameron et al. (1949)	Jahns and Burnham (1969)	London (2005)	Noumas I pegmatite
		of the rare-element minerals in late stage replacement bodies.		
Textures	Intergrowth along the contact zones and the intruding pegmatite.	Mixing of fluids along the contact of the intruding pegmatite.	Porphyritic and intergrowth textures with flux boundary layers clearly visible.	Intergrowth textures are present in all the zones and mixing caused the formation of tourmalines in the wall zone.
Shape of pegmatite body	Symmetrical shape controlled by the area that pegmatite is intruding into	Shape is controlled by the type and structure of the wall rocks.	Shape is controlled by the type and structure of the wall rocks	Emplaced in a granodioritic host rock, with fractures that have undergone folding. The foliation within the Noumas I pegmatite has the same foliation as the granodioritic host rock.
Sub classification	1) Homogeneous simple pegmatites that consist of aggregates of quartz, feldspar and accessory minerals, typically found in groups or swarms with no economically important minerals and 2) Heterogeneous pegmatites usually with a systematic arrangement of constituents and zones that varies in mineralogy and texture (Hugo, 1970).			Heterogeneous complex pegmatite due to the various mineral assemblages and textures hosted within the wall, intermediate and core zone.

The Noumas I pegmatite showed features which are in agreement with Jahns and Burnham's (1969) findings of pegmatites (Chapter 5, Figure 5-21, Table 5-3). Jahns and Burnham (1969) emphasized the importance of a separate (dominantly aqueous) vapour phase in forming pegmatitic textures. When considering the solubility of water in pegmatite melts enriched in F, B, Li, even at very low pressure, it is possible for the pegmatite melt to remain water-undersaturated (London et al., 1989; London, 1996; Thomas et al., 2000, 2003). The majority, although not all, of the factors highlighted in Table 6-19 agree with the model of Jahns and Burnham (1969).

Two chemical families, based on their trace elements present within a pegmatite, can be identified, namely the LCT (lithium, cesium and tantalum) and the NYF (niobium, yttrium and fluorine) family. The Noumas I pegmatite is classified as part of the LCT family, based on the

enrichment of trace elements Li, Be, B, Ta (Chapter 4, Figure 4-29 and Figure 4-30). The elements strongly correlate with S-type granite.

The best example of a LCT pegmatite is the Tanco pegmatite at Bernic Lake, Canada. The pegmatite consists of nine main mineralogical zones (Linnen et al., 2012). The upper intermediate zone produced Li, with Cs production from the pollucite zone and Ta from the central intermediate zone. Within the pegmatite only some zones are concentric, where Ta and Cs occur as different pods within the internal structure of the pegmatite (Linnen et al., 2012). Due to the different locations of mineralization for Li and Ta the two elements are considered as having different mineralization controls. The zones for Tanco and Noumas I pegmatites are summarized in Tables 6-4 and 6-5.

Table 6-20: The mineralogy within the various zones of the Tanco pegmatite.

Zone	Mineralogy	Zone	Mineralogy
1. Wall	Coarse-grained microcline perthite, quartz, albite, tabular mica and tourmaline	5. Upper intermediate	Microcline perthite, amblygonite and petalite
2. Lower intermediate	Microcline perthite and spodumene embedded in medium-grained quartz, albite, tourmaline and lithium micas	6. Central intermediate	Coarse-grained microcline perthite and quartz replaced by an assemblage of fine-grained greenish mica + quartz (MQM) with tantalum and zircon.
3. Transition (wall to the lower intermediate)	Abundant Li-minerals (aluminosilicates: spodumene and petalite, and phosphates: lithiophylite and amblygonite)	7. Quartz	Monomineralic quartz.
4. Aplitic albite	Fine-grained undulating layers of saccharoidal albite and quartz with abundant mica and subordinate tantalum oxides	8. Lepidolite	Fine-grained lithium-muscovite and lepidolite.

The Noumas I pegmatite has a strong similarity to the textural evolutions found at Tanco but does not consist of the same mineralization and zones. The Tanco pegmatite consists of 9 zones (Lichtervelde et al., 2007) including the border zone (Table 6-4). The Noumas I pegmatite is fractionated, due to the presence of Li-bearing minerals, specifically concentrated in the intermediate zone of the pegmatite and has 4 zones.

Table 6-21: The mineralogy within the various zones of the Noumas I pegmatite.

Noumas I pegmatite zonation	Correlating Tanco zone	Mineralogy
1. Border	Wall zone	microcline, plagioclase, qtz, muscovite
2. Wall	Lower intermediate	muscovite, qtz, plagioclase, microcline-perthite, beryl, apatite, garnet, microcline
3. Intermediate	Transition to lepidolite	spodumene, qtz, triplite, [micro-perthite, tantalite-columbite]
4. Core	Quartz zone	milky qtz, microcline-perthite

The Tanco and Noumas I pegmatite pegmatites belong to the same LCT type family with only the zonation and mineralization that differ. This is largely based on the geological setting from which fluids are sourced to produces various mineral enriched zones.

For the Noumas I pegmatite, geochemical data suggested that the element enrichment was of upper crustal origin. Teng's (2005) studies on Li concentrations of the various continental crust, showed a decrease in Li with depth from upper, middle, lower continental crust to the mantle. This reflected the incompatibility of Li during mantle melting and crustal differentiation and provided evidence that the enrichment in Li was from the upper continental crust.

6.4 Summary of results

The Noumas I pegmatite magma intruded along weak zones into a granodiorite host, crosscutting the country rock. It cooled slowly to produce the, 350m long and 25 wide, Noumas I chemical and mineralogical varied pegmatite body. The pegmatite is a dome shaped body with an asymmetrical vertical zoning from a granitic facies, at the bottom in direct contact with granodioritic country-rock. The pegmatite grades into three main zones with differing degrees of enrichment in Li, F, B (±P, Rb, Be).

Mineralogically the border-, wall-, intermediate- and core zones differ with Li-rich minerals concentrated in the intermediate zone (Figure 6-4). Spodumene dominates the Li mineralization within the intermediate zone followed by lepidolite. Other important Li ore minerals in the intermediate zone were petalite, amblygonite and triplite.
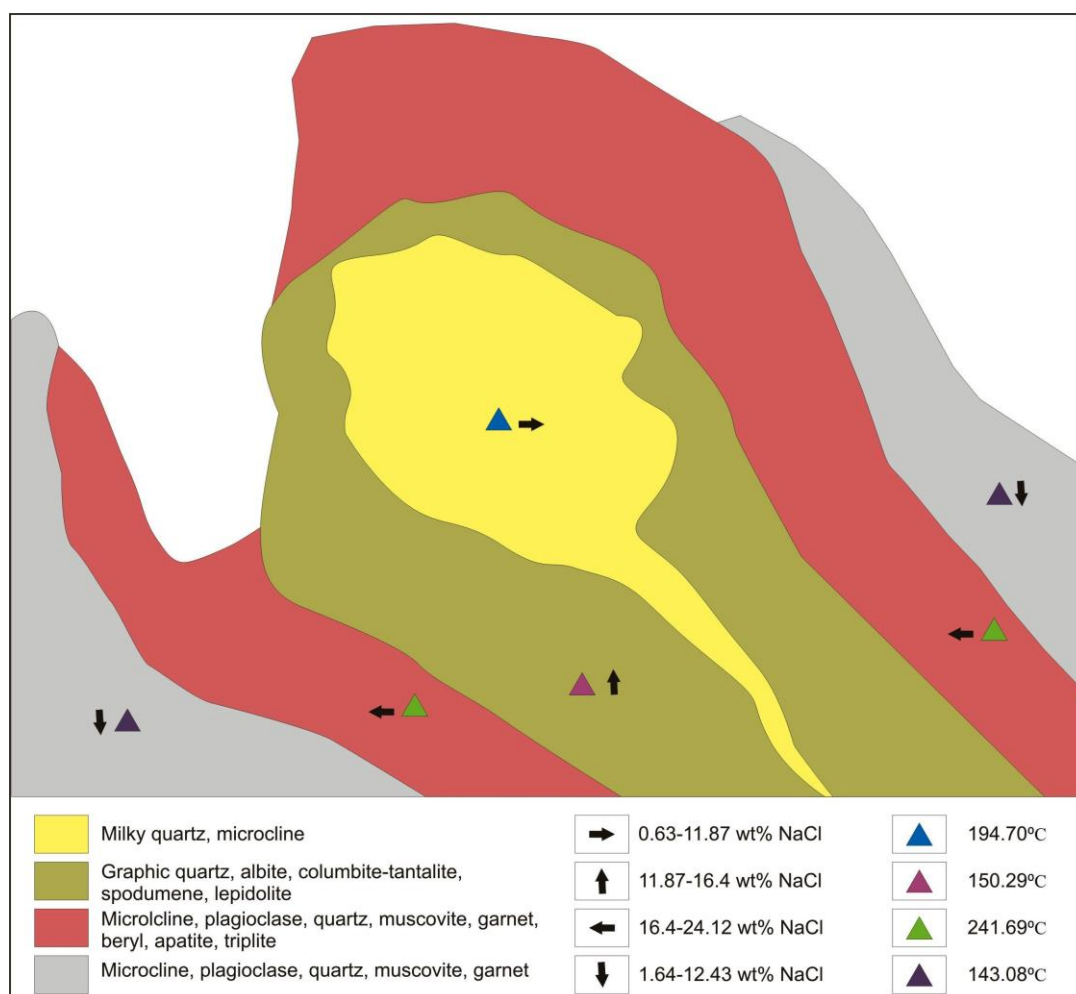
Figure 6-80: Summary of mineralogy and microthermometry for the Noumas I pegmatite within the wall, intermediate and core zones.

The fluids present, during the time of formation, were NaCl dominated with $< Mg + CaCl_2$ present in the intermediate zone. The fluids that formed the Noumas I pegmatite were enriched in Na_2O and depleted in CaO and Sr. The extreme enrichment of Li (6878.20%) within the pegmatite rocks, indicated that the source melts must have been highly Li-enriched.

Textural (Chapter 4) and geochemical (Chapter 5) analyses supports a slow crystal growth rate, that allowed for the separation of the melt. The cooling, growth and nucleation rates can be inferred from the morphology of the crystals, within the wall, intermediate and core zones (London and Morgan, 2012). The minerals forming the intermediate and core zones suggested relative slow cooling with low growth rates. Similar trends were observed in the wall zone, although smaller crystals are present along the contact with the host.

The Noumas I pegmatite strongly agrees with the Jahns and Burnham (1969) pegmatite classification model, where the solidus temperature is lowered after the exsolution of volatiles from the melt. A summary of the Noumas I pegmatite is given in Table 6-6.

Table 6-22: The summary for the studies parameters of the Noumas I pegmatite.

	Noumas I pegmatite
Type of pegmatite	Heterogeneous complex pegmatite
Classification	LCT pegmatite
Age	Younger than 1000 Ma
Depth of emplacement	Primary inclusions 17-20km Secondary inclusions 6-8km (Figure 5-24)
Pressure at time of emplacement	Primary inclusions: 5.5-6 kbar Secondary inclusions: 2-2.5 kbar (Figure 5-24)
Source magma	S-type, peraluminous granite (Table 4-5, Figure 4-16)
Form and zonation	Assymetrical shape, divided into 4 zones namely border, wall, intermediate and core zone.
Country rock	Hosted within a granodioritic host rock
Important minerals	Spodumene, lepidolite, amblygonite, triplite, columbite-tantalite
Secondary and primary fluids	A mixture of NaCl dominated and $Mg+CaCl_2$ was determined within the intermediate zone
Enrichment	A typical granite of 40.5 ppm Li, had to be enriched in Li by 6878.20% factor in order to produce Li-rich zone within the Noumas I pegmatite

Chapter 7: CONCLUSIONS

The Li-rich zoned Noumas I pegmatite (±1000 Ma) formed along fractures and tectonic planes of folded granodioritic host rock. The residual magma, enriched in volatiles and rare elements, intruded along fissures into the surrounding rocks. Akin to other large pegmatite regions of the world, the Noumas I pegmatite is found hosted primarily in the Vioolsdrift suite granodiorites.

The textural, crystal morphology and geochemistry discussed under the petrography, mineralogy and geochemistry studies support a slow cooling rate of the source melts. The depth of emplacement for the pegmatite was estimated (Figure 6-4) for primary inclusions at 17-20km, by using the inferred pressure at 5.5-6 kbar from the quartz-saturated phase relationship (Figure 5-25) for Li-minerals along with the emplacement and metallogenic character of granites from Strong (1988). The formation temperatures for primary inclusions range between 360-560°C. The Tf values indicate the initial emplacement depth, pressure and temperatures at the time of formation. The presence of the secondary fluids at lower pressure between 2-2.5 kbar and temperatures around 100-170°C indicate the change that the pegmatite would have undergone during uplift. SEM-EDX, ICP-MS and XRF showed that the source rocks of the melts were probably from upper continental crustal rocks. This was most evident in the depletion of Nb, Ta, Sr, and Zr in the magma, as it rose through the crust. The granodioritic host rock also played a critical role, during the formation of the pegmatite, especially influencing the minerals closest to the contact zone. Garnet and beryl minerals, found near the contact with the granodiorite, could scavenge Fe and Mg from the host rock. The Noumas I pegmatite thus had a strong magmatic influence during the crystallization period. The negative Ce anomaly indicated the intermediate and core zones were formed during a stronger oxidation period, while the presence of bismuthinite, in the wall zone, indicated a period of reducing conditions.

The Noumas I pegmatite can be classified as a Li-columbite-tantalite pegmatite, derived from peraluminous granites that concentrate Li, Rb, Cs, Be, Sn and Ta, Nb in the presence of B, P and F. The major element compositions support rather a S-type than an I-type granitic source composition. An enrichment factor of 6878.20% was needed to produce the Noumas I pegmatite, with Li-rich minerals from source granite with a concentration of 40 ppm. The major Li-minerals, present in the pegmatite, include spodumene, petalite, lepidolite, amblygonite with accessory beryl, columbite-tantalite, and bismuthinite. The mineral paragenesis indicates a definite change in chemistry and mineralization over the crystallization period of the pegmatite.

Microthermometry, Raman and FTIR studies identified liquid with NaCl as the dominant solute in the fluid. H_2O and CO_2 composition in fluids were present in the wall, intermediate and core zones. The average salinities vary within the pegmatite, the wall has the lowest salinity of 6.47 (wt % NaCl) compared to the intermediate and core zone. This was due to mixing with meteoric fluids, which lowered the homogenization temperature in the wall zones.

Chapter 8: REFERENCES

Ackerman, L., Zacharias, J., and Pudilova, M., 2007. P-T and fluid evolution of barren and lithium pegmatites from Vlastejovice, Bohemian Massif, Czech Republic: *International Journal of Earth Science* (Geol Rundsch) (96) p.623-638.

Akagi, T. and Masuda, A., 1998. A simple thermodynamic interpretation of Ce anomaly, Gechemical Journal, 22:301-314.

Anderson, A.J. and Bodnar, R.J., 1993. An adaption of the spindle stage for geometric analysis of fluid inclusions, *American mineralogist*, 78, 657-664.

Bakker, R.J., 1999. The application of a computerized and optimsed clahrate stability model to fluid inclusion studies, Bol. Soc. Esp. Mineral, 18-1 (abstr.).

Barnes, H.E., 1997. Fluid inclusion studies of hydrothermal ore deposits, I*n: Geochemistry of hydrothermal ore deposits*, John Wiley & Sons Inc., 3rd edition, 657-697.

Beukes, G.J., 1967. 'n Mineralogiese studie van sekere seldsame aardminerale van die Gordonia-Kenhardtgebied, N.W.-Kaapland. Unpubl. M.Sc. thesis, Univ. Bloemfontein.

Beukes, G.J., 1973. 'n Geologiese ondersoek van die gebied suid van Warmbad, Suidwes-Afrika, met spesiale verwysing na die metamorf-magmatiese assosiasies van die voorkambriese gesteentes. Unpubl. Phd. thesis, Univ. Bloemfontein.

Blignault, H.J., 1977. Structural-metamorphic imprint on part of the Namaqua mobile belt in South West Africa, Bulletin, Precambrian Research Unit, University of Cape Town, 23:1-197.

Blignault, H.J., Van Aswegen, G., Van der Merwe, S.W. and Colliston, W.P., 1983. The Namaqualand geotraverse and environs: part of the Proterzoic Namaqua mobile belt, *Spec. Publ. geol. Soc. S. Afr.*, 10:1-29.

Bodnar, R.J and Viryk, M.O., 1994. Intepretation of microthermometric data for H2O-NaCl fluid inclusions, Fluid inclusions in minerals, methods and applications,117-130.

Boelema, R. and Hira, H., 1994*.* Pegmatite deposits, *The mineral resoures of South Africa*, 6th edition, MGC Wilson CR Anhaeusser (editors) Council for Gesciene, 16: 509-521

Boelema, R., 1998. Feldspar, *The mineral resources of South Africa*, 6th edition, MGC Wilson CR Anhaeusser (editors), Council for Geoscience, 16: 267-268.

Bowers, T.S. and Helgeson, H.C., 1983. Calculation of thermodymanic and geochemical consequences of nonideal mixing in the system H2O-CO2-NaCl on phase relations in geologic systems: metamorphic equilibria at high pressures and temperatures, American Mineralogist, vol.68: 1059-1075.

Bullen, W.D., 1998. *In:* Anhaeusser C.R.; Wilson, C.R., 1998. The Mineral Resources of South Africa, Geological. Soc. S. Afr. Johannesburg and Council for Geoscience, 441-443.

Cairncross, B., 2004. Field guide to rocks and minerals of Southern Africa, Struik publishers, 1-292.

Cameron, E.N., Jahns, R.H., McNair, A.H. and Page, L.R., 1949. Internal structure of granitic pegmatites, monograph 2, *Economic Geology*, Publishing Co., 1-112.

Cerny, P., 1991. Rare-element Granitic pegmatites. Part I: Anatomy and internal evolution of pegmatite deposits, *Geoscience Canada*, 18: 49-67.

Cerny, P., London, D. and Milan, N., 2012. Granitic pegmatites as reflections of their sources, *Elements*, 8 (4): 289-294.

Colliston, W.P., and Schoch, A.E., 2002. The structural development of the Aggenys Hills, *South African Journal of Geology*, 105(4): 301-324.

Cornell, D.H.; Thomas, R.J., Moen, H.F.J.; Reid D.L.; Moore, J.M. and Gibson, R.L. The Namaqua-Natal province. *In*: Anhaeusser C.R.; Thomas R.J. 2006. The Geology of South Africa, Geological. Soc. S. Afr. Johannesburg and Council for Geoscience, 325-379.

Deer, W.A., Howie, R.A. and Zussman, J., 1997. *Rock forming minerals*: Single chain silicates, 2nd edition (2A), The Geological Society, 1-668.

Deer, W.A., Howie, R.A. and Zussman, J., 1997. *Rock forming minerals*: Orthosilicates, 2nd edition, (1A), *the Geological Society*, 1-919.

Dewey, J.F., Robb, L., Van Schalkwyk, L., 2006. Did Bushmanland extensionally unroof Namaqualand?, *Precambrian Research* 150: 173-182.

Diamond, L.W.,1994. Introduction to phase relations of CO_2-H_2O fluid inclusions in minerals: Methods and applications: short working course of the working group (IMA) Pontignano-Siena, September 1-4, 131-158.

Fall, A., Rimstidt, D., Bodnar, R.J., 2009. The effect of fluid inclusion size on determination of homogenization temperature and density of liquid-rich aqueous inclusions, *American Mineralogist*, 94 (11-12): 1569-1579.

Faure, G., 2001. *Origin of igneous rocks*, Springe-Verlag New York, 1-10.

Fuertes-Fuente, M., Martin-Izard, A., Bioron, M.C., and Mangas, J., 2000. Fluid evolution of rare-element and muscovite granitic pegmatites from central Galicia, NW Spain, *Mineral Deposits*, 35: 332-345.

Garret, D.E., 2004. Handbook of Lithium and Natural Calcium Chloride, Amsterdam Publishers, 1-235.

Geringer, G. *J.,* Botha, B. J. V. and Slabbert, M. J., 1988. The Keimoes Suite - a composite granitoid batholith along the eastern margin of the Namaqua Mobile Belt, South Africa. *S. Afr. J. Geol.*, 91 (4):465-476.

Gevers, T.W., Partridge, F.C. and Joubert, G.K., 1937. Union of South Africa, *Geological Survey*: The pegmatite area south of the Orange River in Namaqualand, Memoir 31:1-180.

Ginsburg, A.I., 1960. Specific geochemical features of the pegmatitic process, International Geological congress, 21st session, report, part 17, 111-121.

Glover, A.S., Rogers, W.Z., and Barton, J.E., 2012. Granitic pegmatites: Storehouses of Industrial Minerals, *Elements*, 8: 269-273.

Halliday, A.N., Davidson, J.P., Hildreth, W., and Holden, P., 1991. Modelling the petrogenesis of high Rb/Sr silicic magmas, Chemical Geology, 92: 107-114.

Harpum, J.R., 1963. Petrographic classification of granite rocksin Tanganyika by partial chemical analyses, Geological Surv. Tanganyika, 10: 80-88.

Hugo, P.J., 1970. *Geological Survey*: The pegmatites of the Kenhardt and Gordonia districts, Cape Province, Memoir 58: 1-94.

Huizenga, J.M., 2010. Short course in fluid inclusions, Short course handbook, 1-46.

Jacobs, G.K., and Kerrick, D.M., 1981. APL and FORTRAN programs for a new equation of state for H2O, CO2, and their mixtures at supercritical conditions. Comput. Geosci. 7, 131–143.

Jacobsen, S.B., Wills, J., Yin, Q., 2000. Seawater isotope records, crustal evolution, tectonics and atmospheric evolution. Proceeding, Seventh Annual V.M. Goldschmidt Conference, 2000. PDF abstract.

Jahns, R.H. and Burnham, C.W., 1969. Experimental studies of pegmatite genesis: I. a model for the derivation and crystallization of granitic pegmatites, *Economic Geology*, 64: 843-864.

Jiang, S., Yu, J. and Lu, J., 2004. Trace and rare-earth element geochemistry in tourmaline and cassiterite from the Yunlong tin deposit, Yunnan, China: implication for migmatitic-hydrothermal fluid evolution and ore genesis, *Chemical Geology*, 193-213.

Kennedy, B.A., 1990. Surface mining,2nd edition, 194-196.

Keppler, H., 1993. Influence of fluorine on the enrichment of high field strength trace elements in granitic rocks. *Contrib Mineral Petrol* 114: 479-488.

Kerr, P.F., 1950. Formation and occurrence of clay minerals, Clay and clay technology, bull.169: 19-32

Landes, K. K., 1933. American Mineralogist: Origin and Classification of Pegmatites, 18 (2): 5-12.

Levinson, A.A., 1974. Introduction to exploration geochemistry, 2nd addition, Applied publishing ltd., 1-640.

Lichtervelde, M., Linnen, R.L., Salvi, S., Bezia, D., 2007. Tantalum mineralization in the Tanco pegmatite: magmatic *versus* metasomatic processes, *Granitic Pegmatites: The State of the Art – International Symposium. 06th – 12th, Porto, Portugal.*

Linnen, R.L., Van Lichtervelde, M., and Cerny,P., 2012. Granitic pegmatites as source of strategic metals, *Elements*, 8: 275-280.

London, D, Morgan, G.B., Hervig, R.L., 1989. Vapor-undersaturated experiments with Macusani glass + H2O at 200 MPa, and the internal differentiation of granitic pegmatites, *Contrib. Mineral Petrol.,* 102:1-17.

London, D., 2005.Granitic pegmatites: an assessment of current concepts and directions for the future, *Lithos*, 80: 281-303.

London, D. and Burt, D.M., 1982. Alteration of spodumene, montebrasite, and lithiophilite in pegmatites of the White Picacho district, Arizona. *American Mineralogist*, 67: 97-113.

London, D., and Kontak, D.J., 2012. Granitic Pegmatites: scientific wonders and economic bonanzas, *Elements*, 8 (4): 257-263.

London, D., and Morgan, G.B., 2012. The pegmatite puzzle, *Elements*, 8 (4): 263-268.

London, D., 1987. Internal differentiation of rare-element pegmatites: effects of boron, phosphorus and fluorine, *Geochimica et Cosmoschimica acta*, 51: 403-420.

London, D., 1990. Internal differentiation of rare-element pegmatites: A synthesis of recent research: Geological Society of America Special Paper, 246: 35–50.

London, D., 1996. Granitic pegmatites: Transactions of the royal society of Edinburgh, *Earth Sciences*, 87: 305-319.

London, D., 2008. Pegmatites, *Canadian Mineralogist* special publication, 10:1-347.

Lottrmoser, B.G., and Ashley, P.M., 2006. Mobility and retention of trace elements in hardpan-cemented cassiterite tailings, north Queensland, Australia, *Environ Geol*, 50: 835-846.

Martens, F., 1979. A sequence of deformational events in the Ratelpoort fold area, Namaqualand, Master's thesis, University of the Orange Free State, 1-84.

McCarthy, T., and Rubidge, B., 2005. *The story of earth and life*: *a Southern African perspective on a 4.6 billion year journey.* Struik Publishers, 1- 333.

Minnaar, H., and Theart, H.F.J., 2006. The exploitablility of pegmatite deposits in the lower Orange River (Vioolsdrift-Henkries-Steinkopf), *South African Journal of Geology*, 109 (3): 341-352.

Morgan, G.B.V.I., and London, D., 1999. Crystallization of the Little Three layered pegmatite - aplite dike, Ramona District, California, *Contributions to Mineralogy and Petrology*, 136: 310-330.

Nel, L.T., 1965. Beryllium ore deposits in the Republic and in South West Africa: Atom. Energy Bd., Pel., 1-136.

Nesse, W.D., 2004. *Introduction to optical mineralogy*, University of Northern Colorado, Oxford University press, 3rd edition, 1-348.

Patterson, J.E., 1997. The Little 3 Mine "Plug"; Evidence for a Zoned Plutonic Intrusion and a Plausible Parent Source of the Ramona Pegmatite District, Ramona, San Diego County, California, University of Arizona, B.Sc. Honours thesis, 1-152.

Philpotts, A.R., and Ague, J.J., 2009. Principles of Igneous and Metamorphic Petrology second edition, Cambridge University Press, 239-267.

Quirke, T.T., and Kremers, H.E., 1943. Pegmatite crystallization, American Mineralogist, 28: 571-580.

Raeside, R., 2003. *Fluid inclusions: analysis and interpretation*, mineralogical association of Canada, editors: Samson, I., Anderson, A., and Marshall, D., short course series, 32, Vancouver , British Columbia, 1-374.

Robb, L.J., 2005. *Introduction to Ore-Forming Processes,* Blackwell publishing*, 1*-344.

Roedder, E., 1984. Fluid inclusions. *Reviews in Mineralogy*, Mineralogical society of America, 12: 644.

Roedder, E., and Bodnar, R.J., 1980. Geologic pressure determinations from fluid inclusion studies, *Ann. Rev. Earth planet. Sci*, 8: 263-301.

Rudnick, R.L and Gao, S., 2003. Composition of the continental crust, *Treaties of geochemistry*, 3.01:1-56

Schmidt Mumm A., 2008. Introduction to fluid inclusion research, Short course handbook, Department of Geology and Geophysics, Adelaide University, 1-53.

Schutte**,** I.C., 1972. The main pegmatites of the area between Steinkopf, Vioolsdrif and Goodhouse, Geological survey of South Africa, Memoir 60: 1-17.

Schwartz, M.O., 1990. Geochemical criteria for distinguishing magmatic and metasomatic albite enrichment in granitoids- examples from the Ta-Li granite Yichun (China) and the Sn-W deposit Tikus (Indonesia), *Mineral deposita*, 27 (2): 101-108.

Shigley, J.E., and Brown, G.E., 1986. Lithiophilite formation in granitic pegmatites: A reconnaissance experimental study of phosphate crystallization from hydrous aluminosilicate melts, *American Mineralogist*, 71: 356-366.

Sinclair, W.D., 1996. Granitic pegmatites, Canadian Mineral Deposit types, Geological survey of Canada, Geology of Canada, 8: 503-512.

Sohnge, P.G., and De Villiers, J., 1946. Resume of the geology of the Richtersveld and the eastern Sperrgebiet, *Geol. Soc. S. Afr.*, 49.

Stern, L.A., Brown, G.E., Jr., Bird, D.K., Jahns, R.H., Foord, E.E., Shigley, J.E., and Spaulding, L.B., Jr., 1986. Mineralogy and Geochemical Evolution of the Little Three Pegmatite-aplite layered intrusive, Ramona, CA, *American Mineralogist*, 71(3 / 4): 406-427.

Stewart, D.B., 1978. Petrogenesis of lithium-rich pegmatites. *American mineralogist*, 63: 970-980.

Strong, D.F., 1988. A review model for granite-related minerals, 424-445.

Strong, D.F., 1988. A Model for Granophile Mineral Deposits in Roberts, R.G. and Sheahan, P.A. (eds.) Ore deposit Models. Geoscience Canada Reprint Series 3, The Geological Association of Canada. Dept. of Earth Sciences, Memorial University of Newfoundland, 59-66.

Taylor, S.R., and McLennan, S.M., 1985. The continental crust: its composition and evolution. Blackwell, Oxford, 1-312.

Teng, F., 2005. Lithium isotopic systematic of the continental crust, Ph.D Unpublished notes.

Thomas, R., Davidson, P., and Badanina, E., 2009. A melt and fluid inclusion assemblage in beryl from pegmatite in the Orlovka amazonite, East Transbiakalia, Russia: implications for pegmatite-forming melt systems, Mineral Petrol 96: 129-140.

Thomas, R., and Davidson, P., 2007. The formation of granitic pegmatites from the viewpoint of melt and fluid inclusions and new experimental work, Granitic Pegmatites: The state of the art-*International symposium*, 1-27.

Thomas, R., Forster, H-J., and Heinrich, W., 2003. The behaviour of boron in a peraluminous granite-pegmatite system and associated hydrothermal solutions: a melt and fluid-inclusion study, *Contributions to Mineralogy and Petrology*, 144: 457-472.

Thomas, R., Webster, J.D., and Heinrich, W., 2000. Melt inclusions in pegmatite quartz: complete miscibility between silicate melts and hydrous fluids at low pressure. *Contributions to Mineralogy and Petrology* 139, 394-440

Thomas, R.J., Bohmann, D., Bullen, WD., Scogings, AJ. and De Bruin, D., 1994. Unusual spodumene pegmatites from the Late Kibaran of southern Natal, South Africa: *Ore Geology Reviews*, 9(2): 161-182.

Thompson, R.N., 1982. Magmatism of the British Tertiary volcanic province. Scott. J. Geol.,18: 49-107.

Tredoux, M., 2009. Petrochemical applications course notes, GLG364: 1-250.

Van der Merwe, S.W., 1986. The structural development of part of the Namaquland mobile belt in an area between Springbok and Vioolsdrift, Ph.D thesis, Univesity of the Orange Free State, 1-373.

Veksler, I.V., and Thomas, R., 2002. An experimental study of B-, P- and F-rich synthetic granite pegmatite at 0.1 and 0.2 GPa. *Contrib. Mineral. Petrol*. 143: 673-683.

Von Backstrom, J.W., 1964. The geology of an area around Keimoes, Cape Province, with special reference to Phacoliths of Charnockitic Adamellite-phorhyry, Geological survey, Dept. of mines, Republic of South Africa, Memoir 53: 1-218.

Von Backstrom, J.W., 1969. Nuclear reactor materials in South Africa: Minerals Science and Engineering, 1 (2): 24-33.

Von Backstrom, J.W., 1973. Pegmatite deposits in the republic of South Africa, 1-29.

Von Backstrom, J.W., and Nel, L.Y., 1968. Niobium and tantalum mineral deposits in the Republic of South Africa. Atomic Energy Board Report, PEL 177:1-31.

Webster, J.D., Thomas, R., Rhede, Dieter, Foster, H.J and Seltmann, R., 1997. Melt inclusions in quartz from an evolved peraluminous pegmatite: Geochemical evidence for strong tin enrichment in fluorine-rich and phosphorus-rich residual liquids, Geochimica et Cosmochimica Acta, 6 (13): 2589-2604.

Whitworth, M. P., 1991. Petrogenetic implications of garnets associated with lithium pegmatites from SE Ireland, 1-83.

Wood, D.A., Joron, J.L., and Trevil, M., 1979. A re-appraisal of the use of trace elements to classify and discriminate between magma series erupted in different tectonic settings. *Earth Planet. Sci. Lett.*, 45: 326-336.

Appendix 1: SAMPLES

1. Sample collection

During the first visit to the Noumas pegmatite, also known as Blesberg, in the Namaqualand area various samples were taken at different areas along the pegmatite. Random samples were taken in areas in and around areas were extensive mining had occurred (Figures 1 and 2). Of these samples the most promising material was selected containing spodumene, the mineral of interest clearly visible (Table 1).

2. Sample locations

Table 23: GPS coordinates of waypoints taken at the various sample localities in the Namaqualand, between Steinkopf and Viooldrift. Double polished thick and thin (grey) sections made.

SAMPLE	COORDINATES	COMMENT	IN-SITU
BKQ001	S 28°58,56.6" EO17°43'42.2'	Pegmatitic material	Y
BKQ002	S 28°58'57.5" EO17°43'41.8"	Pegmatitic material	Y
BKQ002-1	S 28°59'00.4 EO17°43'40.4	Pegmatitic material	Y
BKQ003-1	S 28°58'59.6" EO17°43'39.3"	Pegmatitic material	Y
BKQ004-2	S 28°58'59.8" EO17°43'39.6"	Pegmatitic material	Y
BKW1	S 28°59'35.9" EO17°42'58.8"	Pegmatitic material	N
DM001	S 28°59'32.2" EO17°44'56.7"	Pegmatitic material	N
GRND1-1	S 29°07'50.7" EO17°38'34.1"	Pegmatitic material	N
NBW	S 29°00'02.2" EO17°42'40.4"	Pegmatitic material	N
NBW1-1	S 29°00'01.1" EO17°42'40.4"	Pegmatitic material	N
NBW1-2	S 29°00'01.2" EO17°42'39.7"	Pegmatitic material	N
PBK1	S 28°58'06.5" EO17°44'19.8"	Pegmatitic material	N
PBK2	S 28°58'06.4" EO17°44'19.6"	Pegmatitic material	N
PEGOUT001	S 29°09'04.3" EO17°37'47.8"	Pegmatitic material	Y
PEGOUT002	S 29°08'52.7" EO17°38'02.8"	Pegmatitic material	Y
PEGOUT003	S 29°08'16.7" EO17°39'43.5"	Pegmatitic material	Y
PEGOUT004	S 29°08'17.1" EO17°39'45.3"	Pegmatitic material	N
PEGOUT005	S 29°05'50.9" EO17°38'15.5"	Pegmatitic material	Y
PEGOUT006	S 29°05'34.1" EO17°38'17.7"	Pegmatitic material	Y
PEGOUT007	S 29°04'59.2" EO17°38'25.3"	Pegmatitic material	N
PEGOUT008	S 29°03'.39.9" EO17°38'50.4"	Pegmatitic material	N
PEGOUT010	S 29°03'18.2" EO17°39'47.9"	Pegmatitic material	N
PEGOUT011	S 29°03'16.8" EO17°40'48.3"	Pegmatitic material	N
PEGUT009	S 29°03'27.1" EO17°39'28.2"	Pegmatitic material	N
POUT1	S 29°02'24.1" EO17°41'28.9"	Pegmatitic material	N
QOUT001	S 28°59'58.6" EO17°42'22.9"	Pegmatitic material	N
QOUT002	S 28°59'59.2" EO17°42'11.8"	Pegmatitic material	N
QOUT003	S 28°59'42.8" EO17°41'46.6"	Pegmatitic material	N
QOUT004	S 29°09'53.0" EO17°37'14.5"	Pegmatitic material	N

SAMPLE	COORDINATES	COMMENT	IN-SITU
QOUT7	S 29°02'47.8" EO17°41'05.7"	Pegmatitic material	N
QURRY001	S 28°58'02.2" EO17°44'00.1"	Pegmatitic material	N
STR1-4	S 29°09'36.1" EO17°37'12.3"	Soil sample	Y
STR2-4	S 29°08'27.5" EO17°38'33.2"	Soil sample	Y
STR3-4	S 29°08'07.4" EO17°39'15.8"	Soil sample	Y
STR4-4	S 29°08'06.5" EO17°39'16.4"	Soil sample	Y
STR5-4	S 29°08'12.9" EO17°39'38.8"	Soil sample	Y
STR6-4	S 29°03'24.5" EO17°40'17.7"	Soil sample	Y
STR7-4	S 29°01'41.5" EO17°41'29.1"	Soil sample	Y
STR8-4	S 29°01'41.2" EO17°41'28.9"	Soil sample	Y
STR9-4	S 28°59'43.7" EO17°43'00.0"	Soil sample	Y

During the follow-up, samples were taken systematically from the different zones (Figure 2) in the vertical as well as the horizontal, along the strike of the pegmatitic body (Table 2).

Table 24: The sampled zones from the border (B), wall (W), intermediate (I) and core (C) zones of the pegmatite (see Figure1 for the position along the pegmatite body). Thick sections (grey).

SAMPLE	Zone	LOCATION	COMMENT
SSO1	B	Southern contact	Qtz, garnet and musc
SSO1A	B	Southern contact	Garnet in qtz
SSO2	B	Northern contact	Qtz , garnet and musc
SSO3	B	Middle qtz	
SSO4	B	Intergrowth zone	Fine disseminated mica distributed along section
SSO5	B	Contact zone	Feldspar, qtz and large mica crystals with beryl
SSO6	W	Contact zone	Qtz, mica and feldspar
SSO7	W	Near contact with host rock	Beryl, mica, garnet in qtz and feldspar
SSO8	C	Inner zone	Qtz in feldspar, green and lilac spodumene, mica.
SW1	W	Wall zone	Qtz "pure"
SW2	I	Contact zone	Color change in qtz (milky), qtz and spodumene contact
SW3	I	Spodumene-rich zone	Spodumene abundant
SW4	C	Spodumene-rich zone	Qtz disseminated in feldspar, beryl and mica
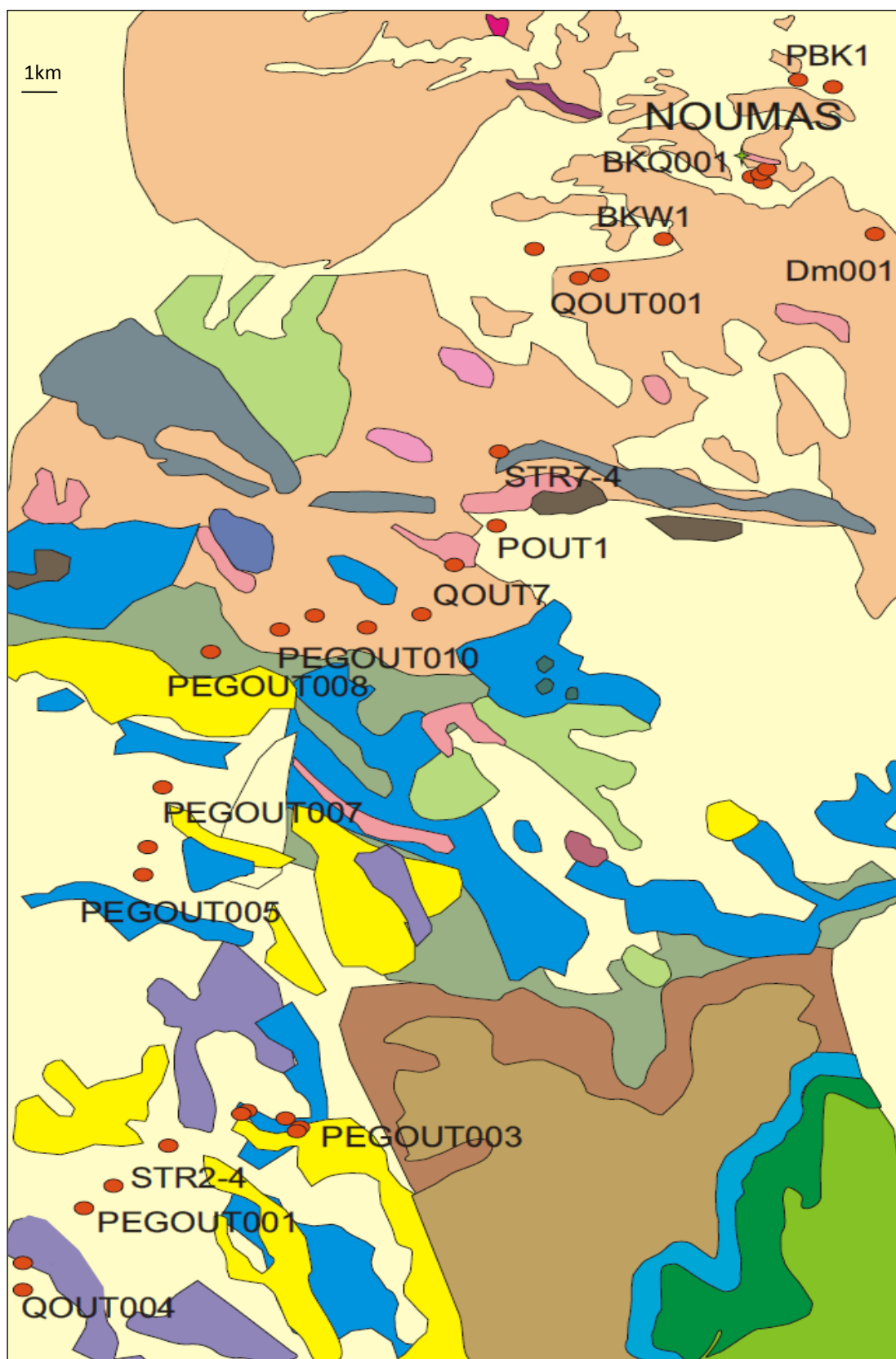
Figure 81: Geological setting of the sampled areas, including the Noumas I pegmatite mining area.
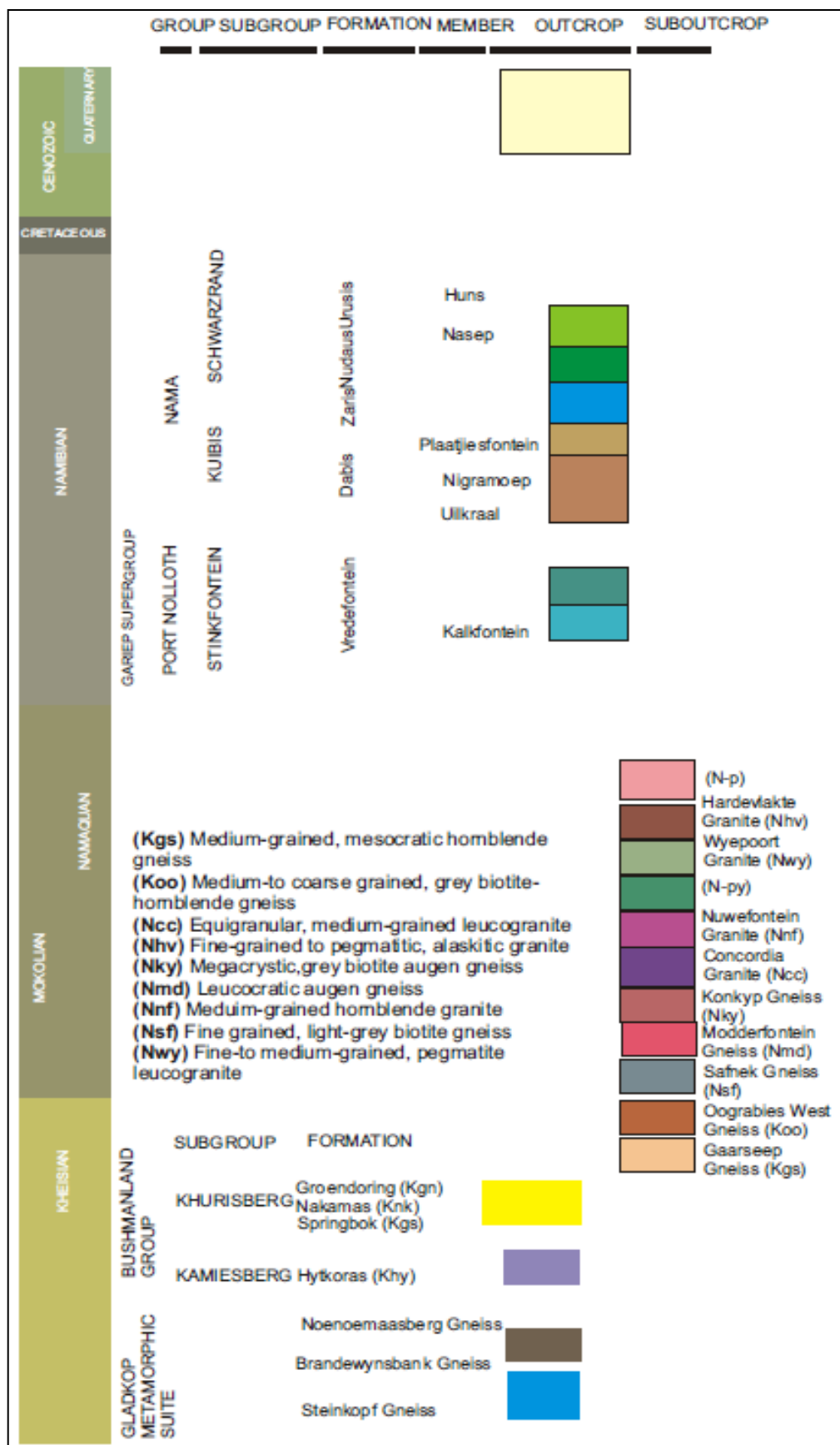
Figure 82: Lithological legend for the geology shown in Figure 1.

Appendix 2: METHODOLOGY

The OLYMPUS BX51 microscope (Table 1) was used to investigate the thin sections from the various zones within the Noumas I pegmatite. It was also used as a pre-estimation for the fluid inclusions within the thick sections. To pin point the areas on the thick sections with fluid inclusions (Chapter 4, Table 4-3, Figure 4-5, Figure 4-6, and Figure 4-7).

Table 25: Detection limits and outlines of Microscopy work at UFS.

	UFS **1.Microscopy**	
Analyze / Used for	Qualitative analysis of mineralogical compositions Identification of minerals and textures	
Data format	Incident and reflected light photographs	
Type	Optical microscopy	
Name, Model	OLYMPUS BX51, microscope	
Samples prep	Polished thin section	

The JEOL JSM 6610 Scanning Electron Microscope (Table 2) was used to estimate the mineral compositions within the thick sections of the Noumas I pegmatite. This was done to identify various phases present in the pegmatite and to establish any compositional variations in the border, wall, intermediate and core zones of the pegmatite (Chapter 4, Figure 4-8, Figure 4-9, Figure 4-10, Table 4-7).

Table 26: Detection limits and outlines of SEM work at UFS

	UFS **2. SEM-EDS**
Analyze / Used for	Qualitative analysis Identification of phases
Data format	Spot analysis, spectra-graphs Elemental and compositional maps
Type	SEM-EDS
Name, Model	JOEL JSM 6610 Scanning Electron Microscope
Standards used	Standard less (internal dataset)
Samples prep	C coated
Accelerating Voltage	20 kV

Whole-rock major and trace elements (Table 3) were analysed by X-ray fluorescence PANanalytical WD-XRF Axois spectrometer using both fused and pressed powder discs. Elemental information for Rb, Sr, Ba, Zr, Nb, Th, Sc, V, Cr, Ga was obtained (Chapter 4, Figure 4-12 to Figure 4-28, Appendix 3, Table 1, Table 2). The pellets and fusion disks were placed and arranged by the PANanalytical WDXRF Axios spectrometer for analyses the major, sodium only, REE-LC and trace elements. The major elements (SiO_2, Al_2O_3, TiO_2, Fe_2O_3, MnO, MgO, CaO, Na_2O, K_2O and P_2O_5) are determined as oxides in wt %. The values of the trace elements are measured in ppm.

Table 27: Detection limits and outlines of XRF work at UFS.
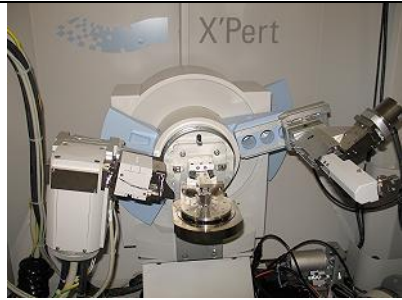
	UFS **3. XRF**
Analyze / Used for	Semi-Quantitative analysis chemistry composition and trace elements
Data format	Major (wt %) and trace elements (ppm)
Type	Wavelength Dispersive XRF
Name, Model	PANalytical WD-XRF Axios spectrometer
Standards used	29 trace and 10 major elements (table 4 Standard names)
Samples prep	Crushed by Retsch KG 5657 Haan BB100, milled by Giebtechnik Labor-Scheibenschwingmmuhle (pellets and fusion disks)
Tube Voltage	4 kW, 60 kV (160 mA)

Table 28: Standards used in the XRF for major and trace elements in wt% and ppm.

Elements	Standard names
Major elements	G-1, W-1, AGV-1, BCR-1, DTS-1, G-2, GSP-1, PCC-1, BHVO-1, MAG-1, SY-2, SY-3, MRG-1, ASK-1, ASK-2, GR,GA, GH, BR, MICA-FE, MICA-MG, DR-N, UB-N, BX-N, DT-N, VS-N, GS-N, FK-N, GL-O, AN-G, BE-N, MA-N, AL-I, IF-G, AC-E, JG-1, JG-1A, JG-2, JG-3, JB-1, JB-1A, JB-2, JB-3,JR-1, JR-2, JA-1, JA-2, JA-3, JF-1, JF-2, JP-1, JGB-1, JCH-1, JDO-1, JLK-1, JLS-1, JSD-1, JSD-2, JSD-3, JSI-1, JSI-2, JR-3, JGB-2, JH-1, NIM-D, NIM-G, NIM-L, NIM-N, NIM-P, NIM-S, SARM-39, SARM-40, SARM-41, SARM-42, SARM-43, SARM-44, SARM-45, SARM-46, SARM-47, SARM-48, SARM-49, SARM-50, SARM-51, SARM-52
Trace elements	AC-E, AGV-1, AL-I, AN-G, ASK-1, ASK-2, BCR-1, BE-N, BHVO-1, BR, BX-N, DR-N, DT-N, DTS-1, FK-N, G1, G2, GA, GH, GL-O, GR, GS-N, GSP-1,IF-G, JA-1, JA-2, JA-3, JB-1. JB-1A. JB-2. JB-3, JCH-1, JDO-1, JF-1, JF-2, JG-1, JG-1A, JG-2, JG-3, JGB-1, JGB-2, JH-1, JLK-1, JLS-1, JP-1, JR-1, JR-2, JR-3, JSD-1, JSD-2, JSD-3, JSI-1, JSI-2, MAG-1, MA-N, MICA-FE, MICA-MG, MRG-1, NIM-D, NIM-G, NIM-L, NIM-N, NIM-P, NIM-S, PCC-1, SARM-39, SARM-40, SARM-41, SARM-42, SARM-43, SARM-44, SARM-45, SARM-46, SARM-47, SARM-48, SARM-49, SARM-50, SARM-51, SARM-52, SY-2, SY-3, TR-2, TR-7, TR-9, TR-14, TRMAC-1, TRMAC-2, TRMAC-3, TRMAC-4, TRMAC-5, TRMAC-6, UB-N, UREM-1, UREM-2, UREM-4, UREM-8, UREM-9, UREM-10, UREM-10/2, UREM-11, VS-N, W-1

After the border, wall, intermediate and core zones were milled the powders were placed into trays for analysis. This was done to identify the minerals that are found within the different zones of the Noumas I pegmatite (Table 5). The results are diffractograms that need to be analysed manually by software packages either 'EVA' or 'HighScore'. The best fit mineral diffractogram patterns with the specific spectral peaks are selected (Chapter 4, Table 4-7, Appendix 3, and Figure 1-8).

Table 29: Detection limits and outlines of XRD work at UFS

	UFS 4. XRD
Analyze / Used for	Mineral identification
Data format	Diffractograms
Type	XRD tube with two Be windows
Name, Model	PANalytical Empyrean X-ray Diffraction
Samples prep	Crushed, milled, powder pressed.
Tube Voltage	60 kV (60mA)

The main objective was to determine the physiochemical properties of the evolved magmatic fluid, temperature of formation, salinities and chemistry of solutes. Microthermometry is used in combination with RAMAN and FTIR techniques to help identify the fluid inclusion compositions.

Fluid inclusions are studied intensely, as they are samples of long-gone fluids once present in the ore body and in some cases can be the actual fluids from which the ore body formed. Fluid inclusions are tiny blebs of fluid (<50μm) trapped within single crystals of both ore and gangue minerals, where normally only the transparent phases are studied (Roedder, 1984). Studies on these trapped fluids can lead to a better understanding of the geological processes involved during the time of formation (Schmidt Mumm, 2008).

There are five basic assumptions regarding fluid inclusion analyses that should not be overlooked, namely:

1) a representative sample of a homogeneous ore-forming fluid is trapped and sealed during the growth of a crystal in an ore deposit,
2) nothing is added or lost from the inclusion after trapping,
3) the volume of the vacuole (cavity) surrounding the inclusion fluid does not increase or decrease after trapping,
4) the relationships are known between the actual trapping event, both in space and particularly in time, and the geologic process of interest, such as deposition of ore and
5) the effects of pressure are insignificant or are known (Barnes, 1997).

It is important to note that most inclusions in general and found at the Noumas I pegmatite do not fulfill one or more of the first three assumptions. If these deviations are known or can

be estimated the resulting complexities can still provide useful information or in some situations not. All the data is discussed to its full possible potential starting under the petrographic section.

After the microscopy located the fluid inclusions, the OLYMPUS BX51 microscope with LINKAM TMSG 600 stage (Table 6) was used to obtain fluid inclusion properties. The thick sections were placed into the stage where it was cooled by liquid nitrogen to below freezing point and then heated homogenitization temperatures. This was done in order to note the different temperatures were only one phase was present and where all phases were in equilibrium (Chapter 5, Figure 5-3, Table 5-1, Figure 5-4 to Figure 5-10, Appendix 4, Table 1).

The petrography allows the identification of fluid inclusion generations and indirectly obtained temperature and fluid composition data into context to give an idea about the formation history. After these microscopic investigations were completed, the Linkam TMSG 600 stage is used on fluid inclusions greater than 10 µm for the freezing and heating measurements. About 230 microthermometric measurements were made in the wall, intermediate and core zones of the Noumas I pegmatite (Appendix 4).
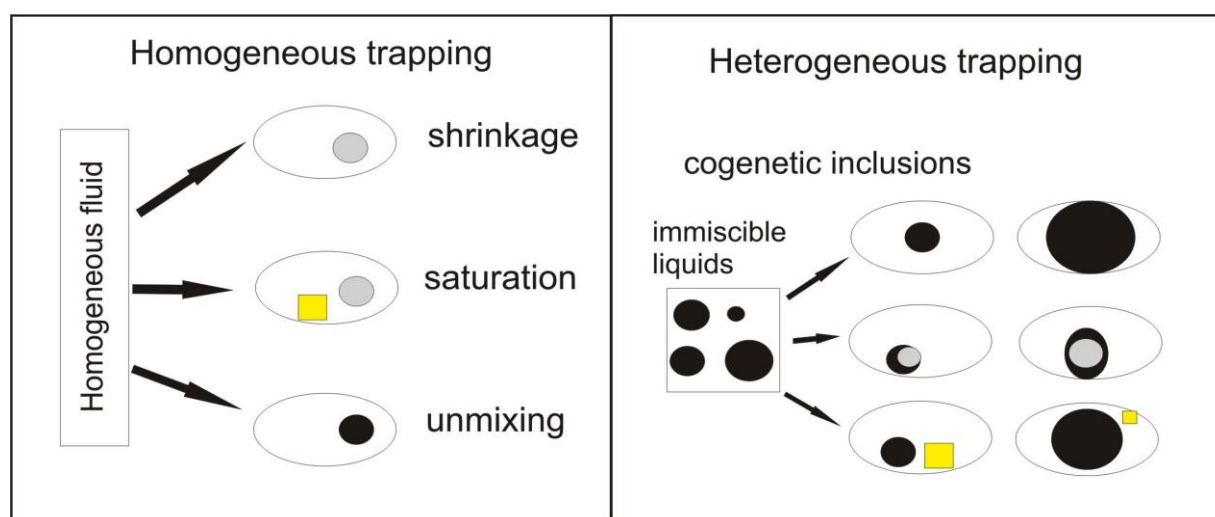
Figure 83: Illustration of homo- and heterogeneously trapped inclusions from various fluids and both types are found at the Noumas I pegmatite (taken form Schmidt Mumm, 2008). Yellow-solid, white-liquid, black-vapour

Pre-selected fluid inclusions were cooled to between -100 and -115°C at a rate of 20°C/minute, then systematically heated at a rate of 1°C/minute. The documented data consisted of the eutectic temperatures (Te), the total melting temperature of ice (Tm_{ice}), and the melting temperature of clathrate (Tm_{CL}) and the total homogenization temperature (Th) (Figure 2).
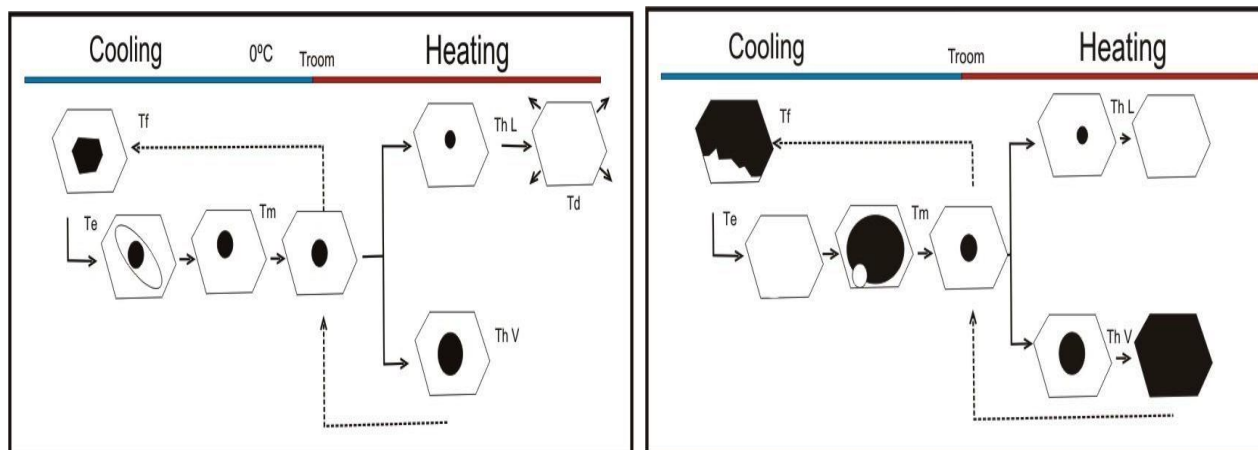
Figure 84: Phase transitions in aqueous and gaseous inclusions during the microthermometry analysis of which the Noumas I pegmatite appears to be more aqueous in nature (taken from Schmidt Mumm, 2008).

Table 30: Detection limits and outlines of Microthermometry work at UFS

	UFS **5. Microthermometry by using Linkam stage**
Analyze / Used for	Fluid inclusion properties
Data format	Fluid inclusion photographs
Type	Microthermometry
Name, Model	OLYMPUS BX51 microscope with LINKAM TMSG 600 stage
Samples prep	Doubly polished thick sections

This method was used in combination with FTIR and Microthermometry to determine the compositions of the fluid inclusions trapped within the border, wall, intermediate and core zones of the Noumas I pegmatite. The RAMAN spectrum (Table 7) provided the basis or reference spectrum to compare the IR spectrums to (Chapter 5, Figure 5-14). FTIR spectrums (Table 8) were taken from mounted thick and thin sections. They were analyzed using Omnic software to indentify the molecular species within the border, wall, intermediate and core zones of the Noumas I pegmatite (Chapter 5, Figure 5-11 to 5-13).

Table 31: Detection limits and outlines of FTIR work done at UFS.

	UFS **6. Raman**
Analyze / Used for	Molecular species in fluids identification of phases
Data format	Infra-red spectra
Type	Raman spectrum plots light intensity (unit, e.g., counts, counts per second or arbitrary units) versus light frequency (relative wavenumbers).
Name, Model	Raman NXR FT-Raman Module
Microscope	Nicolet Continuum FT-IR Microscope
Samples prep	Doubly polished sections (thin and thick) mounted to glass slide

Table 32: Detection limits and outlines of FTIR work done at UFS
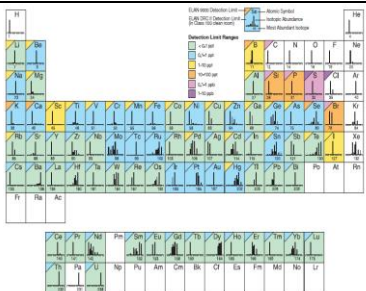
	UFS **7. FTIR**
Analyze / Used for	Molecular species in fluids, Identification of phases
Data format	IR spectrum showing the transmittance (absorbance) of electromagnetic radiation as function of wavelength (wavenumber).
Type	Fourier transform infrared spectroscopy (FTIR) MCT: photoconductive, spectral range $12500 – 400$ cm^{-1}, liquid-nitrogen- cooled using Omnic software
Name, Model	Themo Scientific Nicolet 6700
Samples prep	Doubly polished sections (thin and thick) mounted to glass slide

Table 33: Detection limits and outlines of ICP-MS work done by UFS and GENalysis

	UFS and Genalysis 8. **ICP-MS**
Analyse / Used for	Identification of trace elements Ba, Be, Co, Cs, Ga, Hf, Nb, Rb, Rb, Sn, Sr, Ta, Th, U, V, W, Zr, Y, La, Ce, Pr, Nd, Sm, Eu, Gd, Tb, Dy, Ho, Er, Tm, Yb, Lu.
Name, Model	Shimadzu ICP-MS 8500 mass spectrometer
Samples prep	0.1mg transferred quantitatively to PTFE reaction vessels (Anton Paar Multiwave 3000 Microwave Reaction System) 3 ml nitric acid and 5 ml hydrofluoric acid added then heated 45 min High pressure vessels reached 60 bar pressure and 180°C, after digestion samples were diluted to 100 ml (diluted by a factor of twenty)
Detection limit	lower limit of quantification (QL) 0.01 % (mass)

Appendix 3: XRD, XRF and ICP-MS data
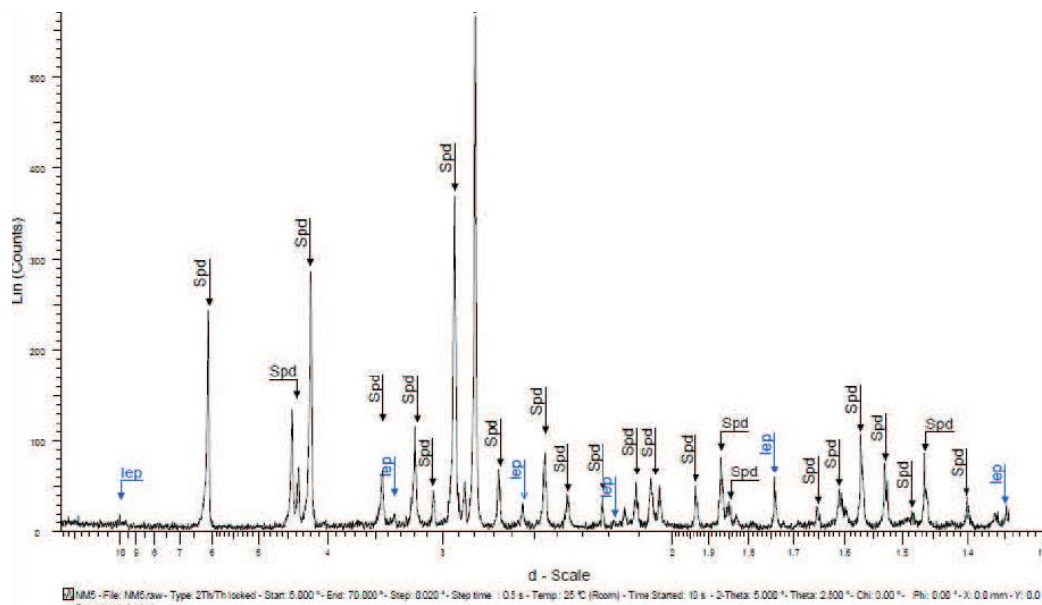
Figure 85: Diffractogram of minerals positively identified from the Noumas I pegmatite in the middle/intermediate zone, sample SW2. lep=leipdolite, spod=spodumene
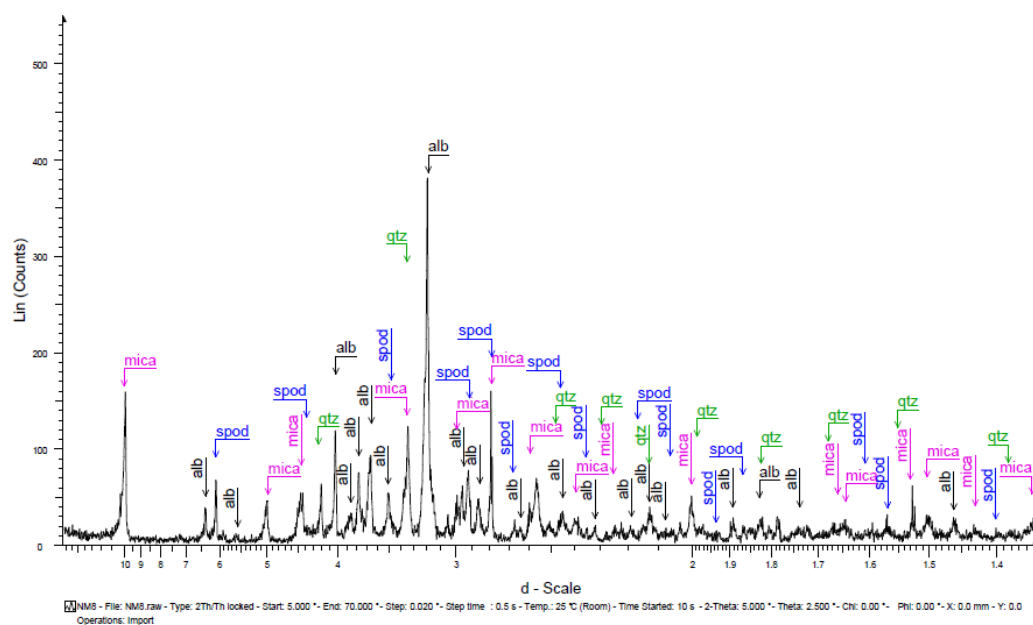
Figure 86: Diffractogram of minerals positively identified from the Noumas I pegmatite in the middle/intermediate zone, sample SW2. alb=albite, qtz=quartz, spod=spodumene
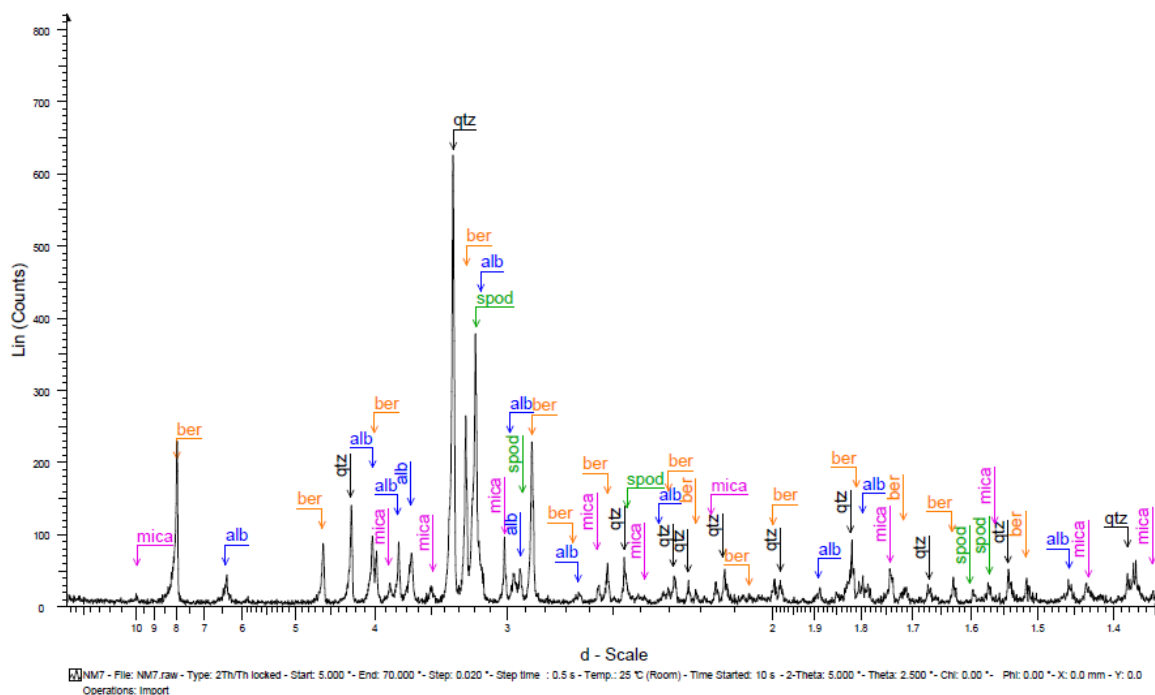
Figure 87: Diffractogram of minerals positively identified from the Noumas I pegmatite in the middle/intermediate zone, sample SW3. alb=albite, ber=beryl, qtz=quartz, spod=spodumene
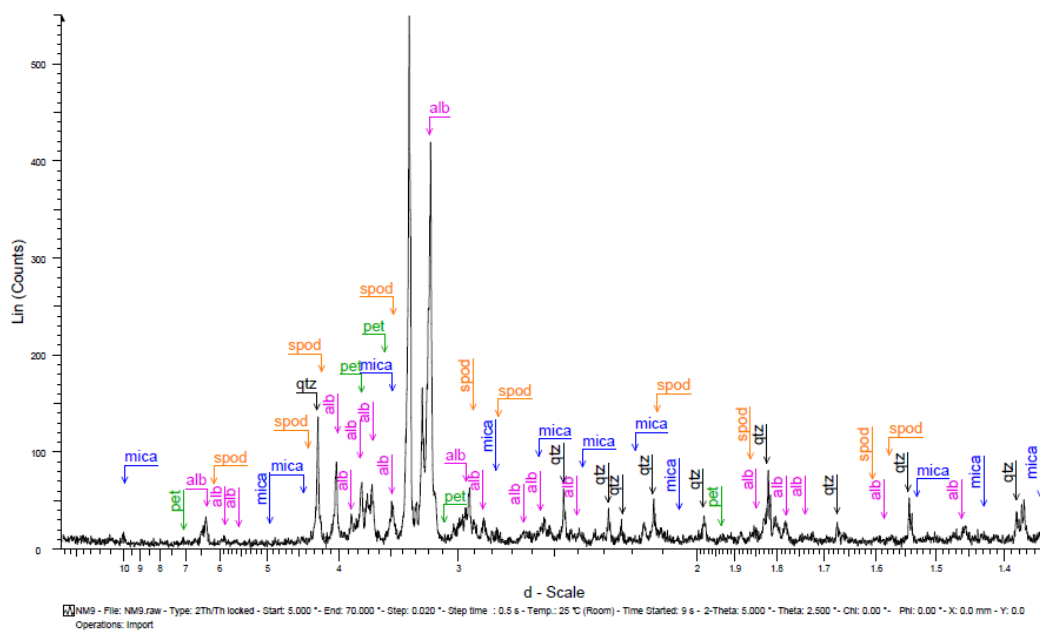
Figure 88: Diffractogram of minerals positively identified from the Noumas I pegmatite in the middle/intermediate zone, sample SW3. alb=albite, pet=petalite, spod=spodumene, qtz=quartz.
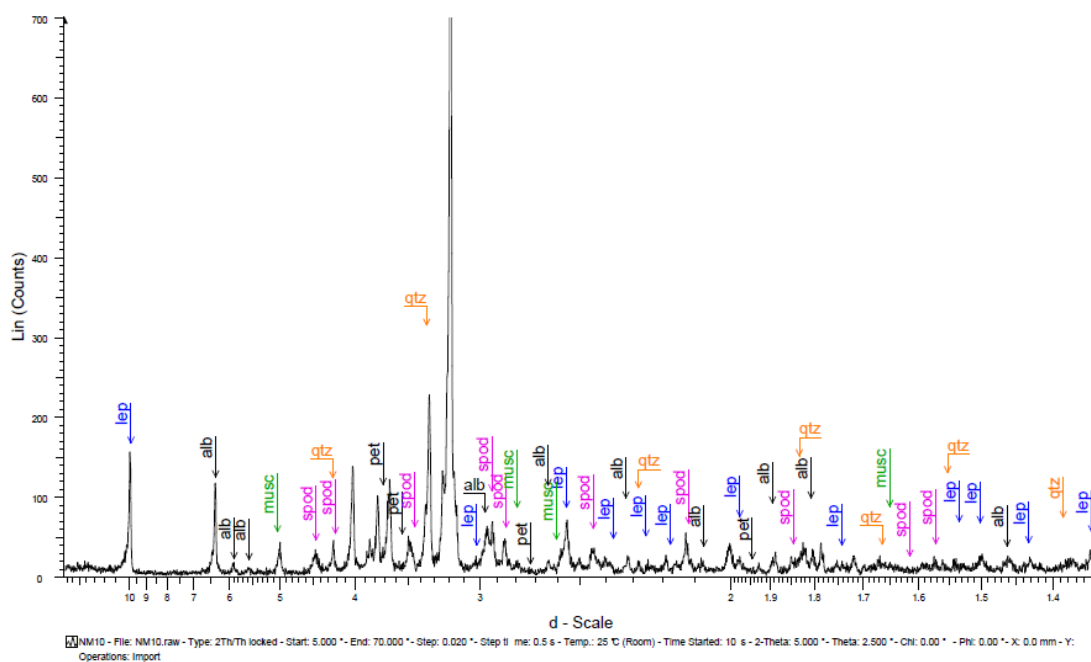
Figure 89: Diffractogram of minerals positively identified from the Noumas I pegmatite in the middle/intermediate zone, sample SW3. alb=albite, lep=lepidolite, musc=muscovite, pet=petalite, qtz=quartz, spod=spodumene
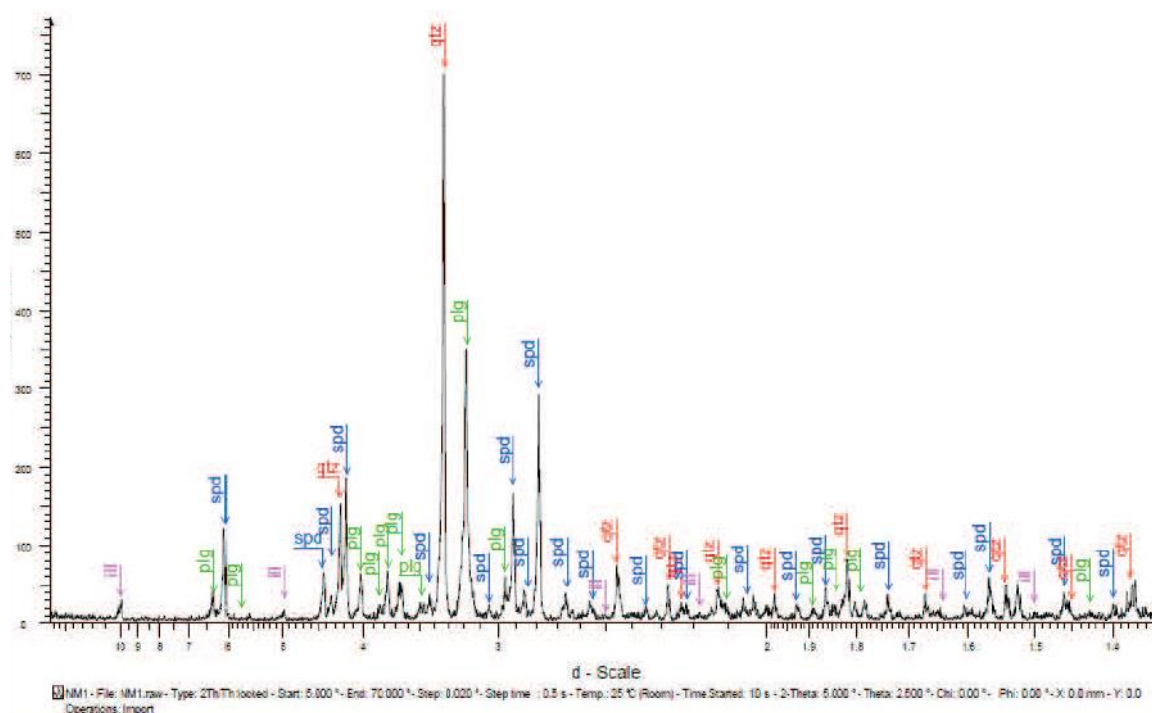
Figure 90: Diffractogram of minerals positively identified from the Noumas I pegmatite on the border of the intermediate zone and the core zone, sample SW3 and SSO8. plag=plagioclase, spd=spodumene, ill=illite, qtz=quartz.
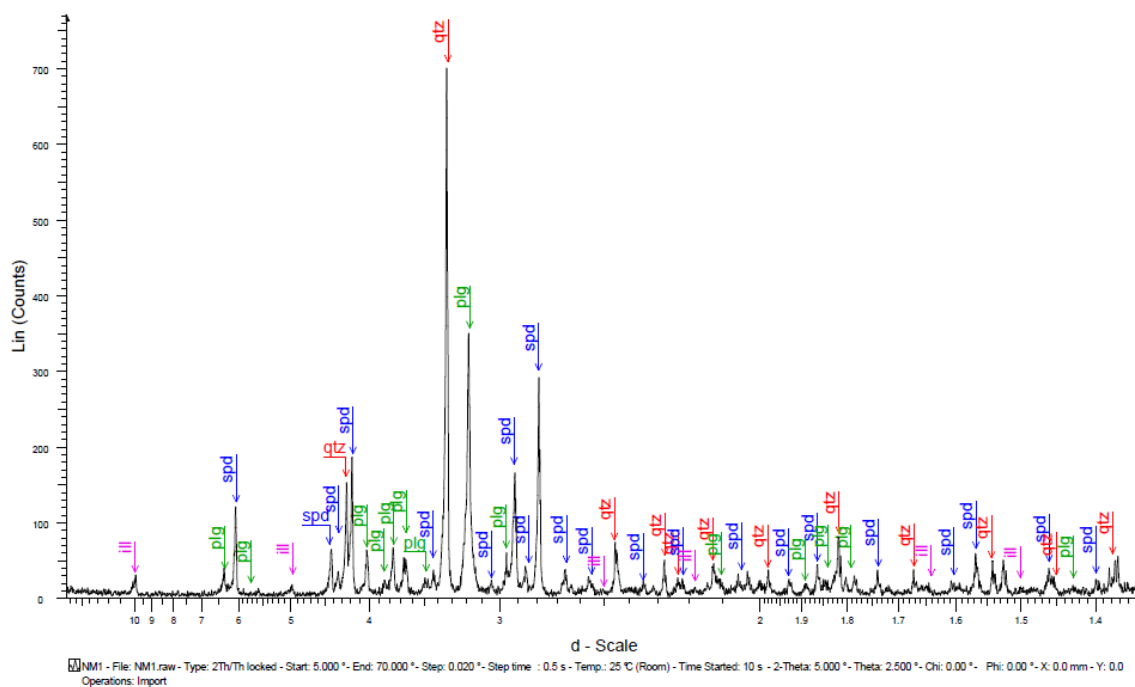
Figure 91: Diffractogram of minerals positively identified from the Noumas I pegmatite on the border of the middle/intermediate zone and the core, sample SW3 and SW4. ill=illite, spd=spodumene, plg-plagioclase, qtz=quartz
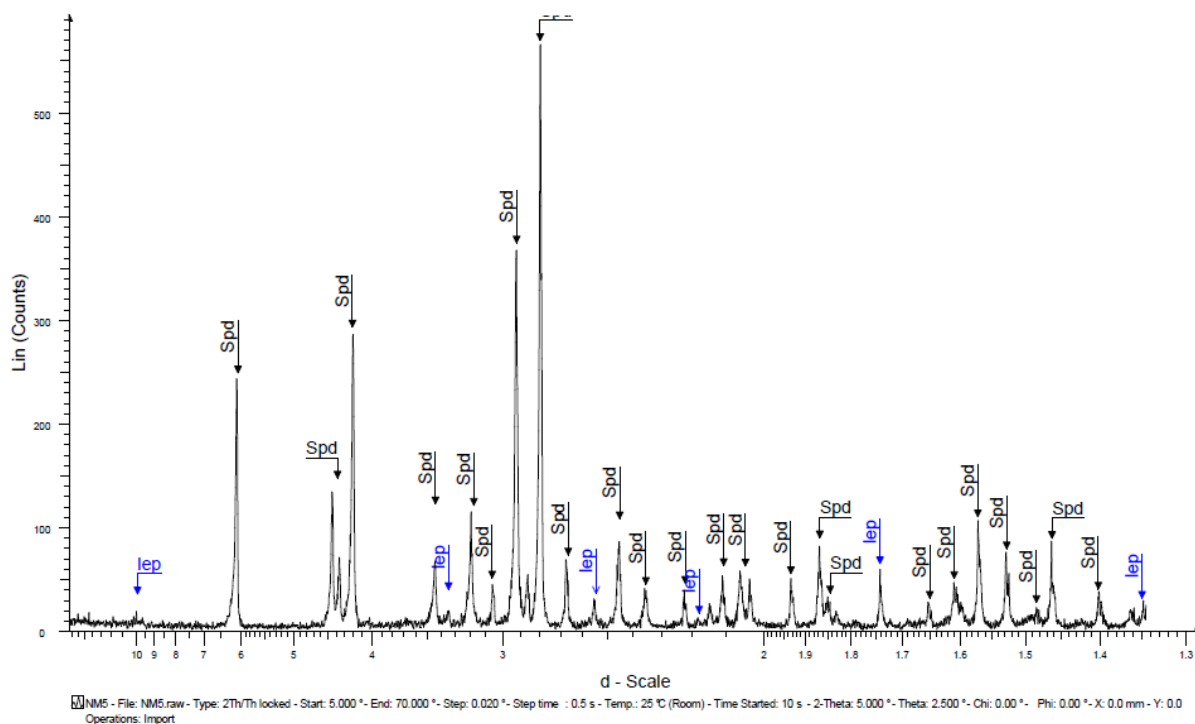
Figure 92: Diffractogram of minerals positively identified from the Noumas I pegmatite in the middle/intermediate zone, sample SW2. lep=leipdolite, spd=spodumene

Table 34: XRF trace element data for the different zones of the Noumas I pegmatite (ppm). B-border, W-wall, I-intermediate and C-core zone.

Sample	SSO1	SSO2	SSO3	SSO4	SSO5	SSO6	SSO7	SSO8	SW2	SW3	SW4
Sc	2.25	1.85	0.43	0.46	0.21	0.34	0.22	2.18	1.70	0.91	0.38
V	1.43	0.47	0.36	3.99	0.29	1.13	1.00	5.02	0.12	4.65	0.23
Cr	2.29	2.88	3.63	21.90	1.76	7.45	1.76	20.46	3.29	28.99	4.61
Co	1.66	1.35	1.58	1.54	0.42	0.63	0.15	1.53	1.46	2.02	3.12
Ni	4.02	5.82	5.45	6.54	1.84	1.43	2.13	6.30	6.37	8.05	8.99
Cu	1.94	5.29	5.92	4.41	7.61	1.80	15.78	4.63	7.34	6.45	8.13
Zn	0.17	0.47	0.80	0.13	40.70	1.40	71.35	0.79	0.65	0.86	5.71
Rb	0.97	1.41	1.93	1.64	556.74	20.97	765.83	0.99	1.88	1.26	38.58
Sr	0.12	0.07	0.12	0.40	37.11	11.29	25.84	0.20	0.27	0.75	4.86
Zr	0.17	0.29	0.29	0.21	7.09	1.42	441.70	0.03	0.63	0.08	1.26
Nb	0.78	0.17	0.20	1.09	3.83	1.43	309.39	0.23	0.03	0.02	2.95
Mo	0.84	0.58	0.40	2.49	0.91	0.33	0.16	2.36	0.29	2.97	0.15
Cd	2.29	0.66	0.65	2.92	1.34	3.39	3.59	0.44	0.90	1.90	3.06
Sn	21.54	17.85	19.69	20.34	19.07	19.63	21.18	20.10	18.37	18.08	21.36
Sb	0.95	1.36	2.11	1.38	1.70	5.16	2.89	1.10	2.27	2.24	0.12
Pb	2.71	2.61	1.89	3.71	2.08	6.38	6.58	2.45	1.85	2.16	2.72
Th	0.59	0.03	1.38	2.13	0.64	0.15	12.18	0.39	0.26	0.94	1.32
Mn	0.007	0.02	0.023	0.021	0.132	0.078	0.034	0.127	0.045	0.118	0.125

Table 35: XRF major element data for the different zones of the Noumas I pegmatite (wt %). B-border, W-wall, I-intermediate and C-core zone

Sample	SSO1	SSO2	SSO3	SSO4	SSO5	SSO6	SSO7	BKQ4.1	BKQ4.3	BKQ5.1	BKQ5.5	14.17.5	BB1	BB2	BB4	SW2	SW3	SW4	SSO8
Zone	B	B	B	B	B	B	W	W	W	W	W	I	I	I	I	I	I	C	C
SiO_2	76.44	68.12	62.79	54.90	78.37	66.85	75.23	64.41	63.99	67.29	70.57	71.84	63.44	59.99	63.46	65.32	54.66	53.14	61.77
Al_2O_3	17.35	17.24	17.25	17.98	19.22	18.33	19.38	18.14	18.42	19.70	17.02	17.16	26.23	26.09	26.72	18.23	20.31	20.11	17.38
Fe_2O_3	0.23	0.55	0.47	0.86	1.44	0.97	1.48	0.21	0.17	1.51	0.53	0.45	1.42	0.27	0.88	0.90	1.23	1.45	0.67
MnO	0.01	0.02	0.02	0.02	0.13	0.08	0.03	0.01	0.01	0.06	0.04	0.17	0.20	0.15	0.18	0.05	0.12	0.13	0.13
MgO	0.08	0.12	0.17	0.04	0.56	0.43	0.78	3.25	3.28	0.28	0.22	0.09	0.24	0.66	0.06	0.24	0.03	0.08	0.36
CaO	0.05	0.03	0.06	0.03	0.11	0.13	0.13	0.01	0.06	0.17	0.13	0.12	0.04	0.11	0.05	0.04	0.03	0.16	0.07
Na_2O	3.28	3.72	3.28	1.78	1.87	5.47	4.89	1.32	1.69	4.85	5.80	3.72	0.08	5.50	0.50	1.27	0.67	0.59	1.73
K_2O	1.24	1.32	3.28	13.31	0.27	0.31	4.50	13.54	13.07	3.09	1.86	1.40	0.22	4.62	0.50	0.44	13.23	13.85	0.22
TiO_2	0.07	0.06	0.04	0.03	0.08	0.02	0.00	28.80	28.76	0.05	0.01	0.01	0.02	0.01	0.02	0.03	0.01	0.05	0.01
P_2O_5	0.04	0.04	0.17	0.16	0.01	0.01	0.01	0.01	0.23	0.12	0.06	0.03	0.01	0.01	0.01	0.00	0.00	0.01	0.01
Totaal	98.78	91.21	87.51	89.12	102.07	92.59	106.44	129.69	129.68	97.10	96.24	94.98	91.89	97.40	92.36	86.52	90.29	89.57	82.35
LOI	-0.044	-0.119	-0.095	-0.174	1.344	0.492	1.344	0.382	0.229	1.541	0.777	0.884	0.181	2.151	0.446	-0.063	-0.157	0.020	-0.088
H_2O	0.001	0.000	0.000	0.001	-0.001	-0.001	0.000	0.000	0.001	0.000	0.001	0.000	0.001	0.000	0.001	0.001	0.001	0.991	0.001

Table 36: ICP-MS data from GENalysis for samples from the wall, intermediate and core zones of the Noumas I pegmatite.

samples	BB-1	BB-2	BB-4	BKQ 4.1	BKQ 4.3	BKQ 5.1a	BKQ 5.5	14.17.5a	BB-1
Be	3	6	4	3	0.05	11	5	6	3
Ce	1	0.025	0.025	0.025	10.4	0.025	0.025	0.025	0.025
Dy	0.05	0.05	0.05	0.05	0.05	0.05	0.05	0.05	0.05
Er	0.05	0.1	0.05	0.05	0.05	0.05	0.05	0.05	0.05
Eu	0.05	0.05	0.05	0.05	0.05	0.05	0.05	0.05	0.05
Ga	78	62	63	11	16	53	34	57	77
Gd	0.2	0.1	0.05	0.1	0.05	0.05	0.05	0.05	0.05
Hf	0.7	0.7	0.5	0.3	0.05	0.2	0.4	4.7	0.6
Ho	0.05	0.05	0.05	0.05	0.05	0.05	0.05	0.05	0.05
La	0.3	0.1	0.1	0.1	0.4	0.1	0.1	0.1	0.1
Li	30067	901	29283	41	11	381	147	9146	31822
Lu	0.025	0.025	0.025	0.025	0.025	0.025	0.025	0.025	0.025
Nb	5	5	5	5	5	106	15	5	5
Nd	0.5	0.4	0.05	0.4	0.2	0.3	0.2	0.2	0.1
Pr	0.11	0.05	0.025	0.05	0.92	0.025	0.025	0.025	0.025
Sm	0.1	0.5	0.1	0.5	0.5	0.5	0.5	0.2	0.5
Sn	1	1	1	1	1	3	1	1	1
Ta	0.3	2.6	0.3	0.05	0.2	27.5	43.7	190.8	0.5
Tb	0.025	0.08	0.025	0.025	0.025	0.025	0.025	0.025	0.025
Th	0.3	2	0.1	0.2	0.1	0.2	1.5	1.9	0.1
Tm	0.025	0.025	0.025	0.025	0.025	0.025	0.025	0.025	0.025
U	0.05	0.1	0.05	0.05	0.05	0.7	0.6	8	0.05
W	12	0.5	16	3	3	11	9	13	12
Y	0.25	0.25	0.25	0.25	0.25	0.25	0.25	0.25	0.25
Yb	0.05	0.05	0.05	0.05	0.05	0.05	0.05	0.05	0.05
Zr	5	2.5	6	21	2.5	2.5	2.5	37	6

Appendix 4: Fluid inclusions (FI)

Table 37: The average salinities, deviations and temperatures for the wall, intermediate and core zone of the Noumas I pegmatite.

Microthermometry	Wall	Intermediate	Core
Avg. Salinity (wt % NaCl)	6.47	12.03	7.37
St. dev. Avg. Sal.	3.62	2.74	0.34
Avg. Te (°C)	-17.58°C	-28.08°C	-24.43°C
St. dev. Avg. Te	8.18	18.93	5.17
Avg. Th (°C)	164.18°C	169.86°C	176.77°C
St. dev. Avg. Th	42.25	25.85	25.37

Table 38: The estimated temperature, pressure for the densities of the two phases as determined by the BULK program.

Phase 1		Phase 2	
55.7698 cc/mol		55.7717 cc/mol	
$x(CO_2)$	0.61 (f = 159.002 MPa)	$x(CO_2)$	0.61 (f = 159.002 MPa)
$x(CH_4)$	0.39 (f = 162.494 MPa)	$x(CH_4)$	0.39 (f = 162.494 MPa)

Table 39: The calculated gas-mixture from the BULK program.

Homogenisation temperature	287.4 °C
Homogenisation pressure	253.901 MPa (1753.66 bar)
Molar volume	55.2948 cc/mole
Density	1.645341 g/cc

Table 40: Fluid inclusion analyses for the Noumas I pegmatite within the border (B), wall (W), intermediate (I) and core (C) zones for primary inclusions.

Sample	Zone	Inclusion Type	Tm	salinity	Th	Te	size V	size L	%V	%L	Tf$_{deep}$
14.17.5a	I	1	-6.5	9.86	144.2	-8.2	6.4	17.89	26.348	73.652	404.2
	I	1	-10	13.94	116.5	-15.2	5.96	21.64	21.594	78.406	376.5
	I	1	-2.2	3.71	138.7	-4.3	5.84	15.12	27.863	72.137	398.7
	I	1	-4.9	7.73	119.9	-8.7	7.75	20	27.928	72.072	379.9
	I	1	-19.6	22.1	216.4	-23.5	10.18	20.35	33.344	66.656	476.4
14.17.5c	I	1	-8.3	12.05	157	-15	3.86	13.69	21.994	78.006	417
	I	1	-6	9.21	166.8	-8.3	4.51	18.57	19.541	80.459	426.8
	I	1	-1.4	2.41	116.9	-3.7	11.53	51.58	18.27	81.73	376.9
	I	1	-20.5	22.71	143.1	-47.6	5.56	20.41	21.409	78.591	403.1
	I	1	-21.1	23.11	150.2	-33.7	8.07	28.77	21.906	78.094	410.2
	I	1	-14.6	18.3	148.2	-86.4	11.58	16.14	41.775	58.225	408.2
	I	1	-13.7	17.52	132.2	-85.3	8.77	45.53	16.151	83.849	392.2
	I	1	-12.8	16.71	278.3	-88.3	6.25	17.19	26.664	73.336	538.3
	I	1	-0.5	0.88	120	-87.7	5.26	22.48	18.962	81.038	380
14.17.5b	I	1	-4.9	7.73	114.3	-69.3	10.53	35.65	22.802	77.198	374.3
	I	1	-14.8	18.47	114.4	-47.3	9.45	30.18	23.846	76.154	374.4
	I	1	-5.3	8.28	150.3	-53.2	10.18	53.14	16.077	83.923	410.3
	I	1	-4.9	7.73	136.2	-54.7	9.48	32.86	22.39	77.61	396.2
	I	1	-3.7	6.01	146.2	-54.7	5.31	32.68	13.977	86.023	406.2
	I	1	-0.4	0.71	116.8	-13.2	8.08	36.72	18.036	81.964	376.8
	I	1	-0.4	0.71	162.9	-22.64	5.02	22.64	18.149	81.851	422.9
	I	1	-10.8	14.77	132.6	-33.7	9.82	37.41	20.792	79.208	392.6
	I	1	-0.7	1.23	179.4	-37.2	10.22	25.7	28.452	71.548	439.4
	I	1	-0.8	1.4	113.9	-37.2	4.96	15.23	24.567	75.433	373.9
	I	1	-1.5	2.57	138.3	-36.3	4.91	18.25	21.2	78.8	398.3
	I	1	-1.1	1.91	145.7	-10.2	10.53	41.28	20.324	79.676	405.7
	I	1	-14.5	18.22	142.9	-35.4	5.26	14.76	26.274	73.726	402.9
	I	1	-0.2	0.35	132.8	-22	3.92	30.93	11.248	88.752	392.8
	I	1	-0.2	0.35	132.7	-33.2	4.21	36.14	10.434	89.566	392.7
	I	1	-0.7	1.23	141.6	-34.2	20.41	40.01	33.78	66.22	401.6
	I	1	-0.5	0.88	133.3	-37.4	5.22	19.31	21.28	78.72	393.3
	I	1	-14.9	18.55	200	-36.6	4.56	12.6	26.573	73.427	460
	I	1	-14.7	18.38	118.5	-36.6	4.56	12.52	26.698	73.302	378.5
	I	1	-3.9	6.3	240.9	-23.5	16.84	29.81	36.099	63.901	500.9
	I	1	-16.6	19.92	149.2	-23.6	4.91	17.11	22.298	77.702	409.2
	I	1	-16.6	19.92	149.2	-23.7	4.56	15.76	22.441	77.559	409.2
	I	1	-3.9	6.3	149.2	-68.7	4.91	17.64	21.774	78.226	409.2

Sample	Zone	Inclusion Type	Tm	salinity	Th	Te	size V	size L	%V	%L	Tf_{deep}
BKQ5.8a	W	1	-20.1	22.44	104.4	-46.8	5.62	45.16	11.067	88.933	364.4
	W	1	-13.1	16.99	268	-43.8	11.01	23.58	31.83	68.17	528
	W	1	-18.4	21.26	218.1	-43.2	3.66	11.36	24.368	75.632	478.1
	W	1	-5.8	8.95	118.5	-53.5	3.51	15.23	18.73	81.27	378.5
	W	1	-5.8	8.95	121.5	-72.3	3.51	10.51	25.036	74.964	381.5
	W	1	-16.9	20.15	152.7	-77.9	9.51	9.65	49.635	50.365	412.7
BB1a	W	1	-3.3	5.41	190.1	-24	5.98	12.36	32.606	67.394	450.1
	W	1	-3.1	5.11	183.5	-12.1	5.61	20.24	21.702	78.298	443.5
	W	1	-3.4	5.56	121	-21.3	6.66	26.64	20	80	381
	W	1	-9.1	12.96	180.8	-55.3	4.51	13.11	25.596	74.404	440.8
	W	1	-2.7	4.49	256.7	-50.5	5.61	15.73	26.289	73.711	516.7
	W	1	-19.1	21.75	248.2	-51.8	14.74	33.02	30.863	69.137	508.2
BB1b	W	1	-15.1	18.72	205.6	-46.3	5.98	14.14	29.722	70.278	465.6
	W	1	-19	21.68	206.2	-57	8.42	29.98	21.927	78.073	466.2
	W	1	-14.6	18.3	224.5	-37.5	50.99	88	36.686	63.314	484.5
	W	1	-1.3	2.24	204.5	-23.6	35.38	65.3	35.141	64.859	464.5
	W	1	-1.9	3.23	183.5	-27.3	14.42	56.32	20.385	79.615	443.5
SSO1	B	1	-20.9	22.98	171.9	-21.7	40	90	30.769	69.231	431.9
	B	1	-1.1	1.91	218	-21.4	50.04	152.43	24.715	75.285	478
	B	1	-4	6.45	163.8	-20.3	26.83	55.17	32.72	67.28	423.8
	B	1	-1.8	3.06	171.2	-18.1	80	221.72	26.515	73.485	431.2
	B	1	-7.8	11.46	155.7	-13.9	45.3	155.2	22.594	77.406	415.7
	B	1	-6.7	10.11	134.9	-18.2	65	98.1	39.853	60.147	394.9
	B	1	-2.3	3.87	132.2	-21.7	5.98	12.36	32.606	67.394	392.2
	B	1	-1.1	1.91	170.1	-21.4	5.61	15.73	26.289	73.711	430.1
	B	1	-4	6.45	143.2	-20.3	5.61	20.24	21.702	78.298	403.2
	B	1	-1.8	3.06	165.2	-18.1	6.66	26.64	20	80	425.2
	B	1	-7.8	11.46	168.2	-13.9	34.56	98.7	25.934	74.066	428.2
	B	1	-1.1	1.91	154.3	-12.3	80	154.99	34.044	65.956	414.3
	B	1	-2.1	3.55	152.3	-21.2	46.31	160.01	22.446	77.554	412.3
	B	1	-2.3	3.87	135.3	-19.1	36.88	89.01	29.295	70.705	395.3
	B	1	-3.1	5.11	167.2	-18.2	52.04	96.21	35.103	64.897	427.2
	B	1	-2.1	3.55	146.9	-12.7	58.86	130.65	31.059	68.941	406.9
	B	1	-7.2	10.73	165.2	-13.7	43.67	219.67	16.583	83.417	425.2
	B	1	-6.8	10.24	134.5	-14.2	59.67	178.4	25.064	74.936	394.5
	B	1	-2.3	3.87	143.2	-18.9	12.22	56.98	17.659	82.341	403.2
	B	1	-2.1	3.55	167.2	-20.1	37.88	78.98	32.415	67.585	427.2
	B	1	-2.1	3.55	143.2	-21.2	54.32	102.32	34.678	65.322	403.2
	B	1	-1.2	2.07	152.1	-20.9	23.45	65.32	26.417	73.583	412.1
sw2	I	1	-3.8	6.16	136.9	-20.1	66	168.01	28.204	71.796	396.9

Sample	Zone	Inclusion Type	Tm	salinity	Th	Te	size V	size L	%V	%L	Tf_{deep}
	I	1	-3.4	5.56	122.8	-19.3	62.64	186.64	25.128	74.872	382.8
	I	1	-0.2	0.35	145.6	-20.4	30	100.44	22.999	77.001	405.6
	I	1	-9.7	13.62	291.6	-17.4	104.02	166.47	38.456	61.544	551.6
	I	1	-8.4	12.16	287.4	-19.1	106.3	2.04	98.117	1.883	547.4
	I	1	-9.4	13.29	291.4	-20.4	20	94	17.544	82.456	551.4
	I	1	-12.6	16.53	286.3	-20.4	25.4	78.3	24.494	75.506	546.3
	I	1	-6.5	9.86	277.6	-14.2	33	112.4	22.696	77.304	537.6
	I	1	-6.6	9.98	156.2	-48.7	32.25	168.58	16.058	83.942	416.2
	I	1	-7.1	10.61	165.8	-49.9	44	126.82	25.758	74.242	425.8
	I	1	-6.7	10.11	268.3	-13.9	12.7	98.4	11.431	88.569	528.3
	I	1	-3.2	5.26	187.5	-9.2	40	78.41	33.781	66.219	447.5
	I	1	-8.5	12.28	297.2	-23.1	50.99	110	31.673	68.327	557.2
	I	1	-12.2	16.15	189.4	-18.7	44.05	94.02	31.904	68.096	449.4
	I	1	-12.4	16.34	293.1	-24.1	58	218.85	20.95	79.05	553.1
	I	1	-7.9	11.58	218.2	-19.4	56	118.07	32.171	67.829	478.2
	I	1	-18.2	21.11	301.1	-34.2	72.03	254.01	22.092	77.908	561.1
	I	1	-7.1	10.61	267.2	20.5	58.41	139.94	29.448	70.552	527.2
	I	1	-18.8	21.54	283.1	-46.7	77.2	356.21	17.812	82.188	543.1
	I	1	-17.2	20.37	278.9	-40.8	67.3	87.9	43.363	56.637	538.9
	I	1	-12.7	16.62	169.4	-21.2	21.1	75.5	21.843	78.157	429.4
	I	1	-13.1	16.99	198.2	-39.7	52.04	96.21	35.103	64.897	458.2
	I	1	-17.8	20.82	159.6	-40.1	58.86	129.52	31.245	68.755	419.6
	I	1	-8.8	12.62	267.4	-21.3	52.04	219.67	19.153	80.847	527.4
	I	1	-12.2	16.15	287.4	-21.5	59.67	178.4	25.064	74.936	547.4
	I	1	-3.4	5.56	256.3	-20.8	22	83.26	20.901	79.099	516.3
	I	1	-0.2	0.35	279.6	-20.2	110.39	129	46.113	53.887	539.6
	I	1	-0.1	0.18	300.1	-20.4	58.03	150.57	27.819	72.181	560.1
	I	1	-12.3	16.24	289.6	-25.1	60.96	145.84	29.478	70.522	549.6
	I	1	-8.1	11.81	297.4	-22.4	54.04	157.63	25.53	74.47	557.4
sw3	I	1	-19.5	22.03	153.4	-25.4	36	82.97	30.26	69.74	413.4
	I	1	-19	21.68	137.8	-31.5	18.44	36.22	33.736	66.264	397.8
	I	1	-12.9	16.8	143.6	-30.7	26.08	64.4	28.824	71.176	403.6
	I	1	-17.4	20.52	143.9	-30.4	25.61	68.26	27.282	72.718	403.9
	I	1	-7.3	10.86	147.8	-40.5	53.14	184.86	22.328	77.672	407.8
	I	1	-3.5	5.71	151.6	-22.2	42.38	103.77	28.998	71.002	411.6
	I	2	-3.8	6.16	109.1	-34	16.12	31.24	34.037	65.963	369.1
	I	1	-3.8	6.16	163.2	-34.8	36.72	119.88	23.448	76.552	423.2
	I	1	-4.7	7.45	118.8	-37.1	20	35.44	36.075	63.925	378.8
	I	1	-6.8	10.24	167.3	-44.2	32.34	65.04	33.21	66.79	427.3
	I	1	-12.6	16.53	155.4	-32.5	17.65	54.32	24.524	75.476	415.4

Sample	Zone	Inclusion Type	Tm	salinity	Th	Te	size V	size L	%V	%L	Tf_{deep}
	I	1	-9.5	13.4	153.3	-36.2	12.4	66.8	15.657	84.343	413.3
	I	1	-18.3	21.19	165.3	-21.8	15.65	89.51	14.882	85.118	425.3
	I	1	-15.3	18.88	134.2	-34.2	43.2	57.4	42.942	57.058	394.2
	I	1	-7.2	10.73	163.2	-41.2	45.32	182.87	19.861	80.139	423.2
	I	1	-12.3	16.24	165.3	-35.2	23.45	117.3	16.661	83.339	425.3
	I	1	-4.2	6.74	145.3	-22.1	34.2	63.21	35.109	64.891	405.3
	I	1	-19.3	21.89	145.3	-31.7	23.4	75.67	23.62	76.38	405.3
	I	1	-13.1	16.99	151.1	-31.2	21.32	64.12	24.953	75.047	411.1
	I	1	-12.4	16.34	149.7	-33.2	26.34	87.97	23.043	76.957	409.7
	I	1	-4.7	7.45	134.2	-23.4	12.73	78.98	13.881	86.119	394.2
	I	1	-8.2	11.93	156.1	-44.1	45.23	67.12	40.258	59.742	416.1
	I	1	-12.8	16.71	161.4	-31.2	34.06	89.65	27.532	72.468	421.4
	I	1	-12.1	16.05	145.7	-33.2	20	37.44	34.819	65.181	405.7
	I	1	-12.7	16.62	156.7	-32	45.01	78.11	36.558	63.442	416.7
	I	1	-7.2	10.73	164.7	-23.1	32.12	67.01	32.402	67.598	424.7
	I	1	-12.4	16.34	154.3	-30.4	27.08	33.24	44.894	55.106	414.3
	I	1	-8.2	11.93	156.1	-41.1	26.04	78.97	24.798	75.202	416.1
	I	1	-12.7	16.62	153.7	-31.9	23.02	68.99	25.019	74.981	413.7
	I	1	-13.2	17.08	161.1	-32.1	34.01	67.11	33.633	66.367	421.1
sw4	C	1	-5.5	8.5	200.3	-26.6	24.33	69.77	25.855	74.145	460.3
	C	1	-6	9.21	201.1	-26.5	16.12	46.17	25.879	74.121	461.1
	C	1	-6.5	9.86	200.3	-26.6	30.07	107.42	21.871	78.129	460.3
	C	1	-4.9	7.73	199.8	-26.8	11.66	26.68	30.412	69.588	459.8
	C	1	-4	6.45	200.2	-26.2	12	70.68	14.514	85.486	460.2
	C	1	-4.5	7.17	200.4	-26.2	29.98	112.32	21.068	78.932	460.4
	C	1	-3.9	6.3	178.2	-27.4	26	81.04	24.29	75.71	438.2
	C	1	-3.8	6.16	198.3	-28.1	31.62	78	28.845	71.155	458.3
	C	1	-4.2	6.74	201	-27.6	48.33	122.44	28.301	71.699	461
	C	1	-3.9	6.3	187.2	-30.1	33.94	132.8	20.355	79.645	447.2
	C	1	-4.9	7.73	189.3	-29.2	28.07	57.69	32.731	67.269	449.3
	C	1	-4.7	7.45	200.1	-29.1	30.27	68.96	30.505	69.495	460.1
	C	1	-6.1	9.34	199.1	-32.1	24.17	111.46	17.821	82.179	459.1
	C	1	-4.3	6.88	179.3	-27.3	43.86	127.28	25.628	74.372	439.3
	C	1	-4.4	7.02	200	-30.1	12.23	87.43	12.272	87.728	460
	C	1	-4.6	7.31	198.2	-29.3	45.65	113.23	28.732	71.268	458.2
	C	1	-4.2	6.74	199.2	-25.8	32.54	79.54	29.033	70.967	459.2
	C	1	-3.9	6.3	201.1	-25.8	35.42	116.43	23.326	76.674	461.1
	C	1	-3.8	6.16	188.2	-26.2	10.78	30.27	26.261	73.739	448.2
	C	1	-3.8	6.16	187.2	-26.5	14.67	85.99	14.574	85.426	447.2
	C	1	-4.1	6.59	197.6	-32.4	26.87	96.78	21.731	78.269	457.6

Sample	Zone	Inclusion Type	Tm	salinity	Th	Te	size V	size L	%V	%L	Tf_{deep}
	C	1	-7	10.49	178.9	-28.7	30.87	73.25	29.648	70.352	438.9
	C	1	-6.8	10.24	197.3	-34.7	45.24	96.09	32.01	67.99	457.3
	C	1	-5.5	8.55	198.2	-28.4	25.16	114.66	17.995	82.005	458.2
	C	1	-4.5	7.17	199.4	-25.4	43.25	98.24	30.568	69.432	459.4
	C	1	-4.3	6.88	187.7	-29.3	30.12	73.78	28.989	71.011	447.7
	C	1	-3.9	6.3	183.2	-26.3	8.99	120.76	6.929	93.071	443.2
	C	1	-4.6	7.31	200.4	-26.3	34.77	112.11	23.672	76.328	460.4
	C	1	-4.9	7.73	200.1	-25.8	36.09	88.93	28.867	71.133	460.1
	C	1	-7.8	11.46	189.8	-26.4	44.99	110.32	28.968	71.032	449.8
sso8	C	1	-4.3	6.88	147.3	-18.5	36.77	182.7	16.754	83.246	407.3
	C	1	-4.3	6.88	147.5	-18	28.07	68.96	28.929	71.071	407.5
	C	1	-5	7.86	142.7	-20.9	55.71	124.58	30.9	69.1	402.7
	C	1	-3.8	6.16	145.8	-19.1	38.05	135.82	21.884	78.116	405.8
	C	1	-4.7	7.45	139.2	-20.8	56.57	137.57	29.139	70.861	399.2
	C	1	-6	9.21	145.7	-21	16.49	61.77	21.071	78.929	405.7
	C	1	-4.1	6.59	144.9	-18.6	26.31	58.31	31.092	68.908	404.9
	C	1	-4.3	6.88	148.5	-18.5	32.56	89.35	26.708	73.292	408.5
	C	1	-5.4	8.41	135.6	-21.3	34.18	73.24	31.819	68.181	395.6
	C	1	-4.6	7.31	146.3	-22.1	51.61	136.37	27.455	72.545	406.3
	C	1	-5.6	8.68	142.1	-20.8	46.39	116.07	28.555	71.445	402.1
	C	1	-5.1	8	154.2	-19.8	46.52	118.83	28.134	71.866	414.2
	C	1	-3.9	6.3	321.1	-18.6	87.73	205.15	29.954	70.046	581.1
	C	1	-1.9	3.23	108.7	-22.6	43.17	235.98	15.465	84.535	368.7
	C	1	-1.9	3.23	111.9	-18.6	36.22	152.12	19.231	80.769	371.9
	C	1	-5.5	8.55	167.8	-19.4	14.16	53.85	20.82	79.18	427.8
	C	1	-5.5	8.55	162.2	-20.4	25.16	114.66	17.995	82.005	422.2
	C	1	-4.1	6.59	154.2	-22.6	8.73	36.74	19.199	80.801	414.2
	C	1	-3.8	6.16	145.7	-21.3	26.17	76.34	25.529	74.471	405.7
	C	1	-4.3	6.88	144.9	-22.6	34.56	94.1	26.861	73.139	404.9
	C	1	-5.4	8.41	148.5	-18.6	55.07	129.43	29.848	70.152	408.5
	C	1	-3.9	6.3	238.4	-21.3	33.78	88.44	27.639	72.361	498.4
	C	1	-1.9	3.23	145.8	-20.4	27.99	62.67	30.874	69.126	405.8
	C	1	-4.3	6.88	149.6	-22.7	25.16	111.4	18.424	81.576	409.6
	C	1	-5.1	8	152.7	-21.8	37.38	100.1	27.189	72.811	412.7
	C	1	-5	7.86	154.3	-21.6	34	89.65	27.497	72.503	414.3
	C	1	-6	9.21	156.4	-23.1	34.22	74.56	31.458	68.542	416.4
	C	1	-3.9	6.3	234.6	-18.4	12.78	66.3	16.161	83.839	494.6
	C	1	-5.5	8.55	171.1	-20.1	18.76	102.2	15.509	84.491	431.1
	C	1	-6	9.21	157.1	-24.3	67.44	99.71	40.347	59.653	417.1

Table 41: Fluid inclusion analyses for the Noumas I pegmatite within the border (B), wall (W), and intermediate (I) zones for secondary inclusions.

Sample	Zone	Inclusion Type	Tm	salinity	Th	Te	size V	size L	%V	%L	$Tf_{shallow}$
14.17.5a	I	2	-1.1	1.91	40.1	-2.3	3.18	11.95	21.018	78.982	99
	I	2	-3.3	5.41	60.7	-6.5	6.7	30.53	17.996	82.004	120
	I	2	-11.1	15.07	76	-52.7	11.93	48.77	19.654	80.346	134
	I	2	-0.9	1.57	39.2	-4.5	7.02	21.05	25.009	74.991	99
14.17.5b	I	2	-3.8	6.16	81	-38.1	3.16	11.62	21.38	78.62	141
14.17.5b	I	2	-15.5	19.05	100	-48.5	5.61	18.88	22.907	77.093	160
	I	2	-5.3	8.28	88.9	-68.5	4.56	23.86	16.045	83.955	148
	I	2	-19.6	22.1	100.5	-91.8	5.66	41.71	11.948	88.052	160
BKQ5.8a	W	2	-21.2	23.18	106.1	-40.3	0	23.09	0	100	166.1
	W	2	-9.8	13.72	89.3	-38.2	9.47	23.16	29.022	70.978	149.3
	W	2	-9.8	13.72	66	-38.9	9.12	29.12	23.849	76.151	126
	W	2	-17.1	20.3	77.4	-50.3	2.83	10.37	21.439	78.561	137.4
	W	2	-5.2	8.14	97.2	-60.1	2.81	11.42	19.747	80.253	157
	W	2	-16.3	19.68	94.3	-47.8	3.16	13.23	19.28	80.72	154
SSO1	B	2	-9	12.85	100	-15	34.06	74.92	31.253	68.747	160
	B	2	-1.2	2.07	104.8	-12.1	32.06	93.34	25.566	74.434	165
	B	2	-2.3	3.87	107.4	-12.7	44.78	65.07	40.765	59.235	167
	B	2	-1.2	2.07	104.3	-12.7	14.74	33.02	30.863	69.137	164
	B	2	-7.1	10.61	102.2	-21.6	14.42	56.32	20.385	79.615	162
	B	2	-1.4	7.02	109.5	-20.9	52.04	83.26	38.463	61.537	170
	B	2	-6.8	10.24	106.3	-12.2	26.89	87.66	23.474	76.526	166
	B	2	-7.2	10.73	102.1	-18.6	41.29	98.67	29.501	70.499	162

Appendix 5: SEM-EDS

Table 42: SEM-EDS analyses on the Noumas I pegmatite for plagioclase.

	BKQ5-2a(4)_pt2	BKQ5-2a(4)_pt4	BKQ5-2a(4)_pt6	BKQ5-2a(4)_pt16
SiO_2	60.88	62.18	61.38	61.04
TiO_2	0.00	0.00	0.00	0.00
Al_2O_3	19.75	19.09	19.63	19.44
Cr_2O_3	0.00	0.00	0.00	0.00
FeO	0.00	0.00	0.00	0.00
MnO	0.00	1.28	0.00	0.00
MgO	0.00	0.00	0.00	0.00
CaO	0.00	0.00	0.00	0.00
Na_2O	19.17	17.44	18.99	19.52
K_2O	0.19	0.00	0.00	0.00
TOTAL	100.00	100.00	100.00	100.00

Table 43: SEM-EDS analyses on the Noumas I pegmatite for quartz.

	BKQ5-2a(12)_pt12	BKQ5-2a(13)_pt1	BKQ5-2a(13)_pt13	BKQ5-2a(13)_pt14	BKQ5-2a(13)_pt17	BKQ5-2a(13)_pt20	BKQ5-3(2)_pt10	BKQ5-3(2)_pt11	BKQ5-3(2)_pt16	BKQ5-3(2)_pt17
SiO_2	100.00	100.00	100.00	98.85	100.00	100.00	95.45	100.00	100.00	99.08
TiO_2	0.00	0.00	0.00	0.00	0.00	0.00	0.00	0.00	0.00	0.00
Al_2O_3	0.00	0.00	0.00	0.73	0.00	0.00	2.46	0.00	0.00	0.32
Cr_2O_3	0.00	0.00	0.00	0.00	0.00	0.00	0.00	0.00	0.00	0.00
FeO	0.00	0.00	0.00	0.00	0.00	0.00	0.00	0.00	0.00	0.00
MnO	0.00	0.00	0.00	0.00	0.00	0.00	0.00	0.00	0.00	0.00
MgO	0.00	0.00	0.00	0.00	0.00	0.00	0.00	0.00	0.00	0.00
CaO	0.00	0.00	0.00	0.00	0.00	0.00	0.00	0.00	0.00	0.00
Na_2O	0.00	0.00	0.00	0.00	0.00	0.00	2.10	0.00	0.00	0.60
K_2O	0.00	0.00	0.00	0.43	0.00	0.00	0.00	0.00	0.00	0.00
TOTAL	100.00	100.00	100.00	100.00	100.00	100.00	100.00	100.00	100.00	100.00

Table 44: SEM-EDS analyses on the Noumas I pegmatite for muscovite

	BKQ5-2b(1)	BKQ5-2b(1)pt2	BKQ5-2b(1)pt4	BKQ5-2b(1)_pt7	BKQ5-2b(1)_pt10	BKQ5-2b(2)_pt2	BKQ5-2b(2)_pt4	BKQ5-2b(2)_pt6	BKQ5-2b(2)_pt7	BKQ5-2b(2)_pt10	BKQ5-2b(2)_pt11	BKQ5-2b(1)_pt2	BKQ5-2b(1)_pt4
SiO$_2$	41.16	41.84	40.98	40.68	40.92	41.01	41.07	41.00	41.65	42.35	41.16	41.84	40.98
TiO$_2$	0.00	0.00	0.00	0.00	0.00	0.00	0.00	0.00	0.00	0.00	0.00	0.00	0.00
Al$_2$O$_3$	39.76	39.64	40.04	40.18	39.70	40.28	39.56	39.46	39.92	35.20	39.76	39.64	40.04
Cr$_2$O$_3$	0.00	0.00	0.00	0.00	0.00	0.00	0.00	0.00	0.00	0.00	0.00	0.00	0.00
FeO	0.73	0.00	0.00	0.00	0.79	0.00	1.18	0.92	0.00	1.37	0.73	0.00	0.00
MnO	0.00	0.00	0.00	0.00	0	0.00	0.00	0.00	0.00	0.00	0.00	0.00	0.00
MgO	0.00	0.00	0.00	0.00	0.00	0.00	0.00	0.00	0.00	0.00	0.00	0.00	0.00
CaO	0.00	0.00	0	0.00	0.00	0.00	0.00	0.00	0.00	0.00	0.00	0.00	0.00
Na$_2$O	0.84	0.00	1.09	1.34	1.08	0.98	0.89	1.30	0.99	2.72	0.84	0.00	1.09
K$_2$O	17.52	18.52	17.89	17.80	17.51	17.73	17.30	17.31	17.44	18.35	17.52	18.52	17.89
TOTAL	100.00	100.00	100.00	100.00	100.00	100.00	100.00	100.00	100.00	100.00	100.00	100.00	100.00

Table 45: SEM-EDS analyses on the Noumas I pegmatite for muscovite continued.

	BKQ5-2b(1)_pt10	BKQ5-2b(1)_pt1	BKQ5-2b(1)_pt2	BKQ5-2b(1)_pt4	BKQ5-2b(1)_pt5	BKQ5-2b(1)_pt7	BKQ5-2b(1)_pt10	BKQ5-2b(3)_pt4	BKQ5-2b(3)_pt6	BKQ5-2b(3)_pt9	BKQ5-2b(3)_pt10	BKQ5-2b(4)_pt3	BKQ5-2b(4)_pt4	BKQ5-2b(4)_pt5	BKQ5-2b(4)_pt6
SiO$_2$	40.92	41.16	41.84	40.98	41.33	40.68	40.92	40.72	41.40	41.27	41.46	46.44	43.81	45.26	45.88
TiO$_2$	0.00	0.00	0.00	0.00	0.00	0.00	0.00	0.00	0.00	0.00	0.00	0.00	0.00	0.00	0.00
Al$_2$O$_3$	39.70	39.76	39.64	40.04	38.55	40.18	39.70	39.70	39.94	39.65	40.05	36.59	32.08	40.41	36.47
Cr$_2$O$_3$	0.00	0.00	0.00	0.00	0.00	0.00	0.00	0.00	0.00	0.00	0.00	0.00	0.00	0.00	0.00
FeO	0.79	0.73	0.00	0.00	0.70	0.00	0.79	0.89	0.67	0.66	0.00	1.12	0.00	1.11	1.20
MnO	0.00	0.00	0.00	0.00	0.00	0.00	0.00	0.00	0.00	0.00	0.00	1.32	1.75	1.98	1.76
MgO	0.00	0.00	0.00	0.00	0.00	0.00	0.00	0.00	0.00	0.00	0.00	0.00	0.00	0.00	0.00
CaO	0.00	0.00	0.00	0.00	0.00	0.00	0.00	0.00	0.00	0.00	0.00	0.00	0.00	0.00	0.00
Na$_2$O	1.08	0.84	0.00	1.09	0.64	1.34	1.08	0.85	1.61	1.75	1.59	0.00	0.58	0.00	0.00
K$_2$O	17.51	17.52	18.52	17.89	18.79	17.80	17.51	17.84	16.38	16.68	16.91	13.77	18.51	10.33	13.79
TOTAL	100.00	100.00	100.00	100.00	100.00	100.00	100.00	100.00	100.00	100.00	100.00	99.25	96.72	99.08	99.10

Table 46: SEM-EDS analyses on the Noumas I pegmatite for muscovite continued

	BKQ 5-2a	BKQ5-2a	BKQ5-2a	BKQ5-2a	BKQ5-2a	BKQ5-2a	BKQ5-2a	BKQ5-2a	BKQ5-2a	BKQ5-2a	BKQ5-2a	BKQ5-2a	BKQ5-2a	BKQ5-2a	BKQ5-2a
SiO_2	46.68	43.61	43.46	45.38	44.81	46.20	51.09	48.30	46.67	43.90	48.04	47.25	43.42	40.72	41.59
TiO_2	0.00	0.00	0.00	0.00	0.00	0.00	0.00	0.00	0.00	0.00	0.00	0.00	0.00	0.00	0.00
Al_2O_3	36.99	34.38	32.56	39.66	33.13	31.46	33.87	32.58	33.04	34.76	34.04	35.21	34.77	40.69	39.61
Cr_2O_3	0.00	0.00	0.00	0.00	0.00	0.00	0.00	0.00	0.00	0.00	0.00	0.00	0.00	0.00	0.00
FeO	1.09	0.00	0.80	0.78	0.76	0.68	0.62	1.83	2.61	0.85	0.83	0.66	1.28	0.00	0.00
MnO	1.19	0.95	1.08	1.18	1.23	0.77	1.54	1.68	1.72	0.92	2.01	1.61	0.83	0.00	0.00
MgO	0.00	0.00	0.00	0.00	0.00	0.00	0.00	0.00	0.00	0.00	0.00	0.00	0.00	0.00	0.00
CaO	0.00	0.00	0.00	0.00	0.00	0.00	0.00	0.00	0.00	0.00	0.00	0.00	0.00	0.00	0.00
Na_2O	0.00	0.00	0.61	0.32	0.00	0.40	0.00	0.00	0.00	0.00	0.25	0.43	0.00	1.85	0.73
K_2O	13.23	18.43	18.03	11.59	18.80	19.53	12.11	14.79	14.92	18.70	13.92	13.66	18.55	16.74	18.06
TOTAL	99.18	97.37	96.54	98.92	98.73	99.03	99.22	99.18	98.95	99.13	99.10	98.82	98.85	100.00	100.00

Table 47: SEM-EDS analyses on the Noumas I pegmatite for muscovite continued

	BKQ5-2b(8)_pt14	BKQ5-2b(8)_pt16	bb2a(4)_pt5	bb2a(4)_pt6	bb2a(4)_pt14	bb2a(4)_pt15	bb2a(4)_pt16	bb2a(4)_pt20	bb2a(5)_pt1	bb2a(5)_pt3	bb2a(5)_pt5	BKQ5-2a(1)_pt6	BKQ5-2a(2)_pt2
SiO_2	44.22	43.85	47.16	42.51	41.49	49.36	41.71	42.26	42.17	42.02	41.74	42.36	45.41
TiO_2	0.00	0.00	0.00	0.00	0.00	0.00	0.00	0.00	0.00	0.00	0.00	0.00	0.00
Al_2O_3	34.17	33.87	31.00	39.26	38.99	28.04	38.95	38.64	38.63	38.87	39.02	38.51	29.65
Cr_2O_3	0.00	0.00	0.00	0.00	0.00	0.00	0.00	0.00	0.00	0.00	0.00	0.00	0.00
FeO	0.98	1.05	0.67	0.00	0.61	0.00	0.00	0.00	0.62	0.00	0.58	0.00	1.55
MnO	1.24	1.30	0.00	0.00	0.00	0.00	0.00	0.00	0.00	0.00	0.00	0.00	0.00
MgO	0.00	0.00	0.00	0.00	0.00	0.00	0.00	0.00	0.00	0.00	0.00	0.00	0.00
CaO	0.00	0.00	0.00	0.00	0.00	0.00	0.00	0.00	0.00	0.00	0.00	0.00	0.00
Na_2O	0.00	0.35	0.32	0.51	0.50	0.73	0.54	0.67	0.48	0.60	0.34	1.08	0.00
K_2O	17.87	18.03	20.86	17.72	18.41	21.49	18.80	18.43	18.09	18.51	18.32	18.04	13.99
TOTAL	98.48	98.45	100.00	100.00	100.00	99.61	100.00	100.00	100.00	100.00	100.00	100.00	90.60

Table 48: SEM-EDS analyses on the Noumas I pegmatite for muscovite continued

	BKQ5-2a	*BKQ5-2a*	*BKQ5-2a*	*BKQ5-2a*	*BKQ5-2a*	*BKQ5-2a*	*BKQ5-2a*	*BKQ5-2a*	*BKQ5-2a*	*BKQ5-2a*	*BKQ5-2a*	*BKQ5-2a*	*BKQ5-2a*	*BKQ5-2a*	*BKQ5-2a*	*BKQ5-2a*
SiO_2	49.19	43.93	48.23	42.50	45.68	44.46	47.65	46.83	44.81	41.14	41.87	48.31	42.38	41.71	41.02	44.37
TiO_2	0.00	0.00	0.00	0.00	0.00	0.00	0.00	0.00	0.00	0.00	0.00	0.00	0.00	0.00	0.00	0.00
Al_2O_3	31.15	33.19	28.58	38.67	30.97	31.32	32.33	31.00	31.35	30.54	38.12	34.92	30.63	31.13	31.05	33.67
Cr_2O_3	0.00	0.00	0.00	0.00	0.00	0.00	0.00	0.00	0.00	0.00	0.00	0.00	0.00	0.00	0.00	0.00
FeO	2.17	0.93	0.00	0.78	3.29	3.35	3.22	4.19	2.88	1.26	0.00	0.00	0.94	1.16	1.11	0.99
MnO	0.00	0.00	0.00	0.00	0.00	0.00	0.00	0.00	0.00	0.00	0.00	0.00	0.00	0.00	0.00	0.00
MgO	0.00	0.00	0.00	0.00	0.00	0.00	0.00	0.00	0.00	0.00	0.00	0.00	0.00	0.00	0.00	0.00
CaO	0.00	0.00	0.00	0.00	0.00	0.00	0.00	0.00	0.00	0.00	0.00	0.00	0.00	0.00	0.00	0.00
Na_2O	0.00	0.17	0.52	0.45	0.00	0.00	0.00	0.00	0.00	0.52	0.46	0.64	0.00	0.51	0.00	0.35
K_2O	14.85	19.27	20.98	17.60	13.77	12.76	14.77	15.62	12.61	17.68	19.54	14.55	17.37	16.39	17.42	18.46
TOTAL	97.36	97.48	98.31	100.00	93.71	91.90	97.97	97.64	91.66	91.14	100.00	98.42	91.32	90.88	90.61	97.84

Table 49: SEM-EDS analyses on the Noumas I pegmatite for apatite.

	BKQ5-2a	*BKQ5-2a*	*BKQ5-2a*	*BKQ5-2a*	*BKQ5-2a*	*BKQ5-2a*	*BKQ5-2a*	*BKQ5-2a*	*BKQ5-2a*	*BKQ5-2a*	*BKQ5-2a*	*BKQ5-2a*	*BKQ5-2a*	*BKQ5-2a*
SiO_2	0.29	0.34	4.62	0.00	0.00	0.00	0.21	0.22	0.18	0.00	0.65	0.00	0.31	0.00
TiO_2	0.00	0.00	0.00	0.00	0.00	0.00	0.00	0.00	0.00	0.00	0.00	0.00	0.00	0.00
Al_2O_3	0.13	0.00	1.46	0.00	0.00	0.00	0.00	0.00	0.00	0.00	0.31	0.00	0.10	0.00
CaO	59.15	57.04	56.46	58.92	59.29	60.62	58.38	58.76	58.67	59.98	60.92	59.22	58.18	59.06
P_2O_3	28.34	28.49	25.63	28.78	28.33	28.29	28.49	28.47	28.72	28.61	27.86	28.49	28.85	28.62
TOTAL	87.90	85.86	89.50	87.69	87.61	88.91	87.08	87.45	87.56	88.59	89.74	87.71	87.43	87.69
F	12.10	14.14	10.50	12.31	12.39	11.09	12.92	12.55	12.44	11.41	10.26	12.29	12.57	12.31

Table 50: SEM-EDS analyses on the Noumas I pegmatite for almandine.

	BB3a(1)_pt1	*BB3a(1)_pt4*	*BB3a(1)_pt6*	*BB3a(1)_pt7*
SiO_2	44.17	38.48	49.06	39.63
TiO_2	0.00	0.00	0.00	0.00
Al_2O_3	20.74	15.34	21.77	20.44
Cr_2O_3	0.00	0.00	0.00	0.00
FeO	22.50	31.13	12.45	26.68
CaO	0.00	0.00	0.00	0.52
Na_2O	12.18	14.80	15.17	12.40
K_2O	0.42	0.25	0.00	0.33
TOTAL	100.00	100.00	98.46	100.00

Table 51: SEM-EDS analyses on the Noumas I pegmatite for K-feldspar

	BK Q5-2a	BK Q5-2a	BKQ 5-2a	BKQ 5-2a	BKQ 5-2a	BKQ 5-2a	BKQ 5-2a	BKQ 5-2a	BKQ 5-2a	BKQ 5-2a	BKQ 5-2a	BKQ 5-2a	BK Q5-2a	BK Q5-2a
SiO_2	50.15	60.88	51.27	55.71	53.38	54.10	55.42	56.04	55.61	55.19	55.69	51.27	53.12	50.75
TiO_2	0.00	0.00	0.00	0.00	0.00	0.00	0.00	0.00	0.00	0.00	0.00	0.00	0.00	0.00
Al_2O_3	29.35	22.60	26.00	19.48	23.05	22.15	19.82	19.01	20.00	20.33	19.30	26.00	24.17	27.84
MnO	0.00	0.00	0.00	0.00	0.00	0.00	0.00	0.00	0.00	0.00	0.00	0.00	0.00	0.00
MgO	0.27	0.00	1.02	0.00	0.68	0.41	0.05	0.00	0.00	0.00	0.00	1.02	0.00	0.00
CaO	0.00	2.17	0.00	0.00	0.00	0.00	0.00	0.00	0.00	0.00	0.00	0.00	0.00	0.00
Na_2O	9.78	2.97	0.69	0.72	0.73	0.79	0.90	0.92	0.83	0.83	0.82	0.69	1.07	0.87
K_2O	10.46	11.37	20.42	24.09	22.16	22.55	23.80	24.03	23.56	23.65	24.18	20.42	21.64	20.54
TOTAL	100.00	100.00	99.39	100.00	100.00	100.00	100.00	100.00	100.00	100.00	100.00	99.39	100.00	100.00

Table 52: SEM-EDS analyses on the Noumas I pegmatite for K-feldspar continued.

	BK Q5-2a	BKQ 5-2a	BKQ 5-2a	BK Q5-2a	BK Q5-2a	BK Q5-2a	BK Q5-2a	BK Q5-2a	BK Q5-2a	BK Q5-2a	BKQ 5-2a	BK Q5-2a	BK Q5-2a	BK Q5-2a	BK Q5-2a
SiO_2	50.67	52.92	45.03	44.89	43.81	55.36	54.21	53.23	45.11	51.24	54.16	55.22	49.43	54.72	54.90
TiO_2	0.00	0.00	0.00	0.00	0.00	0.00	0.00	0.00	0.00	0.00	0.00	0.00	0.00	0.00	0.00
Al_2O_3	28.25	29.11	27.49	31.73	29.23	21.55	20.47	20.01	25.67	23.48	22.91	19.60	25.18	20.10	19.80
FeO	0.00	0.00	0.00	0.00	0.00	0.00	0.00	0.00	0.00	0.00	0.00	0.00	0.00	0.00	0.00
MnO	0.00	0.00	0.00	0.00	0.00	0.00	0.00	0.00	0.00	0.00	0.00	0.00	0.00	0.00	0.00
MgO	0.00	0.00	0.00	0.00	0.00	0.00	0.00	0.00	0.00	0.26	0.00	0.00	0.18	0.00	0.00
CaO	0.00	0.00	0.00	0.00	0.00	0.00	0.00	0.00	0.00	0.00	0.00	0.00	0.00	0.00	0.00
Na_2O	3.52	4.48	7.65	7.07	6.86	2.13	0.76	0.46	0.79	1.27	2.55	0.46	0.33	1.06	0.67
K_2O	17.56	13.49	10.46	11.66	11.51	20.95	24.56	24.86	18.96	19.08	20.38	24.03	21.49	23.58	24.62
TOTAL	100.00	100.00	90.62	95.36	91.42	100.00	100.00	98.56	90.54	95.33	100.00	99.31	96.62	99.46	100.00